AD-A041 864 BOEING COMMERCIAL AIRPLANE CO SEATTLE WASH F/G 9/5
AIR TRAFFIC CONTROL EXPERIMENTATION AND EVALUATION WITH THE NAS--ETC(U)
SEP 76 A D THOMPSON, S C WILSON, P F RIEDER DOT-TSC-707-4
UNCLASSIFIED D6-44049 FAA RD-75-173-4 NL

1 OF 3
ADA041864

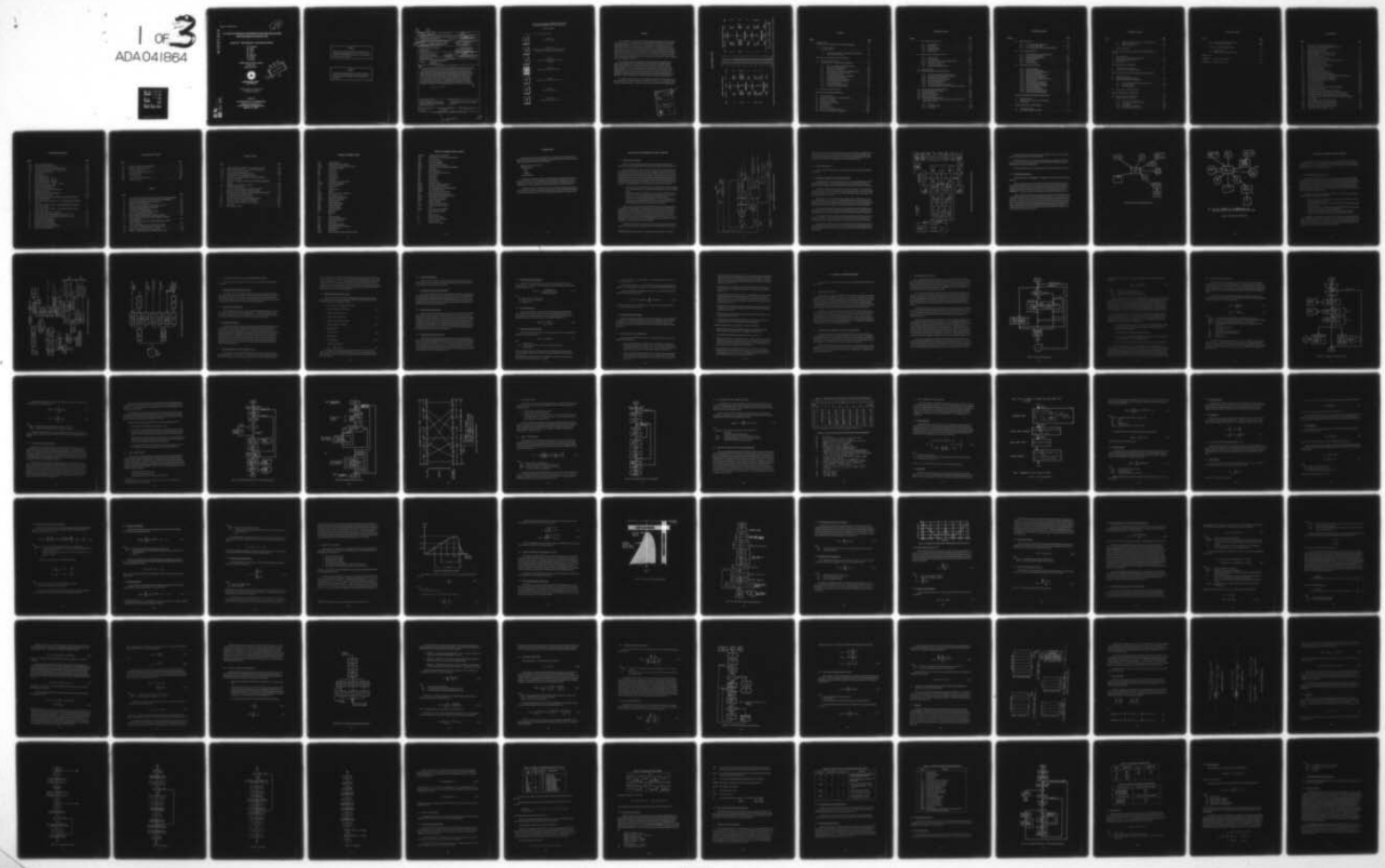

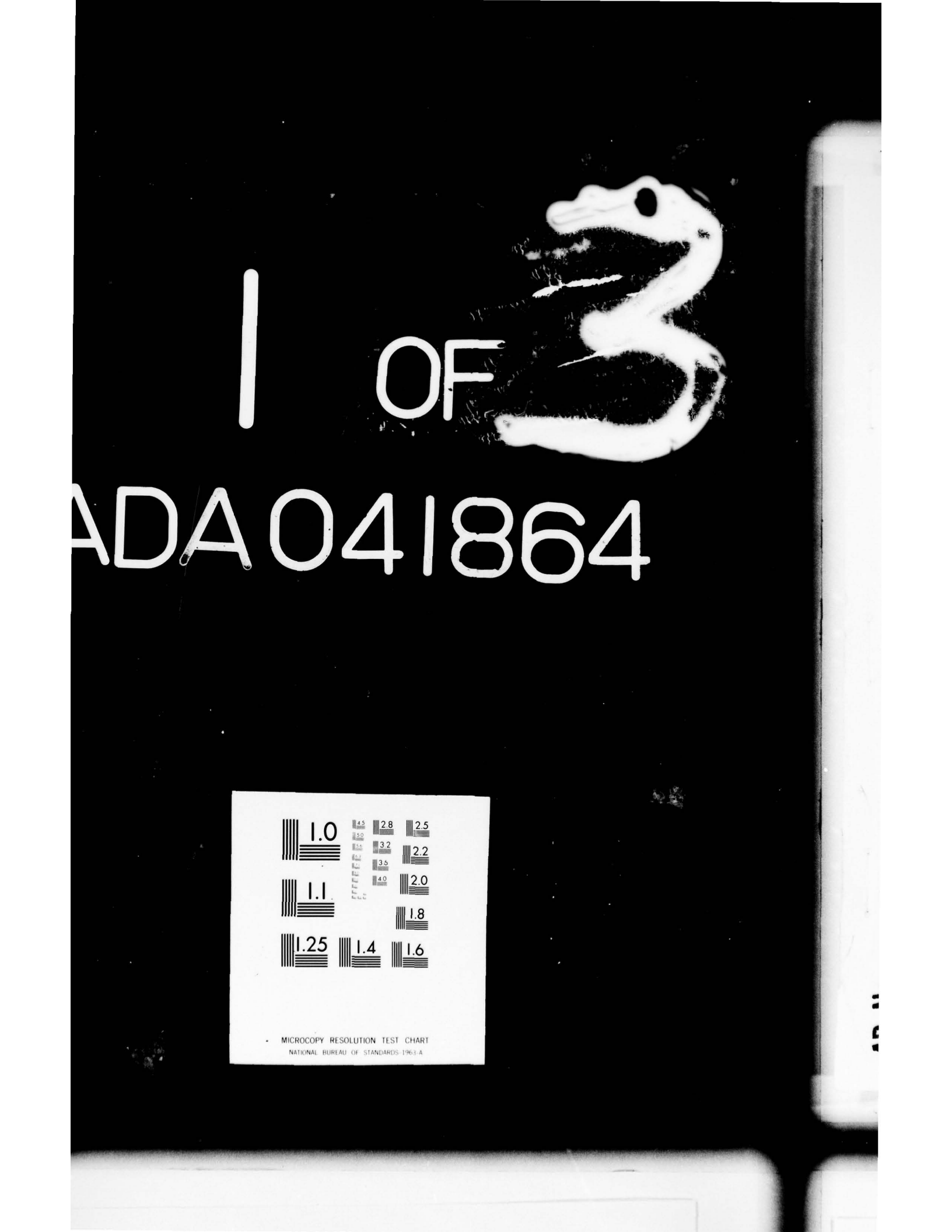
1 OF 3
ADA041864
1.0
1.1
1.25
1.4
1.6
1.8
2.0
2.2
2.5
2.8
3.2
3.6
4.0
4.5
5.0
5.6
MICROCOPY RESOLUTION TEST CHART
NATIONAL BUREAU OF STANDARDS-1963-A

Report No. FAA-RD-75-173, IV

(10)

# AIR TRAFFIC CONTROL EXPERIMENTATION AND EVALUATION WITH THE NASA ATS-6 SATELLITE

## Volume IV: Data Reduction and Analysis Software

A.D. Thompson
S.G. Wilson
P.F. Rieder
W.L. Chu
M.J. Mardesich
C.V. Paulson
P. Alexander

Boeing Commercial Airplane Company
PO Box 3707
Seattle WA 98124




**SEPTEMBER 1976**
**FINAL REPORT**

Document is available to the U.S. public through the
National Technical Information Service,
Springfield, Virginia 22161

Prepared for

U.S. DEPARTMENT OF TRANSPORTATION
Federal Aviation Administration
Systems Research and Development Service
Washington DC 20591

**NOTICE**

This document is disseminated under the sponsorship of the Department of Transportation in the interest of information exchange. The United States Government assumes no liability for its contents or use thereof.

**NOTICE**

The United States Government does not endorse products or manufacturers. Trade or manufacturers' names appear herein solely because they are considered essential to the object of this report.

| 1. Report No. | 2. Government Accession No. | 3. Recipient's Catalog No. |
|---|---|---|
| FAA RD-75-173, IV | | |

**4. Title and Subtitle**
AIR TRAFFIC CONTROL EXPERIMENTATION AND EVALUATION WITH THE NASA ATS-6 SATELLITE
Volume IV, Data Reduction and Analysis Software

**5. Report Date**
September 1976

**6. Performing Organization Code**
DOT-TSC-FAA-77-22, IV

**7. Author(s)**
A.D. Thompson, S.G. Wilson, P.F. Rieder, W.L. Chu, M.J. Mardesich, C.V. Paulson, P. Alexander

**8. Performing Organization Report No.**
D6-44049

**9. Performing Organization Name and Address**
Boeing Commercial Airplane Company*
P.O. Box 3707
Seattle, WA 98124

**10. Work Unit No.**
FA711/R7106

**11. Contract or Grant No.**
DOT-TSC-707-4

**12. Sponsoring Agency Name and Address**
U.S. Department of Transportation
Federal Aviation Administration
Systems Research and Development Service
Washington, DC 20591

**13. Type of Report and Period Covered**
Final Report,
Sep. 1973 to Dec. 1975

**14. Sponsoring Agency Code**

214 p.

**15. Supplementary Notes**
*Under contract to: U.S. Department of Transportation
Transportation Systems Center
Kendall Square
Cambridge, MA 02142

**16. Abstract**


Software used for the reduction and analysis of the multipath prober, modem evaluation (voice, digital data, and ranging), and antenna evaluation data acquired during the ATS-6 field test program is described.

Multipath algorithms include reformatting operations, delay-spectra time histories, delay-Doppler scatter function $S(\tau,\omega)$, noise determination and removal, spread calculations, airborne tape analysis, and other detailed processing including time-domain analysis and various integral and Fourier operations on $S(\tau,\omega)$. Modem and antenna evaluation data processing software includes algorithms for the determination of (1) $C/N_0$ and multipath interference ratio, S/I, (2) digital data bit-error rates, block error statistics, and inter-error spacing, and (3) ranging error statistics and distribution. Sample outputs are given. Program listings and other information are provided in an auxiliary software data package.

The report consists of seven volumes: I – Executive Summary; II – Demonstration of Satellite-Supported Communications and Surveillance for Oceanic Air Traffic Control; III – Summary of U.S. Aeronautical Technology Test Program; IV – Data Reduction and Analysis Software; V – Multipath Channel Characterization Test; VI – Modem Evaluation Test; VII – Aircraft Antenna Evaluation Test.


| 17. Key Words (Suggested by Author(s)) | 18. Distribution Statement |
|---|---|
| ATS-6 Satellite, Multipath, Modem Evaluation, Digital Data, Ranging, Fast Fourier Transform, Data Processing, Algorithms, Envelope Detector Analysis, Scatter Function | Document is available to the U.S. public through the National Technical Information Service, Springfield, Virginia 22161 |

| 19. Security Classif. (of this report) | 20. Security Classif. (of this page) | 21. No. of Pages | 22. Price* |
|---|---|---|---|
| Unclassified | Unclassified | 230 | |

*For sale by the National Technical Information Service, Springfield, Virginia 22151

**AIR TRAFFIC CONTROL EXPERIMENTATION AND EVALUATION WITH THE NASA ATS-6 SATELLITE**

FINAL REPORT

This report consists of the following volumes.

Volume I
Executive Summary

Volume II
Demonstration of Satellite-Supported Communications and Surveillance for Oceanic Air Traffic Control

Volume III
Summary of U.S. Aeronautical Technology Test Program

Volume IV
Data Reduction and Analysis Software

Volume V
Multipath Channel Characterization Test

Volume VI
Modem Evaluation Test

Volume VII
Aircraft Antenna Evaluation Test

## PREFACE

The U.S. Department of Transportation (DOT) aeronautical test program entitled "Air Traffic Control Experimentation and Evaluation with the NASA ATS-6 Satellite" was part of the Integrated ATS-6 L-Band Experiment. The overall ATS-6 L-band experiment was coordinated by the NASA/ Goddard Space Flight Center (GSFC) and was international in scope. The following agencies were participants in the experiment: NASA/Goddard Space Flight Center; DOT/Federal Aviation Administration; DOT/Transportation Systems Center; DOT/U.S. Coast Guard; DOC/Maritime Administration; European Space Agency (ESA); and the Canadian Ministry of Transport and Department of Communications. Each participant performed tests in one or more of three categories: aeronautical, maritime safety, and maritime fleet operations. All tests were conducted in accordance with an overall integrated test plan coordinated by NASA/GSFC.

The U.S. DOT Aeronautical test program was under the direction and sponsorship of the Federal Aviation Administration, Systems Research and Development Service (SRDS), Satellite Branch, with the DOT/TSC conducting the technology tests and the FAA/NAFEC conducting the ATC demonstration tests. The technology tests included multipath channel characterization, modem evaluation, and aircraft antenna evaluation. Results of these tests are presented in volumes III through VII, and the results of the ATC demonstration tests are presented in volume II. The DOT/TSC test program was supported by the Boeing Commercial Airplane Company under contract DOT-TSC-707. Mr. R. G. Bland was the TSC Project Engineer and Contract Technical Monitor.

This volume describes the software used for reduction and analysis of the technology test data. All work described was performed under contract DOT-TSC-707. Sections 4.21 and appendix B of this volume were prepared by CNR, Inc., under subcontract to the Boeing Commercial Airplane Company.

# METRIC CONVERSION FACTORS

## Approximate Conversions to Metric Measures

| Symbol | When You Know | Multiply by | To Find | Symbol |
|---|---|---|---|---|
| | | **LENGTH** | | |
| in | inches | 2.5 | centimeters | cm |
| ft | feet | 30 | centimeters | cm |
| yd | yards | 0.9 | meters | m |
| mi | miles | 1.6 | kilometers | km |
| | | **AREA** | | |
| $in^2$ | square inches | 6.5 | square centimeters | $cm^2$ |
| $ft^2$ | square feet | 0.09 | square meters | $m^2$ |
| $yd^2$ | square yards | 0.8 | square meters | $m^2$ |
| $mi^2$ | square miles | 2.6 | square kilometers | $km^2$ |
| | acres | 0.4 | hectares | ha |
| | | **MASS (weight)** | | |
| oz | ounces | 28 | grams | g |
| lb | pounds | 0.45 | kilograms | kg |
| | short tons (2000 lb) | 0.9 | tonnes | t |
| | | **VOLUME** | | |
| tsp | teaspoons | 5 | milliliters | ml |
| Tbsp | tablespoons | 15 | milliliters | ml |
| fl oz | fluid ounces | 30 | milliliters | ml |
| c | cups | 0.24 | liters | l |
| pt | pints | 0.47 | liters | l |
| qt | quarts | 0.95 | liters | l |
| gal | gallons | 3.8 | liters | l |
| $ft^3$ | cubic feet | 0.03 | cubic meters | $m^3$ |
| $yd^3$ | cubic yards | 0.76 | cubic meters | $m^3$ |
| | | **TEMPERATURE (exact)** | | |
| °F | Fahrenheit temperature | 5/9 (after subtracting 32) | Celsius temperature | °C |


## Approximate Conversions from Metric Measures

| Symbol | When You Know | Multiply by | To Find | Symbol |
|---|---|---|---|---|
| | | **LENGTH** | | |
| mm | millimeters | 0.04 | inches | in |
| cm | centimeters | 0.4 | inches | in |
| m | meters | 3.3 | feet | ft |
| m | meters | 1.1 | yards | yd |
| km | kilometers | 0.6 | miles | mi |
| | | **AREA** | | |
| $cm^2$ | square centimeters | 0.16 | square inches | $in^2$ |
| $m^2$ | square meters | 1.2 | square yards | $yd^2$ |
| $km^2$ | square kilometers | 0.4 | square miles | $mi^2$ |
| ha | hectares (10,000 $m^2$) | 2.5 | acres | |
| | | **MASS (weight)** | | |
| g | grams | 0.035 | ounces | oz |
| kg | kilograms | 2.2 | pounds | lb |
| t | tonnes (1000 kg) | 1.1 | short tons | |
| | | **VOLUME** | | |
| ml | milliliters | 0.03 | fluid ounces | fl oz |
| l | liters | 2.1 | pints | pt |
| l | liters | 1.06 | quarts | qt |
| l | liters | 0.26 | gallons | gal |
| $m^3$ | cubic meters | 35 | cubic feet | $ft^3$ |
| $m^3$ | cubic meters | 1.3 | cubic yards | $yd^3$ |
| | | **TEMPERATURE (exact)** | | |
| °C | Celsius temperature | 9/5 (then add 32) | Fahrenheit temperature | °F |

## CONTENTS

**CONTENTS (Continued)**

**CONTENTS (Continued)**

**CONTENTS (Continued)**

## CONTENTS (Concluded)

## ILLUSTRATIONS

## ILLUSTRATIONS (Continued)

## ILLUSTRATIONS (Concluded)



## TABLES

**TABLES (Concluded)**

## SYMBOLS AND ABBREVIATIONS

| | |
|---|---|
| A/D | analog to digital |
| APD | amplitude probability distribution |
| ATS-6 | *Applications Technology Satellite 6* (NASA) |
| $A_o(\tau)$ | average tap thermal noise |
| bpi | bits per inch |
| bps | bits per second |
| BER | bit-error rate |
| $B_f$ | bandwidth, Hz |
| cw | continuous wave |
| CL | code length |
| $C/N_o$ | carrier-to-noise power density ratio |
| CONUS | Continental United States |
| CP | circular polarization |
| CR | chip rate |
| CRT | cathode ray tube |
| dB | decibel |
| $<\|D\|^2>$ | mean square direct-path signal power |
| DMA | direct memory access |
| DOT | Department of Transportation |
| DRandA | data reduction and analysis |
| $D(\omega)$ | Doppler spectrum |
| ERP | effective radiated power |
| FFT | fast Fourier transform |
| FR(f) | frequency response |
| GMT | Greenwich mean time |
| GOF | goodness of fit |
| H | horizontal |
| i | $\sqrt{-1}$ |
| ips | inches per second |
| $<\|I\|^2>$ | mean square multipath power |
| INS | inertial navigation system |
| I/O | input/output |
| I,Q | in-phase, quadrature-phase |
| IRIG | Inter-Range Instrumentation Group |
| LHC | left-hand circular |
| LPF | low-pass filter |
| NAFEC | National Aviation Facilities Experimental Center |

## SYMBOLS AND ABBREVIATIONS (Concluded)

| | |
|---|---|
| NDandR | noise determination and removal |
| N(f) | multipath-free total noise power spectral density |
| NRZ | nonreturn to zero |
| psd | power spectral density |
| PCM | pulse code modulation |
| PDD | programmable data distributor |
| PLACE | position location and communication equipment |
| PN | pseudo-noise |
| PSK | phase-shift keying |
| $P(\phi)$ | phase probability density function |
| $Q(\tau)$ | delay spectrum |
| R/A | random access |
| R(f) | residual noise |
| RF | radiofrequency |
| RHC | right-hand circular |
| $R(0,\Omega)$ | frequency autocorrelation function |
| $R(\xi,0)$ | time autocorrelation function |
| $R(\xi,\Omega)$ | joint time-frequency autocorrelation function |
| $R_{xy}(\xi)$ | cross-correlation function |
| SACP | satellite aeronautical channel prober |
| S/I | signal-to-multipath interference ratio |
| SRDS | Systems Research and Development Service |
| $S(\tau,\omega)$ | delay-Doppler scatter function |
| TDPC | Test Data Processing Center |
| TFE | telemetry front end |
| TSC | Transportation Systems Center |
| $U(\tau,\xi)$ | tap-gain autocorrelation function |
| V | vertical |
| WBFM | wideband frequency modulation |
| $\lambda$ | electromagnetic wavelength |
| $\mu$ | mean |
| $\sigma$ | standard deviation |
| $\tau,\xi$ | time-delay (lag) variables |
| $\phi_i$ | phase of $i^{th}$ tap received signal |
| $\chi^2$ | chi-squared statistic |
| $\omega,\Omega$ | frequency offset variables. |

# 1. INTRODUCTION

Work performed under contract DOT-TSC-707 includes all software development (for both quick-look and detailed data reduction and analysis), data processing, analysis, and reporting of results for the following U.S. DOT aeronautical technology tests:

Multipath channel characterization
Modem evaluation
- Voice
- Data
- Ranging

Antenna evaluation

This report gives a detailed description of the software and associated hardware used for the reduction and analysis of data acquired during the ATS-6 program for the above tests. Sections 2 through 5 describe software and hardware for reduction and analysis of multipath prober data; sections 6 through 11 provide equivalent information for the modem and antenna evaluation tests.

Program listings and other information relevant to the software described are provided in an auxiliary software data package. The software data package was delivered to DOT/TSC during April 1975. Software developed after April 1975 will be delivered upon completion of the DRandA task.

# 2. MULTIPATH DATA PROCESSING FUNCTIONAL SEQUENCE

## 2.1 SYSTEM BLOCK DIAGRAM

Figure 2-1 depicts the processing steps involved in the reformatting, reduction, and analysis of the recorded multipath SACP signal arrays and the aircraft-transmitter parameter tape.

Received SACP signals[1] are direct recorded in a standard telemetry analog format (serial PCM, NRZ-L). On the analog source tape, two tracks are in general occupied by the multipath data while another of the seven available tracks contains an IRIG-A modulated time code. At the Boeing ground station facility, the data and time tracks are initially processed by telemetry front end (TFE) equipment, which for this particular application routes the played-back serial signals through its PCM subsystem to the programmable data distributor (PDD). The PDD merges time words with the data and distributes the information to one or both of the PDP 11/45 computer I/O buses. The dual PDP computer system is called upon to perform three basic functions:

a. Conversion of the analog recorded data tapes into digital format computer-compatible tapes. The digital tapes are 1/2-in. width with nine parallel tracks written in 1600-bpi density.
b. Quick-look processing of the multipath data. This consists of a playback real-time analysis of the recorded tap outputs and produces individual tap frequency spread, delay spectra, and receiver parameter dumps for all pertinent test data.
c. Calculation of the time-ordered delay-spectra arrays that are used to generate the time history of the multipath channel's delay spectra. The normalization and three-dimensional plotting of this data are performed in the CDC 6600.

The prober data is analyzed in detail by the CDC 6600 computer. This analysis provides a comprehensive characterization of the multipath channel for horizontal and vertical polarization, gathered over a down-looking antenna. The primary output of this routine is the delay-Doppler scatter function of the channel. Also included are the channel's time-frequency autocorrelation function; total scattered intensity; delay spectrum; Doppler spectrum; frequency autocorrelation function; time autocorrelation function; parameter spread values; tap I, Q, and phase distributions; goodness-of-fit test on the tap distributions; tap cross-correlation; tap I and Q dependency tests; and the tap-gain autocorrelation function.

In addition to the SACP receiver data reduction, this report also includes details pertaining to software designed to reduce and analyze the data tape containing airplane and transmitter

[1] Complex I,Q outputs from two delay tap correlator banks, each consisting of 112 elements.

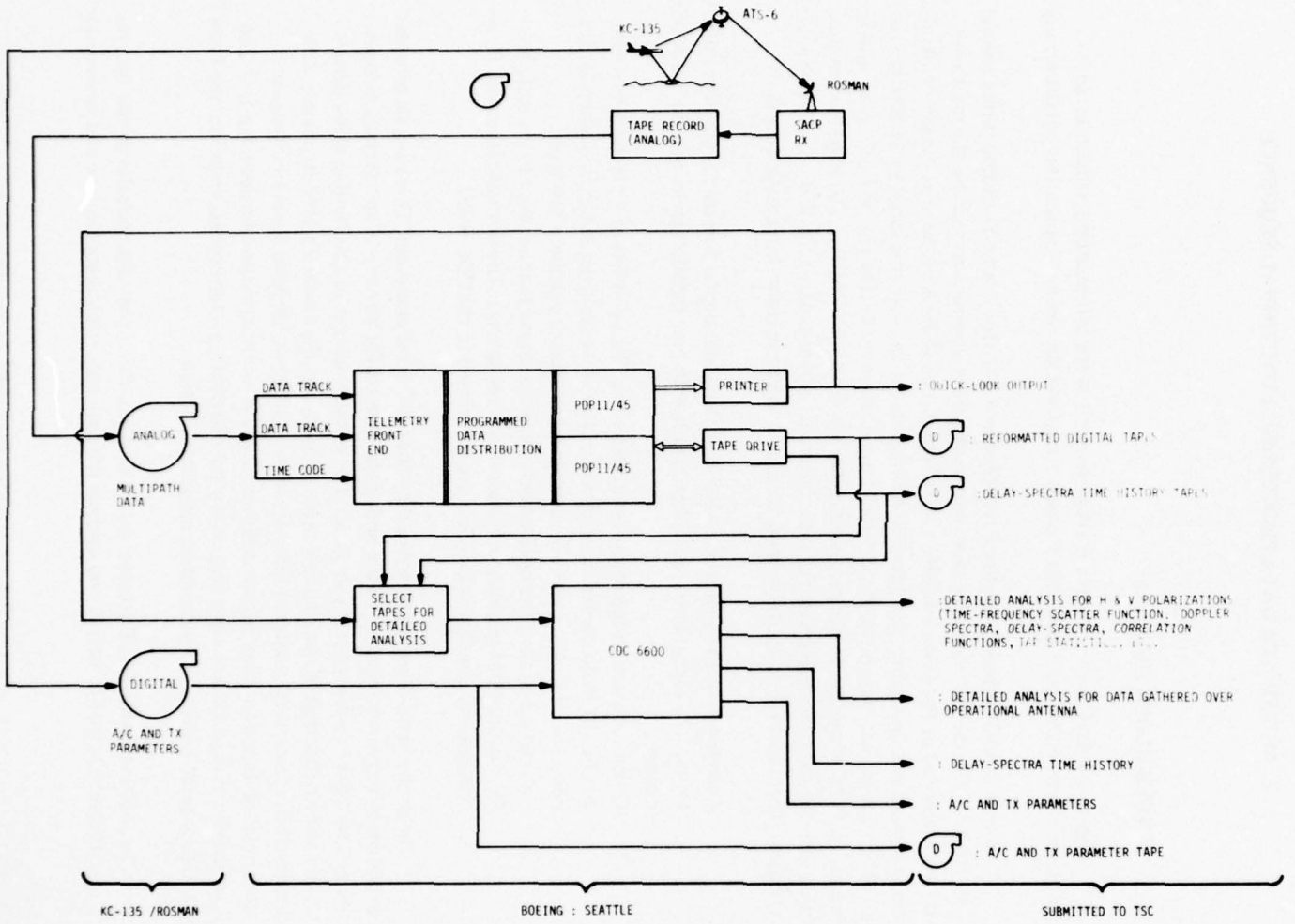


*Figure 2-1. Data Reduction and Analysis Functional Flow*

parameters. The airplane system and transmitter parameters are recorded in a time multiplex-mode of seven-track (six data, one parity) tape that is directly compatible with the Boeing CDC 6600. Data extracted from the airborne system parameters tape will serve as a data collection integrity measure and will be used to augment the logged flight test data for normalization purposes.

## 2.2 SYSTEM DESCRIPTION

In this section, details pertaining to the computer systems used to analyze the multipath data are provided.

### 2.2.1 Boeing Flight Test PDP 11/45 Telemetry Ground Station

The Boeing Flight Test Center ground station is used to convert analog PCM telemetry data to formatted digital information, to perform quick-look reduction including delay-spectra and tap frequency-spread calculations, and to set up the data base for the delay-spectra time history calculation.

The hardware configuration of the ground station is depicted in figure 2-2. Vertical and horizontal data and time code are read simultaneously on the analog tape transport. These data are routed to various components of the telemetry front end (TFE) by the EMR 2793 data matrix, which is manually set up at the start of a test series.

Multipath data is routed to the EMR 720 bit synchronizer where the PCM bit stream is digitized and synchronized to a clock signal. The EMR 720 output is input to the frame synchronizer, which searches for the frame sync bit pattern that heads each frame of data. This action allows for the correlation of specific stream bit segments to real data elements that can be processed by computer.

Frame synchronizer output is processed by the programmable data distributor (PDD), which removes blank words and merges time code information into the data stream. The system setup controller determines the source of the merged time code for the PDD and interrupts for the processor.

Test condition timing control and time code data are generated by the Datum tape search unit and time code translator. A start and stop time is set in this unit, which is used to delimit the test condition interval. When the operator has the TFE set up, system control is transferred to this unit.

Most of the TFE components are set up by control signals from the computers that interface to the TFE through an array of 2763 interfaces. These signals are generated through interpretation of commands either made on the DEC writer terminal by the operator or read in from punched cards by the card reader.

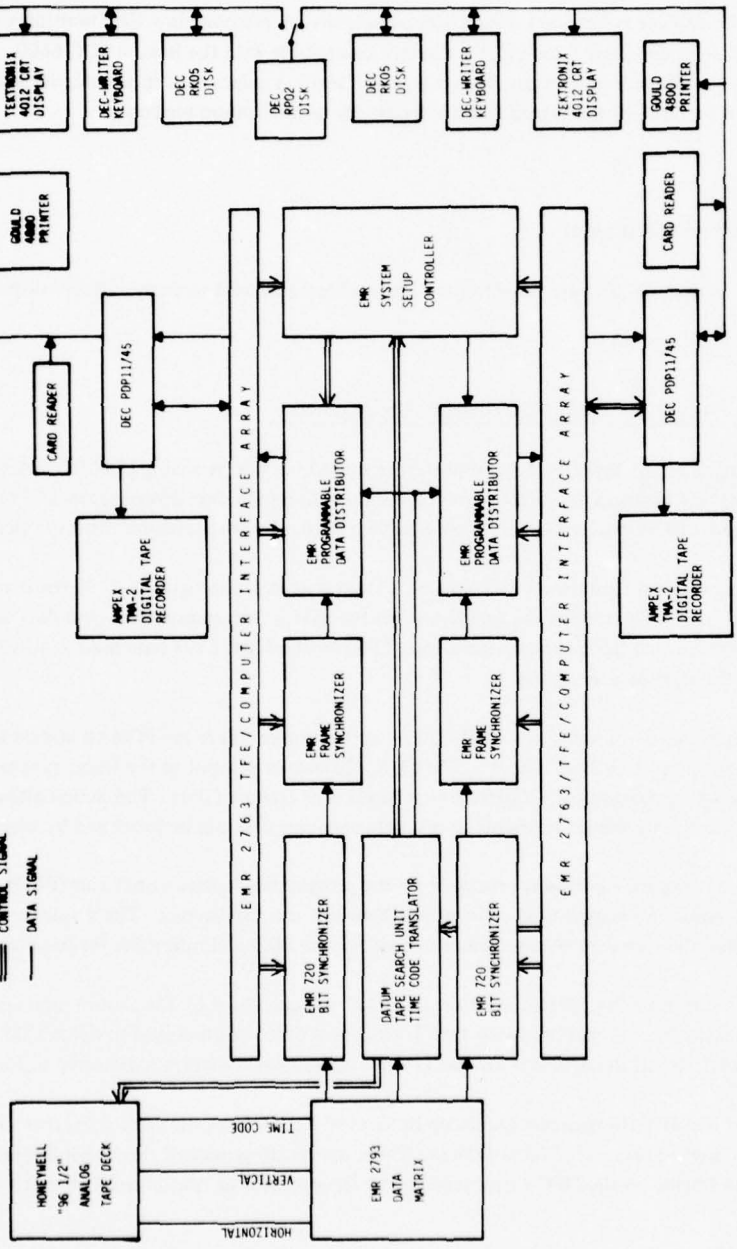


*Figure 2-2. Boeing Flight Test Data Processing EMR Ground Station*

Formatted telemetry data from the PDD is input to the PDP 11/45 memory via a 2763 DMA channel. The data is processed and written to the TMA-2.

Following the reduction of a test condition, the digital tape files containing level quick-look data are read back, with graphic output produced on the Tektronix 4012 CRT display and printed summaries generated on the Gould 4800 printer.

The RK05 and RP02 are used to store programs for the data processing and system operation.

### 2.2.2 CDC 6600 Computer System

A CDC 6600 computer, with KRONOS 2.1 operating system, is used to process the multipath data tapes.

Figure 2-3 gives the data flow for the airborne tape processing. Program inputs consist of a seven-track tape and control data cards. The program, which is run in batch mode on the 6600 computer, produces numerical output and a plot tape that is processed off-line by the CalComp plotter. This plotter was chosen for the quality and size of its plot. The processing program is written in FORTRAN IV. To format the plot tapes, CalComp plot routines from the system library are used.

Figure 2-4 gives the data flow for the delay-spectra time history and the detailed analysis processing. Program inputs consist of the reformatted tape and control data cards. The program is run in batch mode. Temporary storage on disk is used to record the input data. Program outputs include a listing, a save tape (for the scatter function), and a plot tape that is processed off-line on a SC 4020 plotter. The graph produced by the SC 4020 has resolution and size adequate for multipath output. The processing programs are written in FORTRAN IV and CDC 6600 assembly language (2% of the coding). The subroutines used from the system library are relative to random access (R/A) input/output operations and plot tape formatting.

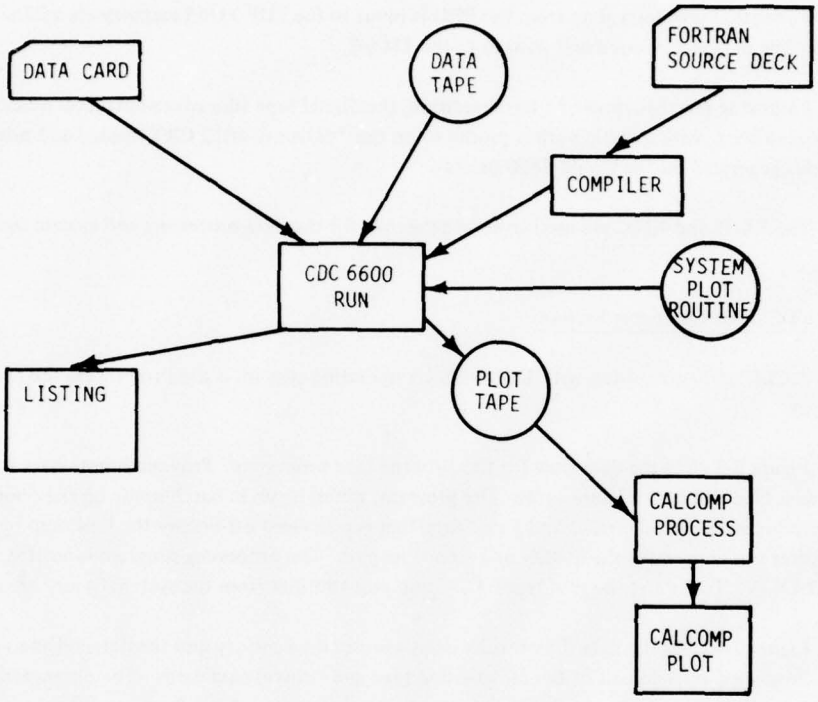


*Figure 2-3. Airborne Tape Processing Data Flow*

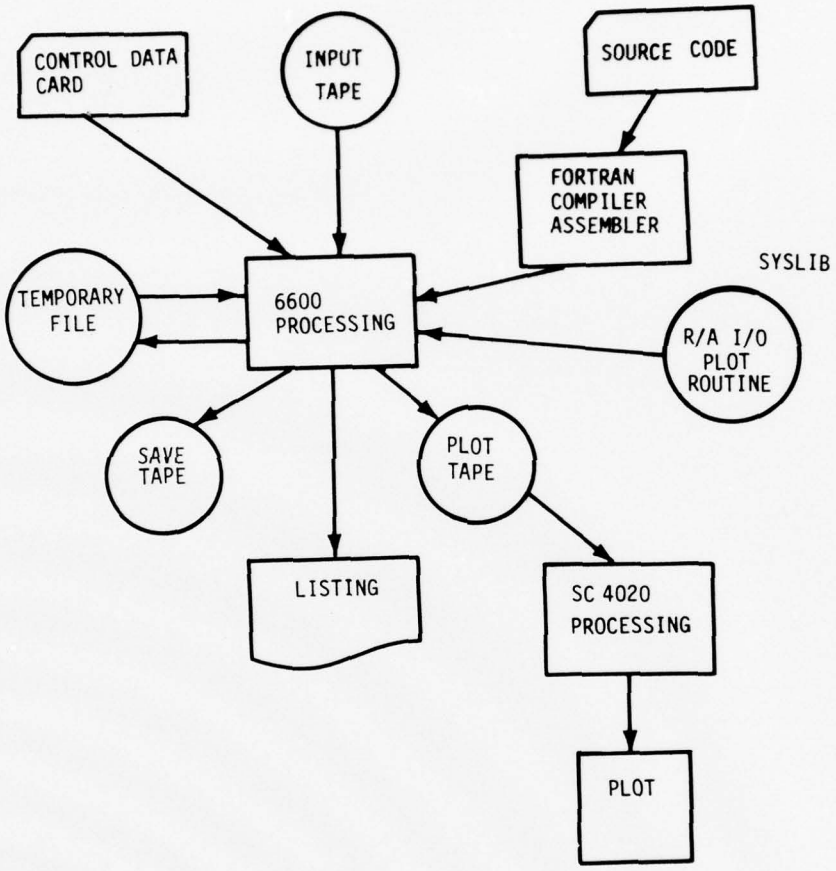


NOTE: SAVE TAPE, TEMPORARY FILE, AND RANDOM ACCESS I/O ROUTINES ARE NOT USED FOR THE DELAY-SPECTRA TIME HISTORY.

*Figure 2-4. Multipath Data Processing Flow*

# 3. MULTIPATH ALGORITHM EXECUTION SEQUENCE

Figures 3-1 and 3-2 depict the algorithm execution sequence for processing the multipath channel data and the receiver system parameters. Detailed descriptions of the indicated block operations are given in section 4. Processing of the airborne system parameters tape is carried out independently from this sequence and is discussed in section 4.23.

## 3.1 ALGORITHM EXECUTION SEQUENCE

The operations described in figures 3-1 and 3-2 are loosely categorized as A/D reformatting, quick-look, delay-spectra time history, extraction of delay-Doppler-related channel parameters, and tap statistical analyses. Common to the four latter categories is in the processing of the SACP receiver and analog tape status parameters. The tape parameters (parity error count, frame lock loss count, data track being processed, polarization of data track) are obtained from the PDP 11/45 software interaction with the TFE equipment, whereas the SACP receiver parameters are embedded in the data frame that contains the correlator outputs.

Through use of the dual-system capabilities of the PDP 11/45 ground station, the algorithm execution sequencing described below is followed:

a. The dual system is used to simultaneously quick-look process the H and V data tracks; this includes generation of tape D3.
b. From the quick-look outputs, periods of data interest and receiver configuration stationarity are identified.
c. The dual system is used to simultaneously reformat the H and V data; each reformatted data stream is recorded on its own separate digital tape, D1.
d. Tape D3 is batch processed for the three-dimensional delay-spectra time history.
e. The reformatted tapes (D1) are batch processed for the detailed data analysis.

Although this execution sequence is considered to be optimum for processing the simultaneously received horizontal and vertical polarization data, it does not have to be strictly followed. For example, one may simultaneously quick-look process and reformat a single polarization data stream or reformat one track while quick-look processing the other. Similarly, any of the processing flow segments could be eliminated without affecting the other operations.

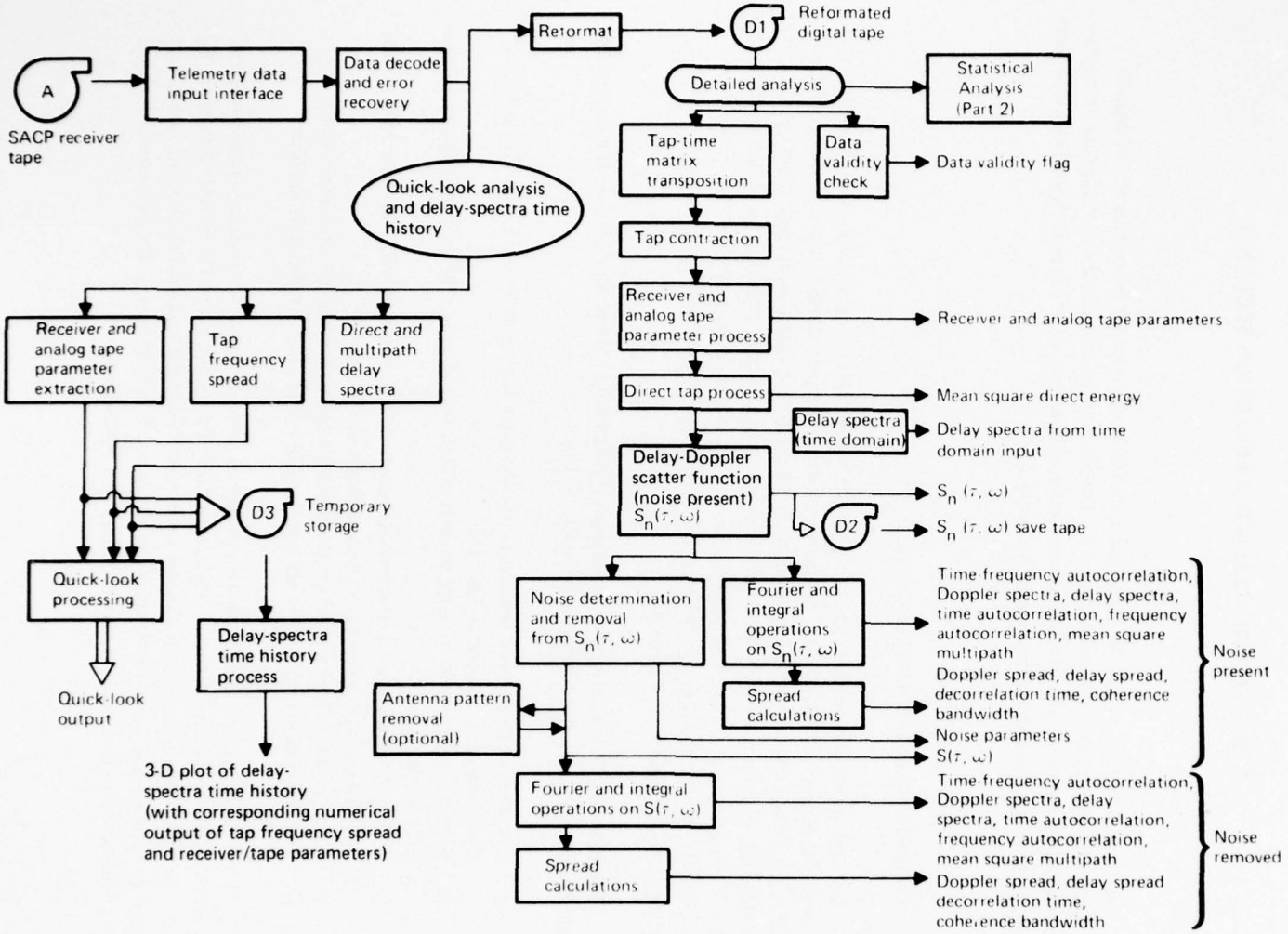


*Figure 3-1. Multipath Algorithm Execution Sequence, Part 1*

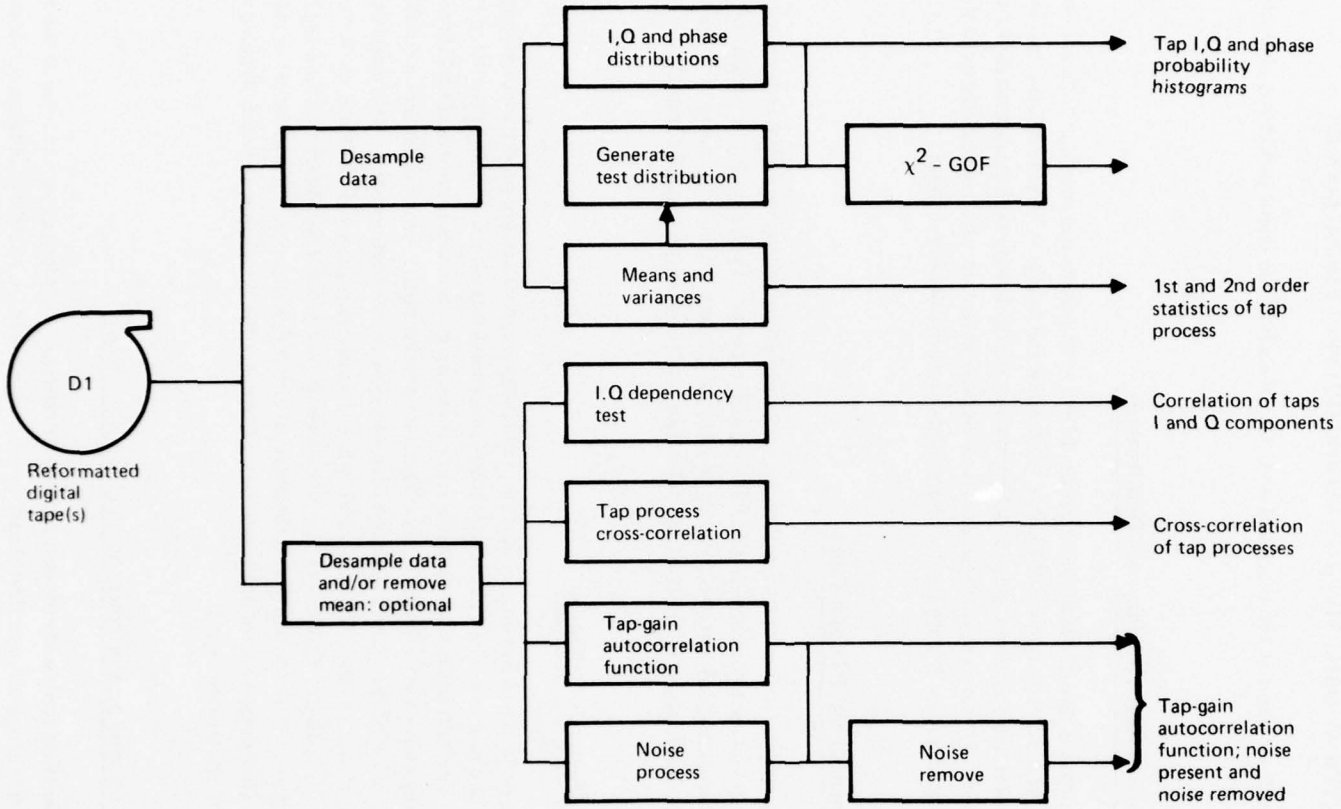


*Figure 3-2. Multipath Algorithm Execution Sequence, Part 2*

## 3.2 ANALYTICAL OBJECTIVES OF ALGORITHM PROCESSING BLOCKS

A brief description of the analytical objective of each of the major processing algorithms is given below.

### 3.2.1 Quick-Look Real-Time Playback Data Analysis

This output is directly available from the PDP 11/45 system and provides both oscilloscope display plots and hard-copy numerical output. From this the operator may investigate receiver parameter configuration, tap frequency spread, delay power spectral density, and analog magnetic tape status descriptors. Primary use of these data is to identify time intervals that provide both steady-state receiver conditions and multipath scatter phenomena of particular importance.

### 3.2.2 Reformatted SACP Digital Tapes

Source analog tapes are processed to provide computer-compatible digital tapes that represent the complex tap voltage time-domain data of the SACP receiver. Typically, those periods of data identified by the quick-look analysis as being of particular interest were reformatted for the CONUS tests. For the oceanic tests, the bulk of the valid data was converted to digital format.

### 3.2.3 Delay-Spectra Time History

For all periods of valid data collection, the scatter channel's delay power spectral density (psd) is determined in a time-running nonoverlapping manner with psd estimates being calculated over a 2-sec interval. The outputs that occur once every 2 sec are given in both numerical and three-dimensional plotted formats. Respectively, these data provide both a quantitative and a comprehensive overview description of the channel's time-variant delay-spectra characteristics. This analysis is of particular importance for the CONUS scatter, where terrain roughness and electrical characteristics vary rapidly with distance. One use of the 3-D overview plot is for isolation of time and tap bank intervals that possess data for which it is desirable to either (1) reference the numerical output to obtain quantitative delay-spectra information or (2) subject the data input string to detailed delay-Doppler psd computer processing.

### 3.2.4 Delay-Doppler Scatter Power Spectral Density, $S(\tau,\omega)$

This function represents the distribution of diffusely scattered power arriving at the receiver with Doppler frequency $\omega$ and time delay $\tau$. For the zero-mean complex Gaussian random-scatter process, $S(\tau,\omega)$ completely characterizes the channel statistics. For each test condition, including

probes conducted over the multipath and operational antenna systems, at least one detailed $S(\tau,\omega)$ function is generated. The output is given in numerical and three-dimensional plotted form. Furthermore, since this parameter is of such fundamental importance for the interpretation, modeling, and application of the scatter channel phenomena, $S(\tau,\omega)$ is also preserved on magnetic tape. This provides a convenient and compact basis from which future analysis may be conducted without going through the time-consuming and expensive computer processing steps required to obtain the delay-Doppler psd from the reformatted SACP digital tapes.

### 3.2.5 Integral and Fourier Operations on $S(\tau,\omega)$

The scatter function $S(\tau,\omega)$ contains all the ingredients needed for derivation of equivalent and lower order channel parameters. Software modules are contained within the detailed analysis routines to derive the following parameters:

a. Joint time-frequency autocorrelation function,

$$R(\xi,\Omega) = \iint S(\tau,\omega)\, e^{i(\Omega\tau+\xi\omega)}\, d\tau d\omega \tag{3-1}$$

b. Time autocorrelation function,

$$R(\xi,0) = \iint S(\tau,\omega)\, d\tau\, e^{i\xi\omega}\, d\omega \tag{3-2}$$

c. Frequency autocorrelation function,

$$R(0,\Omega) = \iint S(\tau,\omega)\, d\omega\, e^{i\Omega\tau}\, d\tau \tag{3-3}$$

d. Doppler spectrum,

$$D(\omega) = \int S(\tau,\omega)\, d\tau \tag{3-4}$$

e. Delay spectrum,

$$Q(\tau) = \int S(\tau,\omega)\, d\omega \tag{3-5}$$

f. Total rms scattered energy,

$$\langle I_T^2 \rangle = \iint S(\tau,\omega)\, d\tau d\omega\,. \tag{3-6}$$

The time-frequency autocorrelation function and its respective axial cuts measure the degree of correlation between two signals delayed in time by $\xi$ and offset in frequency by $\Omega$. These functions are complex and therefore are formatted in terms of their amplitudes and phases in the software output.

### 3.2.6 Channel Spread Parameters

From the $D(\omega)$, $Q(\tau)$, $R(\xi,0)$, and $R(0,\Omega)$ distributions, lower echelon first-order channel parameters such as the Doppler spread, delay spread, decorrelation time, and coherence bandwidth of the scatter channel are easily estimated.

### 3.2.7 Noise Determination and Removal (NDandR)

The outputs of the SACP multipath correlator contain desired signal data, spurious signal terms, low-pass additive thermal noise, and receiver arithmetic noise. Under normal SACP operating conditions, the NDandR algorithm statistically eliminates these noise terms from the data on a tap-by-tap basis. The noise-free estimate of the delay-Doppler function may then be normalized for the low-pass filter attenuation and subjected to the integral, Fourier transform, and spread determination steps as previously outlined.

### 3.2.8 Antenna Pattern Effects Removal

Design criteria for the forward multipath antenna were established to provide a radiation pattern with nearly uniform coverage over the effective scatter region. However, for certain flight direction headings, the fidelity of the channel measurement may be enhanced by applying the antenna effects removal algorithm. This routine operates on the noise-free $S(\tau,\omega)$ estimate to provide an equivalent scatter function that would be measured with a uniform gain antenna. The multipath process performs a 2-into-1 mapping operation wherein two surface returns are mapped into one delay-Doppler point. The application of this algorithm is thus restricted to the in-plane flight goemetry cases where the cosymmetry of the delay contours, Doppler contours, and scatter cross-section (isotropic surface) is exploited.

### 3.2.9 Tap Amplitude and Phase Distributions

Determination of the fundamental statistical properties of the scatter process requires that the received signal's time-domain fluctuations be characterized. The probability distribution and the associated means and variances of these fluctuations are derived for each tap's I component, Q component, and phase angle. The processes' composite signal, which is constructed by vectorially summing the delay tap outputs, is also subjected to these operations. The experimental distributions are compared with prediction for the complex Gaussian channel. These correlations are implemented via the $\chi^2$ goodness-of-fit test.

### 3.2.10 Tap Process Bank Cross-Correlations

The degree of coherency between any two taps in a particular tap bank or in cross-polarized banks (i.e., one is horizontal, the other vertical) is measured through use of the normalized cross-correlation function:

$$R_{X,Y}(\xi) = \frac{\langle X(t)Y^*(t-\xi)\rangle}{\sqrt{\langle X(t)X^*(t)\rangle\langle Y(t)Y^*(t)\rangle}} \quad . \tag{3-7}$$

where:

X = complex tap process in either bank
Y = complex tap process in either bank
$\xi$ = time-lag variable.

### 3.2.11 Tap I and Q Dependency

For random rough surface scattering where the electromagnetic wave undergoes deep phase modulation at the multipath interface, we expect that the I and Q components of the received signals are statistically independent. This condition is explored by determing the zero-lag normalized correlation coefficient between a tap's orthogonal components, i.e.:

$$R_{I,Q}(0) = \frac{\langle IQ\rangle}{\left[\langle I^2\rangle\langle Q^2\rangle\right]^{1/2}} \quad . \tag{3-8}$$

### 3.2.12 Tap-Gain Autocorrelation Function

An estimate[1] of the channel's tap-gain autocorrelation function, $U(\tau,\xi)$, is derived through application of the following operation:

$$U(\tau,\xi) = \langle X_\tau(t)X_\tau^*(t-\xi)\rangle \quad . \tag{3-9}$$

where:

$\tau$ = delay tap value
$X_\tau$ = complex process of tap $\tau$ in bank X (i.e., horizontal or vertical)
$\xi$ = time-lag variable.

This function measures the autocorrelation function of the multipath process on a tap-by-tap basis and is available (magnitude) as a three-dimensional output plot from the software package.

---

[1] *An alternate derivation of this function may be obtained by inverse Fourier transformation of the* $S(\tau,\omega)$ function with respect to the $\omega$ variable.

Two program options exist in this algorithm: (1) cross-polarized estimate of $U(\tau,\xi)$ and (2) noise estimate removal.

The cross-polarized estimate of $U(\tau,\xi)$ is calculated by replacing the conjugated variable in equation (3-9) with the appropriate $Y_\tau$ tap of the bank containing the orthogonal polarized return.

Assuming the independence of multipath and noise, we arrive at a noise-free estimate of the tap-gain autocorrelation function $U_{nr}(\tau,\xi)$:

$$U_{nr}(\tau,\xi) = \langle X_\tau(t)X_\tau^*(t-\xi)\rangle - \frac{1}{N}\sum_{i=1}^{N} \langle X_i(\tau)X_i^*(\tau-\xi)\rangle \quad , \tag{3-10}$$

where $X_i$ is the complex output of a multipath-free tap (usually taken from a region of the bank preceding the specular point return).

### 3.2.13 System Calibration Parameter Data

Magnetically recorded data pertaining to receiver system operation (i.e., direct and multipath channel gains, etc.), transmitter power amplifier outputs, and aircraft flight parameter descriptors are computer reduced to aid in the normalization of the scatter channel power returns. These data also serve as a data collection integrity measure and are used primarily to augment the logged flight test data.

## 3.3 MULTIPATH DATA BASE COMPONENTS

The data base delivered to DOT/TSC relative to the multipath channel characterization test consists of the following items:

a. Library of analog SACP receiver source data tapes. These data were recorded at the NAS ground station on 9600- or 7200-ft reels of 1/2-in. magnetic instrumentation tape using Ampex FR-1900 and/or FR-2000 recorders. The recorded data corresponds to the unprocessed data obtained from the outputs of the SACP receiver during test.

b. Library of reformatted digital data tapes (D1). These 1600-bpi, nine-track digital tapes contain the SACP receiver output data in computer-compatible digital format. The D1 tapes are generated by the Boeing PDP 11/45 facility and have a format as described in section 4.22.1.

c. Library of delay-spectra time history tapes (D3). These 1600-bpi, nine-track digital tapes contain the delay-spectra time history arrays computed by the dual PDP 11/45 computer system. In most cases, the files containing these data are physically located on the same tape as the corresponding reformatted digital data described as D1 (above). Tape format is described in section 4.22.3.

d. Library of $S_n(\tau,\omega)$ save tapes (D2). Tape D2 contains the computed noise-present estimate of the channel's delay-Doppler scatter function. The tape format is described in section 4.22.2.

e. Library of airborne system parameters source tapes. These 800-bpi, seven-track computer-compatible digital tapes were recorded onboard the KC-135 aircraft terminal using a Kennedy 8707 recorder. The tapes contain power level calibration data and other information relevant to the test parameters during test. Information content and tape format are described in section 4.23.

f. Computer programs (card decks) and listings corresponding to the programs used for detailed analysis of the reformatted multipath data (D1) tapes. Description of algorithms are given in sections 3 and 4.

g. Computer programs (card decks) and listings corresponding to the physical optics vector scatter model described in section 5.

h. Punch paper tapes providing radiation distribution plots of antenna range data for the front multipath antenna for various polarizations and pointing angles.

The following additional data base resulted from a subcontract to CNR, Inc.

a. Reformatted 800-bpi, seven-track multipath computer-compatible digital data tapes generated from selected Boeing PDP 11/45, 1600-bpi, nine-track D1 tapes.

b. Transposed multipath digital data tapes listed in volume V, section 5.4.6.

c. Sea-state buoy 800-bpi, seven-track digital data tapes containing measured buoy variables stripped from the analog buoy data source tapes. (Tapes correspond to data acquired on January 29 and 30, 1975, plus March 25 through April 2, 1975.) These PCM data stripping operations employed a capability existing at DOT/TSC.

d. Backup program tape containing the programs used for sea-state buoy data reduction, H-V correlation and statistical analysis, and transpose and scattering function DRandA. These programs are discussed in sections 4.21 and appendix B. Programs can be run on the DOT/TSC PDP 10 in time-share or batch processing modes.

# 4. MULTIPATH ALGORITHM DESCRIPTION

This section provides a more detailed description of the multipath algorithms presented in figures 3-1 and 3-2.

## 4.1 TELEMETRY DATA INPUT

Data processing test conditions on the PDP 11/45 are defined by (1) program type and option, (2) data track or tracks to be analyzed, and (3) the start and stop time of the interval to be processed. Telemetry data input to the PDP 11/45 is preceded by transferring the EMR telemetry front end control to the tape search unit, which causes the analog tape's time code track to be searched for the specified interval start time. When the tape search unit enters the interval, the digitized PCM data is routed to the PDP 11/45 memory in blocks of four frames (each frame word is input as a 16-bit entry; the most significant seven bits are always 0 while the least significant 9 bits contain the data).

The input data is double buffered. When the input of a block of data is completed, an interrupt occurs and causes two events: (1) new data starts entering the second buffer and (2) the process software begins to operate on the buffer that has just been filled. If a TFE frame lock loss event occurs, the processor is notified by another interrupt that enables software to maintain status logic. For both the reformatting and quick-look analysis/delay-spectra time history program operations, data input is typically run at a rate equal to roughly 80,000 words/sec. At a sampling rate of 300 frames/sec, this corresponds to a 2-to-1 processing slowdown factor.

## 4.2 DATA DECODING, ERROR RECOVERY, AND REFORMATTING

To return the data to the form as output from the SACP receiver, it must be parity error checked, stripped of its parity bit, and odd-bit complemented. These three steps are accomplished in one operation, which consists of using the data as an index to a table of reformatted data values and parity error flags. Parity errors are corrected by data replacement from the corresponding data in the preceding frame. An accumulative count of detected parity errors is maintained.

When the reformatted data is written on magnetic tape, it is double-buffer stored in vectors of length equal to 12 frames. These output buffers also contain data pertaining to analog magnetic tape track, frame lock loss count, parity error count and directory, and polarization. The digital tape format is described in section 4.22.

## 4.3 QUICK-LOOK DATA ANALYSIS

Prior to quick-look analysis of the SACP data tapes, we must select the time interval to be processed and establish the subinterval time length over which sample space construction is performed. Typically, the processing interval consists of the entire flight test condition time segment over which log-look records indicate valid data was obtained. We also typically select a subinterval length of 2 sec because this appears to give adequate resolution for the CONUS data runs, which encounter surfaces whose electrical and physical characteristics change rapidly.

For each subinterval sample space, the quick-look process algorithm performs the following operations: (1) extracts the receiver and analog tape status parameters associated with the first and last frame of the subinterval, (2) estimates the multipath tap's frequency spread, (3) estimates the direct and multipath tap's delay spectra, and (4) writes the above as one record on digital tape. The quick-look analysis results are not intended to provide definitive quantitative channel parameter results. Their primary use is to direct attention toward test intervals that warrant further detailed analysis.

An algorithmic flow diagram for the above operations is shown in figure 4-1. By intercepting the receiver and analog tape status parameters at the beginning and end of each subinterval, a measure of receiver parameter stationarity is provided. These data occupy the first 24 bytes of each data set (a data set consists of the SACP data frame preceded by the analog tape system parameters), as described in section 4.22.

The indirect tap bank's frequency-spread estimate is derived by counting the number of times a particular tap's I component crosses the zero voltage level. This is implemented in the PDP 11/45 by maintaining a counter array and a previous sign array in memory. Each element of the two arrays corresponds to a particular SACP tap output. The previous sign array contains sign information (positive or negative) for the last frame processed. This information is compared with the sign of the current array element; if they differ, the corresponding element of the counter array is incremented and the sign of the element in the previous sign array is complemented. These operations take place on each frame that is input to the quick-look program. At the end of a subinterval sample space, the counter array is written on magnetic tape without normalization and is subsequently zeroed for reuse.

For the case of a signal possessing complex Gaussian amplitude statistics, the zero-crossing technique yields a good approximation to its frequency spread as defined in reference 4-1. Because the L-band multipath signal is known to have Rayleigh amplitude statistics, the frequency-spread data is used as a measure of each tap's Doppler spread. This is valid for the taps that possess high signal-to-noise ratio but is invalid for poor signal-to-noise ratios since the zero-crossing counter is activated

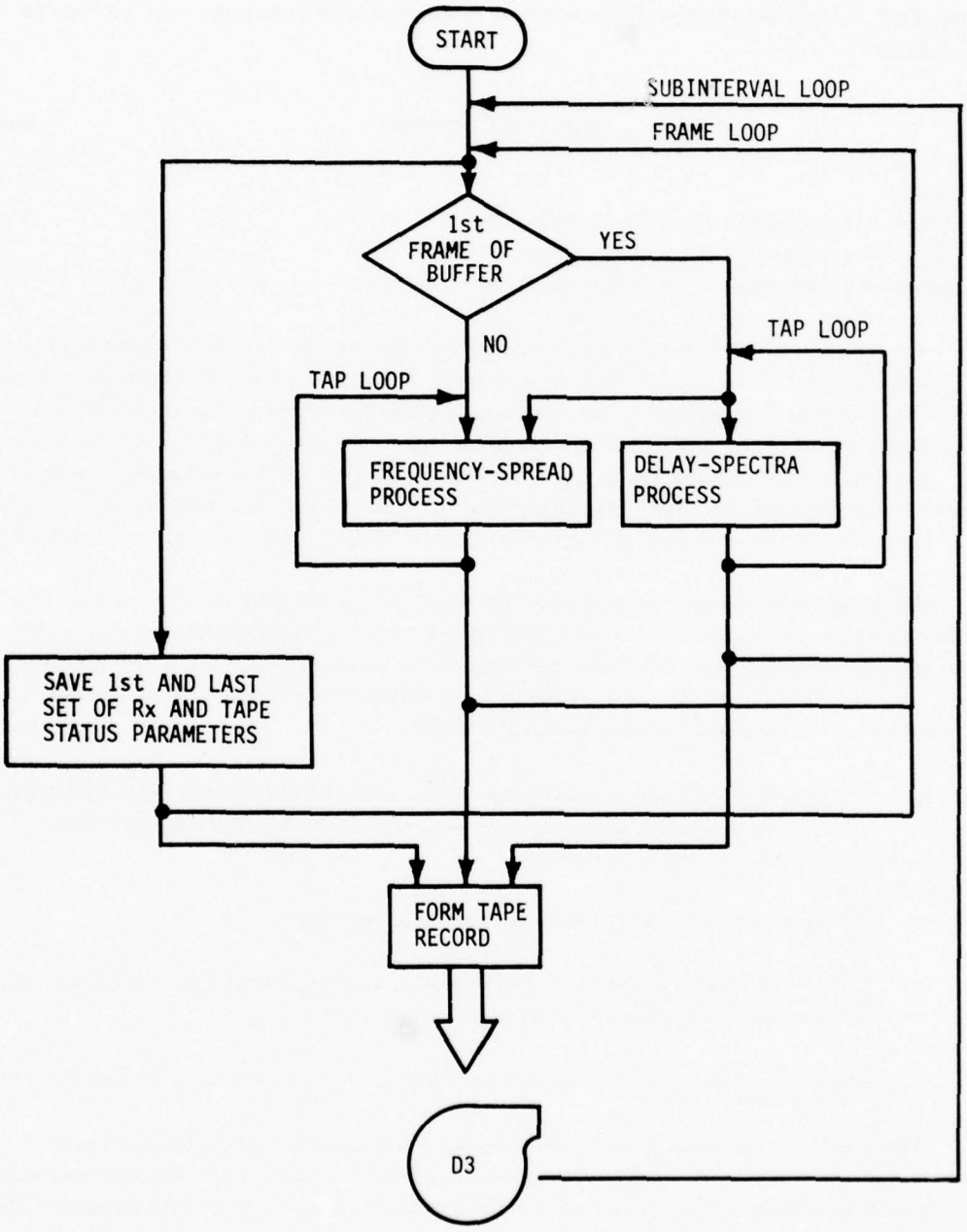


*Figure 4-1. Quick-Look Data Processing*

primarily by the noise fluctuation. For example, the I component of a particular delay tap may be presented as

$$DI(t) = n_I(t) + mp_I(t) \ , \qquad (4\text{-}1)$$

where:

$DI(t)$ = I component of a particular delay tap
$n_I(t)$ = I component of the noise content of the tap
$mp_I(t)$ = I component of the multipath content of the tap .

For the majority of delay taps, $n_I(t)$ is predominantly thermal and would be expected to possess the complex Gaussian statistics and to have a zero-crossing rate that is roughly equivalent to the bandwidth of the low-pass filter operation. The combination of the two processes thus always gives an upper limit measure to the tap's Doppler spread. In the region of the postspecular point return, the algorithm output yields a relatively good estimate of the true Doppler spread. For prespecular point capture and capture far delayed from the specular return, the frequency-spread measure approaches the noise bandwidth. These characteristics are illustrated in the output data described in section 4.24.

The quick-look delay-spectra calculations are based on a sample space constructed from the first frame of each buffer input (i.e., one out of every four frames). This was implemented to speed up the algorithm operation and at the same time improve the independency of the sample space elements (typically the multipath data is oversampled). For each tap, including both the direct and multipath banks, the process algorithm proceeds as follows:

a. The squares of the I and Q components for the particular tap are determined by using the value as an index into a table of squares. This operation is considerably faster than multiplying the number by itself.

b. The squares of the I and Q components are added together.

c. The $I^2 + Q^2$ sum is accumulated from frame to frame by adding it to a memory location corresponding to that tap. A 32-bit result is maintained.

d. At the end of a subinterval condition, the delay-spectra array is written on magnetic tape.

Like the frequency-spread estimate, the delay-spectra measure is contaminated by receiver noise. In this case, however, the effect is not nearly so significant. The receiver noise may be estimated by examining the process output for taps prior to the specular point return to derive a mean estimate of the noise content of a multipath-free tap. This value can be subtracted from the entire induced tap bank. It should be noted, however, that on occasion certain taps are possessed by an anomalous noise content (e.g., taps in the vicinity of 1, 17, 26, 81, and 111 have been observed to fall into this category).

## 4.4 DELAY-SPECTRA TIME HISTORY

The delay-spectra time history algorithm operates on the data records created during the quick-look analysis and preserved on the D3 storage tape. A quick-look analysis data record is generated once every $\Delta S$ sec and contains information on (1) the receiver and analog tape status parameters at the beginning and end of the subinterval, (2) unnormalized frequency-spread estimates for the indirect tap bank, and (3) unnormalized delay-spectra estimates for both the direct and indirect tap banks.

Figure 4-2 illustrates the processing steps associated with this algorithm. Analysis of the receiver and analog tape status parameters is covered separately in section 4.10. The frequency-spread and delay-spectra estimates are normalized as follows:

$$FS(n\tau,t_i) = \left(\frac{1}{\Delta S}\right) FS_i(n\tau) \quad , \tag{4-2}$$

$$Q(n\tau,t_i) = (4/M) Q_i(n\tau) \quad , \tag{4-3}$$

where:

$FS(n\tau,t_i)$ = normalized frequency-spread estimate of the $n^{th}$ tap for time interval $t_i$
$FS_i(n\tau)$ = unnormalized frequency-spread estimate of the $n^{th}$ tap as contained on the $i^{th}$ record
$Q(n\tau,t_i)$ = normalized mean square energy of the $n^{th}$ tap for time interval $t_i$
$Q_i(n\tau)$ = unnormalized mean square energy of the $n^{th}$ tap as contained on the $i^{th}$ record
$n$ = tap number
$\tau$ = chip width of PN sequence
$t_i$ = $t_{start} + i\Delta S$
$\Delta S$ = time length of subinterval (typically 2 sec)
$t_{start}$ = start time of the first record processed
$M$ = SR x $\Delta S$
SR = frame rate ($sec^{-1}$).

The $FS(n\tau,t_i)$ array is presented numerically for all 112 taps. Similarly, the numerical array for $Q(n\tau,t_i)$ is given for all six direct taps and all 112 indirect taps. Any contiguous set of taps including both direct and indirect may be selected for the three-dimensional plotted delay-spectra time history array. This plotted output format gives a concise visual representation of the channel's time-variant delay spectra.

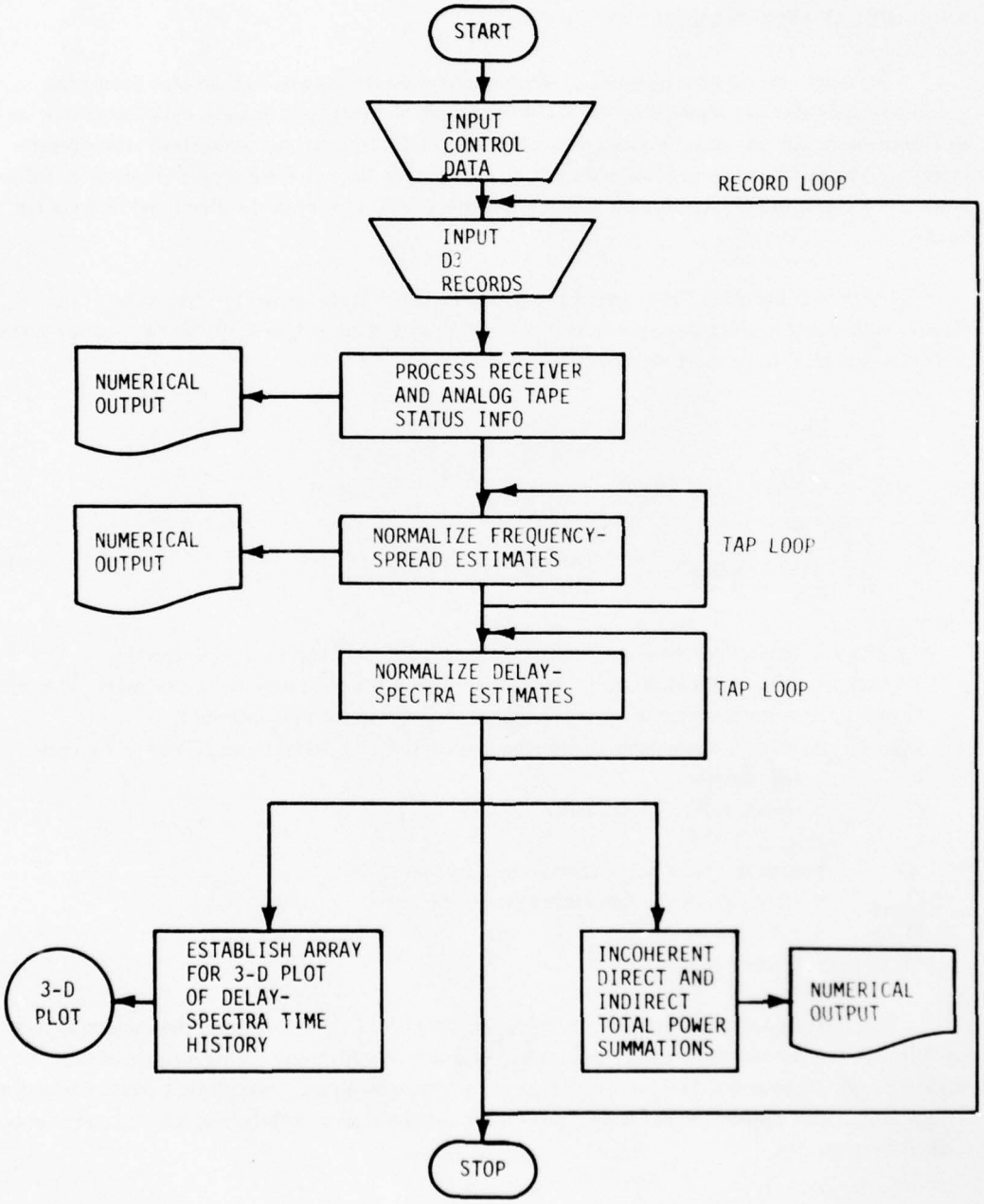


*Figure 4-2. Delay-Spectra Time History Algorithm*

Incoherent power summations of the direct and multipath total energies are also contained in this algorithm and are calculated as follows:

$$PD(t_i) = 4/M \sum_{n_d=1}^{6} Q_i(n_d\tau) , \tag{4-4}$$

$$PI(t_i) = 4/M \sum_{n_I=1}^{112} Q_i(n_I\tau) , \tag{4-5}$$

where:

$PD(t_i)$ = incoherent power summation estimate of the direct tap energy

$PI(t_i)$ = incoherent power summation estimate of the indirect tap energy.

Note that this routine operates on the noise-contaminated frequency-spread and delay-spectra estimates. Thus, the comments in section 4.3 relative to the effects of receiver noise also apply to this algorithm.

## 4.5 TAP-TIME MATRIX TRANSPOSITION

The tap-time matrix transposition operation consists of reordering the input data sequence. Although this operation does not affect the data analysis computations, it is mentioned here for two reasons: (1) to clarify the presentation of the algorithm implementation and (2) to indicate the level of coding and computer time that it requires. For the software discussed in this document, the output of the matrix transposition is used primarily to compute the delay-Doppler scatter function. However, it was implemented as an independent computer program; thus it may be readily used for additional data reduction routines such as tap-amplitude statistics, etc.

The transposition operation consists of reordering the data from a time sequence to a tap sequence. The input data may be viewed as a two-dimensional matrix. A column of the matrix represents the time sequence of one component of one tap. A row of the matrix corresponds to a simultaneous sample of the real or imaginary parts of a particular tap in the bank. The data is input to the computer on a row-by-row basis (i.e., time-ordered). However, for efficient data analysis, the matrix must be accessed by column or tap. The matrix size presents a problem; e.g., for a 512-point complex FFT over the total direct and indirect tap banks, we must work with a data array on the order of 120,000 values of the SACP receiver's eight-bit words.

Memory and disk space with random access are used to perform the transposition operation. For practical reasons, two other operations are performed at the same time the input matrix is being transposed: (1) data validity checks and (2) tap reordering (from the recorded interleaved order to a monotonically increasing order).

The program high-level algorithm (including the coincident operations) is given in figure 4-3. Program input consists of reformatted data tape, number of frames per segment, number of segment tape selected, and 20 characters for case identification. Program outputs consist of the file with tap-ordered data and a history and summary of validity check messages.

The transposition operation, shown in figure 4-4, consists of the following basic steps:

a. Data is input to the CDC 6600 core memory frame by frame.

b. For each frame, the tap data words (I, Q point pairs) are repositioned in core memory to represent a subset of the overall transposed matrix as diagrammed in figure 4-5. In this operation the number of frames processed is sized to occupy a core space of 50K octal.

c. When the allotted core space is filled or when the last frame of a data interval segment has been processed, the transposed subsegment is transferred from core to the random access disk file. Each tap segment is assigned a unique record number.

d. After completing the frame loop, the random access file is accessed and the tap records are rearranged to yield a sequential file representation of the tap-time matrix.

## 4.6 DATA VALIDITY CHECK

The data validity check algorithm provides information pertaining to time (merged IRIG-A) and subframe index counter[1] between adjacent frames that are input to the detailed data analysis routine. For proper operation one expects that: (1) between adjacent frames the time interval will be constant and equal to the reciprocal of the sampling rate and (2) the subframe counter advances by one count. These criteria are checked for each frame of data input to the program. If an error occurs, flags are set without interrupting the program execution. At the end of a data segment input, an error summary is provided to delineate:

Total number of subframe error counts
Total number of time sequence errors
Mean and standard deviation of time intervals between frames.

[1] The SACP data frame contains a subframe counter that runs from 0 to 5 in a continuous cyclic manner by advancing one count per frame.

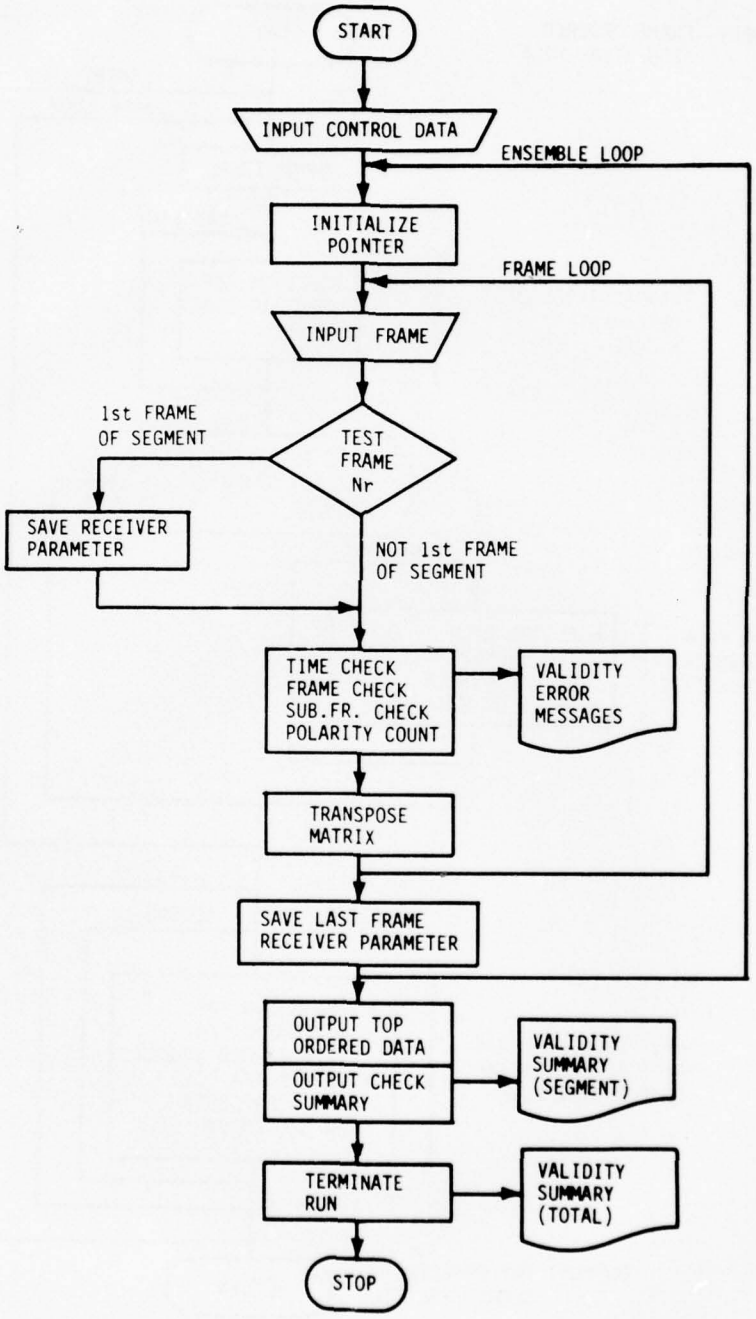


*Figure 4-3. Multipath Data Validity Check and Transposition Algorithm*

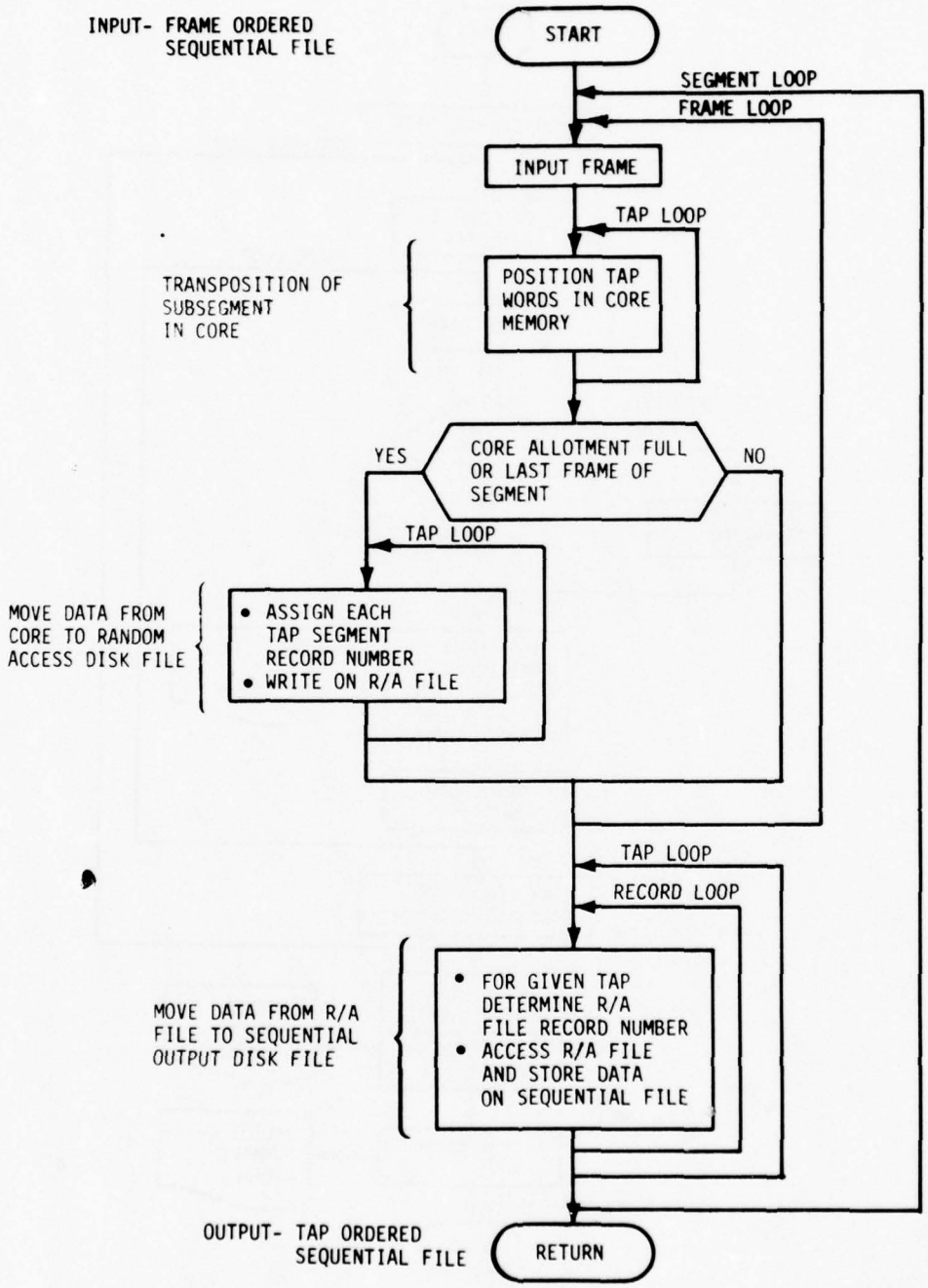


*Figure 4-4. Simplified Transpose Flow Chart*

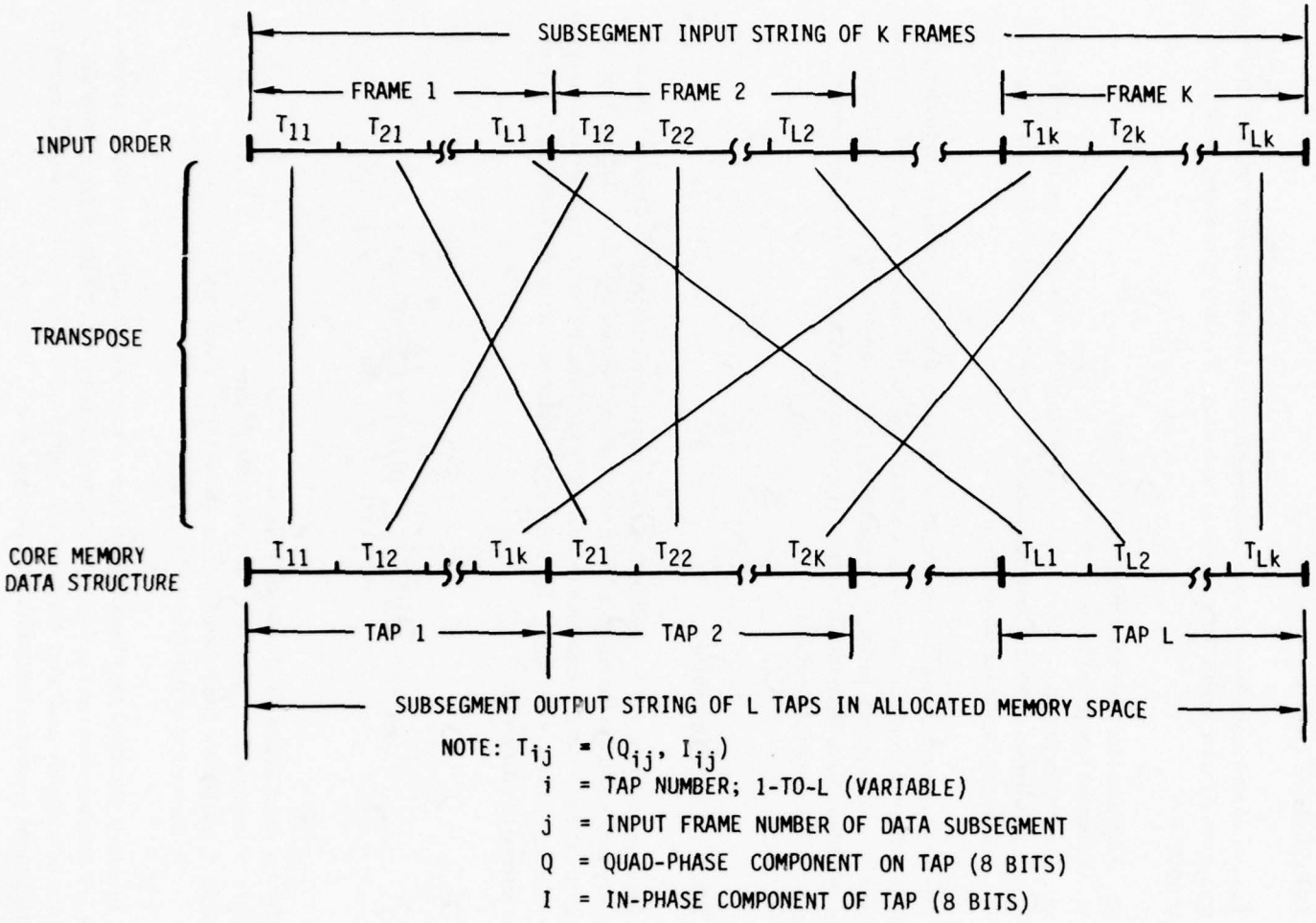


*Figure 4-5. Subinterval Transposition Structure*

## 4.7 TAP CONTRACTION

Tap contraction is a software option, designed primarily to save computer time, which is available to reduce the effective size of the indirect tap bank array. This may take on any or all of the following operations:

a. Eliminate taps from the beginning of the bank.
b. Eliminate taps from the end of the bank.
c. Coherently sum any number of adjacent taps to yield a new array that has a decreased tap resolution width (i.e., one may choose to sum over 7 taps to procure an array of 16 taps as opposed to the original set of 112).

The first two operations are implemented in the matrix transposition algorithm to eliminate taps that are known to contain no significant amount of multipath signal. The coherent tap summation option, if implemented, is performed immediately prior to inputting the data to the scatter function algorithm. Since the resultant decrease in resolution is undesirable, this latter option, although available, is normally not used.

## 4.8 DIRECT TAP PROCESSING

In the interpretation of the multipath signal strength data, it is useful to reference the scattered energy with respect to the energy arriving over the direct line-of-sight path. The total energy contained in the direct signal is estimated by coherently summing the direct tap complex voltage outputs to form a composite direct signal. The mean square value of this signal is then determined over the time interval of interest, i.e.,

$$\langle |D|^2 \rangle = 1/N \sum_{i=1}^{N} \left[ \left( \sum_{j=1}^{6} DI_j(i) \right)^2 + \left( \sum_{j=1}^{6} DQ_j(i) \right)^2 \right], \qquad (4\text{-}6)$$

where:

$\langle |D|^2 \rangle$ = mean square direct composite signal
$DI_j(i)$ = in-phase component of $i^{th}$ sample of the $j^{th}$ direct tap
$DQ_j(i)$ = quad-phase component of $i^{th}$ sample of the $j^{th}$ direct tap
N = the number of points in the sample space .

In general, the direct tap processing algorithm acts on the same data space that is processed for the $S(\tau,\omega)$ determination (see fig. 4-6). The effects of receiver noise on the $\langle |D|^2 \rangle$ estimates are assumed to be negligibly small since the direct link typically operates at a $C/N_o$ density in excess of 60 dB-Hz and the processing bandwidth is on the order of 37.5 Hz.

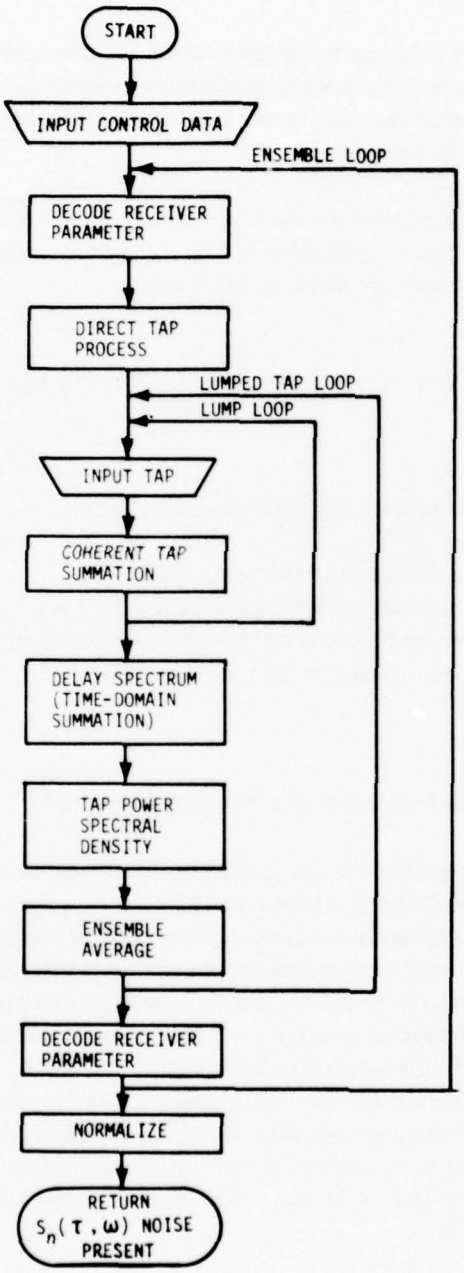


*Figure 4-6. Delay-Doppler Scatter Function Algorithm*

## 4.9 DELAY SPECTRA (TIME–DOMAIN ANALYSIS)

To serve primarily as a check on the integrity of the operations used to derive $S(\tau,\omega)$ we perform a time-domain analysis on the complex tap outputs to derive an estimate of the channel's delay spectra. This estimate may then be compared with the spectra obtained by integrating $S(\tau,\omega)$ (noise not removed) over the Doppler variable.

Inputs to this routine consist of the identical complex tap voltage points utilized in the ensemble array over which $S(\tau,\omega)$ is calculated (see fig. 4-6 for processing sequence). These points are operated on as follows to derive the delay-spectra estimate:

$$Q_{TDA}(n\tau) = 1/N \sum_{i=1}^{N} \left( I^2{}_{n\tau}(i) + Q^2{}_{n\tau}(i) \right) , \qquad (4\text{-}7)$$

where:

| | | |
|---|---|---|
| $Q_{TDA}(n\tau)$ | = | mean square energy arriving at receiver with delay $n\tau$ |
| n | = | tap number |
| $\tau$ | = | chip width of transmitted PN sequence |
| $I_{n\tau}(i)$ | = | in-phase component of $n^{th}$ tap's $i^{th}$ ensemble array value |
| $Q_{n\tau}(i)$ | = | quad-phase component of $n^{th}$ tap's $i^{th}$ ensemble array value |
| N | = | total number of points in the array ensemble . |

## 4.10 RECEIVER AND ANALOG TAPE STATUS PARAMETERS

The receiver and analog tape status reduction algorithm operates on the first 192 bits of a data record contained either on the D1 or D2 digital tape. With the exception of one minor mathematical operation, the algorithm process consists of decoding, labeling, and printing the status parameter bits. The mathematical operation entails determining the ratio of the SACP's direct to indirect receiver tap bank gains. Prior to processing, the bit pattern has the format described in section 4.22. Decoding of the frame counter, lock loss frequency counter, and parity error counter is straightforward and consists of converting the 16-bit binary words into their decimal equivalent. The merged time code words are converted from this BCD format into the hours, minutes, seconds, and decimal fractions of seconds distribution. Bytes 7 and 8 contain data track and polarization status; the polarization byte is not operated on whereas the data track byte is converted to its decimal equivalent. SACP receiver parameters occupy bytes (eight-bit) 13 through 22 plus byte 24 of the data record. They are decoded according to tables 4-1 and 4-2.

*TABLE 4-1. TAPE FORMAT FOR SACP RECEIVER AND TAPE STATUS PARAMETERS*

| Data Byte | Bit | | | | | | | |
|---|---|---|---|---|---|---|---|---|
| | 7 | 6 | 5 | 4 | 3 | 2 | 1 | Ø (LSB) |
| 14 | TSP | CR2 | CR1 | CRØ | AM1 | AMØ | SC1 | SCØ |
| 13 | FLL | TLL | OM1 | OMØ | FT3 | FT2 | FT1 | FTØ |
| 16 | DS4 | DS3 | DS2 | DS1 | DSØ | BW2 | BW1 | BWØ |
| 15 | MS4 | MS3 | MS2 | MS1 | MSØ | IFL | D3Q | --- |
| 18 | TV7 | TV6 | TV5 | TV4 | TV3 | TV2 | TV1 | TVØ |
| 17 | FV15 | FV14 | FV13 | FV12 | FV11 | FV1Ø | FV9 | FV8 |
| 20 | DE7 | DE6 | DE5 | DE4 | DE3 | DE2 | DE1 | DEØ |
| 19 | DE9 | DE8 | HR2Ø | HR1Ø | HR8 | HR4 | HR2 | HR1 |
| 22 | EL | MI4Ø | MI2Ø | MI1Ø | MI8 | MI4 | MI2 | MI1 |
| 21 | --- | SE4Ø | SE2Ø | SE1Ø | SE8 | SE4 | SE2 | SE1 |
| 24 | --- | --- | FV7 | FV6 | FV5 | FV4 | FV3 | FV2 |

Note: The entries in the bit matrix are defined in Table 4-2.

*TABLE 4-2. LEGEND FOR SACP RECEIVER AND TAPE STATUS PARAMETERS*

| | |
|---|---|
| TSP | Ø=T, 1=T/2 |
| CR | CHIP RATE Ø=1ØMHZ, 1=5, 2=2.5, 3=1.25, 4=1.Ø, 5=Ø.5 |
| AM | ANTENNA MODE Ø=MUX, 1=NORM(V), 2=NORM(H) |
| SC | SYSTEM CONFIGURATION Ø=A/C XMIT, 1=A/C RCV A, 2=A/C RCV B |
| FLL | FREQUENCY LOOP MODE, Ø=AUTO, 1=MANUAL |
| TLL | TIMING LOOP MODE, Ø=AUTO, 1=MANUAL |
| OM | OPERATING MODE, Ø=TEST, 1=SEARCH, 2=RUN |
| FT | FREQUENCY LOOP THRESHOLD, THRESHOLD=2**(N+5), IF N=1ØØ1=9, THEN THRESHOLD=2**14=16384 |
| DS | DIRECT TAP SCALE FACTOR, THIS IS A 5 BIT TWOES COMPLIMENT INTEGER WHICH CAN BE CONSIDERED TO BE AN EXPONENT FOR THE DIRECT PATH TAPS WHEN THEY ARE TREATED AS BLOCK COMPLEX NUMBER IF = -3 THEN THE SCALE FACTOR IS .125. |
| BW | MULTIPATH TAP LOW PASS FILTER BANDWIDTH, Ø=6ØØHZ, 1=3ØØHZ, 2=15ØHZ, 3=75HZ, 4=37.5HZ |
| MS | MULTIPATH TAP SCALE FACTOR, SAME INTERPERTATION AS DS |
| IFL | INTERFACE CLOCK PHASE LOCKED LOOP, Ø=NOT LOCKED, 1=LOCKED |
| D3Q | Ø=FREQ LOOP BELOW THRESHOLD, 1=ABOVE THRESHOLD LEVEL |
| TV | TIMING LOOP D-TO-A CONVERTER VOLTAGE |
| FV | FREQUENCY LOOP D-TO-A CONVERTER VOLTAGE (15BITS of DATA) |
| DE | DIRECT PATH TO MULTIPATH TAP SPACING IN CHIPS - DELTA L - (1Ø BITS) |
| EL | EARLY-LATE SWITCH, Ø=T, 1=ET |
| HR | TIME CODE, HOURS |
| MI | TIME CODE, MINUTES |
| SE | TIME CODE, SECONDS. |

## 4.11 DELAY-DOPPLER SCATTER FUNCTION

The multipath channel's delay-Doppler scatter function estimate, $S(\tau,\omega)$, is derived by calculating the discrete power spectral density of the recorded SACP time-domain tap outputs. Figures 4-6 and 4-7 illustrate the fundamental processing steps associated with this algorithm. Five operations are involved in each PSD calculation: (1) application of a data window to the complex time-domain input, (2) FFT calculation of the complex input signal's discrete PSD periodogram, (3) spectral averaging of each periodogram output, (4) ensemble averaging of a set of periodograms, and (5) normalization.

### 4.11.1 Input Data Window

A generalized raised cosine-arch function is used to weight the gated complex fast Fourier transform (FFT) data input. The purpose of this operation is primarily to reduce side lobes in the periodogram's output (i.e., it is assumed the FFT is operating on one cycle of a periodic time-domain process, and thus any difference between the values of the first and last data inputs appears as a sharp signal discontinuity; the data window overcomes this by forcing the leading and trailing values to be nearly identical). The weighting function, W(i), may be expressed as:

$$W(i) \quad \left\{ \begin{array}{ll} = (1/2)\left[1 - \cos\left((i/aN)\pi\right)\right], & i < aN \\ = 1, & aN < 1 < N(1-a) \\ = (1/2)\left[1 - \cos\left(\left(\frac{N-i}{aN}\right)\pi\right)\right], & i > N(1-a) \end{array} \right\} , \qquad (4\text{-}8)$$

where:

- i = the input array point number
- $a$ = the fraction of points over which the leading and trailing edges of the window are applied
- N = total number of points in the array .

Parameter $a$ is a program input; by setting it to 0.5 we obtain the Hanning window.

### 4.11.2 Discrete PSD

The fast Fourier transform algorithm is used to estimate the time-domain's power spectral density. The FFT is merely an efficient algorithm for performing the well-understood discrete Fourier transform. Inputs to the program are in the form of complex tap voltage point pairs. The array size

INPUT : $A(j\Delta t)$ $j^{th}$ SAMPLE OF A COMPLEX TAP OUTPUT, GIVEN EVERY $\Delta t$ SECONDS

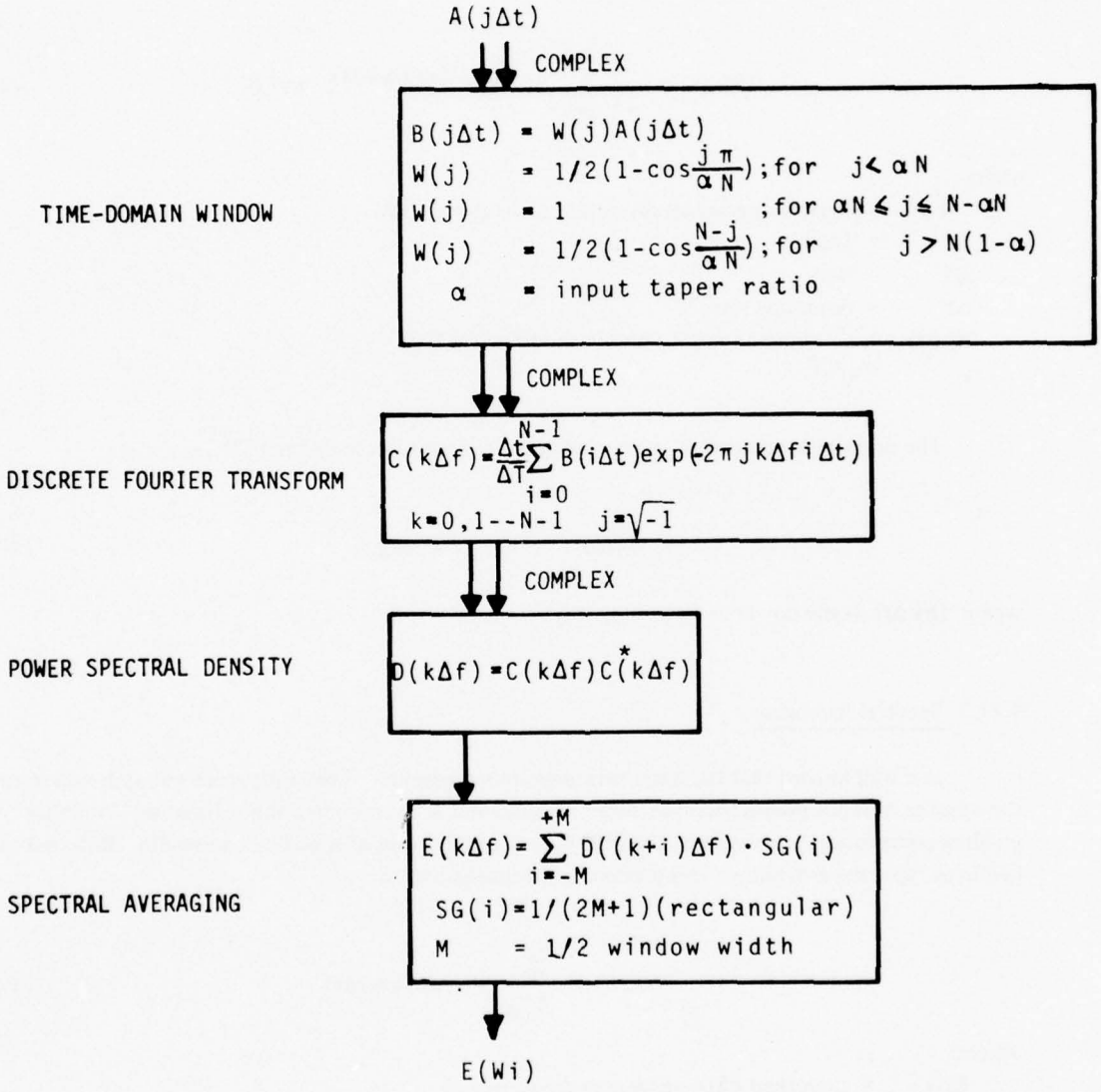


OUTPUT : UNNORMALIZED PSD FOR A COMPLEX TAP INPUT

*Figure 4-7. Tap Power Spectral Density*

may take on any reasonable value; zero-filling is used to extend the array to the nearest $2^n$ value. Outputs from the FFT periodogram occur every $1/\Delta T$ Hz ($\Delta T$ = input gate width in seconds) and are in the form of complex numbers; i.e.,

$$C(k\Delta f) = \frac{\Delta t}{\Delta T} \sum_{i=0}^{N-1} B(i\Delta t)\, e^{-2\pi j(k\Delta f i\Delta t)}; \quad k=1,N \tag{4-9}$$

where:

$C(k\Delta f)$ = complex periodogram output at frequency $k\Delta f$
$\Delta f$ = $1/\Delta T$
$\Delta T$ = $N\Delta t$
$\Delta t$ = (sampling rate)$^{-1}$
$B(i\Delta t)$ = $i^{th}$ complex input point as modified by W(i)
$j$ = $\sqrt{-1}$.

The magnitude squared of the periodogram output represents the PSD; i.e.,

$$D(k\Delta f) = C(k\Delta f)\, C^*(k\Delta f), \tag{4-10}$$

where $D(k\Delta f)$ is the power at frequency $k\Delta f$.

### 4.11.3 Spectral Averaging

It is well known that the basic periodogram's prediction uncertainty does not approach zero as the number of input points becomes large. One technique to overcome this estimation instability involves convolution processing of the PSD with a spectral gate of specified bandwidth. Referred to herein as "spectral averaging," this procedure is represented as:

$$E(k\Delta f) = \sum_{i=-M}^{M} SG(i)D((k+i)\Delta f), \tag{4-11}$$

where:

$E(f)$ = smoothed PSD estimate at frequency $f$
$SG(i)$ = spectral gate function
$D(f)$ = unsmoothed PSD estimate at frequency $f$.

Program options allow for specification of the gate's bandwidth (M) and for use of a rectangular function.

### 4.11.4 Ensemble Averaging

Under conditions of input data stationarity, FFT output stability may be enhanced by averaging the PSD outputs of separate time segments. This procedure consists of sectioning a time interval of interest, applying a separate data window to each section, transforming each section, spectral averaging each section's PSD, and forming the ensemble average of the smoothed periodograms.

### 4.11.5 Normalization

The output of the ensemble average algorithm is normalized to account for the effects of the input data window and the spectral averaging process. To account for these two effects, the periodogram's PSD is multiplied by the ratio of $A_1/A_2$ and divided by the quantity $2M + 1$, where

$$A_1 = \int_0^T dt \quad \Rightarrow \quad \sum_{i=1}^{N} i$$

$$A_2 = \int_0^T W^2(t)\, dt \Rightarrow \sum_{i=1}^{N} W^2(i) . \qquad (4\text{-}12)$$

## 4.12 INTEGRAL AND FOURIER OPERATIONS ON $S(\tau,\omega)$

Both the noise-present and noise-free estimates of the scatter channel's delay-Doppler function may be processed by an algorithm that performs integral and Fourier operations to yield delay spectrum, Doppler spectrum, joint time-frequency correlation function, frequency autocorrelation function, time autocorrelation function, and mean square total multipath power. These operations are described below.

### 4.12.1 Delay Spectrum

For the case where the $S(\tau,\omega)$ function is continuous over both the $\tau$ and $\omega$ variables, the channel's delay spectrum may be derived through the following integral:

$$Q(\tau) = \int_{-\infty}^{\infty} S(\tau,\omega)\, d\omega ,$$

where $Q(\tau)$ is the channel's delay spectrum.

In our case, $S(\tau,\omega)$ is discrete in both dimensions; thus, the delay-spectra estimate is given by

$$Q(\tau_i) = \sum_j S(\tau_i,\omega_j), \tag{4-13}$$

where $Q(\tau_i)$ is the power spectral density of energy arriving with delay $\tau_i$.

As previously described in section 4.9, a time-domain analysis on each tap output may be used to derive an estimate of $Q(\tau_i)$. That analysis, however, is limited to the noise-contamined signal structure whereas the integral operation on $S(\tau,\omega)$ allows one to operate on noise-removed data arrays.

### 4.12.2 Doppler Spectrum

The estimate of the multipath's Doppler spectrum is derived by summing the delay-Doppler function over the delay variable:

$$D(\omega_j) = \sum_i S(\tau_i,\omega_j), \tag{4-14}$$

where $D(\omega_j)$ is the energy arriving at the receiver with Doppler frequency shift $\omega_j$.

In general, the Doppler spectrum is highly asymmetrical and thus both the negative and positive frequency components of $D(\omega)$ are maintained. The discrete outputs are given at the following spectral locations:

$$\omega_j = (2\omega\Delta f)j, \text{ radians/sec}$$

$$\Delta f = \frac{SR}{N} M, \quad \text{hertz}, \tag{4-15}$$

where:

SR = sampling rate of SACP receiver taps
N = number of points in FFT (sec. 4.11)
M = window width of spectral smoothing (sec. 4.11).

These outputs fall between the limits of $\pm SR/2$.

4.12.3 Joint Time-Frequency Autocorrelation Function

In that the channel's delay-Doppler scatter function and joint time-frequency autocorrelation function are Fourier transform pairs, we derive an estimate of $R(\xi,\Omega)$ through application of a double inverse FFT to the $S(\tau,\omega)$ array:

$$R(\xi_x, \Omega_y) = \sum_{m=0}^{M-1} \sum_{n=0}^{N-1} S(\omega_m, \tau_n) \exp\left[2\pi i\left(\frac{xm}{M} + \frac{yn}{N}\right)\right]; \quad \begin{matrix} x = 0,1,\ldots,M-1 \\ y = 0,1,\ldots,N-1 \end{matrix}, \qquad (4\text{-}16)$$

where:

$R(\xi_x,\Omega_y)$ = time-frequency autocorrelation function at time $\xi_x$, frequency $\Omega_y$

M = number of elements in Doppler array extended to a value that is an integer power of 2 (zero-fill if necessary)

N = number of elements in delay coordinate array extended to an integer power of 2 (zero-fill if necessary)

i = $\sqrt{-1}$ .

Parameters $\xi_x$ and $\Omega_y$ take on the following discrete values:

$$\xi_x = \frac{x}{\Delta f M} \; ; \; x = 0,\pm 1,\ldots,\pm\frac{M-1}{2}$$

$$\Omega_y = \frac{y}{\tau N} \; ; \quad y = 0,\pm 1,\ldots,\pm\frac{N-1}{2} \quad ,$$

where:

$\Delta f$ = frequency separation between adjacent Doppler spectra outputs

$\tau$ = the effective tap width of the correlator output.

$R(\xi,\Omega)$ is output (magnitude and phase) in both numerical and three-dimensional plotted form. Since $R(\xi,\Omega) = R^*(-\xi,-\Omega)$, only half of the periodogram output is retained.

4.12.4 Frequency Autocorrelation

An estimate of the channel's frequency autocorrelation function is derived by applying the inverse FFT operation to the delay spectrum[2]:

$$R(0,\Omega_j) = \sum_{k=0}^{N-1} Q(\tau_k)\, e^{2\pi ijk/N}; \quad j = 0, \ldots, N-1, \tag{4-17}$$

where:

$R(0,\Omega_j)$ = frequency autocorrelation function output at frequency $\Omega_j$

N = number of delay taps; zero order extended to be equal to the nearest value that is an integer power of 2

$i = \sqrt{-1}$.

Since $Q(\tau_k)$ is real valued for all $\tau_k$, the $R(0,\Omega)$ distribution is symmetric with respect to $\Omega = 0$. Thus, the algorithm outputs only the positive components of the distribution, which are given at the following frequency locations:

$$\Omega_j = j(1/\tau N) \quad j = 0,1, \ldots, N/2 ,$$

where $\tau$ is the effective tap width of the correlator output. Outputs are given in both numerical and plotted formats.

4.12.5 Time Autocorrelation

Application of the inverse FFT algorithm to the multipath channel Doppler spectrum provides an estimate of the time autocorrelation function. This is represented by:

$$R(\xi_j,0) = \sum_{k=0}^{M-1} D(\omega_k)\, e^{2\pi ijk/M}; \quad j = 0,1, \ldots, N-1, \tag{4-18}$$

[2]As a program option $R(\xi,\Omega)$ may be bypassed; thus we derive the zero-axes cuts; i.e., $R(\xi,0)$ and $R(0,\Omega)$, via a method that does not depend on the availability of $R(\xi,\Omega)$.

where:

$R(\xi_j,0)$ = time autocorrelation function at time $\xi_j$

M = number of $D(\omega)$ array input points extended to a value that is an integer power of 2 (zero-fill if necessary)

i = $\sqrt{-1}$ .

The $R(\xi_j,0)$ function is symmetric with respect to $\xi = 0$ since $D(\omega_k)$ is real valued. Thus, only the positive components of $R(\xi,0)$ are output. These are given at the following discrete time intervals:

$$\xi_j = j/\Delta fM \; ; \; j = 0,1, \ldots , M-1 ,$$

where $\Delta f$ is the frequency separation between adjacent Doppler spectra outputs. The output format of the complex $R(\xi,\Omega)$ array is identical to that used to represent $R(\xi,\Omega)$.

### 4.12.6 Mean Square Total Multipath Power

The multipath channel's mean square power is derived by integrating the delay and Dopper spectra over their respective variables; i.e.,

$$<|I|^2> = \begin{cases} \sum_{i=1}^{N} D(\omega_i) \\ \sum_{i=1}^{M} Q(\tau_i) \end{cases} , \qquad (4\text{-}19)$$

where:

N = number of periodogram outputs

M = number of delay taps .

Both methods are used to give a partial validity check on the spectral transformation operations that have occurred up to this point in the overall computer program (i.e., if the alternate procedures yield different results, then a program error is indicated).

It is noted that the $<|I|^2>$ estimation technique is in essence equivalent to an incoherent power summation of the delay tap outputs. This does not give a true estimate since: (1) adjacent taps (for the usual one-chip tap spacing) have a 50% commonality in the delay area to which they are

partially correlated and (2) the autocorrelation function of the PN m-sequence is not uniform over a chip width but has triangular distribution with peak equal to the sequence length and base equal to −1 at locations ±1 chip from the peak. Assuming the multipath's delay spectra is piecewise constant over a chip width, the above effects are easily calculated to yield an $<|I|^2>$ estimate[3] that is on the order of 1.8 dB lower than would be the case for a coherent tap summation. A coherent summation, in effect, provides a single tap experiment with uniform peak correlation over the entire tap bank range. The tap lumping (contraction) feature of the program allows this to be performed; however, it cannot be employed simultaneously with the detailed single tap resolution $S(\tau,\omega)$ calculation.

## 4.13 SPREAD CALCULATIONS

Spread calculations are performed on the multipath channel's delay spectra, Doppler spectra, frequency autocorrelation function, and time autocorrelation function. The algorithm operates on these distributions to determine the:

a. Maximum, 3-dB, and 1/e levels
b. Spread between the 3-dB levels
c. Spread between the 1/e levels
d. First moment of the distribution
e. Second moment of the distribution with respect to the mean level
f. Second moment of the distribution with respect to the maximum level.

With the exception of the second moment parameters, these quantities are diagrammed in figure 4-8 for an assumed Doppler spectrum.

The spectra and autocorrelation functions upon which the spread calculation algorithm operates are in the form of discrete sample arrays. Assuming an array distribution of the form $y_i = f(x_i)$, the processing begins with a search for the $x_i$ value that produces the maximum $y_i$. These values are designated by $x_{i_{max}}$ and $y_{i_{max}}$, respectively. Two searches are then originated from the $i_{max}$ location (one with i decreasing, the other with i increasing) to determine the $x_i$ values where the distribution first crosses the $y_{i_{max}}/2$ and $y_{i_{max}}/e$ levels. The corresponding differences between the $x_{i_{max}}/2$ and $x_{i_{max}}/e$ levels are then computed to yield the 3-dB and 1/e delay spread values.

[3]Assuming an infinite sampling rate in the digital implementation of the SACP receiver.

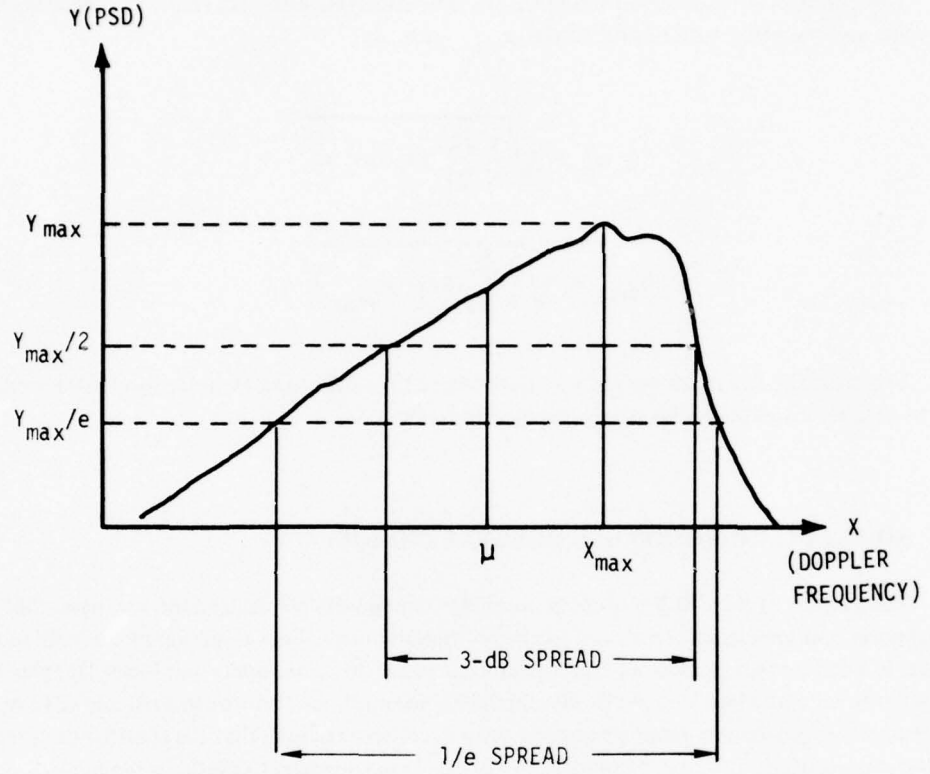


*Figure 4-8. Spread Parameter Illustration*

In determining the distribution mean value, the first step is to calculate the total value of the array sum:

$$S = \sum_{i=1}^{N} y_i \,, \tag{4-20}$$

where:

S = array sum

N = number of points in the array.

The mean value of the array's x-coordinate is then calculated as

$$\mu = \left[ \sum_{i=1}^{N} y_i x_i \right] 1/S \,. \tag{4-21}$$

Two forms of second moment calculations are performed, one with respect to the array's mean value and the other with respect to the $x_{max}$ quantity:

$$\sigma_{\mu} = \sqrt{\frac{1}{S}\sum_{i=1}^{N} (x_i - \mu)^2 \, y_i} \tag{4-22}$$

$$\sigma_{max} = \sqrt{\frac{1}{S}\sum_{i=1}^{N} \left(x_i - x_{i_{max}}\right)^2 y_i} \, . \tag{4-23}$$

Note that the algorithm operates on both sides of the delay and Doppler spectra but considers only the positive x-values for the autocorrelation function.

## 4.14 NOISE DETERMINATION AND REMOVAL (NDandR)

The outputs of the SACP multipath correlator contain desired signal data, low-pass additive thermal noise, spurious signal terms, and receiver arithmetic noise. Determination of the bulk of the tap noise is aided by two factors: (1) for a given time delay, there are upper and lower Doppler frequency limits beyond which it is physically impossible for multipath returns to exist and (2) SACP receiver operator procedures entail replica sequence delay settings such that the specular path return is captured somewhat after the $10^{th}$ tap (oceanic) or $30^{th}$ tap (overland CONUS) in the bank. See figure 4-9 for a plan view of these realms as superimposed upon the delay-Doppler plane of the SACP receiver. Also included are regions X and Y, which are referred to in the following discussion.

The algorithm for noise determination and removal is illustrated in figure 4-10. Delineation of the major features of each processing step is given below.

### 4.14.1 Filter Frequency Response Determination

The SACP complex correlators use digital realizations of Butterworth-Thompson low-pass filters at their outputs. Their frequency response is determined in the NDandR process by emulating the recursive filter algorithm for the case of interest and then subjecting it to a series of unit magnitude sinusoidal inputs that occur at the frequencies of the FFT periodogram for the $S(\tau,\omega)$ function. The amplitude square of the filter output is used to represent the magnitude of the discrete frequency response of the low-pass filter. This is designated FR(f).

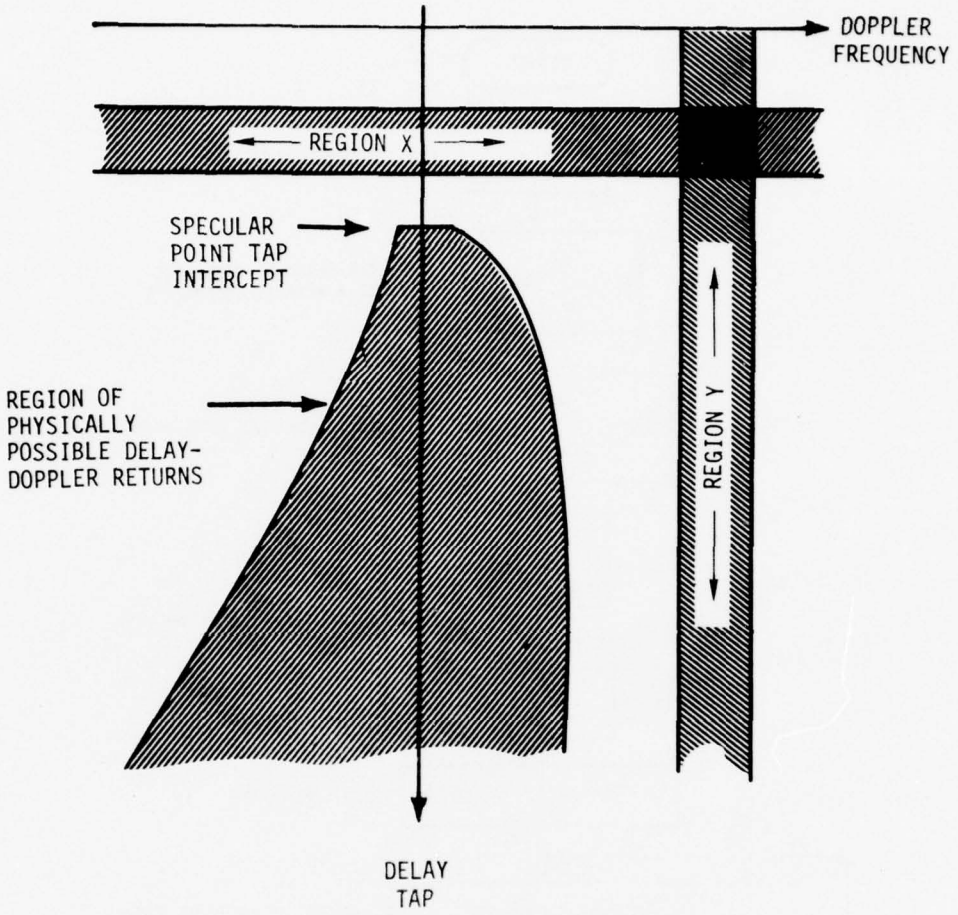


*Figure 4-9. Delay-Doppler Realm of SACP Receiver*

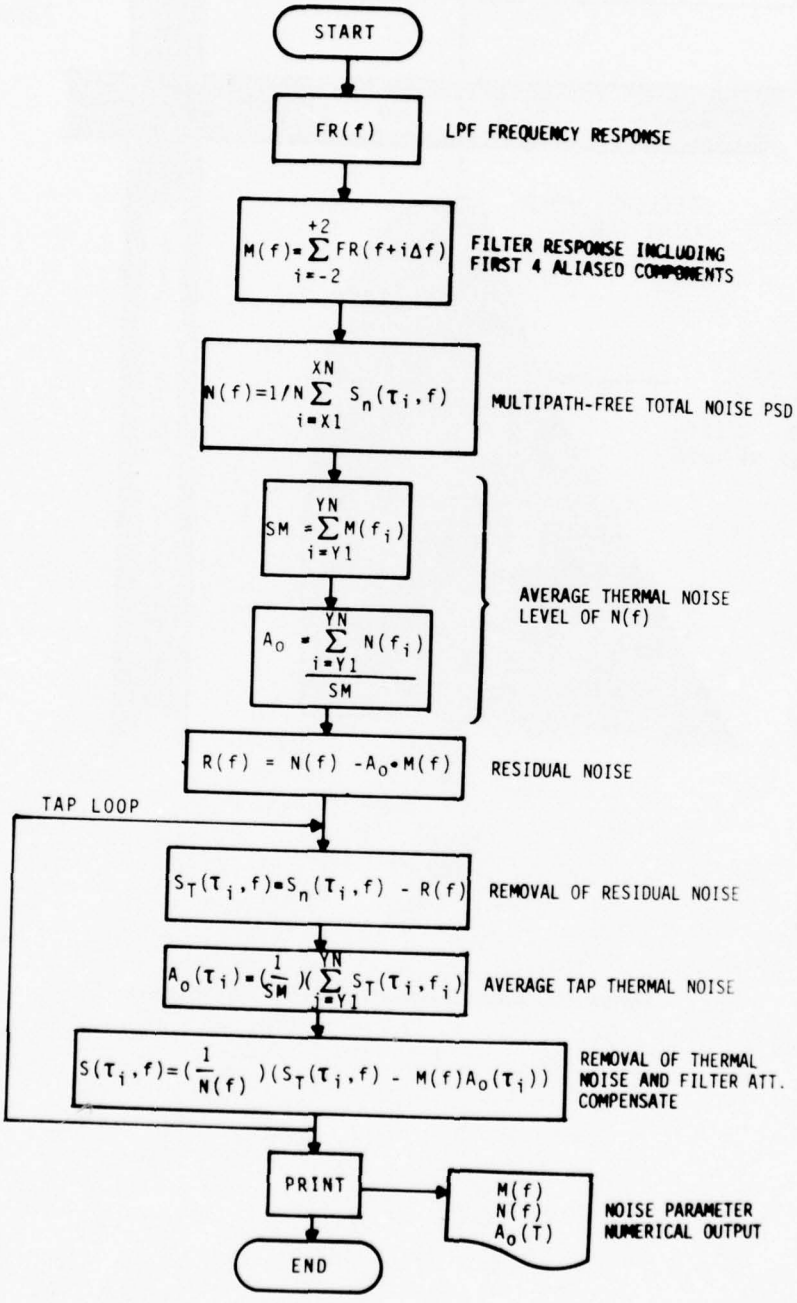


*Figure 4-10. Noise Determination and Removal Algorithm*

### 4.14.2 Filter Response Including Aliased Components

When dealing with a tap's low-pass thermal noise content, we consider not only the basic frequency response of the filter but also the aliased components caused by the implicit periodicity assumption of the FFT algorithm. We include the first four periods of the aliased low-pass filter noise, which is rather significant due to the effective tap sampling rate at only twice the filter's -1 dB frequency. Assuming a white thermal noise content in the SACP receiver, the filter response to thermal noise including the bulk of the aliased components may be expressed as

$$M(f) = \sum_{i=-2}^{+2} FR(f+i\Delta f), \tag{4-24}$$

where:

- $M(f)$ = amplitude of filter response to white noise including first four aliased components
- $\Delta f$ = basic tap sampling rate.

### 4.14.3 Multipath-Free Total Noise Spectra

Once a multipath-free delay region has been determined (i.e., region X of fig. 4-9), its total noise spectra is determined by averaging the $S_n(\tau,\omega)$ array over the delay variable:

$$N(f) = \frac{1}{N} \sum_{i=X1}^{XN} S_n(\tau_i, f), \tag{4-25}$$

where:

- $N(f)$ = multipath-free region's total noise spectra
- $X1$ = first tap of multipath-free region
- $XN$ = last tap of multipath-free region.

An example of a multipath-free region's total noise spectra is given in figure 4-11. For this case, the low-pass filter bandwidth was on the order of 300 Hz and we note the effect of the aliased thermal noise (i.e., the increase in the density at the tails of the distribution). Also in evidence is a large spurious dc noise component, which is caused primarily by the SACP receiver's two's-complement arithmetic.

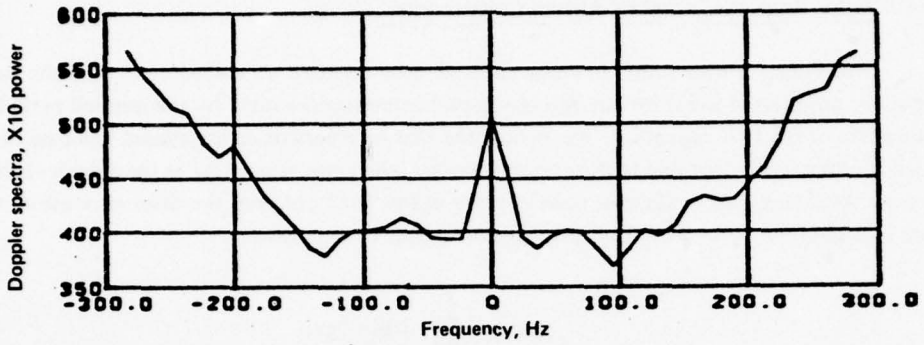


*Figure 4-11. Multipath-Free Noise Spectrum Showing Aliasing and Arithmetic Noise*

4.14.4 Average Thermal Noise Level of N(f)

A tap's thermal noise psd may be represented by $A_o M(f)$, where $A_o$ is tap dependent. To determine $A_o$, we analyze the tap's psd in a frequency region devoid of multipath (i.e., region Y of fig. 4-9). This region is also well removed from the receiver arithmetic noise and the PN code's low-pass spurious response (which has bandwidth characteristics of the multipath signal). Thus, we may assume it to be contaminated by thermal noise alone. For N(f), the $A_o$ estimate is obtained from the following operation:

$$A_o = \frac{\sum_{i=Y1}^{YN} N(f_i)}{SM} , \qquad (4\text{-}26)$$

where:

Y1 = first spectral component in region Y
YN = last spectral component in region Y
$SM = \sum_{i=Y1}^{YN} M(f_i)$.

4.14.5 Residual Noise Determination

By subtracting $A_o M(f)$ from N(f), we obtain what is referred to as the tap bank residual noise estimate:

$$R(f) = N(f) - A_o M(f) . \qquad (4\text{-}27)$$

This parameter thus represents the nonthermal noise content of the psd. It is assumed to be identical for each tap in the bank. The procedures for calculating the residual noise includes the PN correlator's low-pass spurious response to each and every signal that arrives at the receiver. When the residual noise is subtracted from a tap containing multipath return, we are thus removing a portion of low-pass spurious noise that is not present in that particular tap initially. For example, if the tap in question intercepts delay energy $E(\tau_i)$, then we remove a component corresponding to the noise determination interval's uncorrelated PN response to $E(\tau_i)$. For the sequence length typically used in the multipath test (512), this error is very small and amounts to roughly four parts in $10^6$ (power) of the correlated signal.

4.14.6 Residual Noise Removal

Once the residual noise estimate is determined, the NDandR algorithm then enters into a tap loop and proceeds to derive a noise-free estimate of the channel's delay-Doppler function. The first step involves removing R(f) from the particular tap in the loop:

$$S_T(\tau_i,f) = S_n(\tau_i,f) - R(f)\,, \tag{4-28}$$

where:

$S_T(\tau_i,f)$ = the residual noise-free estimate of the $i^{th}$ tap's psd
$S_n(\tau_i,f)$ = the noise-contaminated estimate of the $i^{th}$ tap's psd .

4.14.7 Average Thermal Noise Level of $S_T(\tau_i,f)$

After the residual noise content has been removed from a particular tap's psd, its thermal noise level $A_o(\tau_i)$ is derived in a manner identical to that discussed for the N(t) case; i.e.,

$$A_o(\tau_i) = \frac{\sum_{j=Y1}^{YN} S_T(\tau_i,f_j)}{SM}\,, \tag{4-29}$$

where $A_o(\tau_i)$ is the thermal noise level of the $i^{th}$ delay tap's psd.

### 4.14.8 Thermal Noise Removal and Filter Attenuation Compensation

The final steps in NDandR involve removing $A_o(\tau_i)M(f)$ from $S_T(\tau_i,f)$ and dividing the result by the amplitude response of the low-pass digital filter (which compensates for the filter attenuation on the multipath signal component). This is represented by:

$$S(\tau_i,f) = \frac{S_T(\tau_i,f) - M(f) \times A_o(\tau_i)}{N(f)} \quad , \tag{4-30}$$

where $S(\tau_i,f)$ is the noise-free filter compensated estimate of the multipath psd for the $i^{th}$ receiver tap.

The effectiveness of the NDandR algorithm is illustrated by the sample data presented in section 4.24 (figs. 4-20 through 4-24). In these figures, the delay-Doppler scatter functions, delay spectra, and Doppler spectra for both noise-present and noise-removed conditions are illustrated. Visually, very little difference appears to exist between the noise-present and noise-removed estimates of $S(\tau,\omega)$ (although for lower signal-to-noise cases, the dc offset bias for the noise-removed case exhibits the expected random uncertainty fluctuation about the zero-power-level x-y axis). On the other hand, there is a pronounced difference between noise-present and noise-free Doppler and delay spectra. The noise-free delay spectra have essentially no energy prior to the specular return, approach zero-energy asymptotically as the delay variable becomes much greater than the specular return, and do not possess the extraneous noise in tap 81. By comparison, the noise-free Doppler spectra estimate is virtually signal free for frequencies greater than roughly 150 Hz (the physical upper limit for Doppler return over the tap bank extent for the test condition) and the dc spurious noise contribution has been completely eliminated.

In general, the NDandR algorithm will handle most noise-contamination cases encountered in the multipath tests. It will handle tap-dependent thermal noise conditions (e.g., tap 81 in the above discussion) but will not properly account for conditions where the statistics of the residual noise content vary from tap to tap. The latter cases have been observed to occur during conditions of receiver malfunction and when unwanted signals have entered the tap bank.

## 4.15 AIRBORNE PROBER ANTENNA EFFECTS REMOVAL

To remove the prober aircraft antenna pattern effects from the channel measurements, it is first necessary to make some assumptions regarding the mechanism by which the electromagnetic waves are scattered from the earth surface. In line with the most widely accepted theoretical treatments and the good agreement between experiment and theory as presented in volume V, we base our

analysis upon the vector formulation of the physical optics very rough surface scatter model. Under this assumption the received power from an increment of surface area is expressed as

$$dP_{rcvd} \propto (T_{cf} \times T_{cf}^{*}) P_{ss}(\theta_\eta, \theta_\epsilon) \ , \tag{4-31}$$

where:

$dP_{rcvd}$ = power received from the incremental area

$P_{ss}(\theta_\eta, \theta_\epsilon)$ = probability of incremental area having slope $\theta_\eta$ and $\theta_\epsilon$ in the $\eta$ and $\epsilon$ directions, respectively ($\theta_\eta$ and $\theta_\epsilon$ provide favorable reflections from the surface to satellite)

$T_{cf}$ = complex coefficient that accounts for coupling between incident polarization vector, tilted surface facet, and receiver polarization vector.

The aircraft antenna influence is embodied only in parameter $T_{cf}$, which may be represented as (see sec. 5.2):

$$\begin{aligned} T_{cf} = {} & R_{\|}(a) \left[ A \cos \delta_i + B \sin \delta_i \right] \left[ C \cos \delta_s + D \sin \delta_s \right] \\ & - R_{\perp}(a) \left[ B \cos \delta_i - A \sin \delta_i \right] \left[ -D \cos \delta_s + C \sin \delta_s \right] \ , \end{aligned} \tag{4-32}$$

where:

$R_{\|}(a)$ = parallel Fresnel reflection coefficient

$R_{\perp}(a)$ = perpendicular Fresnel reflection coefficient

$a$ = angle between incident wave and normal of properly tilted (to produce reflection into receiver) surface facet

$\delta_i$ = angle between theta component of incident wave and the incident parallel unit vector (i.e., vertical polarization with respect to tilted surface)

$\delta_s$ = angle between theta component of scattered wave and the reflected parallel unit vector

A.B.C.D = transmitter and receiver complex antenna polarization vector coefficients as described below.

Polarization vectors for the transmit ($\bar{P}_T$) and receive ($\bar{P}_R$) antenna system are given by:

$$\begin{aligned} \bar{P}_T &= A \, \hat{i}_{TT} + B \, \hat{i}_{PT} \\ \bar{P}_R &= C \, \hat{i}_{TR} + D \, \hat{i}_{PR} \ , \end{aligned} \tag{4-33}$$

where:

$\hat{i}_{TT}, \hat{i}_{PT}$ = unit vectors in the theta and phi directions, respectively, with respect to coordinates centered on the transmitter

$\hat{i}_{TR}, \hat{i}_{PR}$ = unit vectors in the theta and phi directions, respectively, with respect to coordinates centered on the receiver.

In our case transmission originates from the KC-135 and is received at the ATS-6 satellite. The satellite antenna is assumed to be right-hand circular (RHC) with 0-dB ellipticity; thus:

$$C = \sqrt{G_S/2}$$

$$D = j\sqrt{G_S/2}\,,$$

where $G_S$ is the gain magnitude of the satellite antenna.

Parameters A and B for the aircraft antenna pattern are derived from scale-model antenna range measurements (see vol. VII of this report). We apply the antenna effects removal algorithm to the specific case where the prober is operating in the simultaneous horizontal/vertical polarization mode. These probe polarization descriptions are nominal in that for aircraft antenna systems one usually expects the presence of cross-polarization terms. Thus for the nominal horizontal polarization probe, B represents the principal polarization term and A is a measure of the cross-polarization term (vice versa for nominal vertical polarization). From the antenna range radiation distribution plots, it is observed that for the various prober antenna pointing directions the ratio of principal-to-cross-polarization terms is typically on the order of 20 dB over the effective "glistening" area of the surface. Hence, to good approximation we consider only the principal terms of the polarization vectors and write $T_{cf}$ for the horizontally polarized probe as:

$$T_{cf} = \sqrt{\frac{G_H G_S}{2}} \left\{ R_{\parallel}(a) \sin\delta_i (\cos\delta_s + j \sin\delta_s) - R_{\perp}(a) \cos\delta_i (\sin\delta_s - j\cos\delta_s) \right\}, \quad (4\text{-}34)$$

and, for the vertically polarized probe,

$$T_{cf} = \sqrt{\frac{G_V G_S}{2}} \left\{ R_{\parallel}(a) \cos\delta_i (\cos\delta_s + j \sin\delta_s) + R_{\perp}(a) \sin\delta_i (\sin\delta_s - j\cos\delta_s) \right\}, \quad (4\text{-}35)$$

where:

$G_H$ = gain of horizontally polarized probe

$G_V$ = gain of vertically polarized probe.

Parameters $G_H$ and $G_V$ do not have constant gain over the scattering surface. To remove this spatial filtering effect, we operate in the delay-Doppler coordinate system of the receiver. The scatter function, $S(\tau,\omega)$, is related to $dP_{rcvd}$ through the following formulation:

$$S(\tau,\omega) = J_1(\tau,\omega)\, dP_{rcvd,1} + J_2(\tau,\omega)\, dP_{rcvd,2} \quad , \tag{4-36}$$

where $j(\tau,\omega)$ is the Jacobian of the transformation from surface coordinates to $(\tau,\omega)$ receiver coordinates.

In the above equation, subscripts 1 and 2 denote the fact that the scattering operation is a 2-into-1 mapping process (that is, two surface points are mapped into one delay-Doppler location). In general, even for isotropic antennas, $dP_{rcvd,1}$ does not equal $dP_{rcvd,2}$; thus without making some assumptions with regard to the $P_{ss}(\theta_\eta,\theta_\epsilon)$ distribution it becomes impossible to properly adjust $S(\tau,\omega)$ for the antenna filtering effects. To circumvent this ambiguity, we restrict our attention entirely to the data gathered during the in-plane legs of the test scenario. The symmetry properties of the delay contours, Doppler contours, and $P_{rcvd}$ function[4] are thereby exploited and we may write $S(\tau,\omega)$ as:

$$S(\tau,\omega) = J_1(\tau,\omega)\, dP'_{rcvd,1}\, (G_1 + G_2) \quad , \tag{4-37}$$

where $dP'_{rcvd,} = dP_{rcvd}/G(\beta)$, i.e., the received engery from incremental area $(\beta)$ given that the antenna illumination is isotropic.

Now under the same geometry and surface assumption we may express $S(\tau,\omega)$ for the isotropic antenna gain case as:

$$\begin{aligned} S_I(\tau,\omega) &= J_1(\tau,\omega)\, dP'_{rcvd,1} + J_2(\tau,\omega)\, dP'_{rcvd,2} \\ &= 2J_1(\tau,\omega)\, dP'_{rcvd,1} \cdot \end{aligned} \tag{4-38}$$

---

[4]Examination of equation (4-31) reveals that for in-plane flight, $dP_{rcvd}$ will be cross-plane symmetrical (apart from antenna asymmetry effects) if (1) the sea-surface slope distribution is isotropic, a valid assumption per data from Cox and Munk (ref. 4-2) and (2) the polarization planes of the transmit and receive antennas are linear and lie either in or perpendicular to the plane containing the KC-135, specular point, and ATS-6 satellite. The latter restriction is necessary to ensure that $T_{cf,1} = T_{cf,2}$. In our case this condition is *not* met since the satellite antenna polarization is circular. However, it can be shown that for grazing angles greater than a few degrees the induced error is relatively small when compared to other factors such as the antenna gain characterization.

Thus for in-plane flight the isotropic antenna scatter function, $S_I(\tau,\omega)$, is related to the antenna-gain-contaminated version $S(\tau,\omega)$ by the simple relationship:

$$S_I(\tau,\omega) = \frac{S(\tau,\omega)}{G(\tau,\omega)} , \tag{4-39}$$

where:

$$G(\tau,\omega) = \frac{G_1 + G_2}{2} . \tag{4-40}$$

In the commonly used steepest descent integration analysis of forward scatter multipath (mathematically appropriate under the constraint that the grazing angle is much greater than the surface rms slope), one usually assumes that the antenna coverage is adequately described by its specular point gain. For this reason we have chosen to relate our antenna-corrected version of the scatter function to the gain directed toward the specular point; i.e.,

$$\begin{aligned} S_{AC}(\tau,\omega) &= S_I(\tau,\omega)\, G(0,0) \\ &= \frac{S(\tau,\omega)}{G(\tau,\omega)} G(0,0) , \end{aligned} \tag{4-41}$$

where:

$S_{AC}(\tau,\omega)$ = antenna-corrected version of the scatter function
$G(0,0)$ = the specular point antenna gain (i.e., $\tau = \omega = 0$).

In addition we also calculate a difference function, $\Delta S(\tau,\omega)$, between the corrected and uncorrected versions of the scattering function:

$$S(\tau,\omega) = S(\tau,\omega) - S_{AC}(\tau,\omega) . \tag{4-42}$$

This function is available as a three-dimensional plot and provides a compact description of the prober's spatial filtering characteristics as translated to the delay-Doppler coordinates of the receiver.

The algorithm for determining $G(\tau,\omega)$ has the following parameters as its basic input: (1) aircraft antenna pattern in the classical theta, phi coordinate system, (2) aircraft altitude, velocity, and height, (3) elevation angle to the satellite, and (4) tap number associated with specular point return.

Using this information the program determines the realm of physically possible $(\tau,\omega)$ point pairs into which the scatter surface can be mapped. Each $S(\tau,\omega)$ density within this realm is then compared to a noise threshold level (to bypass this test, the threshold may be set to zero). If the threshold test is not passed, $S_{AC}(\tau,\omega)$ is set to zero; otherwise standard geometric techniques are used to map $(\tau,\omega)$ into the two sets of surface coordinates that are responsible for the scatter. These locations are in turn translated into antenna pattern coordinates from which a table look-up routine is used to derive the gains $G_1$ and $G_2$, which are then used in equation (4-40) to form the $G(\tau,\omega)$ function. As a secondary output from the algorithm, one may obtain $G(\tau,\omega)$ in both numerical and three-dimensional plotted formats.

## 4.16 TAP I AND Q AMPLITUDE DISTRIBUTION

Amplitude probability distribution in the form of histograms is derived for the I and Q components of a given delay tap through the application of standard numerical grouping techniques. A block diagram illustrating the fundamental components of the APD algorithm is given in figure 4-12. Prior to histogram sorting, three operations are performed on the input data:

a. The data may be optionally desampled to improve the independency of the sample space array.

b. A dither signal is added to each of the desampled data points. This is necessary since the quantizing levels of the digital SACP receiver are not significantly smaller than the bin widths of the histograms. In accord with the two's-complement arithmetic of the receiver, the dither signal is chosen from an ensemble whose values are uniformally distributed between 0 and 1. A new dither signal is used for each signal input value.

c. The mean and standard deviation of the desampled, dithered array is determined:

$$\mu = \frac{1}{N}\sum_{i=1}^{N} x_i \quad , \tag{4-43}$$

$$\sigma = \sqrt{\frac{1}{N}\sum_{i=1}^{N} (x_i-\mu)^2} \quad . \tag{4-44}$$

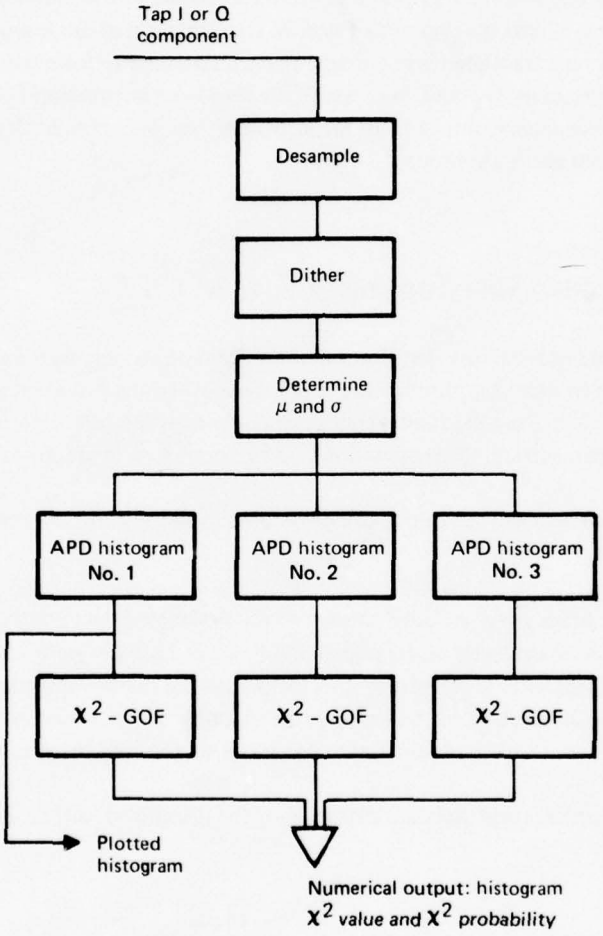


*Figure 4-12. Tap I and Q Amplitude Distribution Algorithm*

After the sample's mean and standard deviation have been determined, the algorithm then sorts the input sample array into three histogram distributions. All three histograms are calculated for each tap component. The sorting techniques are described as follows:

a. Histogram 1 – consists of 20 bins ranging between $-\infty$ and $+\infty$, with the 18 interior bins being of equal width and spanning the range $[-3\sigma, +3\sigma]$.

b. Histogram 2 – similar to No. 1 except bins are combined with their nearest neighbors if the observed frequency is less than a specified (input) percentage.

c. Histogram 3 – bin widths are selected so that the expected frequency (see below for discussion pertaining to expectation model) for each bin is 5%. Thus, there are 20 bins total.

The three histogram distributions are then tested for normality. This is carried out via the $\chi^2$ goodness-of-fit test. The $\chi^2$ statistic is calculated as:

$$\chi^2 = \sum_{i=1}^{N} \frac{(EF_i - 0F_i)^2}{EF_i} \quad , \tag{4-45}$$

where:

$N$ = number of bins in the histogram
$EF_i$ = the expected number of data points falling into the $i^{th}$ bin
$0F_i$ = the observed number of data points falling into the $i^{th}$ bin .

Parameter $EF_i$ is based on the assumption of a Gaussian distribution whose mean and variance are derived from the sample space array; i.e.,

$$EF_i = \frac{1}{\sqrt{2\pi}\sigma} \int_{t_{i-1}}^{t_i} \exp\left(\frac{(x-\mu)^2}{2\sigma^2}\right) dx \quad , \tag{4-46}$$

where $t_i$ is the upper limit of the voltage range associated with the $i^{th}$ bin.

Knowing the $\chi^2$ statistic and the number of degrees of freedom $(N-3) = K$ associated with each particular histogram, we are then able to determine the following cumulative probability:

$$F(\chi^2) = \int_0^{\chi^2} \frac{1}{2^K \Gamma(K/2)} y^{(K-1)} e^{-y} dy \quad . \tag{4-47}$$

This represents the probability that a sample space selected from a Gaussian distribution with the same mean and variance as the test case will produce a $\chi^2$ value less than that of the observed sample (i.e., if $F(\chi^2)$ is consistently greater than 0.9, we would have reason to doubt the normality of the data).

## 4.17 TAP PHASE DISTRIBUTION

We define the phase, $\phi$, of the complex tap received signal as

$$\phi_i = \tan^{-1} Q_i/I_i \,. \tag{4-48}$$

The algorithm for determining the probability distribution histogram of $\phi$ operates on the same desampled dithered I and Q data values that are input to the amplitude statistics routine. Twenty equal-length bins are utilized for the histogram structure, which has a total extent from $-180^o$ to $+180^o$. Via the $\chi^2$ goodness-of-fit test as described in section 4.16, the observed bin densities are compared to a hypothesis resulting from the two-dimensional Gaussian distribution whose quadrature components are independent with nonzero means and nonidentical variances:

$$W(I,Q) = \frac{1}{2\pi\sigma_I\sigma_Q} \exp\left(\frac{(I-\mu_I)^2}{2\sigma_I{}^2} - \frac{(Q-\mu_Q)^2}{2\sigma_Q{}^2}\right), \tag{4-49}$$

where:

$W(I,Q)$ = joint probability density of the tap output taking on the specific I and Q values
$\sigma_I, \sigma_Q$ = standard deviations of the I and Q processes
$\mu_I, \mu_Q$ = means of the I and Q processes.

The phase probability density may be derived by transferring the above relationship to polar coordinates and integrating over the total extent of the radial dimension; i.e.,

$$P(\phi) = \frac{1}{2\pi\sigma_I\sigma_Q}\int_0^\infty \zeta d\zeta \exp\left(-\frac{(\zeta\cos\phi-\mu_I)^2}{2\sigma_I{}^2} - \frac{(\zeta\sin\phi-\mu_Q)^2}{2\sigma_Q{}^2}\right). \tag{4-50}$$

Knowing $P(\phi)$, the expected bin frequencies are then calculated by integrating over the $(\phi)$ range and using steps similar to those described in the previous section to yield the $\chi^2$ statistic and cumulative probability.

## 4.18 TAP PROCESS CROSS-CORRELATION

Given any two complex tap processes, this algorithm computes the normalized cross-correlation function as:

$$R_{XY}(k) = \frac{\sum_{i=1}^{N} X_i Y_{i-k}^*}{\left[\sum_{i}^{N} X_i X_i^* \sum_{i}^{N} Y_i Y_i^*\right]^{1/2}}, \qquad (4\text{-}51)$$

where:

$R_{XY}(k)$ = normalized cross-correlation function between tap processes X and Y for lag offset k

$X_i$ = $i^{th}$ sample of the X tap process (as a program option the mean may be removed prior to processing).

The program is written so that X and Y may be taken from either the same tap bank or from cross-polarized tap banks. A high-level flow diagram for this algorithm is shown in figure 4-13. As indicated, there are two major loops in the routine. The case loop is used to delineate the tap correlation pairs and the number of points to be considered in each calculation. For example, one may request that all 110 taps of the horizontal bank be correlated with their seven closest neighbors of the vertical bank. Because the program performs all correlation simultaneously (i.e., 770 in the above example), the software has been configured to segment the input sequence length into blocks that make machine core usage realistic. We therefore require a segment loop that operates by automatically inputting tape frames to fill the core allotment. Temporary results are then calculated and the process repeats itself until the total requested sample space has been analyzed.

## 4.19 TAP I AND Q DEPENDENCY

The degree of coherence between a tap's I and Q components is calculated for the zero-lag case through application of an algorithm similar to that described in section 4.18. Since I and Q are both real functions, their normalized cross-correlation zero-lag value is given by

$$R_{I,Q}(0) = \frac{\sum_{i=1}^{N} (I_i Q_i)}{\sqrt{\sum_{i=1}^{N} I_i^2 \sum_{i=1}^{N} Q_i^2}}. \qquad (4\text{-}52)$$

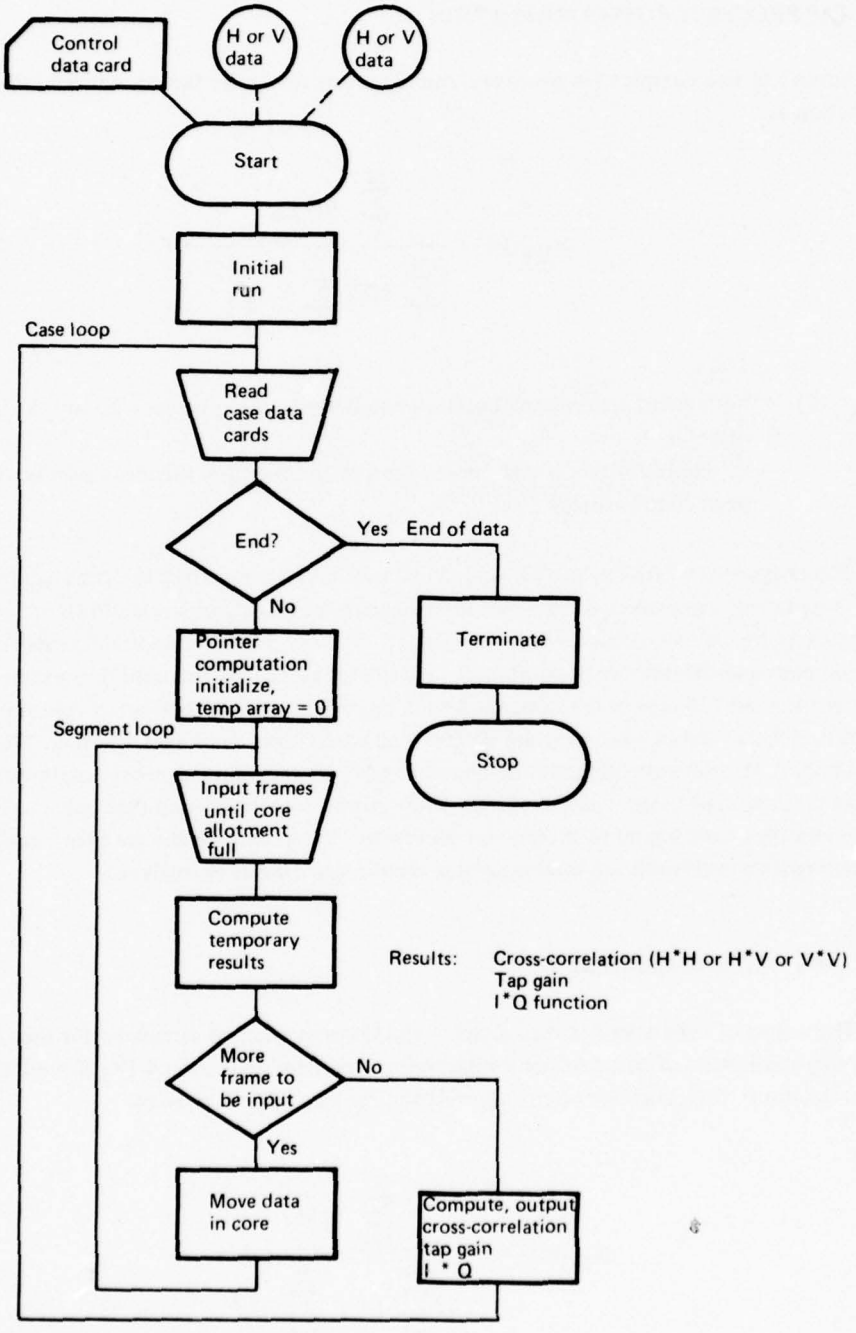


*Figure 4-13. Cross-Correlation Program High-Level Algorithm*

This parameter is given as a numerical output together with the following secondary results:

$$I_{rms} = \sqrt{(1/N)\sum_{i=1}^{N} I_i^2}$$

$$Q_{rms} = \sqrt{(1/N)\sum_{i=1}^{N} Q_i^2}$$

$$A_{rms} = \sqrt{I_{rms}^2 + Q_{rms}^2} \,. \qquad (4\text{-}53)$$

## 4.20 TAP-GAIN AUTOCORRELATION FUNCTION

Prior to application of the noise-removal option, the tap-gain autocorrelation function, $U(\tau,\xi)$, is calculated as a subset of the algorithm described in section 4.18. That is, for the zero tap offset the unnormalized tap correlation function represents the noise-present component of the tap-gain autocorrelation function:

$$U(\tau,\xi) = \frac{1}{N}\sum_{i=1}^{N} X_{\tau,i}\, X^*_{\tau,i-\xi} \,, \qquad (4\text{-}54)$$

where:

$\tau$ = delay value associated with the particular tap
$\xi$ = time-lag variable
X = tap complex process from either the horizontal or vertical polarization bank.

As the program option, the above process may be applied to the cross-polarized tap banks (X and Y); i.e.,

$$U_{XY}(\tau,\xi) = \frac{1}{N}\sum_{i=1}^{N} X_{\tau,i}\, Y^*_{\tau,i-\xi} \,. \qquad (4\text{-}55)$$

A second program option allows one to estimate and remove the noise contribution to the above tap-gain autocorrelation function. The noise estimate is made by applying equations derived in section 4.14 to a multipath-free region of the tap bank; i.e.,

$$U_n(\xi) = \frac{\sum_{i=I}^{I_n} \frac{1}{N} \sum_{j=1}^{N} X_{i,j} X^*_{i,j-\xi}}{I_n - I + 1} , \tag{4-56}$$

where:

$U_n(\xi)$ = estimate of average complex noise contribution to the $U(\tau,\xi)$ function

$X_i$ = tap process in multipath-free region of the correlator bank.

By subtracting $U_n(\xi)$ from $U(\tau,\xi)$ we then obtain an estimate of the noise-free tap-gain autocorrelation function $U_{nf}(\tau,\xi)$:

$$U_{nf}(\tau,\xi) = U(\tau,\xi) - U_n(\xi) . \tag{4-57}$$

## 4.21 COVARIANCE AND CROSS-SPECTRAL DENSITY ESTIMATES OF HORIZONTAL-VERTICAL CHANNEL MULTIPATH DATA

The software described below assumes that the tap transposition programs (sec. 4.5) have been executed for both the horizontal and vertical channel multipath tapes and that the processed data has been placed in a file on either magnetic tape or disk. In addition, the output record length of the tap transposition must be 256 words (512 packed complex samples). The number of records per segment must be less than or equal to four.

### 4.21.1 Data Files

The programs generate eight temporary data files during execution. Their structures are detailed in figure 4-14. HORIZ.DAT and VERT.DAT are horizontal and vertical channel buffers. The variable IREC has a value 1 greater than the number of records per segment in the tap transposition output. NTAPC represents the *n*umber of *tap*s to be used for *c*ross-channel estimates. (The first tap to be used is, of course, an input variable.) The last column in the file structure is a pseudo-tap that has been labeled "carrier." It represents the response of the system to a cw tone at the carrier frequency. It is obtained by summing a set of user-selected taps that ostensibly contain all significant energy. All tap processes have gone through a mean-removal operation before placement in the file data buffers.

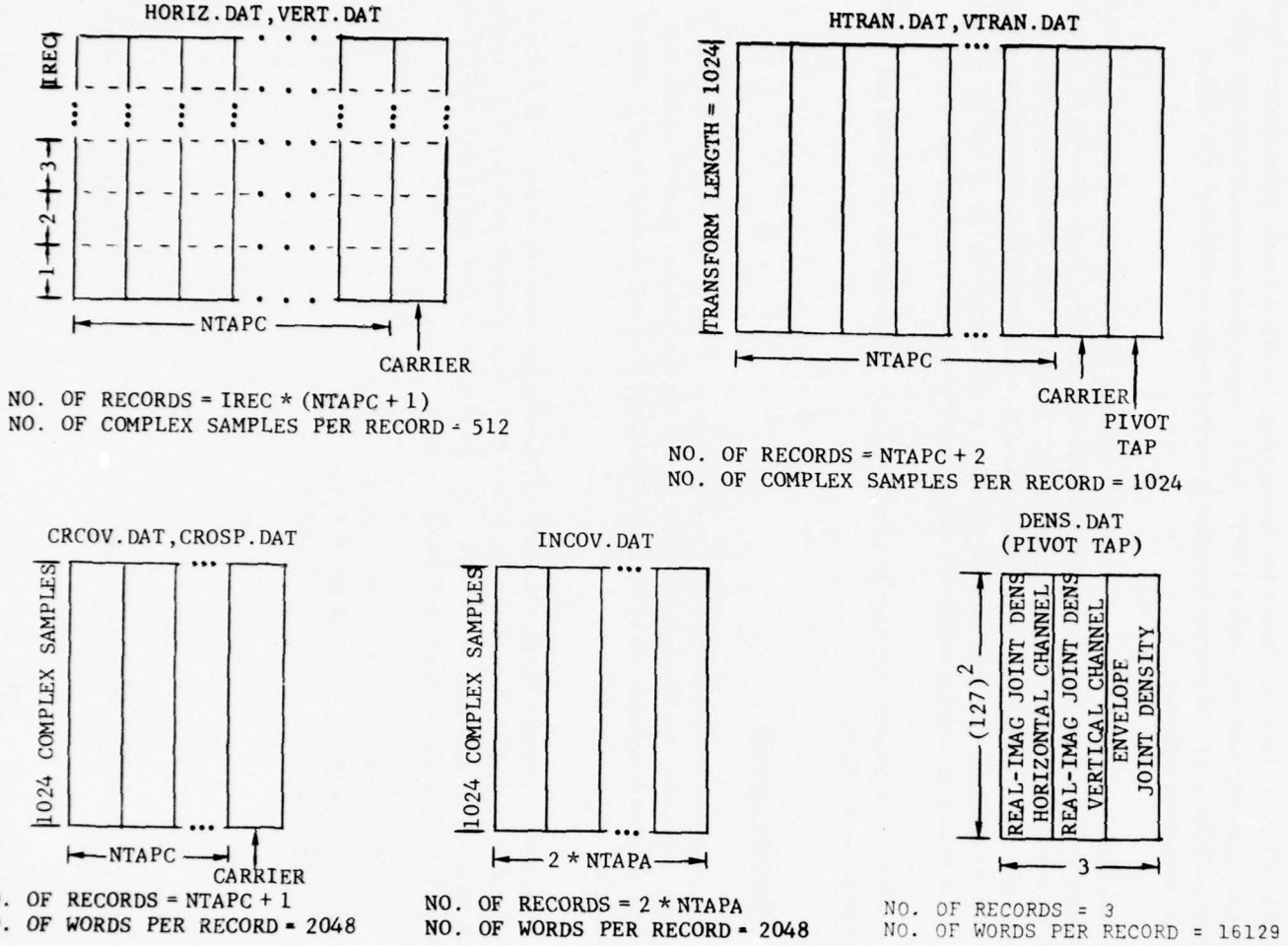


*Figure 4-14. H and V Data File Structure*

HTRAN.DAT and VTRAN.DAT contain one-record delayed transforms of the data in HORIZ.DAT and VERT.DAT. Each transform is two transposition records in length. Intermediate cross-channel covariance estimates are stored in CRCOV.DAT. Intermediate cross-spectral density estimates are stored in CROSP.DAT. All phase information is retained to allow calculation of both cross-power and cross-phase estimates.

As a result of the relatively small amount of additional work required, the program also calculates intertap covariances for both the horizontal and vertical channels. These estimates are located in file INCOV.DAT. The number of records in this file is 2 x NTAPA, where NTAPA represents the *n*umber of *tap*s to be used for intr*a*-channel estimates. A user-selected pivot tap is correlated with each of the NTAPA taps. Horizontal channel intertap covariances are stored in the first set of NTAPA records; vertical channel intertap covariances are stored in the second set of NTAPA records.

DENS.DAT is temporary storage for a joint density description of the horizontal and vertical channel pivot tap processes.

4.21.2 Processing Example

All covariance and spectral estimates are derived via the FFT. These techniques are well known and need not be described here. However, we will briefly describe a novel procedure that allows both estimation algorithms to be executed at the same time while maximum use is made of common information requirements.

Figure 4-15 contains a record description of two complex channel processes. For simplicity, suppose a statistical description of only segment D of the vertical channel data is required. Assume that lag results are required from -512 to +511. Let $\mathcal{F}$ represent the forward FFT and let $\mathcal{F}^{-1}$ represent the inverse operation. Defining the following quantities:

$$\begin{aligned} FA &= \mathcal{F}(A) & FD &= \mathcal{F}(D) \\ FB &= \mathcal{F}(B) & FVIP &= \mathcal{F}(V_i') \\ FC &= \mathcal{F}(C) & FVI1P &= \mathcal{F}(V_{i+1}') , \end{aligned}$$

then,

$$\text{NEGATIVE LAGS} = {}_0\lfloor\mathcal{F}^{-1}(FA \cdot FVIP^*)\rfloor_{511} + {}_0\lfloor\mathcal{F}^{-1}(FB \cdot FVI1P^*)\rfloor_{511} \qquad (4\text{-}58)$$

$$\text{POSITIVE LAGS} = {}_0\lfloor\mathcal{F}^{-1}(FB \cdot FVIP^*)\rfloor_{511} + {}_0\lfloor\mathcal{F}^{-1}(FC \cdot FVI1P^*)\rfloor_{511} \qquad (4\text{-}59)$$

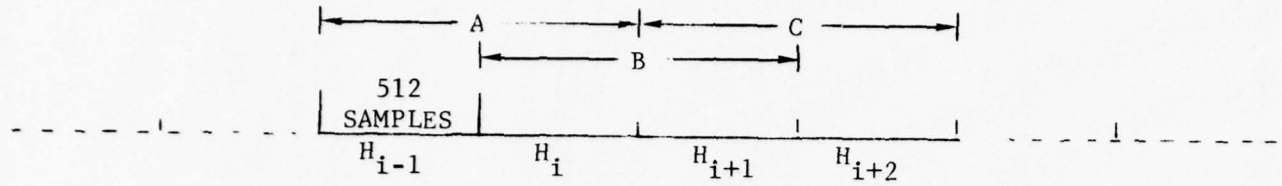


HORIZONTAL CHANNEL DATA

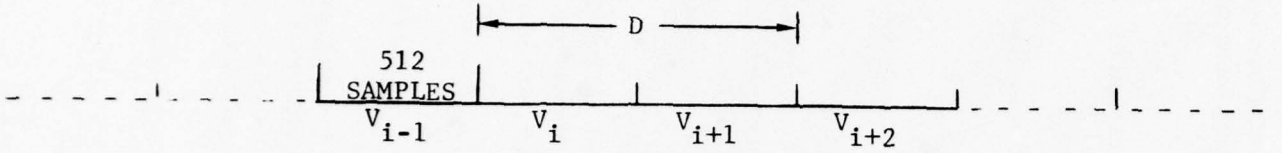


VERTICAL CHANNEL DATA

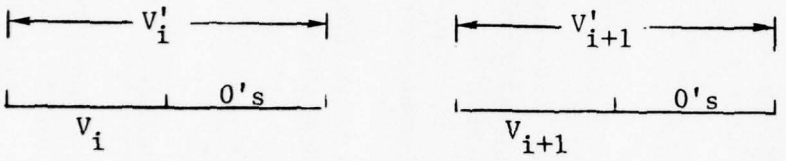


*Figure 4-15. H and V Record Structure*

where the $\lfloor \cdot \rfloor_{511}$ indicates that the first half of the inverse transform is to be used. The last half of the inverse transform contains aliased correlation information and, therefore, is useless. Cross-spectral density information is easily derived by noting that

$$FD(k) = FVIP(k) + (-1)^k FVIIP(k), \tag{4-60}$$

where explicit indexing notation has been introduced for clarity. Thus, FD is easily derived by a set of adds and subtracts

$$\text{Unsmoothed spectral density} = FB \cdot FD^*. \tag{4-61}$$

A data window has not been used, to allow the use of common FFT operations for both estimation procedures. As a result, it is necessary to use a spectral window for spectral density side-lobe suppression. Since cross-spectral estimates are often characterized by a sinusoidal structure, it is necessary to choose a spectral window free of negative excursions to avoid resonance. For this reason, a PARZEN window is employed.

It is clear that if this procedure is followed for NTAPC sets of horizontal-vertical channel tap processes, all the information required for intertap covariance estimates is present in transform representation. Only one additional FFT per channel per record is required for each intratap covariance desired.

### 4.21.3 Flow Chart

A flow chart for the basic program processing loop is detailed in figure 4-16. The terms W, X, Y, Z represent data storage arrays of length equivalent to two tap transposition records. The notation $\lfloor \cdot \rfloor$ denotes that the first half of the data is to be extracted. The notation $\lceil \cdot \rceil$ means that the first half of the data is to be extracted and then shifted in index by one record length. The equation

$$W = \lfloor X \rfloor + \lceil Y \rceil, \tag{4-62}$$

indicates that the first half of W is the same as the first half of X while the second half of W is the same as the first half of Y.

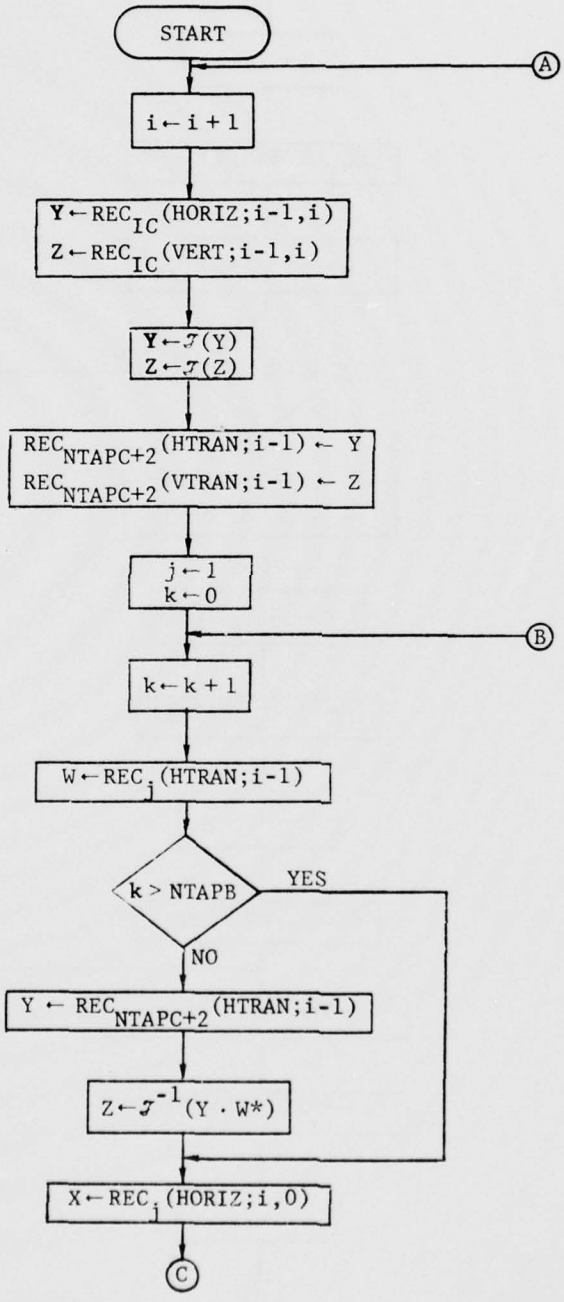


*Figure 4-16. H,V Processing Flow Chart*

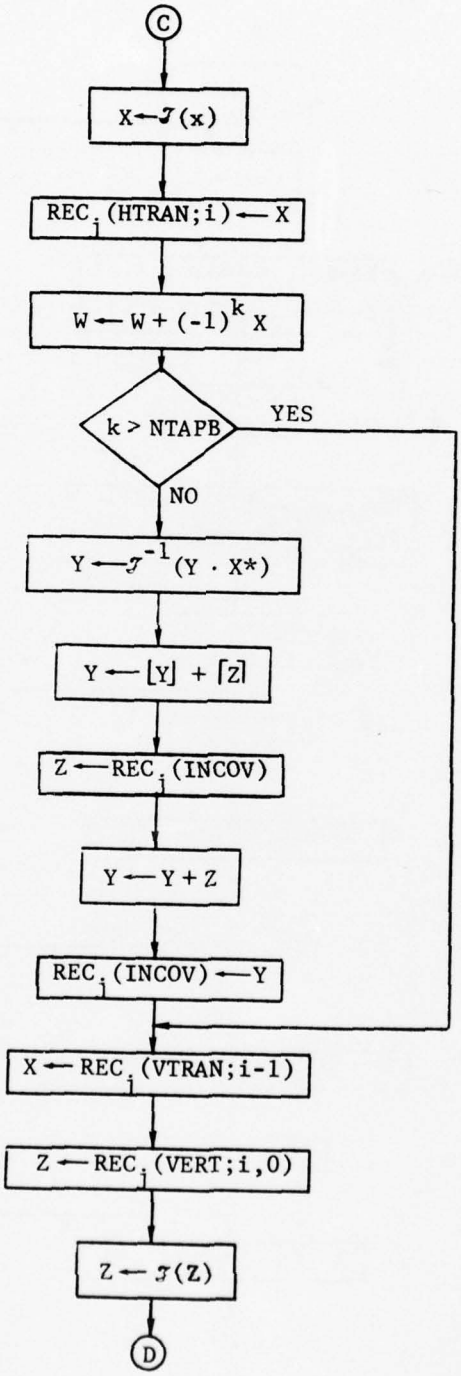


*Figure 4-16. (Continued)*

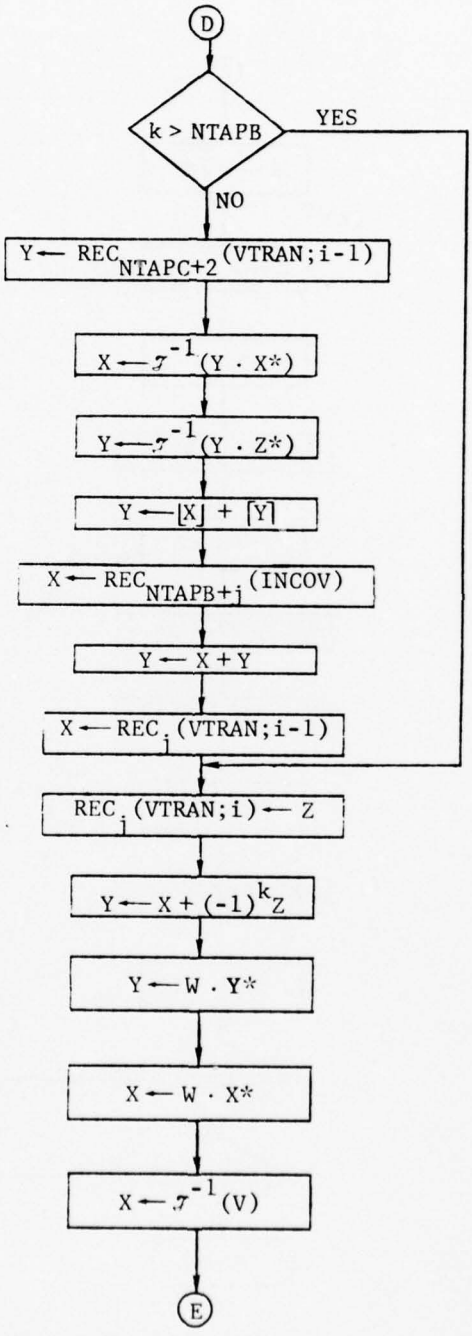


*Figure 4-16. (Continued)*

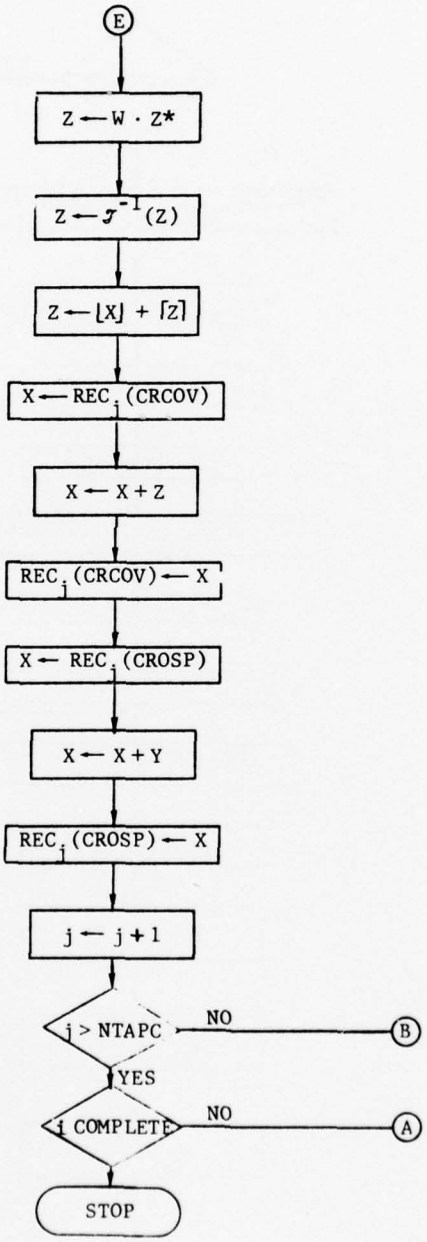


*Figure 4-16. (Concluded)*

Smoothing operations are not explicitly indicated on the flow chart because they are done outside the loop. The flow chart assumes that processing of record i is occurring and that HTRAN.DAT and VTRAN.DAT contain transform information corresponding to the record i-1. In addition, the file transfer indication

$$W \leftarrow REC_{IC}(HORIZ; i; i+1), \tag{4-63}$$

means that records i and i+1 for record IC in file HORIZ.DAT are to be transferred to W. This notation is adopted for convenience only since the data buffering required make the fetch operations much more involved. The notation

$$W \leftarrow REC_{IC}(HORIZ; i, 0), \tag{4-64}$$

means that the second record transferred to W is identically zero. Tap IC is an index of the pivot tap specified by the user.

## 4.22 DIGITAL TAPE FORMATS

Three digital magnetic tapes are created in the overall multipath algorithm execution sequence. Referred to as D1, D2, and D3 in figure 3-1, these tapes are described below.

### 4.22.1 D1: The Reformatted Digital Tape

This tape contains the reformatted SACP frame words together with merged time code, frame count, frame lock loss count, parity error count, and a parity error directory. All physical records written on the tape have a length equal to 12 of the above data sets. A data set is comprised of 292 eight-bit bytes as described in table 4-3.

The frame counter starts at 0 at the first frame of a file and is increased by 1 for every input frame of the file. A file is used to contain the data for one test condition.

The lock loss counter starts at 0 and is incremented by 1 for each frame lock loss encountered in the TFE equipment when data is input from the analog tape.

*TABLE 4-3. FORMAT OF REFORMATTED DIGITAL TAPE, D1*

| Byte number | Number of words | Bits per word | Word description |
|---|---|---|---|
| 1-2 | 1 | 16 | Frame counter |
| 3-4 | 1 | 16 | Lock loss count |
| 5-6 | 1 | 16 | Parity error count |
| 7-8 | 1 | 16 | Data track and polarization |
| 9-12 | 3 | 16 | Merged time code |
| 13-22, 24 | 11 | 8 | Receiver parameters |
| 23 | 1 | 8 | Parity error tipoff |
| 25-36 | 12 | 8 | Direct tap samples |
| 37-260 | 224 | 8 | Indirect tap samples |
| 261-262 | 2 | 8 | Subframe data and index |
| 263-292 | 31 | 8 | Parity error directory |

The parity error count gives the number of parity errors (from the analog input) detected in the frame.

The correspondence between data set byte number and SACP receiver parameter word number is:

| | | | | | | | | | | | |
|---|---|---|---|---|---|---|---|---|---|---|---|
| Data set byte | 14 | 13 | 16 | 15 | 18 | 17 | 20 | 19 | 22 | 21 | 24 |
| SACP receiver word | 1 | 2 | 3 | 4 | 5 | 6 | 7 | 8 | 9 | 10 | 11. |

The SACP receiver words are described in section 4.10.

The data track and polarization descriptors are encoded as numeric and ASCII words; they occupy the first four bits of the $7^{th}$ and $8^{th}$ data set bytes, respectively.

The merged-time code words are encoded as shown in table 4-4.

The parity error tipoff byte is encoded as 0 if no parity errors were detected in the frame; it is nonzero otherwise. The parity error directory contains encoded addresses where parity errors were detected – one per 16-bit word. The addresses are decoded as follows: receiver parameters are numbered $130_{10}$ to $120_{10}$ (descending); the taps are numbered $119_{10}$ to 1 where each value corresponds to a Q,I point pair. The last entry in the table is followed by a word containing -1.

The direct tap samples are in the order:

Q1, I1, Q4, I4, Q2, I2, Q5, I5, Q3, I3, Q6, I6.

*TABLE 4.4. MERGED-TIME CODE FORMAT*

| Bytes | Bit 15 14 13 12 | 11 10 9 8 | 7 6 5 4 | 3 2 1 0 |
|---|---|---|---|---|
| 9, 10 | Units BCD seconds | Hundreds | Tens BCD milliseconds | Units |

| Bytes | Bit 15 14 | 13 12 11 10 | 9 8 7 | 6 5 4 3 | 2 1 0 |
|---|---|---|---|---|---|
| 11, 12 | Tens | Units BCD hours | Tens | Units BCD minutes | Tens BCD seconds |

The indirect tap samples are in the order:

$$Q1,\ I1,\ Q57,\ I57,\ Q2,\ I2, \ldots, Q56,\ I56,\ Q112,\ I112.$$

The subframe data word is blank whereas the index counts from 0 to 5 and then recycles.

4.22.2 D2: The $S_n(\tau,\omega)$ Save Tape

Tape D2 contains the noise-present estimate of the scatter channel's delay-Doppler function. Also present on the tape is a directory that lists the identity of the data on the files. The directory file delineates the identification, creation date, and time associated with all the tape files. Each $S_n(\tau,\omega)$ array occupies its own tape file. The scatter function array is accompanied by data and polarization test descriptors plus the receiver and analog tape status parameters that occur at the beginning and end of the sample space interval. Under the CDC 6600 KRONOS 2.1 operating environment, the following FORTRAN binary write statements fully describe the data arrangement of each $S_n(\tau,\omega)$ file:

```
      WRITE (IU) (BUF(I), I=1,20)
      WRITE (IU) (BUF(I), I=1,20), (TIT(I), I=1,4)
      WRITE (IU) NFREQ, NTAP
      WRITE (IU) (FR(I), I=1, N FREQ)
      WRITE (IU) (TNB(I), I=1, NTAP)
      DO 10 I=1, NTAP
10    WRITE (IU) (SF(J,I), J=1, NFREQ)
```

IU is the FORTRAN output unit (2).

BUF is an array of 20 words. These contain the receiver and analog tape status parameters associated with the first frame of the ensemble used to calculate the scatter function.

BUF1 is an array of 20 words corresponding to the receiver and analog tape status parameters associated with the end of the sample space.

TIT is a four-word array identifying date and polarization of the test condition.

NFREQ is the number of frequency points saved from the periodogram output.

NTAP is the number of taps processed.

FR is the frequency array in hertz.

TNB is the tap number array.

SF is the scatter function array with SF(1,1) corresponding to FR(1), TNB(1)
SF(2,1) FR(2), TNB(1)
SF(1,2) RF(1), TNB(2).

### 4.22.3 D3: The Delay-Spectra Time History Storage Tape

Tape D3 is used primarily to contain the record elements of the delay-spectra time history array. It is generated by the quick-look process algorithm, with each subinterval condition's output being written as a separated physical record. The record structure is as shown in table 4-5. A tape file is used to contain all the records for a particular test condition.

## 4.23 AIRBORNE SYSTEM PARAMETERS

In its normal mode of operation, the multipath prober test utilizes wideband PN-PSK sequence transmissions from the KC-135 aircraft. Airborne system parameters necessary for proper interpretation and normalization of multipath scatter return include (1) modulator mode characteristics, (2) aircraft pitch, roll, heading, groundspeed, and altitude, (3) aircraft location, (4) antenna mode and polarization, and (5) RF power input levels at the antennas. With the exception of aircraft location, which is obtained from a manual log of INS waypoints, these data are recorded over all flight test intervals during which scatter channel probing takes place. In this section the recorded parameters, the recording format, and the data conversion are described.

*TABLE 4-5. FORMAT OF DELAY-SPECTRA TIME HISTORY TAPE, D3*

| Byte number | Number of words | Bits per word | Description |
|---|---|---|---|
| 1-24 | 24 | 8 | Receiver and analog tape status data at start of test subinterval (see bytes 1-24 of D1) |
| 25-48 | 24 | 8 | Receiver and analog tape status data at end of test subinterval |
| 49-272 | 112 | 16 | Indirect tap frequency-spread in the order: Tap 1, tap 57, tap 2, tap 58, . . . , tap 56, tap 112 |
| 273-296 | 6 | 32 | Direct tap delay spectra in the order: Tap 1, tap 4, tap 2, tap 5, tap 3, tap 6 |
| 297-742 | 112 | 32 | Indirect tap delay spectra in the order: Tap 1, tap 57, tap 2, . . . , tap 112 |

4.23.1 Recorded Parameters and Recording Format

Airborne system parameters are recorded on computer-compatible 800-bpi, seven-track tape (six bits plus parity) using a Kennedy 8707 recorder. Byte size is six bits. Data is segregated into records containing 484 bytes. The record format is given in table 4-6.

Apart from the time code words, the sixth bit of each data byte contains no information. Thus, the power monitor data and aircraft parameters are digitized at a resolution level of 10 bits.

4.23.2 Data Conversion and Processing

Figure 4-17 illustrates the basic CDC 6600 software algorithm processing steps associated with reduction and analysis of the airborne system parameters tape. The first step involves unpacking, decommutation, and processing of the time-multiplexed calibration signals, which in general will precede the airborne system data. The calibration file is analyzed to yield upper and lower calibration levels for the appropriate channels. The signal data is subsequently processed according to the following paragraphs. (The output description is given in section 4.24.)

*TABLE 4-6. AIRCRAFT PARAMETERS RECORD FORMAT*

| Bytes | Description |
|---|---|
| 0-3 | IRIG-B time code |
| 4 | SACP modulator mode |
| 5 | RF subsystem mode |
| 6,7 | Spare (no data) |
| 8,9 | Internal power monitor, direct channel PA |
| 10,11 | Power meter, direct channel (HP 435A) |
| 12,13 | Internal power monitor, V channel PA |
| 14,15 | Power meter, V channel (HP 435A) |
| 16,17 | DC power supply, 100-W PA |
| 18,19 | Internal power monitor, H channel PA |
| 20,21 | Power meter, H channel (HP 435A) |
| 22,23 | Aircraft altitude (feet) |
| 24,25 | Aircraft coarse heading (degrees) |
| 26,27 | Aircraft fine heading (degrees) |
| 28,29 | Aircraft roll angle (degrees) |
| 30,31 | Aircraft pitch angle (degrees) |
| 32,33 | Aircraft ground speed (knots) |
| 34,35 | Spare (no data) |
| 36-483 | 15 additional scans of parameters contained in bytes 6 to 35 with the last scan truncated at aircraft groundspeed |

4.23.3 SACP Modulator Mode Code

The five data bits contained in the fourth byte of each record are used to designate the SACP modulator chip rate (bits 2,3,4) and code length (bits 0,1). Switches that set these parameters provide coded bits to the recording system according to table 4-7.

4.23.4 RF Subsystem Mode

The aircraft antenna and the nominal polarization over which SACP transmissions take place are delineated by the four least significant bits of the fifth record byte. Coding is shown in table 4-8.

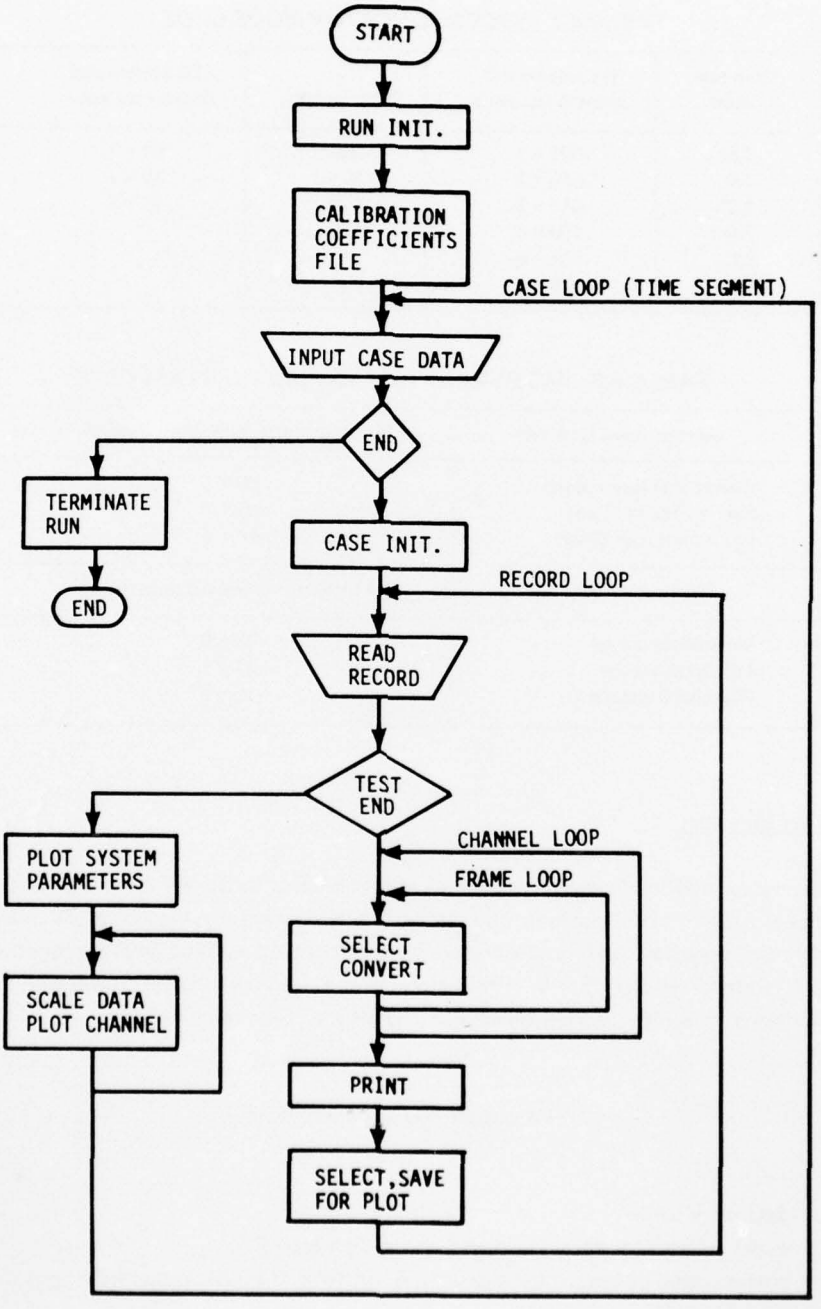


*Figure 4-17. Airborne Tape Processing – High-Level Program Algorithm*

*TABLE 4-7. SACP MODULATOR MODE CODE*

| Chip rate, Mbps | Bit pattern and decimal no. equiv | Code length | Bit pattern and decimal no. equiv |
|---|---|---|---|
| 0.5 | 001 = 1 | 255 | 01 = 1 |
| 1.0 | 010 = 2 | 511 | 10 = 2 |
| 1.25 | 011 = 3 | 1023 | 11 = 3 |
| 2.5 | 100 = 4 | | |
| 5.0 | 101 = 5 | | |
| 10.0 | 110 = 6 | | |

*TABLE 4-8. ANTENNA TYPE AND POLARIZATION CODE*

| Antenna type (bits 1,2) | Bit pattern and decimal no. equivalent |
|---|---|
| Operational (slot-dipole) | 00 = 0 |
| Side multipath (SMP) | 01 = 1 |
| Front multipath (FMP) | 10 = 2 |
| **Polarization (bits 3,4)** | **Bit pattern and decimal no. equivalent** |
| Vertical/horizontal | 00 = 0 |
| Left-hand circular | 01 = 1 |
| Right-hand circular | 10 = 2 |

4.23.5 Power Monitors

With the exception of the three power monitors internal to the RF amplifiers used for the direct, horizontal, and vertical channels, the recorded power monitor values from the external RF power meters are converted directly to a voltage level and output without further reduction, i.e., output voltage = (word value/$2^9$) x 5.0 V. The internal power monitor data are converted to their respective channel power amplifier readings through the following linear relationship:

$$\text{PA output} = (X/UC)A, \text{ watts,}$$

where:

X = data word value

UC = upper calibration signal (recorded on the first tape file)

A = power amplifier output (as measured when calibration file is created, input to routine via data card).

4.23.6 Aircraft Parameters

Aircraft groundspeed is derived through the following relationship:

$$\text{Groundspeed} = (X/512)(500), \text{ knots},$$

where x is the data word value.

All the other aircraft parameters are obtained through use of the following relationship:

$$\text{A/C parameter} = \frac{X - LC}{UC - LC}(A_1 - A_2) + A_2,$$

where:

- X = data word value
- UC = upper calibration voltage level
- LC = lower calibration voltage level
- $A_1$ = parameter value corresponding to UC
- $A_2$ = parameter value corresponding to LC.

The UC and LC values are obtained from the tape file containing calibration readings. The $A_1$ and $A_2$ values are set internally in the computer program and have been derived from information supplied by NAFEC.

As previoulsy noted, fine and coarse headings are components of the aircraft system parameters data. Fine heading varies from $0^o$ to $10^o$, whereas coarse heading is given over the full $360^o$ range. In general, the aircraft actual heading is obtained by rounding down the coarse reading to the nearest $10^o$ and then adding the fine heading. Due to calibration uncertainties, this procedure may cause large errors if the actual heading is close to a mod-$10^o$ value (e.g., if coarse heading reads 321 and fine heading reads 9, then the actual heading is undoubtably closer to $319^o$ than $329^o$). To circumvent such potential problems, the following logic may be applied to the output to derive the aircraft heading:

$$\text{A/C heading} \begin{cases} = CH_{rd} - 10 + FH & \text{for } \Delta+2 < FH \\ = CH_{ru} + FH & \text{for } \Delta-2 > FH \\ = CH_{rd} + FH & \text{otherwise}, \end{cases}$$

where:

$CH_{rd}$ = rounded-down (nearest $10^{o}$) coarse heading
$CH_{ru}$ = rounded-up (nearest $10^{o}$) coarse heading
FH = fine heading
$\Delta$ = $CH - CH_{rd}$ .

## 4.24 SAMPLE MULTIPATH ANALYSIS OUTPUT

In this section, sample numerical and plotted outputs are illustrated and described for each of the previously presented algorithms.

### 4.24.1 Quick-Look Analysis

Immediately following the processing of a quick-look test condition, the results are displayed in graphic and tabular form on the Tektronix 4012 display and Gould 4800 printer, respectively. An example of the numerical hard-copy output is given in table 4-9. The top line of the output delineates the analog tape description: name (e.g., AT 127), file, and record number from which the data was dumped. We then have two rows of data words corresponding to the analog tape and SACP receiver parameters (see sec. 4.10 for the format description) as they existed at the beginning (start) and end (stop) of the subinterval sample space. Data arrays for the indirect tap frequency spread (titled DOPPLER), the direct delay psd (titled DIRECT DELAY), and the indirect tap bank delay psd (titled DELAY) follow the start/stop receiver parameters. The direct delay taps are interleaved and thus the row array represents tap 1, 4, 2, 5, 3, 6. The indirect tap Doppler and delay data are arranged in order, reading from left to right on a row-by-row basis (each row is preceded by the tap number associated with the adjacent data value). As indicated in section 4.1, the quick-look results are unnormalized for the size of the sample space. For the example output presented, a 2-sec sample space was processed and the sampling rate was approximately 610 $sec^{-1}$. Thus, for normalization, the frequency-spread data is divided by 2 and the delay spectra data by 305 (only every fourth point is processed for delay-spectra calculation).

The 4012 quick-look display presents a graph of the numerical data arrays described above. The fields (e.g., DOPPLER, DIRECT DELAY, and DELAY) are separately and automatically scaled to improve detail and resolution. Up to five subinterval segments may be displayed at one time. The data field arrangement is shown in figure 4-18. For this particular example, the indirect taps are occupied not only by multipath return but also by the direct signal from the multipath prober antenna, located roughly at tap 10.

AD-A041 864 BOEING COMMERCIAL AIRPLANE CO SEATTLE WASH F/G 9/5
AIR TRAFFIC CONTROL EXPERIMENTATION AND EVALUATION WITH THE NAS--ETC(U)
SEP 76 A D THOMPSON, S C WILSON, P F RIEDER DOT-TSC-707-4
UNCLASSIFIED D6-44049 FAA RD-75-173-4 NL

2 OF 3
ADA041864

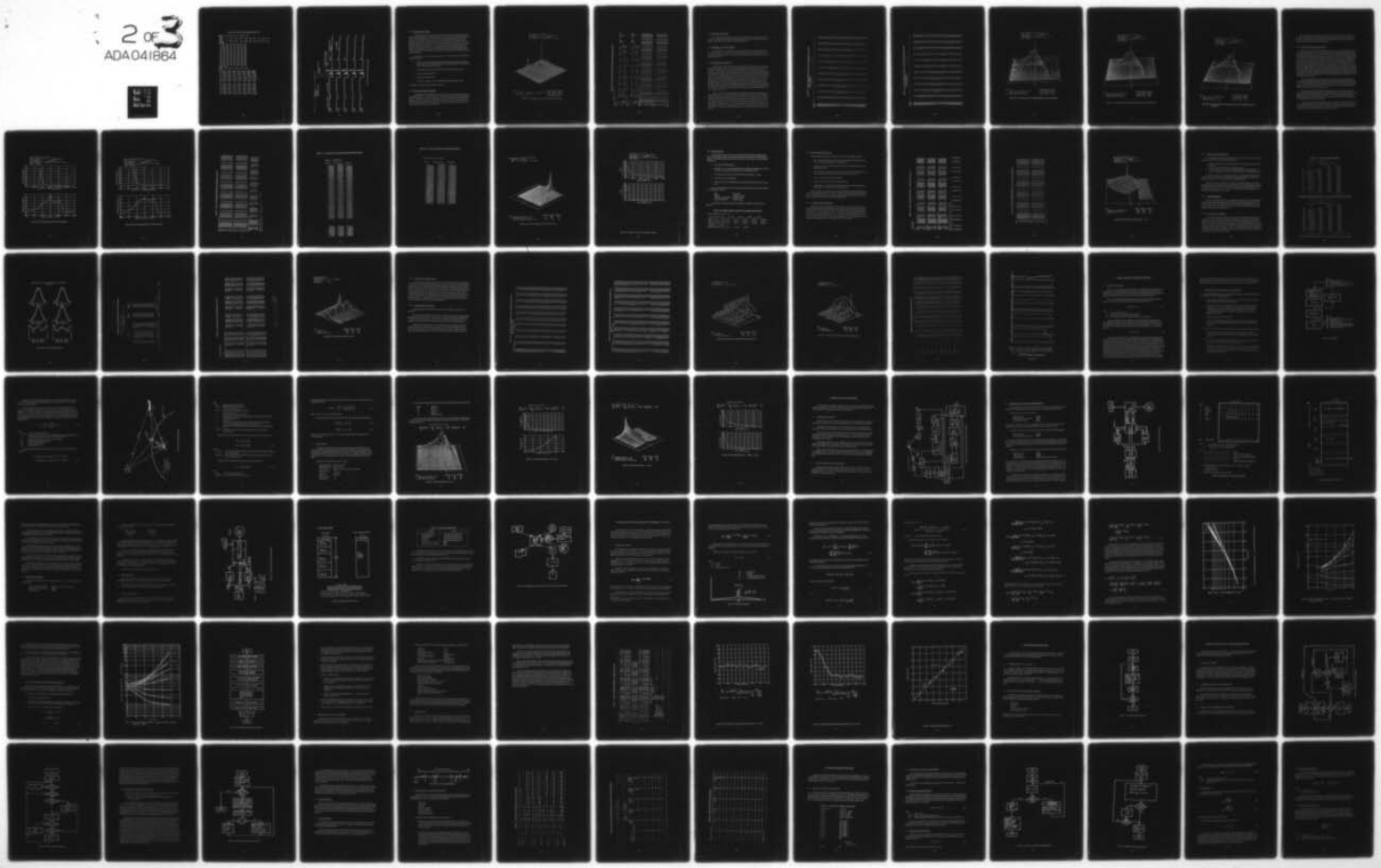

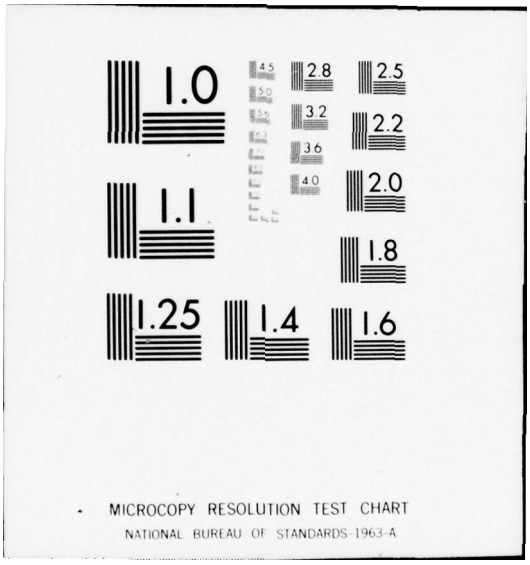
1.0
1.1
1.25
1.4
1.6
1.8
2.0
2.2
2.5
2.8
3.2
3.6
4.0
4.5
5.0
MICROCOPY RESOLUTION TEST CHART
NATIONAL BUREAU OF STANDARDS-1963-A

*TABLE 4-9. QUICK-LOOK NUMERICAL OUTPUT*

```
TAPE AT  127 DUMP OF FILE  0, RECORD  340
START
  52644  0  0  44003  10564  21112  20020 -4057 -4003  4144  20111  304
STOP
  55150  0  0  44003  30561  21112  20020 -4057 -4003  4144  21111  304
DOPPLER
  1  594  611  634  604  646  596  646
  8  626  658  643  652  652  617  623
  15  656  645  637  651  666  633  650
  22  634  628  636  622  625  649  634
  29  642  633  664  644  645  612  642
  36  646  613  316  300  403  453  480
  43  545  554  571  598  646  622  610
  50  598  607  631  620  624  648  596
  57  613  644  608  592  676  647  622
  64  602  641  633  609  626  647  625
  71  609  622  629  598  644  610  638
  78  642  646  621  665  638  633  661
  85  635  631  663  637  629  615  657
  92  620  624  623  609  622  621  667
  99  642  648  600  622  633  657  634
  106  647  660  637  613  686  655  617
DIRECT DELAY
  2344  4904  1211969  2025  1294765  1876
DELAY
  1  37153  35532  37351  34181  35575  32679  38228
  8  34824  36381  32309  34641  36957  33283  35558
  15  37384  35228  35280  38244  33815  34777  36987
  22  37791  38298  34363  37679  34772  36362  39355
  29  35011  35059  32871  37131  39159  41732  33432
  36  34091  36636  152195  140635  66293  77420  62704
  43  52545  53936  46029  45969  45446  44437  39076
  50  41254  39261  35420  35475  39624  40292  39543
  57
  57  39154  35862  33564  36346  40120  38077  38485
  64  35548  36028  37567  36430  35585  33199  33191
  71  39234  40506  34093  33746  35609  30427  36106
  78  35164  33092  31709  38841  38544  36661  34155
  85  35720  35806  35238  35693  33033  39445  36648
  92  32413  36277  33906  35268  32750  34713  34342
  99  37445  36060  32386  32321  35047  33755  36339
  106  38203  36014  38568  35987  34622  203159  35307
```

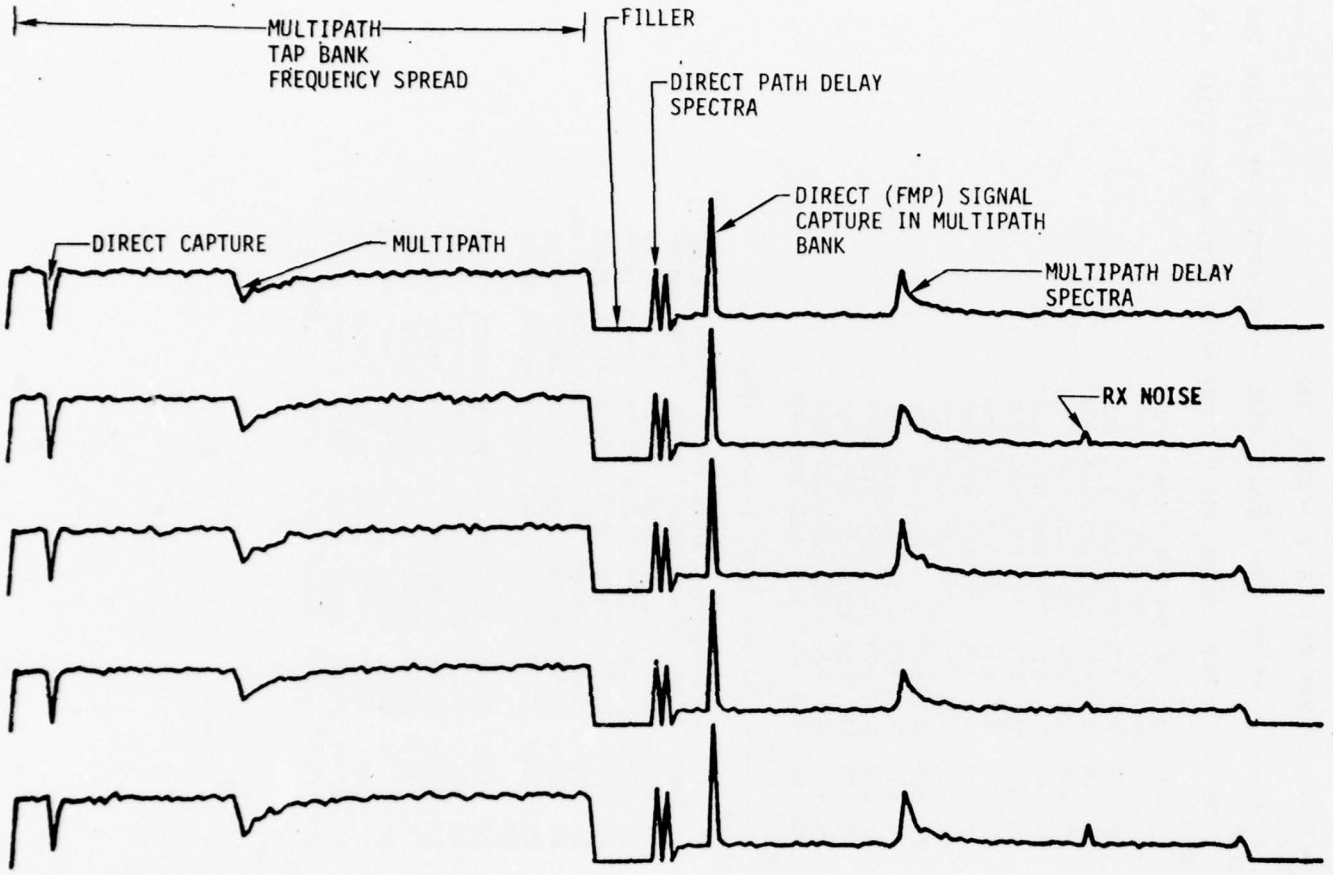


*Figure 4-18. Quick-Look Graphical Display*

### 4.24.2 Delay-Spectra Time History

Three-dimensional plots with hidden lines removed and numerical output representations are provided for the delay-spectra time history distribution. Figure 4-19 represents a sample plotted output for a overland CONUS data run. The plot title contains information pertaining to test data, polarization, tap resolution or width, and the time interval over which the time history is plotted. Typically, the subintervals over which a delay spectrum is calculated are on the order of 2 sec, and 60 distributions per graph are usually plotted. Thus, the time interval subtended spans roughly 2 min. The grid is labeled according to the (x,y,z) coordinate system, with axis descriptors given at the bottom of the output page. This form of axis description is used to facilitate the labeling software required to support the option available in the 3-D program that allows for the arbitrary choice of any desired point of view.

Corresponding to each subinterval delay spectrum is a set of numerical output containing the following information:

a. Receiver and analog tape status parameters corresponding to conditions existing at the beginning and end of the subinterval over which the following parameters are determined (see following paragraph for description)

b. The frequency-spread estimate associated with each of the indirect channel taps

c. The direct-tap bank delay spectra

d. The indirect-tap delay spectra

e. The total rms energies in the direct and multipath tap banks (signal plus noise).

An example of a numerical output is presented in table 4-10.

### 4.24.3 Receiver and Analog Tape Parameters

A typical output from the algorithm that analyzes the SACP receiver and analog tape parameters is given in table 4-10. The output begins with a descriptor indicating the track designation from which the analog data was extracted. Following are two rows of parameters delineating the receiver status descriptors, the time merged from the IRIG-A time code track, the frame counter, the frame lock loss counter, and the parity error counter. The counters are referenced to the first frame processed for a given test condition on the PDP 11/45.

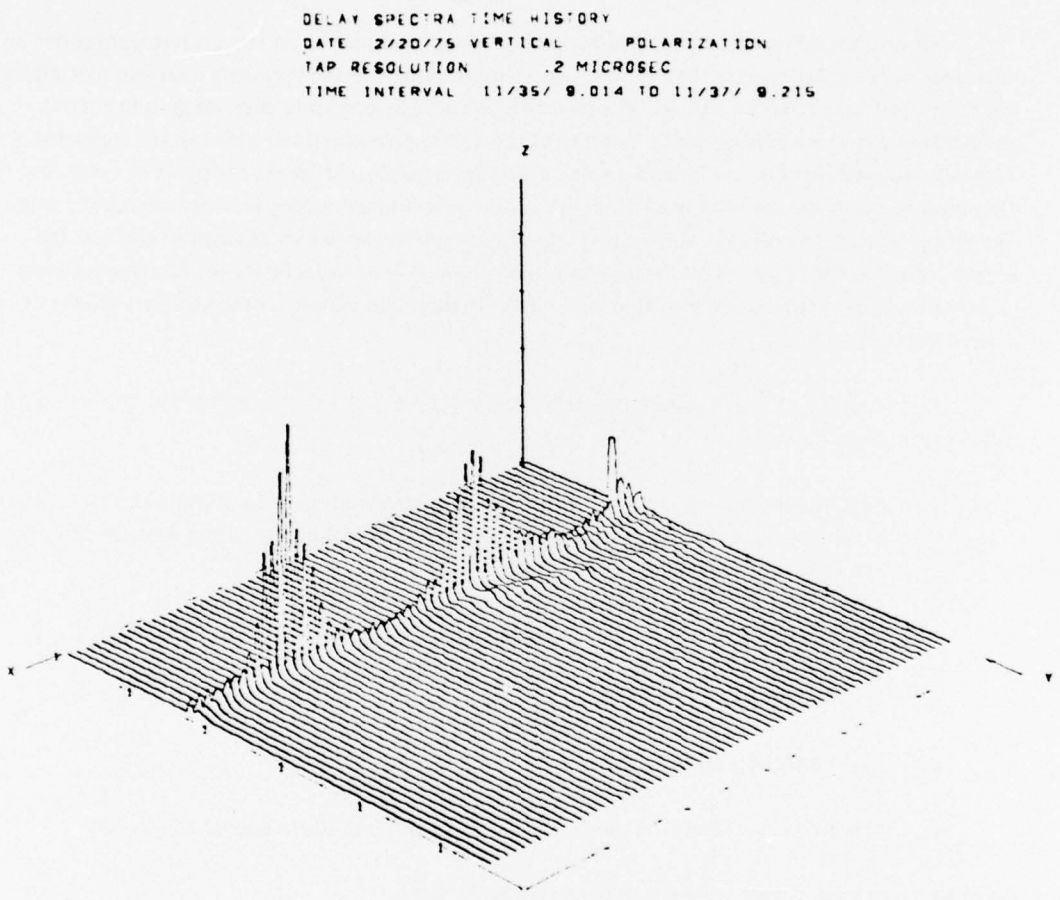


| AXIS | | MINIMUM | MAXIMUM | INCREMENT |
|---|---|---|---|---|
| X | EXPERIMENT TIME RELATIVE TO T-START(SEC) | 0.00 | 120.00 | 20.00 |
| Y | DELAY TAP ( .2 MICROSEC. WIDTH) | 0.00 | 120.00 | 20.00 |
| Z | DELAY PSD (LINEAR) | 0.001 | 5000.00 | 3000.00 |

*Figure 4-19. Three-Dimensional Plot of Delay-Spectra Time History*

## TABLE 4-10. DELAY-SPECTRA TIME HISTORY NUMERICAL OUTPUT

2/18/75 HORIZONTAL
RECORD 24 ------

TRACK 3

| TIME | SYSTEM CONFIG | ANTENA MODE | BIT RATE MB/S | BANDWITH HZ | DELTA L BITS | EARLY/ LATE | SCALE F. DIR | SCALE F. IND | D/I SC. FAC | OPERATUR MODE | FREQ LOOP MODE |
|---|---|---|---|---|---|---|---|---|---|---|---|
| 12/40/46 | A/C XMIT | MUX | 5. | 300 | 80 | T | .00781 | .12500 | .06250 | RUN | AUTO |

| MERGED TIME | TIME LOOP MODE | FR.LOOP THRESH | FR.LOOP THRESH | FR.LOOP D/A (V) | TIME LOOP D/A (V) | INT CLK PLL | FRAME COUNTER | LOCK LOSS FREQ | PAR.ER COUNT |
|---|---|---|---|---|---|---|---|---|---|
| 12/40/46.4950 | AUTO | 32.0000 | ABOVE | 6.28E+04 | 3 | LOCKED | 43531 | 0 | 0 |

TRACK 3

| TIME | SYSTEM CONFIG | ANTENA MODE | BIT RATE MB/S | BANDWITH HZ | DELTA L BITS | EARLY/ LATE | SCALE F. DIR | SCALE F. IND | D/I SC. FAC | OPERATOR MODE | FREQ LOOP MODE |
|---|---|---|---|---|---|---|---|---|---|---|---|
| 12/40/48 | A/C XMIT | MUX | 5. | 300 | 80 | T | .00781 | .12500 | .06250 | RUN | AUTO |

| MERGED TIME | TIME LOOP MODE | FR.LOOP THRESH | FR.LOOP THRESH | FR.LOOP D/A (V) | TIME LOOP D/A (V) | INT CLK PLL | FRAME COUNTER | LOCK LOSS FREQ | PAR.ER COUNT |
|---|---|---|---|---|---|---|---|---|---|
| 12/40/48.4920 | AUTO | 32.0000 | ABOVE | 6.30E+04 | 3 | LOCKED | 44751 | 0 | 0 |

INDIVIDUAL TAP DOPPLER SPREAD

| | | | | | | | | | | | | | | | | | | | |
|---|---|---|---|---|---|---|---|---|---|---|---|---|---|---|---|---|---|---|---|
| 1 | 326.00 | 2 | 324.00 | 3 | 315.00 | 4 | 312.50 | 5 | 312.50 | 6 | 323.50 | 7 | 328.00 | 8 | 328.50 | 9 | 309.50 | 10 | 314.50 |
| 11 | 313.00 | 12 | 309.00 | 13 | 313.50 | 14 | 327.50 | 15 | 328.00 | 16 | 330.50 | 17 | 299.00 | 18 | 328.50 | 19 | 323.00 | 20 | 323.00 |
| 21 | 305.00 | 22 | 308.50 | 23 | 313.00 | 24 | 313.50 | 25 | 339.50 | 26 | 330.50 | 27 | 322.00 | 28 | 319.50 | 29 | 325.50 | 30 | 317.00 |
| 31 | 326.50 | 32 | 309.50 | 33 | 330.00 | 34 | 308.50 | 35 | 91.00 | 36 | 326.00 | 37 | 314.50 | 38 | 320.00 | 39 | 312.00 | 40 | 328.00 |
| 41 | 313.00 | 42 | 102.00 | 43 | 86.50 | 44 | 156.00 | 45 | 211.50 | 46 | 179.50 | 47 | 246.00 | 48 | 260.50 | 49 | 241.50 | 50 | 255.00 |
| 51 | 290.00 | 52 | 272.50 | 53 | 294.00 | 54 | 302.00 | 55 | 311.00 | 56 | 294.00 | 57 | 292.00 | 58 | 305.50 | 59 | 308.00 | 60 | 288.00 |
| 61 | 300.00 | 62 | 308.00 | 63 | 291.00 | 64 | 308.00 | 65 | 296.50 | 66 | 312.00 | 67 | 312.50 | 68 | 314.00 | 69 | 311.00 | 70 | 312.00 |
| 71 | 299.00 | 72 | 297.50 | 73 | 314.00 | 74 | 314.50 | 75 | 319.00 | 76 | 315.00 | 77 | 331.50 | 78 | 294.50 | 79 | 306.00 | 80 | 317.00 |
| 81 | 324.00 | 82 | 303.50 | 83 | 300.00 | 84 | 316.00 | 85 | 305.00 | 86 | 308.00 | 87 | 309.00 | 88 | 306.50 | 89 | 312.00 | 90 | 290.00 |
| 91 | 310.00 | 92 | 303.50 | 93 | 321.00 | 94 | 296.50 | 95 | 302.00 | 96 | 334.50 | 97 | 314.50 | 98 | 317.00 | 99 | 327.50 | 100 | 319.00 |
| 101 | 300.00 | 102 | 307.00 | 103 | 329.50 | 104 | 304.50 | 105 | 302.50 | 106 | 319.00 | 107 | 308.00 | 108 | 301.50 | 109 | 323.00 | 110 | 313.50 |
| 111 | 300.00 | 112 | 313.00 | | | | | | | | | | | | | | | | |

DIRECT DELAY PSD

| | | | | | | | | | | | | | | | | | | | |
|---|---|---|---|---|---|---|---|---|---|---|---|---|---|---|---|---|---|---|---|
| 1 | 1.80 | 2 | 7320.34 | 3 | 6741.80 | 4 | 12.37 | 5 | 1.83 | 6 | 2.14 | | | | | | | | |

INDIRECT DELAY PSD

| | | | | | | | | | | | | | | | | | | | |
|---|---|---|---|---|---|---|---|---|---|---|---|---|---|---|---|---|---|---|---|
| 1 | 27.23 | 2 | 25.15 | 3 | 25.41 | 4 | 27.69 | 5 | 29.01 | 6 | 28.37 | 7 | 29.07 | 8 | 27.67 | 9 | 25.38 | 10 | 31.89 |
| 11 | 34.19 | 12 | 29.24 | 13 | 31.45 | 14 | 29.88 | 15 | 28.62 | 16 | 26.93 | 17 | 28.16 | 18 | 29.72 | 19 | 30.55 | 20 | 27.24 |
| 21 | 30.58 | 22 | 30.12 | 23 | 27.14 | 24 | 31.32 | 25 | 26.65 | 26 | 25.52 | 27 | 24.25 | 28 | 31.60 | 29 | 30.30 | 30 | 29.86 |
| 41 | 29.87 | 42 | 285.32 | 43 | 366.46 | 44 | 164.22 | 45 | 78.29 | 46 | 71.14 | 47 | 46.37 | 48 | 32.86 | 49 | 55.52 | 50 | 52.43 |
| 51 | 37.10 | 52 | 43.42 | 53 | 41.47 | 54 | 37.45 | 55 | 34.48 | 56 | 38.34 | 57 | 34.15 | 58 | 32.85 | 59 | 30.94 | 60 | 34.90 |
| 61 | 32.35 | 62 | 31.45 | 63 | 33.60 | 64 | 33.50 | 65 | 35.26 | 66 | 29.51 | 67 | 31.43 | 68 | 27.19 | 69 | 31.30 | 70 | 28.82 |
| 71 | 31.73 | 72 | 31.08 | 73 | 28.33 | 74 | 33.25 | 75 | 28.18 | 76 | 34.61 | 77 | 30.10 | 78 | 30.47 | 79 | 32.83 | 80 | 31.04 |
| 81 | 46.78 | 82 | 33.31 | 83 | 29.43 | 84 | 31.77 | 85 | 31.30 | 86 | 28.45 | 87 | 30.86 | 88 | 29.62 | 89 | 30.27 | 90 | 29.27 |
| 91 | 30.22 | 92 | 32.66 | 93 | 29.91 | 94 | 33.20 | 95 | 28.31 | 96 | 32.62 | 97 | 29.90 | 98 | 28.20 | 99 | 29.62 | 100 | 30.43 |
| 101 | 29.71 | 102 | 31.93 | 103 | 34.05 | 104 | 29.75 | 105 | 31.61 | 106 | 30.49 | 107 | 33.29 | 108 | 33.42 | 109 | 29.76 | 110 | 31.88 |
| 111 | 162.62 | 112 | 29.34 | | | | | | | | | | | | | | | | |

RMS DIR,INDIR 118.757 27.223

### 4.24.4 Mean Square Direct Energy

The mean square direct energy is calculated within the program loop that performs the $S(\tau,\omega)$ calculation. A numerical output from this algorithm is provided at the end of the total ensemble calculation. An example of such an output is included in section 4.24.7.

### 4.24.5 Delay-Spectra Time-Domain Analysis

As mentioned in section 4.9, the delay spectra as determined from a time-domain analysis of the complex tap outputs are calculated to serve as an integrity check on the delay-Doppler function and associated integral operations. The output from this algorithm is given numerically and is treated further in section 4.24.7.

### 4.24.6 Delay-Doppler Scatter Function

Identical output formats are used for the noise-present and noise-free estimates of the scatter channel's delay-Doppler function. Numerical and three-dimensional plotted outputs (with or without the removal of hidden lines) are used to represent this function. Examples of numerical output segments are given in table 4-11 (noise present) and table 4-12 (noise removed). The page begins with a heading descriptor delineating test date, polarization, and whether the estimate is noise free. Following is the $S(\tau, \omega)$ array presented in matrix form. The left-hand column corresponds to the frequency in hertz of the smoothed periodogram output. This is given once every $W_{1/2}\Delta f$ hertz, where $W_{1/2}$ is the half width of the spectra smoothing window and $\Delta f$ is the unsmoothed periodogram output sampling rate that is equal to the frame rate divided by the number of complex points used for the FFT input. With the exception of the frequency delineator, the top row of the matrix corresponds to the delay tap number associated with the PSD (linear relative watts) given in the below column. From these figures it is seen that the form of the numerical output gives an easily recognized display of the $S(\tau,\omega)$ energy concentration.

Figures 4-20 and 4-21 represent examples of the hidden-line-removed, three-dimensionally plotted outputs of $S(\tau,\omega)$ for the noise-present and noise-removed cased, respectively. The hidden-line-present plot for the noise-removed case is given in figure 4-22. Each plot contains a title describing the test date, polarization, tap width or resolution, time interval over which the scatter function was calculated, and whether the plot corresponds to a noise-removed or noise-present estimate. The grid is labeled according to the (x,y,z) coordinate systems, with axis labels given at the bottom of the output page. This form of axis description is used to facilitate the labeling software required to support the option available in the 3-D program that allows for the arbitrary choice of any desired point of view.

## TABLE 4-11. DELAY-DOPPLER SCATTER FUNCTION NUMERICAL OUTPUT (NOISE PRESENT)

2/27/75 - H C NOISE PRESENT

| FREQUENCY HERTZ | TAP 32 | TAP 33 | TAP 34 | TAP 35 | TAP 36 | TAP 37 | TAP 38 | TAP 39 | TAP 40 | TAP 41 | TAP 42 |
|---|---|---|---|---|---|---|---|---|---|---|---|
| -285.9 | .06 | .07 | .07 | .09 | .05 | .08 | .07 | .03 | .06 | .07 | .07 |
| -274.0 | .07 | .06 | .07 | .08 | .06 | .08 | .06 | .07 | .06 | .07 | .07 |
| -262.1 | .07 | .06 | .06 | .07 | .06 | .07 | .07 | .07 | .06 | .07 | .07 |
| -250.2 | .07 | .06 | .06 | .06 | .05 | .06 | .06 | .07 | .05 | .07 | .17 |
| -238.3 | .06 | .06 | .06 | .06 | .06 | .06 | .07 | .07 | .05 | .10 | .00 |
| -226.4 | .05 | .06 | .06 | .05 | .06 | .06 | .07 | .07 | .07 | .49 | 1.01 |
| -214.5 | .05 | .06 | .05 | .06 | .06 | .06 | .06 | .05 | .28 | 1.16 | .87 |
| -202.5 | .05 | .05 | .05 | .06 | .06 | .06 | .06 | .13 | 1.07 | 1.27 | .61 |
| -190.6 | .05 | .04 | .05 | .06 | .05 | .07 | .07 | .81 | 1.80 | .85 | .53 |
| -178.7 | .05 | .05 | .05 | .05 | .05 | .06 | .35 | 1.43 | 1.54 | .55 | .47 |
| -166.8 | .05 | .05 | .05 | .05 | .05 | .14 | 1.41 | 2.10 | .93 | .48 | .39 |
| -154.9 | .05 | .04 | .04 | .05 | .05 | .30 | 3.35 | 1.44 | .62 | .46 | .29 |
| -143.0 | .05 | .04 | .04 | .06 | .25 | 2.76 | 3.13 | 1.03 | .54 | .39 | .24 |
| -131.1 | .05 | .04 | .05 | .07 | 1.57 | 3.84 | 2.04 | .37 | .57 | .33 | .22 |
| -119.1 | .05 | .04 | .05 | .06 | 4.16 | 3.17 | 1.57 | .55 | .44 | .30 | .19 |
| -107.2 | .05 | .04 | .06 | 2.37 | 5.28 | 2.15 | 1.16 | .07 | .40 | .26 | .19 |
| -95.3 | .05 | .04 | .40 | 5.80 | 3.72 | 1.83 | .32 | .34 | .45 | .24 | .20 |
| -83.4 | .04 | .04 | 2.55 | 6.51 | 2.47 | 1.51 | .31 | .32 | .40 | .24 | .18 |
| -71.5 | .04 | .13 | 7.21 | 5.15 | 2.20 | 1.04 | .75 | .47 | .27 | .26 | .15 |
| -59.6 | .05 | .34 | 9.94 | 3.41 | 1.83 | .91 | .58 | .42 | .22 | .22 | .14 |
| -47.7 | .04 | 3.48 | 8.72 | 2.58 | 1.41 | .87 | .50 | .37 | .24 | .18 | .13 |
| -35.7 | .07 | 7.22 | 6.17 | 2.24 | 1.21 | .82 | .45 | .32 | .26 | .15 | .13 |
| -23.8 | .15 | 10.33 | 4.54 | 2.16 | 1.21 | .75 | .43 | .31 | .28 | .15 | .16 |
| -11.9 | .32 | 11.07 | 4.17 | 2.08 | 1.32 | .75 | .54 | .33 | .26 | .22 | .25 |
| .0 | .40 | 9.37 | 4.32 | 2.17 | 1.36 | .75 | .70 | .43 | .32 | .28 | .34 |
| 11.9 | .23 | 9.17 | 4.14 | 2.46 | 1.37 | .83 | .75 | .43 | .31 | .28 | .26 |
| 23.8 | .06 | 6.19 | 5.16 | 2.79 | 1.03 | 1.17 | .73 | .44 | .32 | .26 | .21 |
| 35.7 | .04 | 1.77 | 6.23 | .12 | 1.41 | 1.21 | .75 | .04 | .39 | .32 | .28 |
| 47.7 | .05 | .33 | 3.09 | 5.83 | 3.35 | 1.37 | .92 | .37 | .51 | .45 | .34 |
| 59.6 | .05 | .20 | .85 | 3.77 | .15 | 2.04 | 1.72 | .22 | .33 | .02 | .45 |
| 71.5 | .05 | .25 | .17 | .03 | 2.17 | 2.03 | 2.36 | 2.23 | 1.55 | .35 | .71 |
| 83.4 | .04 | .04 | .03 | .19 | .25 | 1.23 | 1.33 | 2.37 | 2.56 | 2.13 | 1.45 |
| 95.3 | .04 | .04 | .00 | .14 | .11 | .13 | .17 | .33 | 1.59 | 1.72 | 1.66 |
| 107.2 | .05 | .05 | .05 | .10 | .14 | .09 | .07 | .03 | .68 | .21 | .70 |
| 119.1 | .05 | .05 | .04 | .08 | .12 | .04 | .05 | .03 | .03 | .05 | .05 |
| 131.1 | .04 | .04 | .05 | .05 | .08 | .12 | .07 | .03 | .05 | .04 | .05 |
| 143.0 | .05 | .04 | .03 | .05 | .05 | .09 | .10 | .03 | .05 | .05 | .05 |
| 154.9 | .04 | .05 | .03 | .05 | .05 | .05 | .10 | .04 | .05 | .05 | .06 |
| 166.8 | .04 | .04 | .05 | .05 | .06 | .05 | .10 | .04 | .05 | .05 | .06 |
| 178.7 | .04 | .05 | .03 | .05 | .05 | .04 | .05 | .05 | .07 | .06 | .05 |
| 190.6 | .05 | .05 | .03 | .06 | .06 | .05 | .05 | .05 | .06 | .07 | .06 |
| 202.5 | .06 | .05 | .04 | .05 | .06 | .06 | .06 | .05 | .06 | .07 | .06 |
| 214.5 | .06 | .06 | .03 | .06 | .06 | .06 | .06 | .05 | .05 | .08 | .06 |
| 226.4 | .05 | .06 | .05 | .05 | .06 | .07 | .06 | .05 | .05 | .07 | .06 |
| 238.3 | .06 | .06 | .05 | .05 | .06 | .07 | .05 | .04 | .05 | .07 | .06 |
| 250.2 | .06 | .06 | .05 | .06 | .06 | .06 | .05 | .04 | .06 | .07 | .06 |
| 262.1 | .06 | .07 | .06 | .07 | .06 | .06 | .06 | .07 | .06 | .06 | .06 |
| 274.0 | .06 | .07 | .05 | .07 | .07 | .05 | .07 | .07 | .07 | .06 | .06 |
| 285.9 | .05 | .06 | .07 | .05 | .07 | .07 | .07 | .04 | .07 | .07 | .07 |

## TABLE 4-12. DELAY-DOPPLER SCATTER FUNCTION NUMERICAL OUTPUT (NOISE REMOVED)

2/27/75 _ H C NOISE REMOVED

| FREQUENCY HERTZ | TAP 32 | TAP 33 | TAP 34 | TAP 35 | TAP 36 | TAP 37 | TAP 38 | TAP 39 | TAP 40 | TAP 41 | TAP 42 |
|---|---|---|---|---|---|---|---|---|---|---|---|
| -285.9 | -.00 | .00 | .00 | .02 | -.02 | .01 | -.01 | -.02 | -.01 | -.01 | -.00 |
| -274.0 | .01 | -.00 | .00 | .02 | -.01 | .01 | .00 | -.01 | -.01 | -.01 | -.01 |
| -262.1 | .02 | .00 | .01 | .01 | -.01 | .00 | -.02 | -.01 | -.01 | -.01 | .00 |
| -250.2 | .02 | .01 | .00 | .01 | -.01 | -.00 | -.01 | -.02 | -.02 | -.00 | .12 |
| -238.3 | .01 | .01 | .00 | -.00 | .00 | -.00 | .00 | .00 | -.01 | .03 | .59 |
| -226.4 | -.00 | .01 | .00 | -.00 | -.00 | -.00 | .00 | -.01 | .00 | .45 | 1.02 |
| -214.5 | -.00 | .00 | -.01 | .00 | -.00 | -.00 | -.01 | -.02 | .23 | 1.16 | .86 |
| -202.5 | -.00 | -.00 | -.01 | .01 | .00 | .01 | -.01 | .07 | 1.06 | 1.26 | .58 |
| -190.6 | -.00 | -.01 | -.01 | .00 | -.00 | .01 | .01 | .78 | 1.81 | .82 | .50 |
| -178.7 | -.00 | -.00 | .00 | .00 | -.01 | .00 | .30 | 1.38 | 1.54 | .51 | .42 |
| -166.8 | .00 | .01 | .01 | .00 | -.01 | .00 | 1.31 | 2.11 | .90 | .43 | .34 |
| -154.9 | .01 | -.00 | -.00 | .01 | .00 | .87 | 3.42 | 1.42 | .58 | .41 | .24 |
| -143.0 | .00 | -.01 | -.00 | .01 | .21 | 2.71 | 3.05 | 1.00 | .54 | .34 | .19 |
| -131.1 | .00 | -.00 | .01 | .03 | 1.55 | 3.87 | 2.08 | .38 | .53 | .27 | .17 |
| -119.1 | .00 | -.00 | .00 | .42 | 4.20 | 3.14 | 1.54 | .81 | .39 | .25 | .15 |
| -107.2 | .01 | -.00 | .01 | 2.98 | 5.32 | 2.14 | 1.06 | .63 | .35 | .21 | .14 |
| -95.3 | .00 | -.00 | .36 | 5.86 | 3.70 | 1.84 | .77 | .54 | .40 | .19 | .14 |
| -83.4 | -.00 | -.00 | 2.54 | 6.54 | 2.45 | 1.47 | .77 | .47 | .35 | .16 | .13 |
| -71.5 | .00 | .09 | 7.20 | 5.08 | 2.16 | .99 | .70 | .41 | .22 | .14 | .10 |
| -59.6 | .00 | .80 | 9.94 | 3.38 | 1.79 | .86 | .62 | .37 | .17 | .17 | .09 |
| -47.7 | .00 | 3.46 | 8.72 | 2.55 | 1.57 | .83 | .45 | .31 | .19 | .13 | .08 |
| -35.7 | .03 | 7.17 | 6.12 | 2.13 | 1.16 | .77 | .40 | .27 | .21 | .09 | .08 |
| -23.8 | .11 | 10.52 | 4.47 | 2.12 | 1.16 | .71 | .38 | .26 | .21 | .10 | .11 |
| -11.9 | .22 | 10.97 | 4.07 | 1.90 | 1.22 | .64 | .44 | .29 | .17 | .11 | .15 |
| .0 | .25 | 9.22 | 4.17 | 2.02 | 1.20 | .61 | .54 | .33 | .17 | .12 | .18 |
| 11.9 | .13 | 9.06 | 4.04 | 2.30 | 1.27 | .82 | .54 | .34 | .20 | .17 | .15 |
| 23.8 | .02 | 6.15 | 5.14 | 2.71 | 1.59 | 1.02 | .71 | .39 | .27 | .22 | .16 |
| 35.7 | .00 | 1.73 | 6.23 | 4.07 | 1.96 | 1.17 | .70 | .58 | .34 | .26 | .23 |
| 47.7 | .01 | .29 | 3.67 | 5.81 | 3.32 | 1.83 | .97 | .82 | .47 | .39 | .34 |
| 59.6 | .00 | .02 | .73 | 3.74 | 4.15 | 2.66 | 1.67 | 1.15 | .78 | .56 | .40 |
| 71.5 | .00 | .01 | .13 | .59 | 2.04 | 2.62 | 2.92 | 2.22 | 1.50 | .90 | .65 |
| 83.4 | -.00 | .00 | .05 | .10 | .20 | 1.19 | 1.80 | 2.34 | 2.54 | 2.10 | 1.42 |
| 95.3 | -.00 | -.00 | .01 | .09 | .06 | .05 | .12 | .38 | 1.55 | 1.67 | 1.03 |
| 107.2 | .01 | .00 | .00 | .05 | .09 | .04 | .02 | .01 | .03 | .16 | .66 |
| 119.1 | .00 | .00 | -.00 | .02 | .07 | .05 | .02 | .01 | .00 | -.01 | -.00 |
| 131.1 | .00 | -.00 | .00 | .01 | .03 | .05 | .02 | .01 | .00 | -.01 | -.00 |
| 143.0 | .00 | .00 | .00 | .01 | .00 | .04 | .05 | .03 | -.00 | -.01 | .00 |
| 154.9 | -.00 | .00 | .01 | .01 | .00 | .01 | .07 | .03 | -.00 | -.01 | .01 |
| 166.8 | -.01 | -.00 | .00 | .01 | .01 | -.00 | .04 | .03 | .00 | -.01 | .00 |
| 178.7 | -.01 | -.00 | .00 | .01 | .00 | -.00 | .00 | .02 | .02 | -.00 | -.00 |
| 190.6 | -.00 | -.00 | -.00 | .01 | .00 | .00 | -.01 | -.00 | .02 | .00 | .00 |
| 202.5 | .01 | -.01 | -.00 | .00 | .00 | -.00 | -.00 | -.02 | .00 | .01 | -.00 |
| 214.5 | .01 | .00 | -.00 | -.01 | .00 | -.00 | -.00 | -.02 | -.02 | .01 | -.00 |
| 226.4 | -.00 | .00 | .00 | -.01 | -.00 | .01 | -.01 | -.01 | -.02 | .00 | -.00 |
| 238.3 | .00 | .00 | -.00 | -.01 | -.01 | -.00 | -.02 | -.01 | -.01 | -.01 | .00 |
| 250.2 | .01 | .00 | .00 | -.00 | -.01 | -.02 | -.01 | -.01 | -.01 | -.01 | -.01 |
| 262.1 | .01 | .01 | -.00 | .01 | -.01 | -.01 | .00 | -.01 | -.01 | -.00 | -.01 |
| 274.0 | -.01 | .01 | -.00 | .01 | -.00 | .00 | -.01 | -.01 | -.01 | -.00 | -.01 |
| 285.9 | -.01 | -.01 | -.00 | .01 | .00 | -.00 | -.01 | -.00 | -.01 | -.02 | -.01 |

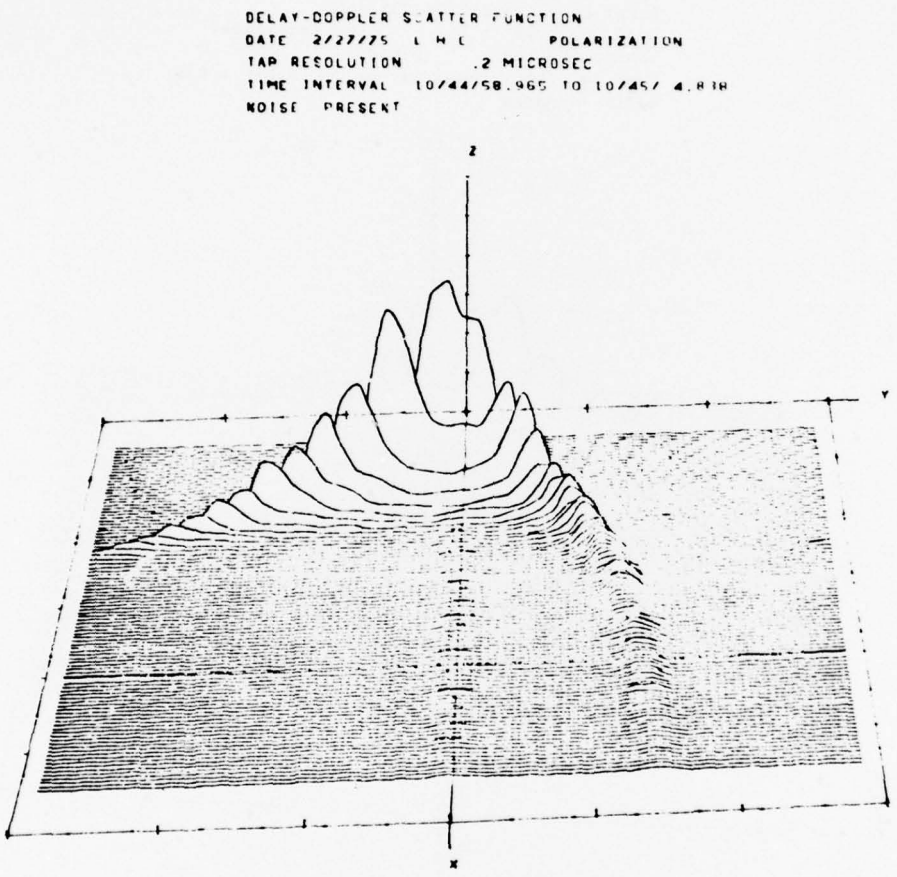


| AXIS | | MINIMUM | MAXIMUM | INCREMENT |
|---|---|---|---|---|
| X | DELAY TAP ( .2 MICROSEC. WIDTH) | .00 | 120.00 | 20.00 |
| Y | DOPPLER FREQUENCY (HERTZ) | -300.00 | 300.00 | 100.00 |
| Z | DELAY-DOPPLER PSD (LINEAR) | .00 | 12.00 | 2.00 |

*Figure 4-20. Three-Dimensional Plot of Delay-Doppler Function (Noise Present)*

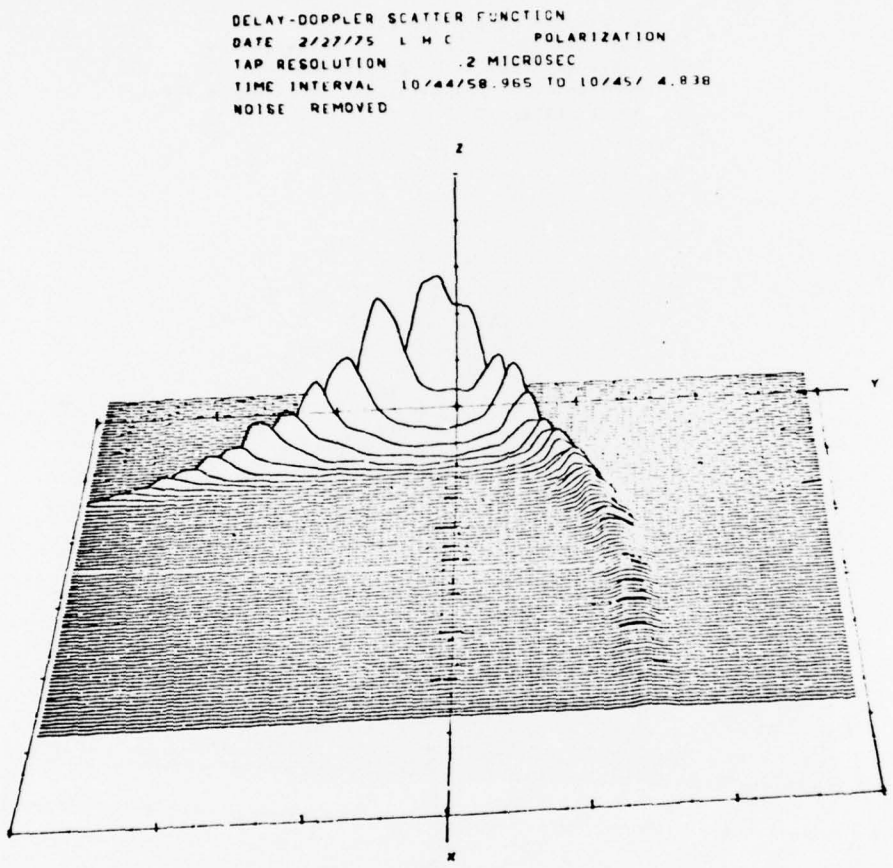


*Figure 4-21. Three-Dimensional Plot of Delay-Doppler Function (Noise Removed)*

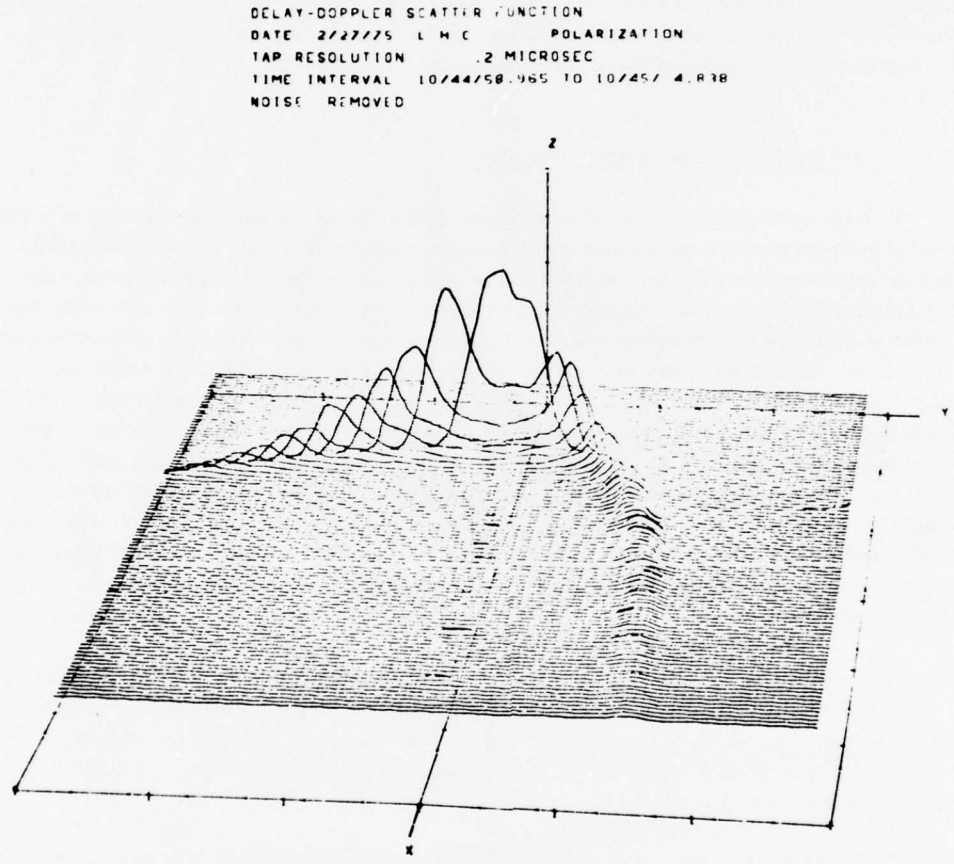


| AXIS | | MINIMUM | MAXIMUM | INCREMENT |
|---|---|---|---|---|
| X | DELAY TAP ( .2 MICROSEC. WIDTH) | .00 | 120.00 | 20.00 |
| Y | DOPPLER FREQUENCY (HERTZ) | -300.00 | 300.00 | 100.00 |
| Z | DELAY-DOPPLER PSD (LINEAR) | -3.00 | 12.00 | 3.00 |

*Figure 4-22. Three-Dimensional Plot of Delay-Doppler Function (Noise Removed, Hidden Lines Present)*

The intended purpose of plotting the $S(\tau,\omega)$ functions is twofold: (1) to give the observer a quick and concise description of the energy distribution characteristics of the $S(\tau,\omega)$ spectra and (2) to provide a visual directory from which one may access the numerical results to key in on areas of interest or anomolous behavior of the scattering function.

4.24.7 Integral and Fourier Operations on $S(\tau,\omega)$

Both the noise-present and noise-free estimates of the $S(\tau,\omega)$ function are subjected to operations that yield the scatter channel's delay spectra, Doppler spectra, frequency autocorrelation function, time autocorrelation function, and total rms energy. For the delay and Doppler spectra, numerical and plotted output are given, as shown in figure 4-23 and 4-24 and table 4-13. As previously mentioned in section 4.14, plotted spectra for both the noise-present and noise-removed algorithm outputs are presented. This is done to give an indication of the effectiveness of the ND and R operations. Also included in the numerical outputs of table 4-13 are: (1) the delay spectra from input (or time-domain analysis), (2) the mean square total indirect energy (integration over delay variable = T, integration over Doppler variable = F), (3) the mean square total indirect energy for the noise-present case, and (4) the composite mean square energy of the direct signal. The T and F integrations are identical as would be expected and they are substantially less than the signal-plus-noise integration. The direct and multipath mean square energies are not normalized to remove differences in antenna ERP, receiver channel gains, etc. This step is performed in the data interpretation phase of the analysis, which is not a DRandA software component.

Numerical and plotted output formats are used to represent the multipath $R(\xi,\Omega)$ function. An example illustrating the distribution of $|R(\xi,\Omega)|$ is given in the three-dimensional plot of figure 4-25. To enhance the fidelity of the output, the plot routine has in this case been operated in a mode whereby both the constant $\xi$ and constant $\Omega$ contours, which occur at the discrete periodogram output values, are drawn with hidden lines removed.

The frequency and time autocorrelation functions are given in the form of numerical and plotted output. For both numerical outputs, the amplitude and phase are tabulated relative to the frequency (hertz) or time (seconds) variable, respectively. Numerical examples of the $R(0,\Omega)$ and $R(\xi,0)$ distributions are given in tables 4-14 and 4-15. Sample plotted results of the autocorrelation function magnitudes are presented in figure 4-26.

The frequency and time autocorrelation functions are given only in the form of numerical output. For both distributions, the voltage amplitude and phase in degrees are tabulated relative to the frequency (hertz) or time (seconds) variable. Examples of the algorithm outputs for the frequency and time autocorrelation functions are given in figures 4-25 and 4-26.

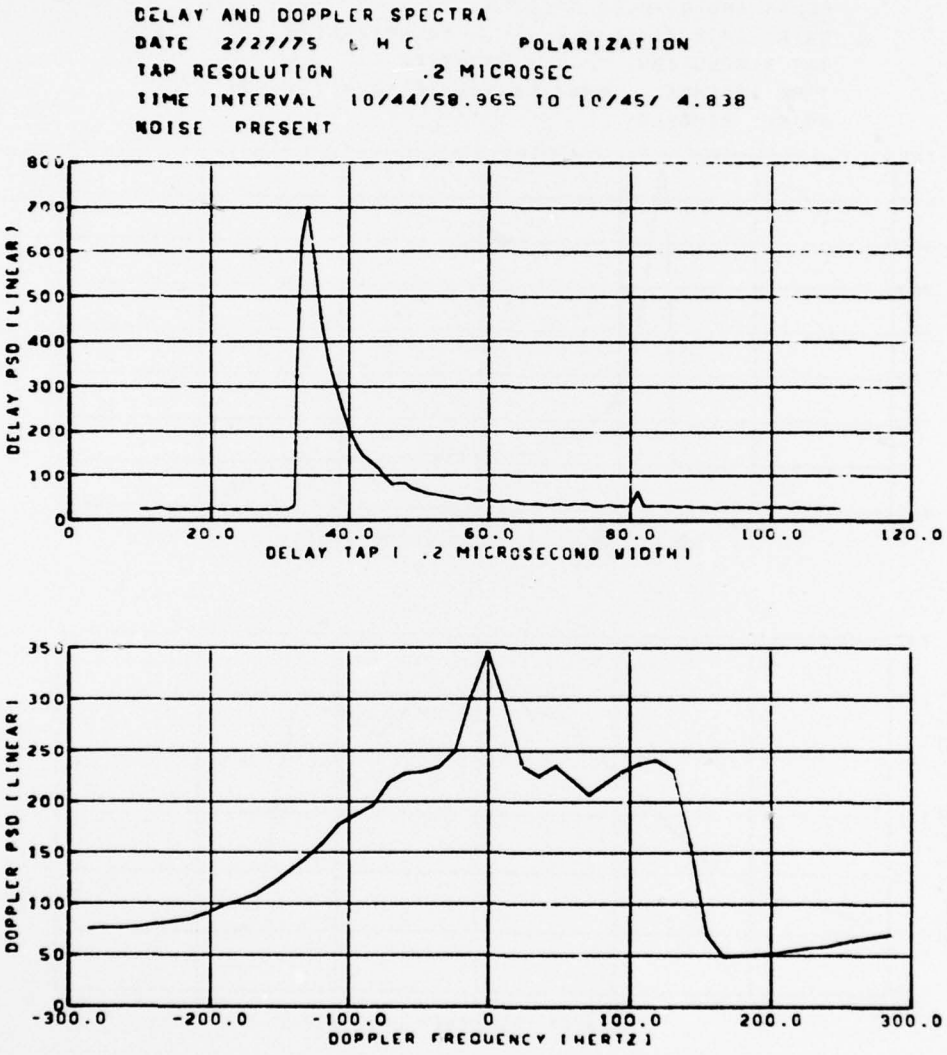


*Figure 4-23. Delay and Doppler Spectra Plot (Noise Present)*

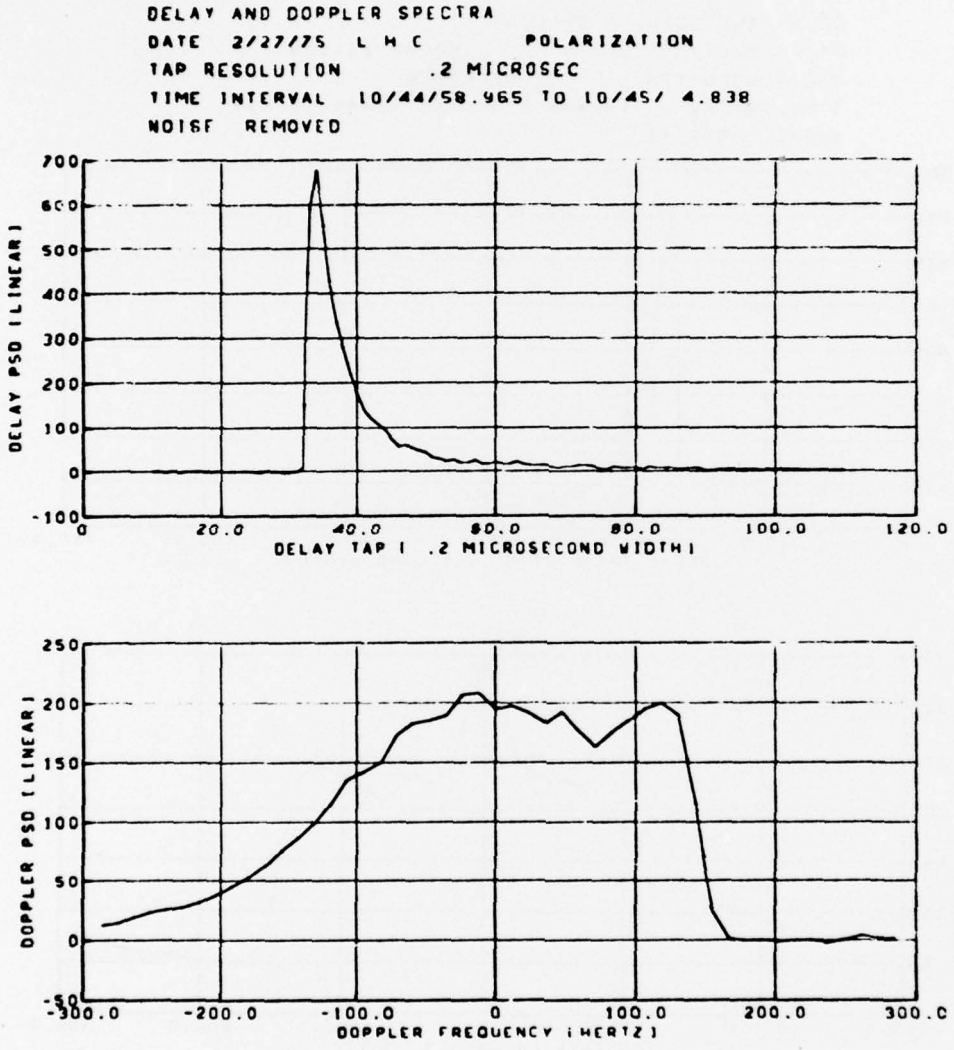


*Figure 4-24. Delay and Doppler Spectra Plot (Noise Removed)*

## TABLE 4-13. DELAY AND DOPPLER SPECTRA NUMERICAL OUTPUT

DELAY SPECTRA FROM INPUT

| | | | | | | | | | | | | | | | |
|---|---|---|---|---|---|---|---|---|---|---|---|---|---|---|---|
| 10 | 2.684E+01 | 11 | 2.596E+01 | 12 | 2.669E+01 | 13 | 2.834E+01 | 14 | 2.667E+01 | 15 | 2.721E+01 | 16 | 2.663E+01 | 17 | 2.806E+01 |
| 18 | 2.680E+01 | 19 | 2.687E+01 | 20 | 2.812E+01 | 21 | 2.735E+01 | 22 | 2.657E+01 | 23 | 2.643E+01 | 24 | 2.712E+01 | 25 | 2.670E+01 |
| 26 | 2.727E+01 | 27 | 2.612E+01 | 28 | 2.589E+01 | 29 | 2.615E+01 | 30 | 2.726E+01 | 31 | 2.976E+01 | 32 | 3.483E+01 | 33 | 6.158E+02 |
| 34 | 7.187E+02 | 35 | 5.674E+02 | 36 | 4.460E+02 | 37 | 3.631E+02 | 38 | 3.002E+02 | 39 | 2.524E+02 | 40 | 2.133E+02 | 41 | 1.687E+02 |
| 42 | 1.464E+02 | 43 | 1.328E+02 | 44 | 1.182E+02 | 45 | 9.918E+01 | 46 | 8.435E+01 | 47 | 8.943E+01 | 48 | 8.793E+01 | 49 | 7.508E+01 |
| 50 | 6.896E+01 | 51 | 6.197E+01 | 52 | 5.309E+01 | 53 | 5.769E+01 | 54 | 5.852E+01 | 55 | 5.371E+01 | 56 | 4.785E+01 | 57 | 5.274E+01 |
| 58 | 4.509E+01 | 59 | 4.787E+01 | 60 | 4.883E+01 | 61 | 4.810E+01 | 62 | 4.407E+01 | 63 | 4.153E+01 | 64 | 4.309E+01 | 65 | 4.181E+01 |
| 66 | 4.051E+01 | 67 | 4.189E+01 | 68 | 3.939E+01 | 69 | 3.773E+01 | 70 | 4.052E+01 | 71 | 3.916E+01 | 72 | 3.973E+01 | 73 | 4.129E+01 |
| 74 | 3.999E+01 | 75 | 3.578E+01 | 76 | 3.409E+01 | 77 | 3.866E+01 | 78 | 3.679E+01 | 79 | 3.483E+01 | 80 | 3.474E+01 | 81 | 6.696E+01 |
| 82 | 3.596E+01 | 83 | 3.604E+01 | 84 | 3.634E+01 | 85 | 3.485E+01 | 86 | 3.358E+01 | 87 | 3.133E+01 | 88 | 3.507E+01 | 89 | 3.360E+01 |
| 90 | 3.269E+01 | 91 | 3.096E+01 | 92 | 3.141E+01 | 93 | 3.292E+01 | 94 | 3.333E+01 | 95 | 3.307E+01 | 96 | 3.105E+01 | 97 | 3.304E+01 |
| 98 | 3.093E+01 | 99 | 3.196E+01 | 100 | 3.175E+01 | 101 | 3.322E+01 | 102 | 3.237E+01 | 103 | 3.063E+01 | 104 | 3.253E+01 | 105 | 2.860E+01 |
| 106 | 3.016E+01 | 107 | 3.084E+01 | 108 | 2.945E+01 | 109 | 3.079E+01 | 110 | 3.115E+01 | | | | | | |

DELAY SPECTRA (TAP,PSD)

| | | | | | | | | | | | | | | | |
|---|---|---|---|---|---|---|---|---|---|---|---|---|---|---|---|
| 10 | 2.552E+01 | 11 | 2.456E+01 | 12 | 2.551E+01 | 13 | 2.716E+01 | 14 | 2.490E+01 | 15 | 2.578E+01 | 16 | 2.522E+01 | 17 | 2.667E+01 |
| 18 | 2.465E+01 | 19 | 2.561E+01 | 20 | 2.718E+01 | 21 | 2.611E+01 | 22 | 2.531E+01 | 23 | 2.535E+01 | 24 | 2.587E+01 | 25 | 2.529E+01 |
| 26 | 2.574E+01 | 27 | 2.495E+01 | 28 | 2.446E+01 | 29 | 2.499E+01 | 30 | 2.588E+01 | 31 | 2.838E+01 | 32 | 3.309E+01 | 33 | 6.212E+02 |
| 42 | 1.466E+02 | 43 | 1.324E+02 | 44 | 1.179E+02 | 45 | 9.861E+01 | 46 | 8.058E+01 | 47 | 8.283E+01 | 48 | 8.502E+01 | 49 | 7.300E+01 |
| 50 | 6.728E+01 | 51 | 6.137E+01 | 52 | 5.838E+01 | 53 | 5.630E+01 | 54 | 5.466E+01 | 55 | 5.138E+01 | 56 | 4.713E+01 | 57 | 5.186E+01 |
| 66 | 3.875E+01 | 67 | 4.092E+01 | 68 | 3.758E+01 | 69 | 3.629E+01 | 70 | 3.945E+01 | 71 | 3.817E+01 | 72 | 3.858E+01 | 73 | 3.981E+01 |
| 82 | 3.453E+01 | 83 | 3.486E+01 | 84 | 3.484E+01 | 85 | 3.366E+01 | 86 | 3.257E+01 | 87 | 3.004E+01 | 88 | 3.390E+01 | 89 | 3.202E+01 |
| 98 | 2.940E+01 | 99 | 3.079E+01 | 100 | 3.038E+01 | 101 | 3.179E+01 | 102 | 3.120E+01 | 103 | 2.951E+01 | 104 | 3.119E+01 | 105 | 2.744E+01 |
| 106 | 2.891E+01 | 107 | 2.960E+01 | 108 | 2.842E+01 | 109 | 2.970E+01 | 110 | 2.971E+01 | | | | | | |

DOPPLER SPECTRA (FREQ,PSD)

| | | | | | | | | | | | |
|---|---|---|---|---|---|---|---|---|---|---|---|
| -285.9 | 7.545E+01 | -274.0 | 7.629E+01 | -262.1 | 7.688E+01 | -250.2 | 7.788E+01 | -238.3 | 8.012E+01 | -226.4 | 8.311E+01 |
| -214.5 | 8.601E+01 | -202.5 | 9.105E+01 | -190.6 | 9.828E+01 | -178.7 | 1.034E+02 | -166.8 | 1.096E+02 | -154.9 | 1.212E+02 |
| -143.0 | 1.326E+02 | -131.1 | 1.452E+02 | -119.1 | 1.596E+02 | -107.2 | 1.731E+02 | -95.3 | 1.880E+02 | -83.4 | 1.970E+02 |
| -71.5 | 2.193E+02 | -59.6 | 2.287E+02 | -47.7 | 2.290E+02 | -35.7 | 2.347E+02 | -23.8 | 2.508E+02 | -11.9 | 3.056E+02 |
| .0 | 3.478E+02 | 11.9 | 2.979E+02 | 23.8 | 2.357E+02 | 35.7 | 2.253E+02 | 47.7 | 2.351E+02 | 59.6 | 2.219E+02 |
| 71.5 | 2.881E+02 | 83.4 | 2.198E+02 | 95.3 | 2.307E+02 | 107.4 | 2.331E+02 | 119.1 | 2.417E+02 | 131.1 | 2.315E+02 |
| 143.0 | 1.560E+02 | 154.9 | 7.003E+01 | 166.8 | 4.846E+01 | 178.7 | 4.951E+01 | 190.6 | 5.107E+01 | 202.5 | 5.262E+01 |
| 214.5 | 5.432E+01 | 226.4 | 5.709E+01 | 238.3 | 5.849E+01 | 250.2 | 6.136E+01 | 262.1 | 6.366E+01 | 274.0 | 6.774E+01 |
| 285.9 | 7.044E+01 | | | | | | | | | | |

SUM OF SQUARE (T,F,I) 7.347E+03 7.347E+03 7.477E+03

COMPOSITE DIRECT MEAN SQUARE 9.837171E+03

## TABLE 4-14. FREQUENCY AUTOCORRELATION FUNCTION OUTPUT

FREQUENCY AUTOCORRELATION

| FREQUENCY | AMPLITUDE(VOLT) | PHASE(DEG) |
|---|---|---|
| .0 | 1.0000E+00 | .0 |
| 3.9063E+04 | 8.9285E-01 | 7.7328E+01 |
| 7.8125E+04 | 7.4585E-01 | 1.4462E+02 |
| 1.1719E+05 | 6.5425E-01 | -1.5049E+02 |
| 1.5625E+05 | 5.6775E-01 | -8.8584E+01 |
| 1.9531E+05 | 5.2336E-01 | -2.6814E+01 |
| 2.3438E+05 | 4.6593E-01 | 3.5152E+01 |
| 2.7344E+05 | 4.2903E-01 | 9.4934E+01 |
| 3.1250E+05 | 3.9176E-01 | 1.5473E+02 |
| 3.5156E+05 | 3.7683E-01 | -1.4710E+02 |
| 3.9063E+05 | 3.5641E-01 | -8.5096E+01 |
| 4.2969E+05 | 3.2576E-01 | -2.5656E+01 |
| 4.6875E+05 | 2.9879E-01 | 3.3310E+01 |
| 5.0781E+05 | 2.8891E-01 | 8.8592E+01 |
| 5.4688E+05 | 2.8976E-01 | 1.5141E+02 |
| 5.8594E+05 | 2.5245E-01 | -1.4979E+02 |
| 6.2500E+05 | 2.3354E-01 | -9.1d73E+01 |
| 6.6406E+05 | 2.1839E-01 | -3.0658E+01 |
| 7.0313E+05 | 2.1782E-01 | 1.9692E+01 |
| 7.4219E+05 | 2.1611E-01 | 8.3202E+01 |
| 7.8125E+05 | 1.9490E-01 | 1.3564E+02 |
| 8.2031E+05 | 2.0432E-01 | -1.4279E+02 |
| 8.5938E+05 | 1.8853E-01 | -1.9462E+02 |
| 8.9844E+05 | 1.8046E-01 | -9.0349E+01 |
| 9.3750E+05 | 1.7058E-01 | 1.6334E+01 |
| 9.7656E+05 | 1.5852E-01 | 7.2116E+01 |
| 1.0156E+06 | 1.5874E-01 | 1.295?E+02 |
| 1.0547E+06 | 1.6444E-01 | -1.7543E+02 |
| 1.0938E+06 | 1.5926E-01 | -1.1362E+02 |
| 1.1328E+06 | 1.4483E-01 | -6.0987E+01 |
| 1.1719E+06 | 1.5261E-01 | 2.2449E+00 |
| 1.2109E+06 | 1.2877E-01 | 5.3992E+01 |
| 1.2500E+06 | 1.3049E-01 | 1.2277E+02 |
| 1.2891E+06 | 1.1986E-01 | -1.7730E+02 |
| 1.3281E+06 | 1.3190E-01 | -1.2595E+02 |
| 1.3672E+06 | 1.3185E-01 | -6.3767E+01 |
| 1.4063E+06 | 1.2681E-01 | -1.4331E+01 |
| 1.4453E+06 | 1.3562E-01 | 4.8414E+01 |
| 1.4844E+06 | 1.1629E-01 | 1.2460E+02 |
| 1.5234E+06 | 1.2890E-01 | 1.6351E+02 |
| 1.5625E+06 | 1.1439E-01 | -1.3652E+02 |
| 1.6016E+06 | 1.1940E-01 | -6.3348E+01 |
| 1.6406E+06 | 1.1568E-01 | -1.6290E+01 |
| 1.6797E+06 | 1.0929E-01 | 4.0853E+01 |
| 1.7188E+06 | 9.8749E-02 | 1.0088E+02 |
| 1.7578E+06 | 1.0552E-01 | 1.5962E+02 |
| 1.7969E+06 | 1.1775E-01 | -1.3730E+02 |
| 1.8359E+06 | 9.3154E-02 | -7.6280E+01 |
| 1.8750E+06 | 1.0370E-01 | -2.1293E+01 |
| 1.9141E+06 | 9.2990E-02 | 4.1474E+01 |
| 1.9531E+06 | 1.0248E-01 | 9.6154E+01 |
| 1.9922E+06 | 9.7894E-02 | 1.5347E+02 |
| 2.0313E+06 | 7.6410E-02 | -1.5713E+02 |
| 2.0703E+06 | 8.5653E-02 | -9.7248E+01 |
| 2.1094E+06 | 8.2230E-02 | -4.4329E+01 |
| 2.1484E+06 | 8.8410E-02 | 2.2532E+01 |
| 2.1875E+06 | 7.0714E-02 | 7.5245E+01 |
| 2.2266E+06 | 9.4122E-02 | 1.3186E+02 |
| 2.2656E+06 | 8.2752E-02 | -1.6064E+02 |
| 2.3047E+06 | 9.2467E-02 | -1.1161E+02 |
| 2.3438E+06 | 8.9819E-02 | -3.8655E+01 |
| 2.3828E+06 | 6.9710E-02 | 9.1683E+00 |
| 2.4219E+06 | 7.4736E-02 | 6.8256E+01 |
| 2.4609E+06 | 6.5909E-02 | 1.1662E+02 |

*TABLE 4-15. TIME AUTOCORRELATION FUNCTION OUTPUT*

TIME AUTOCORRELATION FUNCTION

| TIME | AMPLITUDE(VOLT) | PHASE(DEG) |
|---|---|---|
| .0 | 1.0000E+00 | .0 |
| 1.3115E-03 | 8.7967E-01 | 1.3860E+02 |
| 2.6230E-03 | 6.6992E-01 | -8.4751E+01 |
| 3.9344E-03 | 5.0223E-01 | 4.9337E+01 |
| 5.2459E-03 | 3.3748E-01 | -1.7688E+02 |
| 6.5574E-03 | 2.1820E-01 | -4.5221E+01 |
| 7.8689E-03 | 1.6115E-01 | 8.3312E+01 |
| 9.1803E-03 | 1.0058E-01 | -1.5035E+02 |
| 1.0492E-02 | 5.2663E-02 | -2.5425E+01 |
| 1.1803E-02 | 2.9139E-02 | 1.0414E+02 |
| 1.3115E-02 | 2.3768E-02 | -1.4254E+02 |
| 1.4426E-02 | 2.5111E-02 | 4.4548E+00 |
| 1.5738E-02 | 8.0562E-03 | 1.0512E+02 |
| 1.7049E-02 | 2.4922E-02 | 1.7679E+02 |
| 1.8361E-02 | 1.3695E-02 | -2.6621E+01 |
| 1.9672E-02 | 1.2693E-02 | 5.9928E+01 |
| 2.0984E-02 | 2.8293E-02 | -1.5820E+02 |
| 2.2295E-02 | 1.1677E-02 | -7.2030E+01 |
| 2.3607E-02 | 1.1919E-02 | 2.6045E+01 |
| 2.4918E-02 | 1.1376E-02 | -8.1437E+01 |
| 2.6230E-02 | 5.6512E-03 | 5.0540E+01 |
| 2.7541E-02 | 1.4727E-02 | 1.6144E+02 |
| 2.8852E-02 | 1.4709E-02 | -4.1563E+01 |
| 3.0164E-02 | 3.9302E-03 | -2.7095E-01 |
| 3.1475E-02 | 1.4241E-02 | -1.4581E+02 |
| 3.2787E-02 | 1.2124E-02 | -2.8562E-01 |
| 3.4098E-02 | 4.7684E-03 | 1.9315E+01 |
| 3.5410E-02 | 7.8573E-03 | -7.1355E+01 |
| 3.6721E-02 | 1.8536E-03 | 5.2781E+01 |
| 3.8033E-02 | 3.1045E-03 | 4.0875E+01 |
| 3.9344E-02 | 6.3787E-03 | 3.2947E+00 |
| 4.0656E-02 | 4.4454E-03 | -5.5808E+01 |

TIME FREQUENCY AUTOCORRELATION FUNCTION
CASE1/20/75 VERTICAL
TIME 0/ 2/ 5.3020 0/ 2/ 5.3020

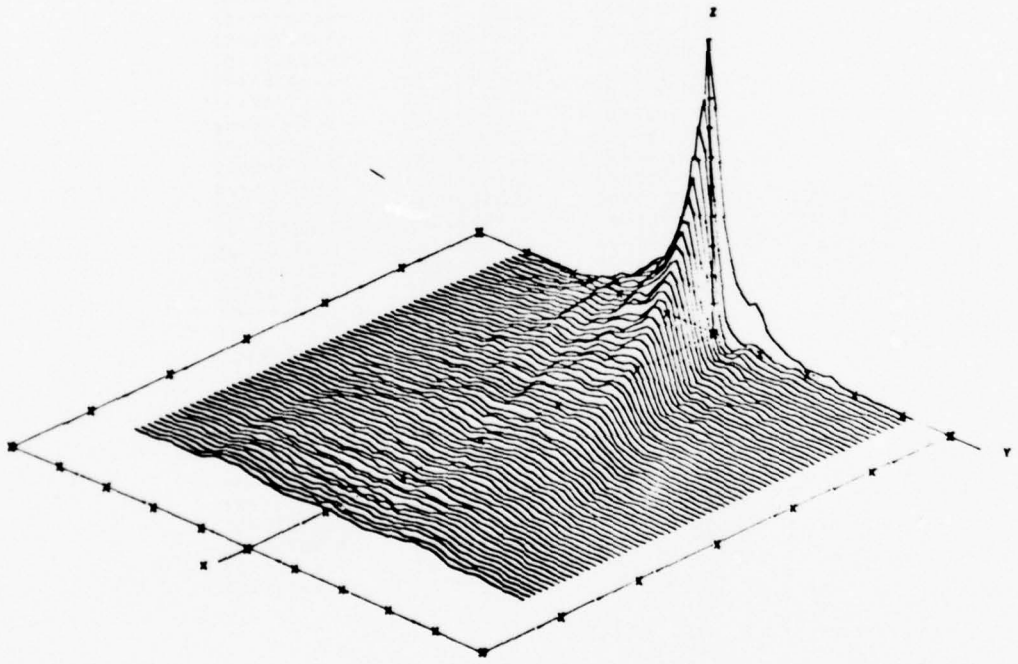


| AXIS | | MINIMUM | MAXIMUM | INCREMENT |
|---|---|---|---|---|
| X | FREQUENCY SEPARATION ( KHZ ) | 0 | 3000 | 500 |
| Y | TIME SEPARATION ( MILLISEC ) | -50.0 | 50.0 | 10.0 |
| Z | TIME-FREQ. AUTOCOR. FUNCTION (PWR) | .00 | 1.00 | .10 |

*Figure 4-25. Joint Time-Frequency Autocorrelation Function*

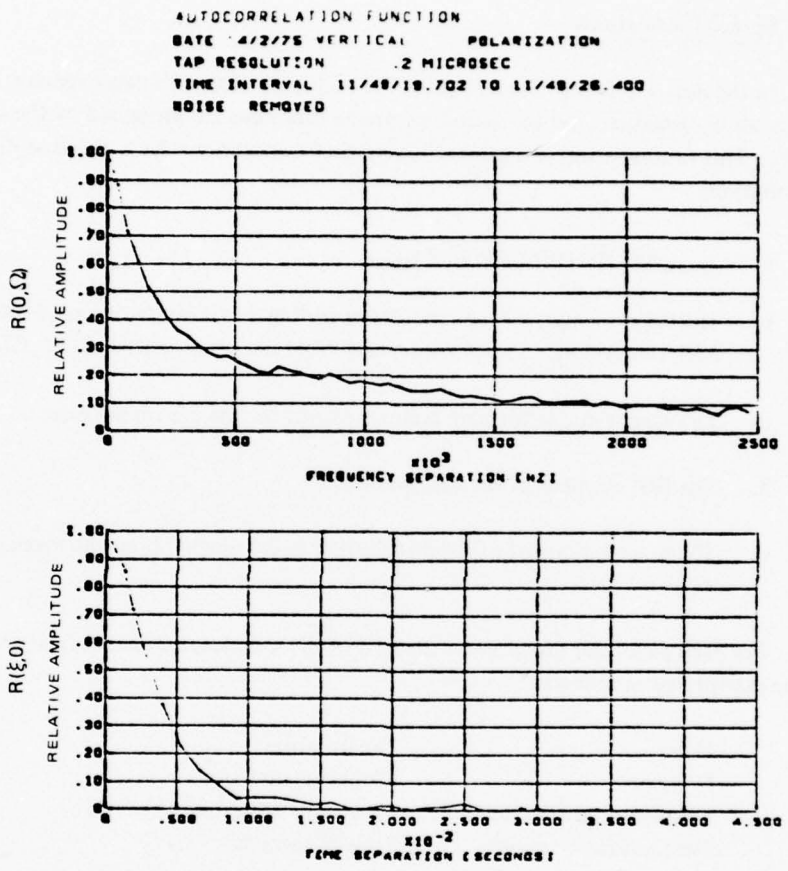


*Figure 4-26. Frequency and Time Autocorrelation Functions*

4.24.8 Spread Calculations

In the detailed data analysis routine, the multipath channel's delay spectra, Doppler spectra, freqency autocorrelation, and time autocorrelation functions are processed by the spread calculation software. This routine assumes a density function of the form y = f(x). It has as its output numerical calculations of:

a. $y_{max}$ and the corresponding $x_{max}$

b. The value of $y_{max}/2$ and its corresponding x-axis intersections (the first ones to occur on both sides of $x_{max}$) and the separation of the x-axis intersections (DX)

c. The same value as for item b above except for the 1/e spread case, i.e., $y_{max}/e$

d. The first moment of the distribution

e. The second moment of the distribution as calculated about the mean and about the $x_{max}$ value.

For each particular distribution the unit of the x-parameter output from the spread calculation is to be interpreted as follows:

| | |
|---|---|
| Delay: | Tap number |
| Doppler: | Frequency in hertz |
| Frequency autocorrelation: | Frequency in hertz |
| Time autocorrelation: | Time in seconds. |

A sample output for the spread or moment calculation on a Doppler spectrum is given in table 4-16.

*TABLE 4-16. MOMENT COMPUTATION OUTPUT (DOPPLER SPECTRUM)*

```
MOMENT COMPUTATION ON DOPPLER SPECTRA

 X OF MAX, YMAX,YMAX/2,YMAX/E   -1.1914E+01     2.5391E+02     1.2696E+02     9.3410E+01
 INTER. AT .5 MAX,   (LEVEL,X1,X2,DX)     1.2696E+02    -4.7210E+01     4.7834E+01     9.5045E+01
 INTER. AT 1./E MAX, (LEVEL,X1,X2,DX)     9.3410E+01    -5.0583E+01     6.0851E+01     1.1143E+02
 INTER. AT 1/10 MAX, (LEVEL,X1,X2,DX)     2.5391E+01    -8.6657E+01     1.1313E+02     1.9978E+02
 FIRST MOMENT     8.1562E+00
SECOND MOMENT RELATIVE TO MEAN AND MAX     6.0117E+01     6.4328E+01
```

4.24.9 Noise Determination and Removal

In determining the characteristics of the SACP receiver noise, the algorithm calculates:

a. N(f) – the total noise power spectral density in a tap region that precedes the specular point return and is thus considered to be multipath free

b. $A_0M(f)$ – an estimate of the thermal noise psd content of the total noise power in the multipath-free region

c. R(f)– the difference between items a and b, which is referred to as the residual noise content and is assumed to be a representative value for any given indirect tap

d. $A_0(\tau)$ – the thermal noise content for each tap

e. The mean value of the I and Q voltage inputs for each tap

f. FR(f) and M(f) – the filter frequency response with no aliasing and the filter response including the first four aliased components, respectively.

With the exception of the FR(f) spectra, all the above parameters are provided as numerical outputs. Samples are given in tables 4-17 and 4-18. Parameters M(f), R(f), and N(f) are presented as frequency (hertz) and psd point pairs. The I and Q voltage means are given as tap number and mean voltage. The array $A_0(\tau)$ is given as tap number and psd point pairs.

4.24.10 Antenna Pattern Effects Removal

The primary output from the antenna effects removal is the $S_{AC}(\tau,\omega)$ array. This array is passed into additional processing algorithms, as shown in figure 3-1, and is also output in numerical and plotted formats. These formats are identical to those previously described for the uncorrected $S(\tau,\omega)$ function. A secondary output, $G(\tau,\omega)$, which provides a visual indication of the antenna's spatial filtering properties as mapped into the $(\tau,\omega)$ coordinate system, is given in figure 4-27 and illustrates that for this representative case very little filtering occurs over the realm responsible for the majority of the multipath return (i.e., the shoulders of the $S(\tau,\omega)$ function).

## TABLE 4-17. NOISE PARAMETER OUTPUTS – M(f), R(f), N(f), $A_0$, $A_0$ (τ)

NOISE REMOVAL
**********

M(F)

| | | | | | | | | | |
|---|---|---|---|---|---|---|---|---|---|
| -285.9 | 1.472E+00 | -274.0 | 1.443E+00 | -262.1 | 1.407E+00 | -250.2 | 1.363E+00 | -238.3 | 1.315E+00 | -226.4 | 1.273E+00 |
| -214.5 | 1.225E+00 | -202.5 | 1.191E+00 | -190.6 | 1.155E+00 | -178.7 | 1.125E+00 | -166.8 | 1.104E+00 | -154.9 | 1.081E+00 |
| -143.0 | 1.067E+00 | -131.1 | 1.053E+00 | -119.1 | 1.045E+00 | -107.2 | 1.038E+00 | -95.3 | 1.035E+00 | -83.4 | 1.025E+00 |
| -71.5 | 1.027E+00 | -59.6 | 1.024E+00 | -47.7 | 1.019E+00 | -35.7 | 1.023E+00 | -23.8 | 1.018E+00 | -11.9 | 1.020E+00 |
| .0 | 1.019E+00 | 11.9 | 1.020E+00 | 23.8 | 1.018E+00 | 35.7 | 1.023E+00 | 47.7 | 1.019E+00 | 59.6 | 1.024E+00 |
| 71.5 | 1.027E+00 | 83.4 | 1.025E+00 | 95.3 | 1.033E+00 | 107.2 | 1.038E+00 | 119.1 | 1.045E+00 | 131.1 | 1.055E+00 |
| 143.0 | 1.067E+00 | 154.9 | 1.081E+00 | 166.8 | 1.104E+00 | 178.7 | 1.125E+00 | 190.6 | 1.155E+00 | 202.5 | 1.191E+00 |
| 214.5 | 1.225E+00 | 226.4 | 1.273E+00 | 238.3 | 1.315E+00 | 250.2 | 1.363E+00 | 262.1 | 1.407E+00 | 274.0 | 1.443E+00 |
| 285.9 | 1.472E+00 | | | | | | | | | | |

RESIDU ⇒ R(f)

| | | | | | | | | | | | |
|---|---|---|---|---|---|---|---|---|---|---|---|
| -285.9 | 2.652E-01 | -274.0 | 2.350E-01 | -262.1 | 2.241E-01 | -250.2 | 2.219E-01 | -238.3 | 2.122E-01 | -226.4 | 2.330E-01 |
| -214.5 | 1.944E-01 | -202.5 | 1.881E-01 | -190.6 | 1.891E-01 | -178.7 | 1.854E-01 | -166.8 | 1.762E-01 | -154.9 | 1.739E-01 |
| -143.0 | 1.730E-01 | -131.1 | 1.653E-01 | -119.1 | 1.640E-01 | -107.2 | 1.735E-01 | -95.3 | 1.767E-01 | -83.4 | 1.658E-01 |
| -71.5 | 1.640E-01 | -59.6 | 1.670E-01 | -47.7 | 1.637E-01 | -35.7 | 1.642E-01 | -23.8 | 1.613E-01 | -11.9 | 1.726E-01 |
| .0 | 3.916E-01 | 11.9 | 2.746E-01 | 23.8 | 1.606E-01 | 35.7 | 1.710E-01 | 47.7 | 1.643E-01 | 59.6 | 1.591E-01 |
| 71.5 | 1.676E-01 | 83.4 | 1.701E-01 | 95.3 | 1.690E-01 | 107.2 | 1.688E-01 | 119.1 | 1.689E-01 | 131.1 | 1.665E-01 |
| 143.0 | 1.784E-01 | 154.9 | 1.786E-01 | 166.8 | 1.810E-01 | 178.7 | 1.852E-01 | 190.6 | 1.901E-01 | 202.5 | 1.869E-01 |
| 214.5 | 1.908E-01 | 226.4 | 2.015E-01 | 238.3 | 2.153E-01 | 250.2 | 2.252E-01 | 262.1 | 2.223E-01 | 274.0 | 2.265E-01 |
| 285.9 | 2.465E-01 | | | | | | | | | | |

AVERAGE NOISE TAP USED ⇒ N(f)

| | | | | | | | | | | | |
|---|---|---|---|---|---|---|---|---|---|---|---|
| -285.9 | 2.652E-01 | -274.0 | 2.350E-01 | -262.1 | 2.241E-01 | -250.2 | 2.219E-01 | -238.3 | 2.122E-01 | -226.4 | 2.330E-01 |
| -214.5 | 1.944E-01 | -202.5 | 1.881E-01 | -190.6 | 1.891E-01 | -178.7 | 1.854E-01 | -166.8 | 1.762E-01 | -154.9 | 1.739E-01 |
| -143.0 | 1.730E-01 | -131.1 | 1.653E-01 | -119.1 | 1.640E-01 | -107.2 | 1.735E-01 | -95.3 | 1.767E-01 | -83.4 | 1.658E-01 |
| -71.5 | 1.640E-01 | -59.6 | 1.670E-01 | -47.7 | 1.637E-01 | -35.7 | 1.642E-01 | -23.8 | 1.613E-01 | -11.9 | 2.726E-01 |
| .0 | 3.916E-01 | 11.9 | 2.746E-01 | 23.8 | 1.606E-01 | 35.7 | 1.710E-01 | 47.7 | 1.643E-01 | 59.6 | 1.591E-01 |
| 71.5 | 1.676E-01 | 83.4 | 1.701E-01 | 95.3 | 1.690E-01 | 107.2 | 1.688E-01 | 119.1 | 1.689E-01 | 131.1 | 1.665E-01 |
| 143.0 | 1.784E-01 | 154.9 | 1.786E-01 | 166.8 | 1.810E-01 | 178.7 | 1.852E-01 | 190.6 | 1.901E-01 | 202.5 | 1.869E-01 |
| 214.5 | 1.908E-01 | 226.4 | 2.015E-01 | 238.3 | 2.153E-01 | 250.2 | 2.252E-01 | 262.1 | 2.223E-01 | 274.0 | 2.265E-01 |
| 285.9 | 2.465E-01 | | | | | | | | | | |

THERMAL NOISE FOR 10TAPS 4.2027E-02 - ⇒ $A_0$

RELATIVE THERMAL NOISE DENSITY FOR EACH TAP ⇒ A(τ)

| | | | | | | | | | | | | | | | |
|---|---|---|---|---|---|---|---|---|---|---|---|---|---|---|---|
| 1 | .0 | 2 | .0 | 3 | .0 | 4 | .0 | 5 | .0 | 6 | .0 | 7 | .0 | 8 | .0 |
| 9 | .0 | 10 | .0 | 11 | .0 | 12 | .0 | 13 | .0 | 14 | .0 | 15 | .0 | 16 | .0 |
| 17 | .0 | 18 | .0 | 19 | .0 | 20 | .0 | 21 | .0 | 22 | .0 | 23 | .0 | 24 | .0 |
| 25 | .0 | 26 | .0 | 27 | .0 | 28 | .0 | 29 | .0 | 30 | .0 | 31 | .0 | 32 | .0 |
| 33 | .0 | 34 | .0 | 35 | .0 | 36 | .0 | 37 | .0 | 38 | .0 | 39 | .0 | 40 | .0 |
| 41 | .0 | 42 | .0 | 43 | .0 | 44 | .0 | 45 | .0 | 46 | .0 | 47 | .0 | 48 | .0 |
| 49 | .0 | 50 | .0 | 51 | .0 | 52 | .0 | 53 | .0 | 54 | .0 | 55 | .0 | 56 | .0 |
| 57 | .0 | 58 | .0 | 59 | .0 | 60 | .0 | 61 | .0 | 62 | .0 | 63 | .0 | 64 | .0 |
| 65 | .0 | 66 | .0 | 67 | .0 | 68 | .0 | 69 | .0 | 70 | .0 | 71 | .0 | 72 | .0 |
| 73 | .0 | 74 | .0 | 75 | .0 | 76 | .0 | 77 | .0 | 78 | .0 | 79 | .0 | | |

## TABLE 4-18. NOISE PARAMETER OUTPUT (I and Q VOLTAGE MEANS)

| | | | | | | | | | | | | |
|---|---|---|---|---|---|---|---|---|---|---|---|---|
| IMEAN | | | | | | | | | | | | |
| 1 | -1.8132E+00 | 2 | -1.2424E+00 | 3 | -2.0477E+00 | 4 | -1.5803E+00 | 5 | -1.4070E+00 | 6 | -9.2245E-01 | |
| 7 | -1.4081E+00 | 8 | -3.0425E+00 | 9 | -1.4996E+00 | 10 | -1.5065E+00 | 11 | -1.3746E+00 | 12 | -1.6284E+00 | |
| 13 | -1.4155E+00 | 14 | -7.8979E-01 | 15 | -1.7481E+00 | 16 | -1.4324E+00 | 17 | -1.0491E+00 | 18 | -1.0391E+00 | |
| 19 | -1.1208E+00 | 20 | -1.5996E+00 | 21 | -2.2612E+00 | 22 | -1.5572E+00 | 23 | -1.4444E+00 | 24 | -1.6436E+00 | |
| 25 | -1.4087E+00 | 26 | -1.7466E+00 | 27 | -1.5102E+00 | 28 | -1.7070E+00 | 29 | -1.2449E+00 | 30 | -1.0545E+00 | |
| 31 | -2.3103E+00 | 32 | -1.7109E+00 | 33 | -1.9909E+00 | 34 | -1.1967E+00 | 35 | -1.5437E+00 | 36 | -1.7708E+00 | |
| 37 | -9.7559E-01 | 38 | -8.1519E-01 | 39 | -2.1011E+00 | 40 | -2.0901E+00 | 41 | -1.5237E+00 | 42 | -1.5994E+00 | |
| 43 | -1.6130E+00 | 44 | -1.4551E+00 | 45 | -1.1006E+00 | 46 | -1.4224E+00 | 47 | -1.4570E+00 | 48 | -1.8022E+00 | |
| 49 | -1.4404E+00 | 50 | -2.0540E+00 | 51 | -1.8137E+00 | 52 | -1.7063E+00 | 53 | -1.2605E+00 | 54 | -1.3564E+00 | |
| 55 | -1.4529E+00 | 56 | -1.5483E+00 | 57 | -2.2505E-01 | 58 | -2.0176E+00 | 59 | -1.5354E+00 | 60 | -1.8043E+00 | |
| 61 | -1.5112E+00 | 62 | -1.2717E+00 | 63 | -1.4353E+00 | 64 | -2.1140E+00 | 65 | -1.7217E+00 | 66 | -1.5122E+00 | |
| 67 | -1.7673E+00 | 68 | -9.9072E-01 | 69 | -1.2959E+00 | 70 | -2.0200E+00 | 71 | -2.2827E+00 | 72 | -2.1033E+00 | |
| 73 | -1.5864E+00 | 74 | -1.3145E+00 | 75 | -1.4490E+00 | 76 | -1.4434E+00 | 77 | -8.3813E-01 | 78 | 3.9600E+00 | |
| 79 | 1.9038E+00 | | | | | | | | | | | |
| Q MEAN | | | | | | | | | | | | |
| 1 | -1.4775E+00 | 2 | -1.0334E+00 | 3 | -1.9184E+00 | 4 | -1.1213E+00 | 5 | -1.0031E+00 | 6 | -7.2852E-01 | |
| 7 | -1.6658E+00 | 8 | -1.4453E+00 | 9 | -1.9411E+00 | 10 | -1.7056E+00 | 11 | -1.1846E+00 | 12 | -1.3107E+00 | |
| 13 | -1.1843E+00 | 14 | -7.4927E-01 | 15 | -1.6826E+00 | 16 | -1.2249E+00 | 17 | -8.6411E-01 | 18 | -8.9722E-01 | |
| 19 | -7.7856E-01 | 20 | -1.2148E+00 | 21 | -1.8179E+00 | 22 | -2.5544E-01 | 23 | -1.0945E+00 | 24 | -7.9175E-01 | |
| 25 | -1.0044E+00 | 26 | -1.5023E+00 | 27 | -1.1421E+00 | 28 | -1.3489E-01 | 29 | -1.0194E+00 | 30 | -1.1726E+00 | |
| 31 | -1.5544E+00 | 32 | -1.4307E+00 | 33 | -1.8375E+00 | 34 | -7.4121E-01 | 35 | -1.3594E+00 | 36 | -1.2195E+00 | |
| 37 | -5.4736E-01 | 38 | -9.3408E-01 | 39 | -1.9554E-01 | 40 | -1.0491E+00 | 41 | -5.9322E-01 | 42 | -1.4449E+00 | |
| 43 | -1.4595E+00 | 44 | -1.2964E+00 | 45 | -1.0277E+00 | 46 | -1.2385E+00 | 47 | -1.2419E+00 | 48 | -1.6201E+00 | |
| 49 | -1.2551E+00 | 50 | -1.4586E+00 | 51 | -1.2312E+00 | 52 | -1.2759E+00 | 53 | -1.1324E+00 | 54 | -1.0496E+00 | |
| 55 | -1.0789E+00 | 56 | -1.3357E+00 | 57 | -7.0264E-01 | 58 | -1.0718E+00 | 59 | -1.1470E+00 | 60 | -1.6641E+00 | |
| 61 | -1.2122E+00 | 62 | -1.1724E+00 | 63 | -1.4817E+00 | 64 | -1.7677E+00 | 65 | -1.5081E+00 | 66 | -1.3635E+00 | |
| 67 | -1.3059E+00 | 68 | -9.2920E-01 | 69 | -1.3479E+00 | 70 | -1.5095E+00 | 71 | -1.7551E+00 | 72 | -1.7112E+00 | |
| 73 | -1.2917E+00 | 74 | -9.7283E-01 | 75 | -1.3927E+00 | 76 | -1.4458E+00 | 77 | -8.1716E-01 | 78 | -1.7927E+00 | |
| 79 | -9.4092E-01 | | | | | | | | | | | |
| I,Q MEAN | -1.4281E | | -1.21-1( | | | | | | | | | |

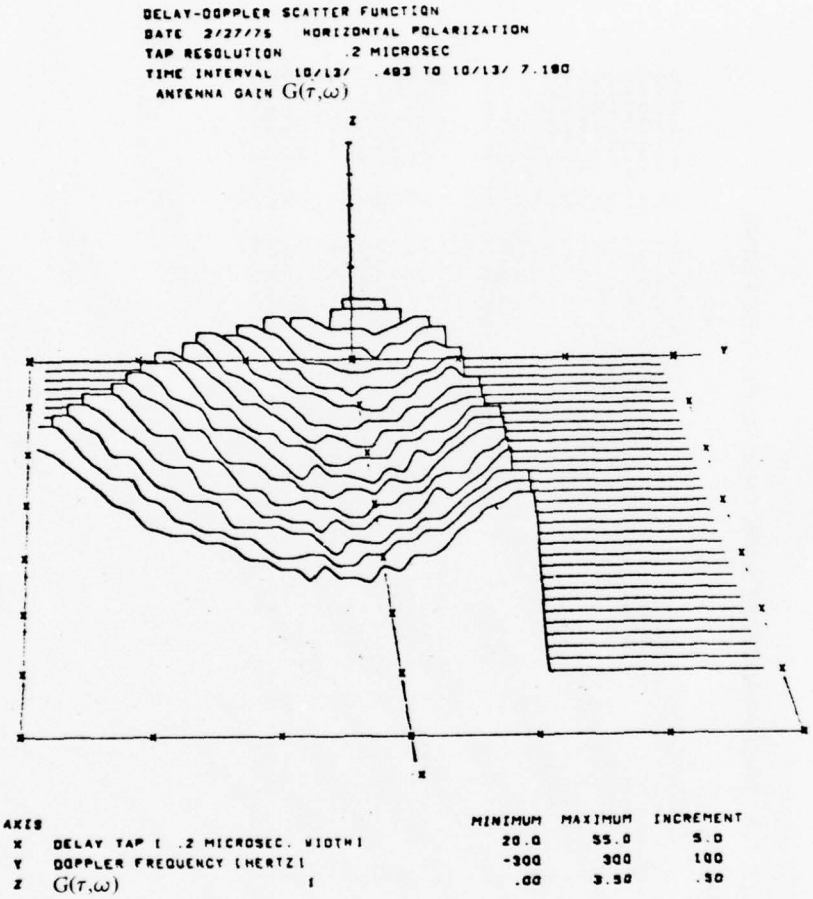


*Figure 4-27. Antenna Effects Removal Output – $G(\tau,\omega)$*

### 4.24.11 Tap I and Q Amplitude Distribution

The amplitude probability distribution algorithm is applied to both I and Q and for each component has as its primary output the following information:

a. Numeric tabulation of each of the three histogram's observed frequencies and expected frequencies
b. The $\chi^2$ value and probability for each of the histograms
c. A plot of the observed and expected distribution associated with the histogram constructed by subdividing the $(-3\sigma, +3\sigma)$ amplitude range into 18 equal-length bin widths.

An example of outputs a and b is presented in table 4-19. This represents that portion of the output associated with the histogram corresponding to bin width selection based on equal bin frequency expectation (e.g., 5% expected in each bin; total population 1024).

Figure 4-28 contains an example of output option c. Plotted on one page are the I, Q, and phase distributions for two taps. Bar charts and continuous curves are used to represent the observed and expected frequencies, respectively. For the I and Q distribution, the markers along the x-axis are $\sigma/3$ apart and span the range from $-3\sigma$ to $+3\sigma$. The scale mark for the phase distribution is given every $20^{o}$ over the range from $-180^{o}$ to $+180^{o}$.

### 4.24.12 Tap Phase Distribution

Numerical and plotted output formats are available to present the results of the tap phase distribution testings. An example illustrating the plotted format has been given in figure 4-28. The numerical output consists of a tabulation of the observed and expected histogram values, the calculated $\chi^2$ statistic, and the probability of obtaining a $\chi^2$ value less than the observed. Table 4-20 contains a representative numerical output set.

### 4.24.13 Tap Process Cross-Correlation

For complex time-domain processes, such as represented by the SACP tap voltages, the cross-correlation function has both real and imaginary components. The tap process cross-correlation algorithm numerically outputs these results in the form of magnitude and phase and also provides a three-dimensional plot of the magnitude. An example of a numerical tabulation is given in table 4-21. Columns are lumped in groups of three (LAG, AMP, PH) corresponding to time lag in microseconds, function normalized amplitude, and phase in degrees. A sample plotted output is given in figure 4-29. This output format is configured to display on one graph all cross-correlations that are made with a particular tap (referred to as the principal tap).

## TABLE 4-19. TAP I AND Q APD HISTOGRAMS

C4.02.7% FR IN-PLANE IQ-ANGLE

CHI - SQUARED STATISTICS I OF TAP 27
( INDIRECT TAP )

| INTERVAL | | | EXPECTED FREQS. | OBSERVED FREQS. |
|---|---|---|---|---|
| LE. | | -25.73 | 51.19 | 55.00 |
| GT. | -25.73 LE. | -20.17 | 51.19 | 49.00 |
| GT. | -20.17 LE. | -16.42 | 51.15 | 48.00 |
| GT. | -16.42 LE. | -13.43 | 51.23 | 57.00 |
| GT. | -13.43 LE. | -10.87 | 51.14 | 52.00 |
| GT. | -10.87 LE. | -8.56 | 51.51 | 44.00 |
| GT. | -8.56 LE. | -6.43 | 51.19 | 52.00 |
| GT. | -6.43 LE. | -4.44 | 50.42 | 61.00 |
| GT. | -4.44 LE. | -2.47 | 51.72 | 51.00 |
| GT. | -2.47 LE. | -.54 | 51.34 | 38.00 |
| GT. | -.54 LE. | 1.39 | 51.34 | 49.00 |
| GT. | 1.39 LE. | 3.37 | 51.72 | 52.00 |
| GT. | 3.37 LE. | 5.36 | 50.42 | 54.00 |
| GT. | 5.36 LE. | 7.49 | 51.19 | 56.00 |
| GT. | 7.49 LE. | 9.80 | 51.51 | 40.00 |
| GT. | 9.80 LE. | 12.36 | 51.14 | 56.00 |
| GT. | 12.36 LE. | 15.34 | 51.23 | 47.00 |
| GT. | 15.34 LE. | 19.09 | 51.15 | 59.00 |
| GT. | 19.09 LE. | 24.65 | 51.19 | 56.00 |
| GT. | | 24.65 | 51.19 | 52.00 |

OBSERVED CHI - SQUARES = 13.92908 WITH 17 D.F.

THE PROBABILITY OF OBTAINING A VALUE OF CHI – SQUARES LESS THAN THE OBSERVED CHI IS .32788

C4.02.7% FR IN-PLANE IQ-ANGLE

CHI - SQUARED STATISTICS Q OF TAP 27
( INDIRECT TAP )

| INTERVAL | | | EXPECTED FREQS. | OBSERVED FREQS. |
|---|---|---|---|---|
| LE. | | -20.59 | 51.19 | 44.00 |
| GT. | -20.59 LE. | -16.66 | 51.19 | 57.00 |
| GT. | -16.66 LE. | -13.66 | 51.15 | 44.00 |
| GT. | -13.66 LE. | -10.96 | 51.23 | 54.00 |
| GT. | -10.96 LE. | -8.48 | 51.14 | 52.00 |
| GT. | -8.48 LE. | -6.19 | 51.51 | 57.00 |
| GT. | -6.19 LE. | -4.05 | 51.19 | 55.00 |
| GT. | -4.05 LE. | -3.03 | 50.42 | 55.00 |
| GT. | -3.03 LE. | -1.02 | 51.72 | 57.00 |
| GT. | -1.02 LE. | -.05 | 51.34 | 43.00 |
| GT. | -.05 LE. | 1.93 | 51.34 | 45.00 |
| GT. | 1.93 LE. | 3.14 | 51.72 | 53.00 |
| GT. | 3.14 LE. | 4.76 | 50.42 | 43.00 |
| GT. | 4.76 LE. | 6.56 | 51.19 | 48.00 |
| GT. | 6.56 LE. | 8.39 | 51.51 | 46.00 |
| GT. | 8.39 LE. | 10.47 | 51.14 | 54.00 |
| GT. | 10.47 LE. | 12.91 | 51.23 | 61.00 |
| GT. | 12.91 LE. | 15.97 | 51.15 | 44.00 |
| GT. | 15.97 LE. | 20.50 | 51.19 | 55.00 |
| GT. | | 20.50 | 51.19 | 52.00 |

OBSERVED CHI - SQUARES = 13.07459 WITH 17 D.F.

THE PROBABILITY OF OBTAINING A VALUE OF CHI – SQUARES LESS THAN THE OBSERVED CHI IS .26882

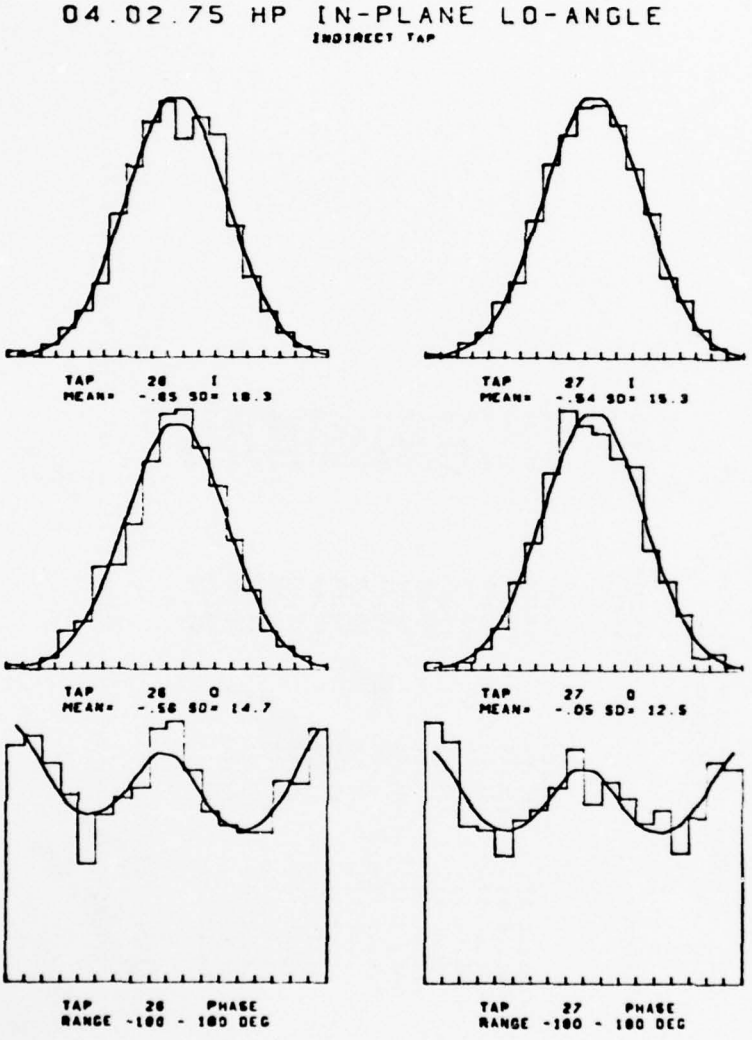


*Figure 4-28. Tap I, Q, and Phase Histograms*

## TABLE 4-20. TAP PHASE DISTRIBUTION HISTOGRAM

64,62,75 EP IN-PLANE IC-ANGLE

CHI - SQUARED STATISTICS PHASE OF TAP 27
( INDIRECT TAP )

| | INTERVAL | | EXPECTED FREQS. | OBSERVED FREQS. |
|---|---|---|---|---|
| LE. | | -160.00 | 71.42 | 80.00 |
| GT. | -180.00 LE. | -140.00 | 64.30 | 74.00 |
| GT. | -140.00 LE. | -120.00 | 55.51 | 46.00 |
| GT. | -120.00 LE. | -100.00 | 49.25 | 47.00 |
| GT. | -100.00 LE. | -80.00 | 44.75 | 34.00 |
| GT. | -80.00 LE. | -60.00 | 49.09 | 50.00 |
| GT. | -60.00 LE. | -40.00 | 52.81 | 53.00 |
| GT. | -40.00 LE. | -20.00 | 59.85 | 60.00 |
| GT. | -20.00 LE. | .00 | 65.57 | 72.00 |
| GT. | .00 LE. | 20.00 | 65.45 | 55.00 |
| GT. | 20.00 LE. | 40.00 | 59.55 | 62.00 |
| GT. | 40.00 LE. | 60.00 | 52.49 | 57.00 |
| GT. | 60.00 LE. | 80.00 | 47.61 | 49.00 |
| GT. | 80.00 LE. | 100.00 | 44.33 | 53.00 |
| GT. | 100.00 LE. | 120.00 | 49.82 | 40.00 |
| GT. | 120.00 LE. | 140.00 | 55.09 | 51.00 |
| GT. | 140.00 LE. | 160.00 | 63.97 | 68.00 |
| GT. | | 180.00 | 71.28 | 66.00 |

OBSERVED CHI - SQUARES = 11.32580 WITH 14 D.F.

THE PROBABILITY OF OBTAINING A VALUE OF CHI - SQUARES LESS THAN THE OBSERVED CHI IS .33973

## TABLE 4-21. CROSS-CORRELATION NUMERICAL OUTPUT

4-2-75 HORIZONTAL

CORRELATION OF TAP 29 WITH TAP 24

| | | | | | | | | | | | | |
|---|---|---|---|---|---|---|---|---|---|---|---|---|
| LAG,AMP,PH | -49.2 | .0085 | 75.6 | -47.5 | .0062 | 54.7 | -45.9 | .0016 | 45.0 | -44.3 | .0154 | 38.8 |
| LAG,AMP,PH | -42.6 | .0174 | 7.2 | -41.0 | .0202 | -8.1 | -39.3 | .0131 | -12.4 | -37.7 | .0092 | -84.1 |
| LAG,AMP,PH | -36.1 | .0064 | -34.2 | -34.4 | .0123 | -116.7 | -32.8 | .0092 | -140.8 | -31.1 | .0107 | -121.4 |
| LAG,AMP,PH | -29.5 | .0114 | -170.1 | -27.9 | .0089 | -112.0 | -26.2 | .0069 | 174.9 | -24.6 | .0169 | 59.7 |
| LAG,AMP,PH | -23.0 | .0141 | 80.1 | -21.3 | .0087 | 84.0 | -19.7 | .0162 | 39.7 | -18.0 | .0163 | 15.1 |
| LAG,AMP,PH | -16.4 | .0141 | 8.0 | -14.8 | .0037 | 1.1 | -13.1 | .0155 | -4.8 | -11.5 | .0112 | -36.1 |
| LAG,AMP,PH | -9.8 | .0113 | -13.2 | -8.2 | .0150 | -60.5 | -6.6 | .0093 | 165.6 | -4.9 | .0037 | -147.8 |
| LAG,AMP,PH | -3.3 | .0091 | -154.7 | -1.6 | .0060 | -156.3 | .0 | .0061 | 114.0 | 1.6 | .0075 | 103.3 |
| LAG,AMP,PH | 3.3 | .0059 | 51.5 | 4.9 | .0131 | 122.2 | 6.6 | .0142 | 101.2 | 8.2 | .0140 | 90.2 |
| LAG,AMP,PH | 9.8 | .0136 | 105.0 | 11.5 | .0014 | 161.3 | 13.1 | .0117 | 140.5 | 14.8 | .0016 | 163.1 |
| LAG,AMP,PH | 16.4 | .0048 | 174.0 | 18.0 | .0079 | -137.8 | 19.7 | .0077 | -156.7 | 21.3 | .0034 | 144.3 |
| LAG,AMP,PH | 23.0 | .0040 | 60.3 | 24.6 | .0077 | 127.9 | 26.2 | .0083 | -60.9 | 27.9 | .0037 | 90.6 |
| LAG,AMP,PH | 29.5 | .0065 | 61.2 | 31.1 | .0053 | 53.7 | 32.8 | .0050 | -122.4 | 34.4 | .0073 | 24.9 |
| LAG,AMP,PH | 36.1 | .0049 | 28.8 | 37.7 | .0104 | 3.8 | 39.3 | .0076 | -42.8 | 41.0 | .0124 | -24.0 |
| LAG,AMP,PH | 42.6 | .0123 | -37.4 | 44.3 | .0134 | -146.8 | 45.9 | .0104 | -55.5 | 47.5 | .0126 | -70.3 |
| LAG,AMP,PH | 49.2 | .0130 | 36.4 | | | | | | | | | |

CORRELATION OF TAP 29 WITH TAP 25

| | | | | | | | | | | | | |
|---|---|---|---|---|---|---|---|---|---|---|---|---|
| LAG,AMP,PH | -49.2 | .0142 | -49.2 | -47.5 | .0173 | -49.3 | -45.9 | .0206 | -37.5 | -44.3 | .0174 | -29.3 |
| LAG,AMP,PH | -42.6 | .0177 | -51.6 | -41.0 | .0189 | -65.0 | -39.3 | .0196 | -61.4 | -37.7 | .0174 | -73.6 |
| LAG,AMP,PH | -36.1 | .0107 | -65.8 | -34.4 | .0169 | -79.2 | -32.8 | .0167 | -81.9 | -31.1 | .0153 | -94.9 |
| LAG,AMP,PH | -29.5 | .0110 | -99.5 | -27.9 | .0118 | -121.6 | -26.2 | .0109 | -97.2 | -24.6 | .0083 | -133.3 |
| LAG,AMP,PH | -23.0 | .0067 | -112.0 | -21.3 | .0054 | -119.8 | -19.7 | .0042 | -121.3 | -18.0 | .0040 | -103.3 |
| LAG,AMP,PH | -16.4 | .0037 | -147.1 | -14.8 | .0079 | -50.2 | -13.1 | .0051 | -90.5 | -11.5 | .0051 | -94.2 |
| LAG,AMP,PH | -9.8 | .0075 | -137.6 | -8.2 | .0086 | -105.8 | -6.6 | .0080 | -147.7 | -4.9 | .0064 | -128.3 |
| LAG,AMP,PH | -3.3 | .0119 | -141.9 | -1.6 | .0105 | -155.0 | .0 | .0085 | -164.2 | 1.6 | .0062 | 171.0 |
| LAG,AMP,PH | 3.3 | .0090 | 173.4 | 4.9 | .0043 | 156.9 | 6.6 | .0055 | 155.2 | 8.2 | .0036 | 174.3 |
| LAG,AMP,PH | 9.8 | .0132 | 159.3 | 11.5 | .0026 | 146.1 | 13.1 | .0059 | 165.0 | 14.8 | .0074 | 169.8 |
| LAG,AMP,PH | 16.4 | .0061 | 119.3 | 18.0 | .0039 | 153.9 | 19.7 | .0064 | 168.3 | 21.3 | .0049 | 160.8 |
| LAG,AMP,PH | 23.0 | .0045 | -167.4 | 24.6 | .0078 | 123.6 | 26.2 | .0093 | 152.7 | 27.9 | .0096 | 134.6 |
| LAG,AMP,PH | 29.5 | .0071 | 166.5 | 31.1 | .0077 | 141.1 | 32.8 | .0083 | 93.9 | 34.4 | .0070 | 82.0 |
| LAG,AMP,PH | 36.1 | .0064 | 98.2 | 37.7 | .0056 | 94.0 | 39.3 | .0063 | 140.9 | 41.0 | .0011 | 121.3 |
| LAG,AMP,PH | 42.6 | .0013 | 66.8 | 44.3 | .0061 | 122.1 | 45.9 | .0070 | 144.8 | 47.5 | .0066 | 91.8 |
| LAG,AMP,PH | 49.2 | .0045 | 103.3 | | | | | | | | | |

CORRELATION FUNCTION
4-2-75 HORIZONTAL
TIME INTERVAL 11/ 0/ .492 11/ 0/13.636
PRINCIPLE TAP 28
TAP RESOLUTION .20

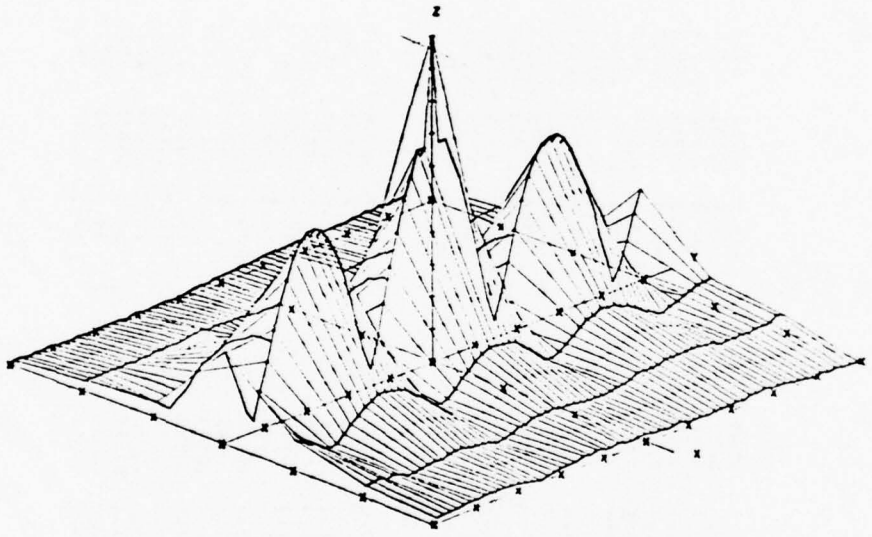


| AXIS | | MINIMUM | MAXIMUM | INCREMENT |
|---|---|---|---|---|
| X | TAP OFFSET | -3.00 | 3.00 | 1.00 |
| Y | TIME LAG (MSEC) | -50.0 | 50.0 | 10.0 |
| Z | CORRELATION (MAGNITUDE) | .00 | 1.00 | .10 |

*Figure 4-29. Tap Process Cross-Correlation Output*

### 4.24.14 Tap-Gain Autocorrelation Function

Numerical and three-dimensional plot formats are used to represent the derived tap-gain autocorrelation function. Both magnitude and phase are given numerically, whereas only the magnitude of the function is plotted. Example numerical results for the function magnitude and phase are given in tables 4-22 and 4-23, respectively. The output format in both cases is self-explanatory (the time-lag column is in milliseconds). This particular example corresponds to the noise-removed option applied to horizontally polarized in-plane flight data and is seen to be characterized by a process whose specular return falls in tap 25. Corresponding to the same data base used for the numerical example, we present a sample plotted output in figures 4-30 and 4-31 for noise-present and noise-removed options, respectively. As indicated, the receiver noise, which appears as a spike train along the $\xi = 0$ axis, is effectively eliminated by the noise-removal algorithm.

### 4.24.15 Airborne System Parameters Tape

Numerical line print and stacked CalComp plots are used to display the airborne system parameters.

The printed output example presented in table 4-24 illustrates the presentation format. Each page begins with the experiment date. Underneath is a columnar listing of the time (HR/MIN/SEC); the status bits for the bit rate, sequence length, antenna, and polarization; followed by the 13 data channel samples corresponding to the power monitor sensors and the aircraft flight parameters.

CalComp plots stacked vertically over a common time base are used to display the SACP modulator mode data, the RF subsystem data, and any nine of the aircraft flight parameters and power meter readings. These data are plotted with a time scale of 1 in/min. In general, one plot is used to represent a single flight test leg (14 to 20 min). Figure 4-32 presents a typical output plot.

## TABLE 4-22. TAP-GAIN AUTOCORRELATION FUNCTION (MAGNITUDE) NUMERICAL OUTPUT

| TAP GAIN AUTO COR LAG | TAP 21 | TAP 22 | TAP 23 | AMPLITUDE TAP 24 | TAP 25 | TAP 26 | TAP 27 | TAP 28 | TAP 29 | TAP 30 |
|---|---|---|---|---|---|---|---|---|---|---|
| -49.18 | 1.46 | 1.22 | .24 | 3.59 | 201.20 | 152.29 | 89.37 | 100.90 | 52.00 | 37.64 |
| -47.54 | 5.65 | 3.77 | 2.24 | 2.23 | 215.79 | 149.98 | 108.21 | 97.51 | 58.36 | 31.53 |
| -45.90 | 1.48 | 3.33 | 2.02 | 4.83 | 224.66 | 137.61 | 133.40 | 73.48 | 68.41 | 46.73 |
| -44.26 | 1.00 | 1.39 | 1.27 | 2.76 | 238.95 | 123.92 | 157.42 | 61.87 | 69.49 | 66.77 |
| -42.62 | 1.35 | 2.74 | 1.93 | 9.17 | 243.95 | 114.14 | 181.39 | 43.57 | 68.32 | 82.78 |
| -40.98 | .75 | 2.13 | 1.66 | 3.89 | 256.32 | 90.98 | 192.57 | 43.30 | 64.04 | 92.03 |
| -39.34 | 1.47 | 2.81 | 2.61 | 8.18 | 271.07 | 79.28 | 208.81 | 55.59 | 52.17 | 100.77 |
| -37.70 | 2.51 | 2.17 | .42 | 5.24 | 275.66 | 62.22 | 222.29 | 79.37 | 37.37 | 100.64 |
| -36.07 | 2.18 | 1.20 | .99 | .82 | 284.24 | 44.26 | 225.86 | 96.19 | 21.89 | 94.98 |
| -34.43 | .08 | 1.59 | 1.66 | .66 | 297.32 | 26.35 | 229.61 | 119.98 | 8.66 | 81.65 |
| -32.79 | 1.71 | 1.74 | .73 | 1.73 | 306.91 | 11.45 | 225.87 | 138.51 | 17.12 | 60.48 |
| -31.15 | 3.42 | 2.17 | 2.25 | 3.46 | 313.71 | 27.83 | 222.38 | 157.41 | 33.01 | 38.73 |
| -29.51 | 2.13 | 3.14 | 2.38 | 4.12 | 331.00 | 54.34 | 201.00 | 161.46 | 52.19 | 25.82 |
| -27.87 | 1.08 | .94 | 1.06 | 2.34 | 334.60 | 76.27 | 187.87 | 162.55 | 73.28 | 46.42 |
| -26.23 | 2.00 | 3.64 | 2.24 | 2.60 | 346.32 | 103.91 | 168.84 | 166.15 | 81.68 | 71.67 |
| -24.59 | 1.62 | 1.73 | 2.87 | 1.60 | 354.64 | 129.65 | 147.82 | 155.33 | 90.67 | 93.88 |
| -22.95 | .77 | 3.58 | 3.17 | 8.66 | 366.37 | 154.22 | 126.15 | 143.85 | 100.87 | 119.69 |
| -21.31 | 3.77 | 1.07 | 4.17 | 1.36 | 372.89 | 173.66 | 109.67 | 124.40 | 93.38 | 125.56 |
| -19.67 | 1.06 | 2.02 | 2.38 | 9.53 | 376.16 | 201.84 | 94.77 | 100.01 | 87.02 | 133.59 |
| -18.03 | 4.28 | 2.16 | 5.97 | 5.96 | 385.99 | 223.63 | 92.18 | 71.30 | 77.73 | 121.71 |
| -16.39 | 2.69 | 4.25 | 2.80 | 3.49 | 386.96 | 246.66 | 104.38 | 39.29 | 60.13 | 111.40 |
| -14.75 | 4.93 | 1.29 | 3.66 | 1.65 | 397.45 | 271.91 | 130.16 | 16.09 | 37.87 | 86.71 |
| -13.11 | 3.02 | .90 | 3.42 | 5.01 | 404.90 | 289.23 | 153.36 | 38.93 | 20.99 | 63.88 |
| -11.48 | 2.61 | .95 | 2.82 | 5.76 | 410.62 | 314.05 | 183.35 | 74.79 | 11.81 | 34.25 |
| -9.84 | .49 | .21 | .57 | 3.47 | 409.63 | 326.02 | 211.15 | 108.27 | 34.16 | 20.39 |
| -8.20 | 4.28 | .48 | 4.55 | 4.53 | 419.62 | 343.30 | 238.55 | 142.30 | 57.37 | 54.85 |
| -6.56 | 2.28 | 1.12 | 1.71 | 4.88 | 420.77 | 349.85 | 258.78 | 165.20 | 78.08 | 81.71 |
| -4.92 | .50 | 2.28 | 2.74 | 5.84 | 425.92 | 365.90 | 279.97 | 189.41 | 99.66 | 120.41 |
| -3.28 | 3.70 | 3.71 | 3.02 | 1.02 | 423.95 | 366.25 | 288.36 | 205.19 | 117.03 | 131.97 |
| -1.64 | 1.86 | 2.08 | 1.90 | 2.70 | 426.91 | 369.67 | 301.88 | 213.52 | 123.29 | 149.63 |
| .00 | 1.28 | 2.72 | 4.00 | 3.52 | 429.91 | 378.42 | 305.72 | 220.78 | 126.54 | 150.90 |
| 1.64 | 1.86 | 2.08 | 1.90 | 2.70 | 426.91 | 369.67 | 301.88 | 213.52 | 123.29 | 149.63 |
| 3.28 | 3.70 | 3.71 | 3.02 | 1.02 | 423.95 | 366.25 | 288.36 | 205.19 | 117.03 | 131.97 |
| 4.92 | .50 | 2.28 | 2.74 | 5.84 | 425.92 | 365.90 | 279.97 | 189.41 | 99.66 | 120.41 |
| 6.56 | 2.28 | 1.12 | 1.71 | 4.88 | 420.77 | 349.85 | 258.78 | 165.20 | 78.08 | 81.71 |
| 8.20 | 4.28 | .48 | 4.55 | 4.53 | 419.62 | 343.30 | 238.55 | 142.30 | 57.37 | 54.85 |
| 9.84 | .49 | .21 | .57 | 3.47 | 409.63 | 326.02 | 211.15 | 108.27 | 34.16 | 20.39 |
| 11.48 | 2.61 | .95 | 2.82 | 5.76 | 410.62 | 314.05 | 183.35 | 74.79 | 11.81 | 34.25 |
| 13.11 | 3.02 | .90 | 3.42 | 5.01 | 404.90 | 289.23 | 153.36 | 38.93 | 20.99 | 63.88 |
| 14.75 | 4.93 | 1.29 | 3.66 | 1.65 | 397.45 | 271.91 | 130.16 | 16.09 | 37.87 | 86.71 |
| 16.39 | 2.69 | 4.25 | 2.80 | 3.49 | 386.96 | 246.66 | 104.38 | 39.29 | 60.13 | 111.40 |
| 18.03 | 4.28 | 2.16 | 5.97 | 5.96 | 385.99 | 223.63 | 92.18 | 71.30 | 77.73 | 121.71 |
| 19.67 | 1.06 | 2.02 | 2.38 | 9.53 | 376.16 | 201.84 | 94.77 | 100.01 | 87.02 | 133.59 |
| 21.31 | 3.77 | 1.07 | 4.17 | 1.36 | 372.89 | 173.66 | 109.67 | 124.40 | 93.38 | 125.56 |
| 22.95 | .77 | 3.58 | 3.17 | 8.66 | 366.37 | 154.22 | 126.15 | 143.85 | 100.87 | 119.69 |
| 24.59 | 1.62 | 1.73 | 2.87 | 1.60 | 354.64 | 129.65 | 147.82 | 155.33 | 90.67 | 93.88 |
| 26.23 | 2.00 | 3.64 | 2.24 | 2.60 | 346.32 | 103.91 | 168.84 | 166.15 | 81.68 | 71.67 |
| 27.87 | 1.08 | .94 | 1.06 | 2.34 | 334.60 | 76.27 | 187.87 | 162.55 | 73.28 | 46.42 |
| 29.51 | 2.13 | 3.14 | 2.38 | 4.12 | 331.00 | 54.34 | 201.00 | 161.46 | 52.19 | 25.82 |
| 31.15 | 3.42 | 2.17 | 2.25 | 3.46 | 313.71 | 27.83 | 222.38 | 157.41 | 33.01 | 38.73 |

## TABLE 4-23. TAP-GAIN AUTOCORRELATION FUNCTION (PHASE) NUMERICAL OUTPUT

TAP GAIN AUTO COR PHASE

| LAG | TAP 21 | TAP 22 | TAP 23 | TAP 24 | TAP 25 | TAP 26 | TAP 27 | TAP 28 | TAP 29 | TAP 30 |
|---|---|---|---|---|---|---|---|---|---|---|
| -49.18 | 36.72 | -143.71 | -141.09 | 53.19 | 96.32 | -84.20 | 13.50 | -145.25 | -102.49 | -160.97 |
| -47.54 | 143.53 | -51.56 | -10.49 | 175.97 | 93.59 | -89.15 | -2.52 | -149.37 | -112.69 | -132.01 |
| -45.90 | -170.34 | -11.84 | 152.53 | -4.58 | 88.18 | -87.32 | -16.87 | -142.43 | -117.86 | -101.72 |
| -44.26 | 130.80 | -111.02 | 25.45 | 58.26 | 86.13 | -90.90 | -26.59 | -133.40 | -126.02 | -98.53 |
| -42.62 | 176.91 | -44.14 | 168.53 | 3.05 | 81.75 | -96.24 | -35.42 | -116.60 | -130.37 | -100.02 |
| -40.98 | 142.20 | 5.51 | -156.48 | -78.80 | 78.31 | -94.83 | -44.75 | -89.17 | -143.42 | -106.27 |
| -39.34 | 102.02 | -144.88 | 4.02 | 65.32 | 74.61 | -92.97 | -52.91 | -63.76 | -152.33 | -111.39 |
| -37.70 | -145.96 | 55.15 | -24.54 | 9.27 | 70.90 | -95.06 | -60.91 | -55.55 | -150.30 | -115.85 |
| -36.07 | -175.42 | 11.40 | -3.68 | 144.31 | 69.16 | -91.59 | -68.89 | -55.44 | -157.23 | -125.47 |
| -34.43 | -134.83 | -101.97 | 76.54 | -16.31 | 64.54 | -72.34 | -77.12 | -53.19 | -94.20 | -127.02 |
| -32.79 | 120.47 | -35.24 | -140.20 | 57.86 | 61.25 | .77 | -86.39 | -57.58 | -29.79 | -129.39 |
| -31.15 | 171.21 | 31.35 | -47.23 | -84.46 | 58.46 | 27.40 | -93.85 | -61.77 | -25.18 | -114.61 |
| -29.51 | 139.28 | -89.99 | 47.16 | -1.08 | 55.47 | 42.86 | -102.84 | -64.39 | -29.96 | -75.41 |
| -27.87 | -148.83 | 93.73 | -26.74 | -26.14 | 51.87 | 41.33 | -111.99 | -69.66 | -35.86 | -44.56 |
| -26.23 | -166.08 | 46.67 | -104.48 | 33.64 | 48.24 | 41.10 | -123.09 | -74.31 | -43.20 | -34.69 |
| -24.59 | -47.48 | -109.26 | 100.55 | 62.33 | 45.68 | 41.89 | -134.32 | -78.56 | -51.65 | -34.80 |
| -22.95 | -47.87 | 79.61 | -111.49 | 11.37 | 42.25 | 38.67 | -144.04 | -84.58 | -62.13 | -42.14 |
| -21.31 | 105.94 | -178.41 | -59.68 | -124.43 | 38.82 | 36.76 | -171.40 | -88.57 | -70.35 | -49.37 |
| -19.67 | -118.44 | 157.70 | 3.93 | -52.19 | 35.33 | 34.60 | 167.71 | -92.84 | -79.64 | -55.84 |
| -18.03 | 148.34 | 102.06 | -46.78 | 41.28 | 33.00 | 33.33 | 136.71 | -92.27 | -88.05 | -63.09 |
| -16.39 | -86.41 | 53.33 | -164.93 | 160.42 | 29.54 | 30.35 | 115.59 | -99.06 | -102.75 | -73.02 |
| -14.75 | -137.79 | 32.25 | 45.72 | 76.39 | 27.53 | 27.15 | 90.52 | -40.89 | -111.23 | -79.14 |
| -13.11 | 178.48 | 167.79 | -15.85 | -23.19 | 24.06 | 23.44 | 73.19 | 19.72 | -128.74 | -79.50 |
| -11.48 | 164.19 | 77.10 | -35.42 | -19.39 | 20.74 | 20.39 | 61.16 | 26.23 | 62.61 | -67.03 |
| -9.84 | 171.98 | -112.99 | 12.39 | 44.89 | 18.20 | 18.59 | 50.63 | 31.00 | 64.86 | 2.29 |
| -8.20 | -58.72 | -1.28 | 126.38 | -22.68 | 14.88 | 14.94 | 40.38 | 24.69 | 45.10 | 30.89 |
| -6.56 | 89.18 | -44.45 | -119.11 | -8.81 | 12.51 | 12.21 | 30.45 | 22.56 | 34.88 | 27.63 |
| -4.92 | -7.86 | 17.16 | -167.29 | -24.40 | 9.08 | 9.56 | 23.67 | 15.76 | 26.29 | 22.73 |
| -3.28 | 173.23 | -54.82 | 59.23 | 46.69 | 5.69 | 5.88 | 14.95 | 10.99 | 18.36 | 14.57 |
| -1.64 | -6.74 | 115.88 | -119.51 | -6.52 | 3.16 | 3.59 | 7.46 | 5.92 | 9.10 | 8.59 |
| .00 | 180.00 | 180.00 | .00 | .00 | .00 | .00 | .00 | .00 | .00 | .00 |
| 1.64 | 6.74 | -115.88 | 119.51 | 6.52 | -3.16 | -3.59 | -7.46 | -5.92 | -9.10 | -8.59 |
| 3.28 | -173.23 | 54.82 | -59.23 | -46.69 | -5.69 | -5.88 | -14.95 | -10.99 | -18.36 | -14.57 |
| 4.92 | 7.86 | -17.16 | 167.29 | 24.40 | -9.08 | -9.56 | -23.67 | -15.76 | -26.29 | -22.73 |
| 6.56 | -89.18 | 44.45 | 119.11 | 8.81 | -12.51 | -12.21 | -30.45 | -22.56 | -34.88 | -27.63 |
| 8.20 | 58.72 | 1.28 | -126.38 | 22.68 | -14.88 | -14.94 | -40.38 | -24.69 | -45.10 | -30.89 |
| 9.84 | -171.98 | 112.99 | -12.39 | -44.89 | -18.20 | -18.59 | -50.63 | -31.00 | -64.86 | -2.29 |
| 11.48 | -164.19 | -77.10 | 35.42 | 19.39 | -20.74 | -20.39 | -61.16 | -26.23 | -62.61 | 67.03 |
| 13.11 | -178.48 | -107.79 | 15.85 | 23.19 | -24.06 | -23.44 | -73.19 | -19.72 | 128.74 | 79.50 |
| 14.75 | 137.79 | -32.25 | -45.72 | -76.39 | -27.53 | -27.15 | -90.52 | 40.89 | 111.23 | 79.14 |
| 16.39 | 86.41 | -53.33 | 164.93 | -160.42 | -29.54 | -30.35 | -115.59 | 99.06 | 102.75 | 73.02 |
| 18.03 | -148.34 | -102.06 | 46.78 | -41.28 | -33.00 | -33.33 | -136.71 | 92.27 | 88.05 | 63.09 |
| 19.67 | 118.44 | -157.70 | -3.93 | 52.19 | -35.33 | -34.60 | -167.71 | 92.84 | 79.64 | 55.84 |
| 21.31 | -105.94 | 178.41 | 59.68 | 124.43 | -36.82 | -36.76 | 171.40 | 88.57 | 70.35 | 49.37 |
| 22.95 | 47.87 | -79.61 | 111.49 | -11.37 | -42.25 | -38.67 | 149.04 | 84.58 | 62.13 | 42.14 |
| 24.59 | 47.48 | 109.26 | -100.55 | -62.33 | -45.68 | -41.89 | 134.32 | 78.56 | 51.65 | 34.80 |
| 26.23 | 166.08 | -46.67 | 104.48 | -33.64 | -48.24 | -41.10 | 123.09 | 74.31 | 43.20 | 34.69 |
| 27.87 | 148.83 | -93.73 | 20.74 | 26.14 | -51.87 | -41.33 | 111.99 | 69.66 | 35.86 | 44.56 |
| 29.51 | -139.28 | 89.99 | -47.16 | 1.08 | -55.47 | -42.86 | 102.84 | 64.39 | 29.96 | 75.41 |
| 31.15 | -171.21 | -31.35 | 47.23 | 84.46 | -58.46 | -27.40 | 93.85 | 61.77 | 25.18 | 114.61 |

TAP AUTOCORRELATION FUNCTION
4-2-75 HORIZONTAL
TIME INTERVAL 11/ 8/ .492 11/ 8/ 2.217

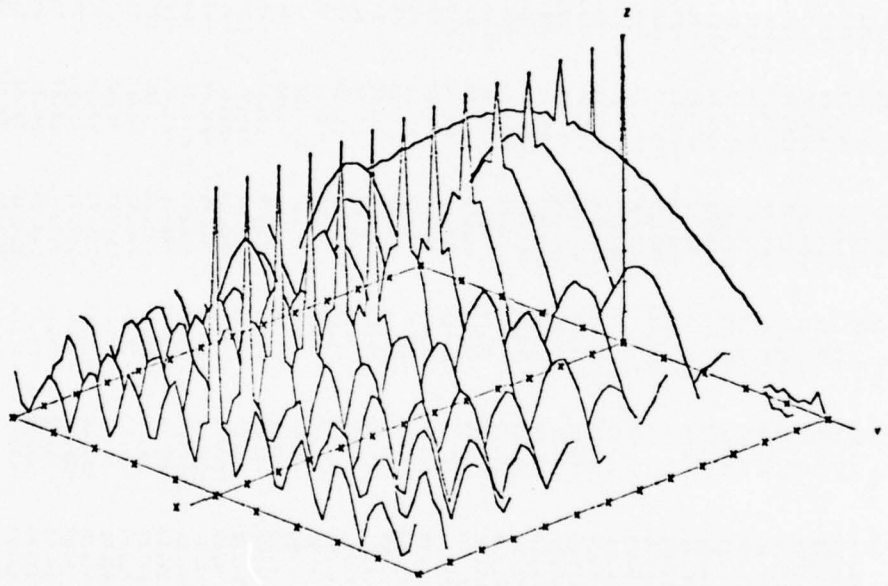


| AXIS | | MINIMUM | MAXIMUM | INCREMENT |
|---|---|---|---|---|
| X | TAP NUMBER | 23.0 | 36.0 | 1.0 |
| Y | TIME LAG (MSEC) | -50.0 | 50.0 | 10.0 |
| Z | AUTOCORRELATION (MAGNITUDE) | .00 | 1.00 | .10 |

*Figure 4-30. Tap-Gain Autocorrelation Function (Noise Present)*

TAP AUTOCORRELATION FUNCTION
4-2-75 HORIZONTAL
TIME INTERVAL 11/ 0/ .492 11/ 0/ 2.217

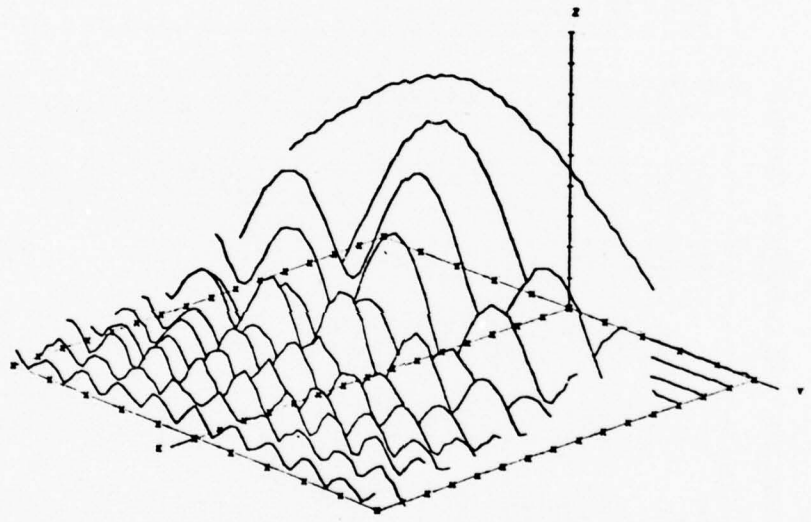


| AXIS | | MINIMUM | MAXIMUM | INCREMENT |
|---|---|---|---|---|
| X | TAP NUMBER | 21.0 | 36.0 | 1.0 |
| Y | TIME LAG (MSEC) | -50.0 | 50.0 | 10.0 |
| Z | TAP GAIN AUTOCORRELATION | 0 | 450 | 50 |

*Figure 4-31. Tap-Gain Autocorrelation Function (Noise Removed)*

## TABLE 4-24. AIRBORNE TAPE NUMERICAL OUTPUT

3/27/75

| | | | | | | | | | | | | | | | | | | |
|---|---|---|---|---|---|---|---|---|---|---|---|---|---|---|---|---|---|---|
| | | | | | | OH | P40 | VP | P4V | VP-DC | HP | P4H | ALT. | C-AD | F-AD | ROLL | PITCH | S-SPD |
| | | | | | | V | W | V | W | V | V | W | FEET | DEG | DEG | DEG | DEG | KN |
| 10/ 0/ 3 | 5 | 3 | 1 | 0 | | 3.30 | 22.0 | .72 | 91.7 | 3.80 | 3.20 | 26.5 | 28657 | 159.7 | 5.33 | 1.8 | -4.9 | 439.5 |
| | | | | | | 3.32 | 22.0 | .72 | 93.4 | 3.81 | 3.20 | 26.5 | 28417 | 158.8 | 5.33 | 1.9 | -5.1 | 440.4 |
| | | | | | | 3.32 | 21.7 | .72 | 91.7 | 3.80 | 3.20 | 27.4 | 28417 | 159.7 | 5.44 | 2.1 | -5.1 | 439.5 |
| | | | | | | 3.31 | 22.0 | .72 | 93.4 | 3.80 | 3.23 | 27.4 | 28732 | 158.0 | 5.33 | 2.1 | -5.2 | 435.5 |
| 10/ 0/ 5 | 5 | 3 | 1 | 0 | | 3.30 | 21.7 | .72 | 91.7 | 3.80 | 3.20 | 27.4 | 28732 | 159.7 | 5.42 | 1.8 | -5.1 | 443.4 |
| | | | | | | 3.31 | 22.0 | .72 | 93.4 | 3.79 | 3.13 | 28.3 | 29033 | 158.0 | 5.42 | 2.1 | -5.2 | 434.6 |
| | | | | | | 3.32 | 22.0 | .72 | 93.4 | 3.80 | 3.23 | 27.4 | 28657 | 158.0 | 5.33 | 2.1 | -5.0 | 434.6 |
| | | | | | | 3.30 | 22.0 | .73 | 93.4 | 3.80 | 3.13 | 27.4 | 28417 | 157.2 | 5.37 | 2.0 | -4.9 | 435.5 |
| 10/ 0/ 6 | 5 | 3 | 1 | 0 | | 3.32 | 22.0 | .73 | 93.4 | 3.81 | 3.13 | 26.5 | 28732 | 158.0 | 5.33 | 2.1 | -5.0 | 431.6 |
| | | | | | | 3.31 | 22.0 | .72 | 91.7 | 3.79 | 3.20 | 27.4 | 28732 | 157.2 | 5.37 | 2.2 | -4.8 | 435.5 |
| | | | | | | 3.30 | 22.0 | .73 | 91.7 | 3.81 | 3.20 | 26.5 | 28732 | 158.8 | 5.37 | 1.3 | -4.7 | 439.5 |
| | | | | | | 3.31 | 22.0 | .72 | 91.7 | 3.80 | 3.13 | 27.4 | 28732 | 158.8 | 5.33 | 2.1 | -4.9 | 445.3 |
| 10/ 0/ 7 | 5 | 3 | 1 | 0 | | 3.30 | 22.0 | .72 | 93.4 | 3.81 | 3.13 | 26.5 | 28657 | 158.0 | 5.35 | 2.2 | -4.8 | 435.5 |
| | | | | | | 3.31 | 22.0 | .72 | 91.7 | 3.80 | 3.13 | 26.5 | 28582 | 158.8 | 5.33 | 1.8 | -4.7 | 441.4 |
| | | | | | | 3.30 | 21.7 | .72 | 93.4 | 3.81 | 3.13 | 26.5 | 28732 | 159.7 | 5.42 | 2.2 | -5.3 | 441.4 |
| | | | | | | 3.32 | 22.0 | .72 | 91.7 | 3.79 | 3.20 | 27.4 | 28417 | 158.0 | 5.44 | 2.1 | -5.1 | 439.5 |
| 10/ 0/ 9 | 5 | 3 | 1 | 0 | | 3.30 | 22.0 | .72 | 91.7 | 3.80 | 3.13 | 27.4 | 28417 | 158.8 | 5.33 | 1.8 | -4.9 | 446.3 |
| | | | | | | 3.31 | 21.7 | .72 | 91.7 | 3.80 | 3.20 | 27.4 | 28732 | 159.7 | 5.44 | 2.1 | -4.8 | 443.4 |
| | | | | | | 3.31 | 22.0 | .72 | 93.4 | 3.79 | 3.13 | 27.4 | 28732 | 158.0 | 5.33 | 2.3 | -5.0 | 434.6 |
| | | | | | | 3.32 | 22.0 | .72 | 93.4 | 3.79 | 3.13 | 27.4 | 28657 | 158.0 | 5.37 | 2.4 | -4.8 | 435.5 |
| 10/ 0/10 | 5 | 3 | 1 | 0 | | 3.31 | 22.0 | .72 | 93.4 | 3.79 | 3.13 | 28.3 | 28417 | 158.0 | 5.42 | 2.1 | -5.1 | 436.5 |
| | | | | | | 3.31 | 22.0 | .73 | 93.4 | 3.80 | 3.13 | 27.4 | 28732 | 158.0 | 5.37 | 2.5 | -4.7 | 439.5 |
| | | | | | | 3.30 | 22.2 | .73 | 93.4 | 3.81 | 3.13 | 27.4 | 28732 | 157.2 | 5.35 | 2.7 | -4.6 | 434.6 |
| | | | | | | 3.31 | 22.0 | .73 | 93.4 | 3.81 | 3.20 | 26.5 | 28657 | 159.7 | 5.37 | 2.5 | -4.6 | 440.4 |
| 10/ 0/11 | 5 | 3 | 1 | 0 | | 3.31 | 22.2 | .73 | 93.4 | 3.79 | 3.13 | 27.4 | 28417 | 157.2 | 5.37 | 2.2 | -4.6 | 437.5 |
| | | | | | | 3.31 | 21.7 | .73 | 91.7 | 3.80 | 3.20 | 26.5 | 28732 | 158.8 | 5.35 | 2.4 | -4.6 | 440.4 |
| | | | | | | 3.30 | 22.0 | .72 | 91.7 | 3.81 | 3.20 | 27.4 | 29033 | 158.1 | 5.37 | 2.6 | -4.7 | 446.3 |
| | | | | | | 3.32 | 21.7 | .72 | 91.7 | 3.79 | 3.20 | 27.4 | 28732 | 159.7 | 5.33 | 2.8 | -4.8 | 444.3 |
| 10/ 0/12 | 5 | 3 | 1 | 0 | | 3.30 | 22.0 | .72 | 91.7 | 3.80 | 3.20 | 27.4 | 28417 | 158.8 | 5.35 | 2.7 | -4.8 | 441.4 |
| | | | | | | 3.30 | 21.7 | .72 | 91.7 | 3.81 | 3.13 | 27.4 | 28417 | 160.5 | 5.37 | 2.5 | -4.8 | 440.4 |
| | | | | | | 3.31 | 22.0 | .72 | 93.4 | 3.79 | 3.13 | 28.3 | 28417 | 158.0 | 5.33 | 3.2 | -4.9 | 437.5 |
| | | | | | | 3.31 | 22.0 | .72 | 93.4 | 3.79 | 3.20 | 27.4 | 28657 | 158.0 | 5.37 | 3.1 | -4.7 | 430.7 |
| 10/ 0/14 | 5 | 3 | 1 | 0 | | 3.31 | 22.0 | .72 | 93.4 | 3.79 | 3.20 | 28.3 | 29033 | 158.0 | 5.33 | 4.8 | -4.8 | 438.5 |
| | | | | | | 3.31 | 22.0 | .73 | 93.4 | 3.80 | 3.13 | 26.5 | 28417 | 158.8 | 5.37 | 3.1 | -4.7 | 431.6 |
| | | | | | | 3.31 | 22.0 | .72 | 93.4 | 3.78 | 3.13 | 28.3 | 28732 | 157.2 | 5.35 | 3.3 | -4.6 | 431.6 |
| | | | | | | 3.31 | 22.0 | .73 | 93.4 | 3.80 | 3.13 | 26.5 | 28732 | 158.0 | 5.33 | 3.1 | -4.7 | 437.5 |
| 10/ 0/15 | 5 | 3 | 1 | 0 | | 3.31 | 22.0 | .72 | 93.4 | 3.79 | 3.13 | 27.4 | 28732 | 158.0 | 5.35 | 3.4 | -4.6 | 430.7 |
| | | | | | | 3.30 | 22.2 | .73 | 93.4 | 3.80 | 3.13 | 27.4 | 28657 | 157.2 | 5.35 | 3.0 | -4.6 | 435.5 |
| | | | | | | 3.31 | 22.0 | .73 | 91.7 | 3.80 | 3.20 | 26.5 | 28417 | 158.8 | 5.37 | 2.9 | -4.6 | 443.4 |
| | | | | | | 3.31 | 22.0 | .72 | 93.4 | 3.80 | 3.20 | 26.5 | 29033 | 157.2 | 5.37 | 2.9 | -4.8 | 441.4 |

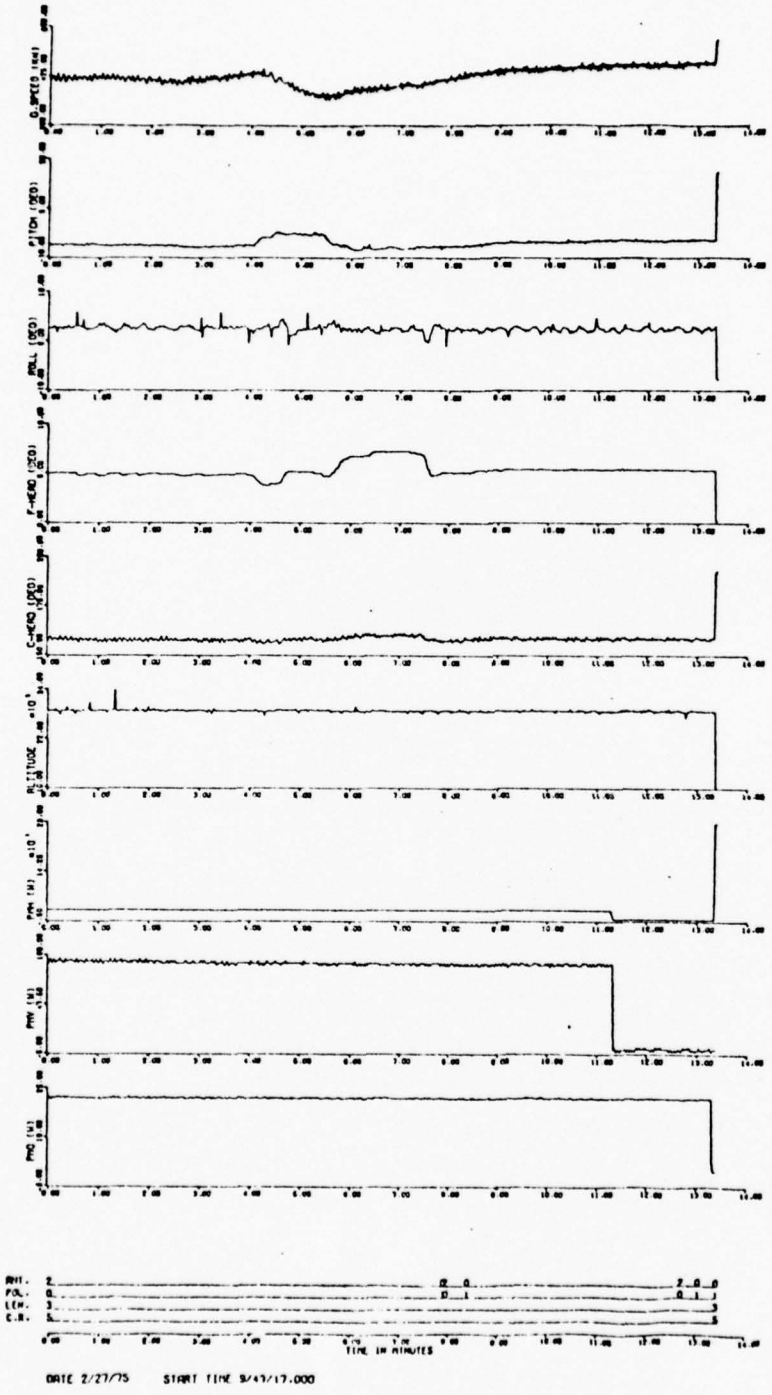


*Figure 4-32. Airborne Tape Plotted Results*

# 5. PHYSICAL OPTICS SCATTER MODEL PREDICTIONS

## 5.1 MODEL INTRODUCTION

The choice of an appropriate model for the analysis of electromagnetic surface scatter is determined almost exclusively by the roughness characteristics of the reflecting medium. Surfaces are usually classified as slightly rough, very rough, or composite depending on the magnitude of the height irregularities. In general, different scatter theories are used for each of these situations.

For the case of L-band aeronautical satellite oceanic scatter, the surface will almost always appear to be very rough; this implies that the following is approximately satisfied:

$$\frac{2\pi}{\lambda}\,\sigma_H \cos\theta_i > 1.0\ , \tag{5-1}$$

where:

$\lambda$ = electromagnetic wavelength
$\sigma_H$ = standard deviation of surface height irregularities
$\theta_i$ = incident angle of ray upon the surface as measured from the normal.

Analysis of scattering from very rough surfaces is usually developed through the physical optics tangent-plane method. Commonly called the Kirchhoff approximation, this model is based on the assumption of a locally plane surface over the distance of many wavelengths. This constraint is considered to be satisfied if the radius of curvatuve of the surface undulations ($\delta_c$) is much greater than $\lambda$; i.e.,

$$\lambda \ll 4\pi\,\delta_c \cos\theta_i\ . \tag{5-2}$$

For this analysis we employ the vector formulation of the physical optics model and are thus able to properly account for the electromagnetic polarization dependences of each particular scattering facet on the surface. Because of the immense complexity of this model, it is not possilble to arrive at adequate channel parameter solutions in a closed form. This is circumvented through use of a computerized technique that subdivides the sperical scatter surface into incrementally small areas and then determines the scatter cross section (including polarization transformation factors), Doppler shift, and time delay associated with each area. The complex vector representation of the scattered signal is coupled to the receiver antenna characteristics, thereby providing an estimation of the received power from the particular surface path and thus allowing the channel's delay-Doppler scatter function, $S(\tau,\omega)$, to be constructed. From $S(\tau,\omega)$, steps identical to those described in section 4.12 are followed to determine the channel's time-frequency autocorrelation function, delay spectrum, Doppler

spectrum, time autocorrelation function, frequency autocorrelation function, total energy content, and spread values of the unidimensional distributions. Described below are the most important scatter theory relationships of the computer routine as well as typical sample outputs in a plotted format.

## 5.2 ALGORITHM EXECUTION SEQUENCE AND DESCRIPTION

A block diagram illustrating the computer model's input/output and basic processing function is given in figure 5-1. Inputs to the program include:

a. System geometry parameters (aircraft altitude, speed, velocity vector direction, grazing angle at specular point, and transmitted frequency)

b. Complex polarization vectors of airplane and satellite antenna (satellite polarization characteristics are assumed to be isotropic over the scatter surface; antenna radiation distribution characteristics may be accounted for mathematically or by including a azimuthal-elevation angle look-up table to derive complex horizontal and vertical polarization coefficients)

c. RMS surface slope and electrical parameters

d. Surface area resolution parameter (determines the size of the incremental surface area used in the surface integration routine and thus ultimately affects the fidelity of the predictions)

The basic processing function of the computer code may be broken down into three categories.

a. For each incremental surface area (dS) considered in the integration, calculate the received scattered power (dP), the time delay ($\tau$), and Doppler shift ($\omega$) associated with the return.

b. Sort the power returned from each incremental area into a two-dimensional array ($\tau,\omega$) to yield an estimate of the channel's scatter function $S(\tau,\omega)$.

c. Perform Fourier and integral operations on $S(\tau,\omega)$ to derive the channel's time-frequency autocorrelation function, time autocorrelation function, frequency autocorrelation function, Doppler spectrum, delay spectrum, total rms scattered energy, and the spread values of the unidimensional parameters.

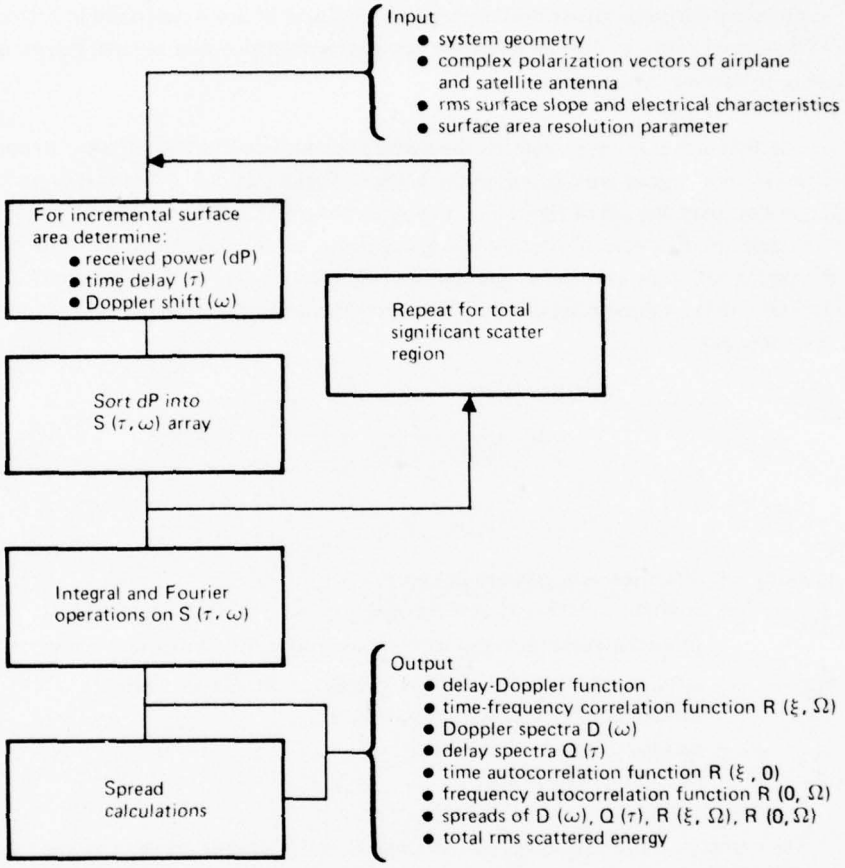


*Figure 5-1. Scatter Model*

Category c utilizes algorithmic operations identical to those described in sections 4.12 and 4.13. The second category (b) is a relatively straightforward two-dimensional bin-sorting algorithm and needs no further explanation.

The first category (a) represents the surface scatter boundary-interface component of the model and is, to a large extent, based on the work of Peake (ref. 5-1). Drawing from this source we briefly present, with the aid of figure 5-2, the underlying mathematics associated with the derivation of dP, $\tau$, and $\omega$. For ease of interpretation, parameter dP is calculated relative to the power received over the direct path link whereas $\tau$ and $\omega$ are evaluated relative to the direct path Doppler and the specular point delay values, respectively. The normalized received power from incremental area dS is thus expressed as

$$dP = \frac{1}{4\pi} \frac{r_d^2}{r_1^2 r_2^2} \frac{(T_{cf}\, T_{cf}^*)}{|\bar{G}_p \cdot \bar{G}_s|^2} \sigma_{xs}\, dS, \tag{5-3}$$

where:

$r_1, r_2, r_d$ = distances as illustrated in figure 5-2

$T_{cf}$ = complex coefficient that accounts for coupling between incident polarization vector, tilted dielectric surface element, and receiver polarization vector

$\bar{G}_p$ = airplane complex polarization vector for direct link path

$\bar{G}_s$ = satellite complex polarization vector

$\sigma_{xs}$ = surface scatter cross section

dS = elemental surface area.

The complex transmission coefficient embodies the aircraft antenna spatial filtering and is calculated as:

$$T_{cf} = (DI) \Big| R_{\parallel}(a)\,(A\cos\delta_i + B\sin\delta_i)\,(C\cos\delta_s + D\sin\delta_s) - R_{\perp}(a)\,(B\cos\delta_i - A\sin\delta_i)\,(-D\cos\delta_s + C\sin\delta_s) \Big| . \tag{5-4}$$

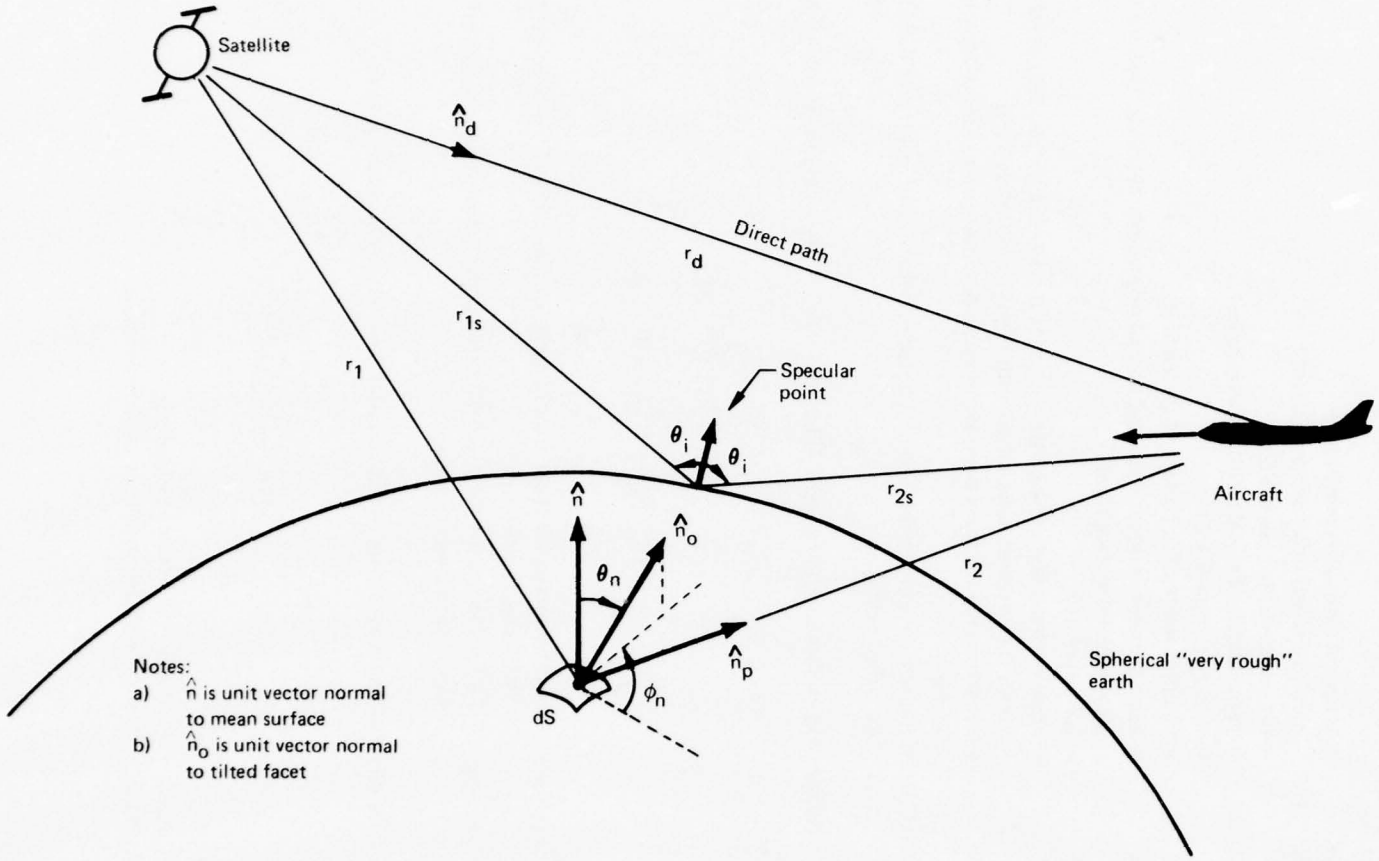


*Figure 5-2. Scatter Model Geometry*

where:

| | | |
|---|---|---|
| DI | = | spherical earth divergence factor |
| $R_{\parallel}(a)$ | = | parallel Fresnel reflection coefficient |
| | = | $(\epsilon^2 \cos a - E)(\epsilon^2 \cos a + E)$ |
| $R_{\perp}(a)$ | = | perpendicular Fresnel reflection coefficient |
| | = | $(\cos a - E)(\cos a + E)$ |
| $\epsilon$ | = | complex index of refraction of the surface |
| $a$ | = | angle between incident wave and normal of properly tilted (to produce reflection into receiver) surface facet |
| E | = | $(\epsilon^2 - \sin^2 a)^{1/2}$ |
| $\delta_i$ | = | angle between theta component of incident wave and the incident parallel unit vector (i.e., vertical polarization with respect to tilted surface) |
| $\delta_s$ | = | angle between the theta component of scattered wave and the reflected parallel unit vector |
| A,B,C,D | = | transmitter and receiver complex antenna polarization vector coefficients as described below. |

Polarization vectors for the transmit ($\bar{P}_T$) and receive ($\bar{P}_R$) antenna system are given by:

$$\bar{P}_T = A\hat{L}_{TT} + B\hat{L}_{PT}$$

$$\bar{P}_R = C\hat{L}_{TR} + D\hat{L}_{PR}, \qquad (5\text{-}5)$$

where:

| | | |
|---|---|---|
| $\hat{L}_{TT}, \hat{L}_{PT}$ | = | unit vectors in the theta and phi directions, respectively, with respect to coordinates centered on transmitter |
| $\hat{L}_{TR}, \hat{L}_{PR}$ | = | unit vectors in the theta and phi directions, respectively, with respect to coordinates centered on receiver. |

The physical optics very rough surface scatter cross section is obtained from:

$$\sigma_{xs} = \frac{\pi}{\cos\theta_n} P_{ss}(\theta_n, \phi_n) \ , \qquad (5\text{-}6)$$

where:

| | | |
|---|---|---|
| $\theta_n, \phi_n$ | = | angles as illustrated in figure 5-2 |
| $P_{ss}(\theta_n, \phi_n)$ | = | surface slope probability density function. |

For this particular analysis the slope probability density function was assumed to be isotropic with the following Gaussian form:

$$P_{ss}(\theta_n,\phi_n) = \frac{\cos\theta_n}{\pi\eta^2} \exp\left(-\frac{\tan^2\theta_n}{\eta^2(1+2\eta^2)}\right), \tag{5-7}$$

where $\eta^2 = \langle \tan^2\theta_n \rangle$ = mean square surface slope.

The delay and Doppler variables associated with a given incremental area are determined from

$$\omega = \frac{2\pi f_o}{c}\left\{-\bar{n}_p \cdot \bar{v} + \bar{n}_d \cdot \bar{v}\right\} \tag{5-8}$$

$$\tau = \frac{1}{c}\left\{r_1 + r_2 - r_{1s} - r_{2s}\right\}, \tag{5-9}$$

where $f_o$ is the transmitted frequency, c is the velocity of light, and the other parameters are as illustrated in figure 5-2.

## 5.3 SAMPLE OUTPUT

To facilitate the comparison between theoretical expectation and experimental results, the scatter channel model's output formats have been configured to resemble as closely as possible those associated with the multipath data reduction routines. Thus, for the most part, the applicable output format description given in section 4.23 is pertinent to this section. To illustrate the degree of model sophistication, a set of sample plotted results associated with a typical production run is presented here.

Input parameters for this sample run were as follows:

| | |
|---|---|
| Satellite polarization: | Right-hand circular |
| Airplane polarization: | Horizontal-omni |
| Aircraft velocity: | 200 m/sec, great circle path toward satellite |
| Aircraft altitude: | 10 km |
| Frequency | 1650 MHz |
| Surface type: | Sea water |
| Surface rms slope: | $6^o$ |
| Grazing angle: | $19^o$ |

A cross-reference relating figure number with the model's parameter prediction is given below:

| *Figure* | *Parameter* |
|---|---|
| 5-3 | $S(\tau,\omega)$ |
| 5-4 | $D(\omega)$, $Q(\tau)$ |
| 5-5 | $\lvert R(\xi,\Omega)\rvert$ |
| 5-6 | $\lvert R(0,\Omega)\rvert$, $\lvert R(\xi,0)\rvert$. |

It is of interest to note that the example run entailed a division of the effective surface scatter area into more than roughly 80,000 elemental patches and required a total of 380 sec of CDC 6600 central processor time.

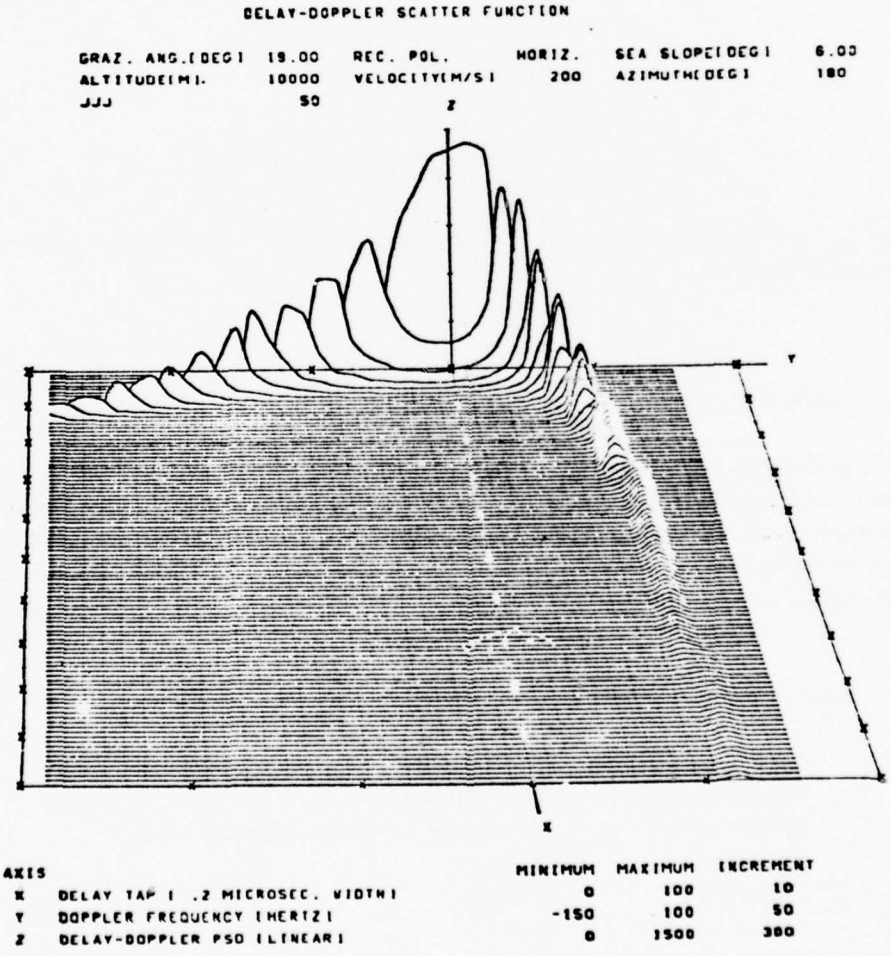


*Figure 5-3. Scatter Model Prediction – $S(\tau,\omega)$*

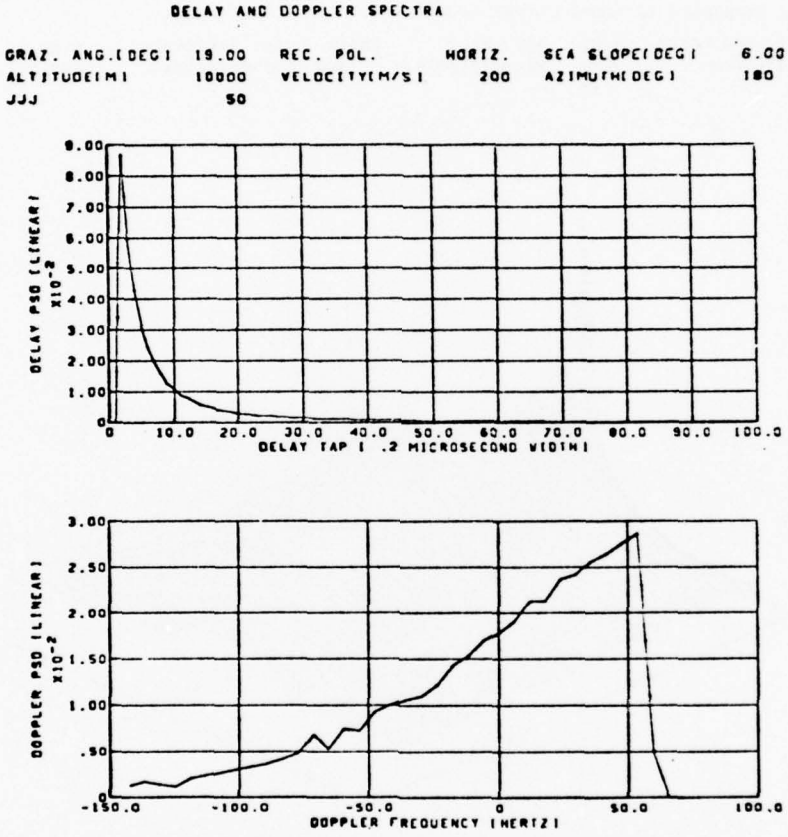


*Figure 5-4. Scatter Model Predictions – $D(\omega)$, $Q(\tau)$*

TIME FREQUENCY AUTOCORRELATION FUNCTION

| | | | | | |
|---|---|---|---|---|---|
| GRAZ. ANG.(DEG) | 19.00 | REC. POL. | HORIZ. | SEA SLOPE(DEG) | 6.00 |
| ALTITUDE(M) | 10000 | VELOCITY(M/S) | 200 | AZIMUTH(DEG) | 180 |
| JJJ | 50 | | | | |

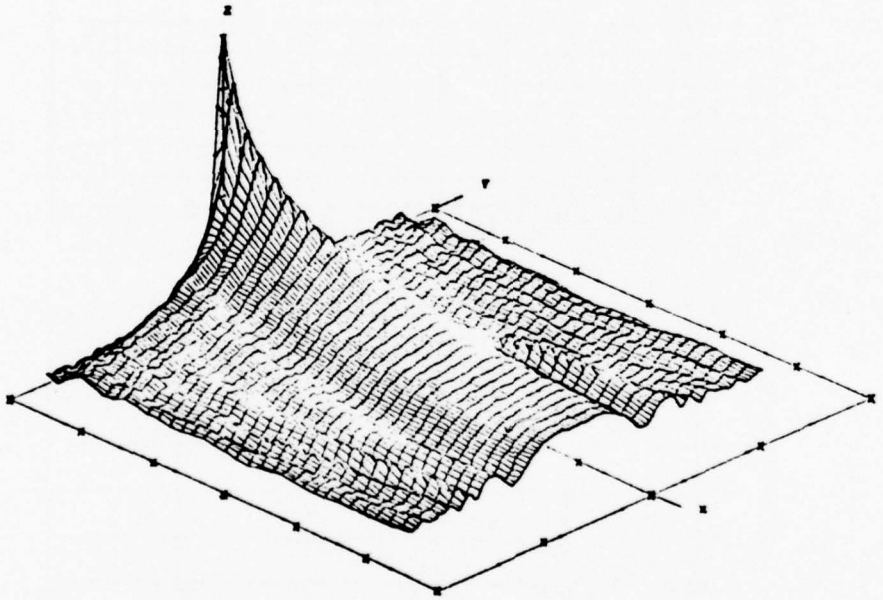


| AXIS | | MINIMUM | MAXIMUM | INCREMENT |
|---|---|---|---|---|
| X | FREQUENCY SEPARATION ( KHZ) | 0 | 3000. | 500 |
| Y | TIME SEPARATION ( MILLISEC ) | -100 | 100 | 50 |
| Z | TIME-FREQ. AUTOCOR. FUNCTION (PWR) | .00 | 1.00 | .10 |

*Figure 5-5. Scatter Model Prediction – $|R(\xi,\Omega)|$*

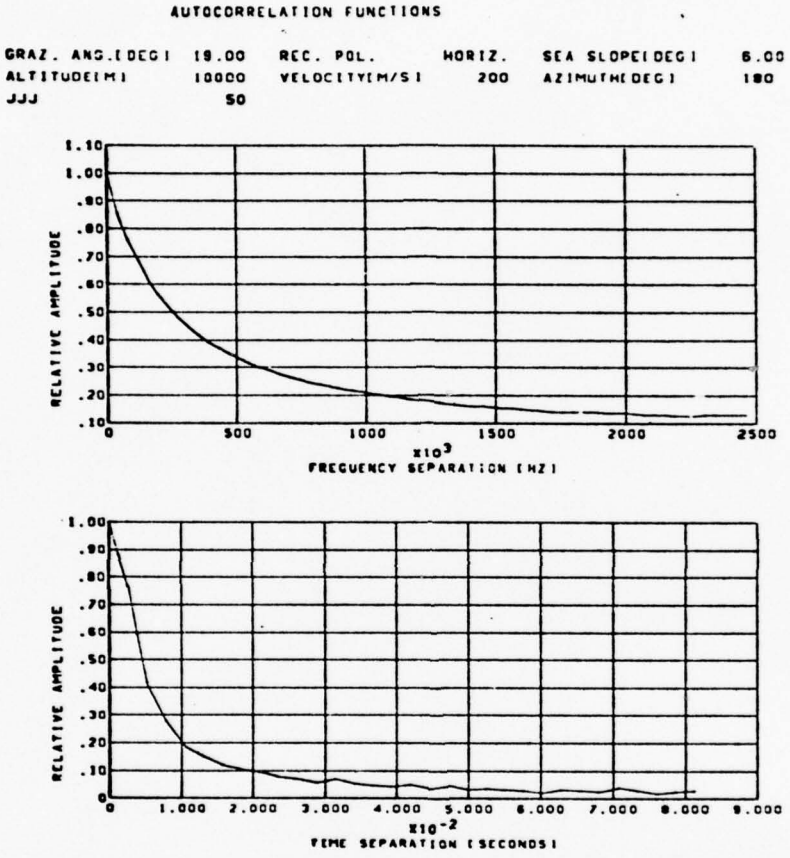


*Figure 5-6. Scatter Model Predictions — $|R(0,\Omega)|$, $|R(\xi,0)|$*

# 6. MODEM/ANTENNA DATA PROCESSING

The data gathered for the digital modem, voice modem, hybrid voice and data modem, ranging modem, and antenna tests on the KC-135 airplane is in the form of analog tapes, written logs, and onboard strip charts. Processing of this raw data is described below.

## 6.1 SYSTEM BLOCK DIAGRAM

Figure 6-1 illustrates the flow of data in the data reduction and analysis system. The diagram shows the various machine processes and human judgment processes constituting the total system.

The airborne logs and strip charts are used to determine the valid voice test periods. The selected voice channels are transcribed to 1/4-in. tapes for intelligibility scoring by CBS Laboratories.

Tape logs are used to determine input parameters that are furnished to the Boeing Test Data Processing Center (TDPC) along with the analog source tapes. These parameters include type of test data, tracks to process, time segments to process, analog source tape speed, and kind of output desired (digital tape or stripout).

Airplane logs, onboard strip charts, and TDPC strip charts are used to determine which time segments of the digital tapes are to be analyzed. The time segment information is sent with the digital tape to the CDC 6600 for processing with the applicable analysis programs.

Output from the CDC 6600 includes $C/N_o$ and S/I statistics, bit-error rates, bit-error statistics, and ranging data analysis. This output is manually merged with other data such as voice intelligibility scores and aircraft parameters to give final outputs. Outputs include those described in the DRandA plan.

## 6.2 TEST DATA PROCESSING CENTER (TDPC)

Processing of the analog data at TDPC is subdivided into two basic systems, with each system having modes dependent on the data being processed. One system processes antenna, voice, and ranging data; the other system processes the digital communication data. The systems are described more fully in the following paragraphs.

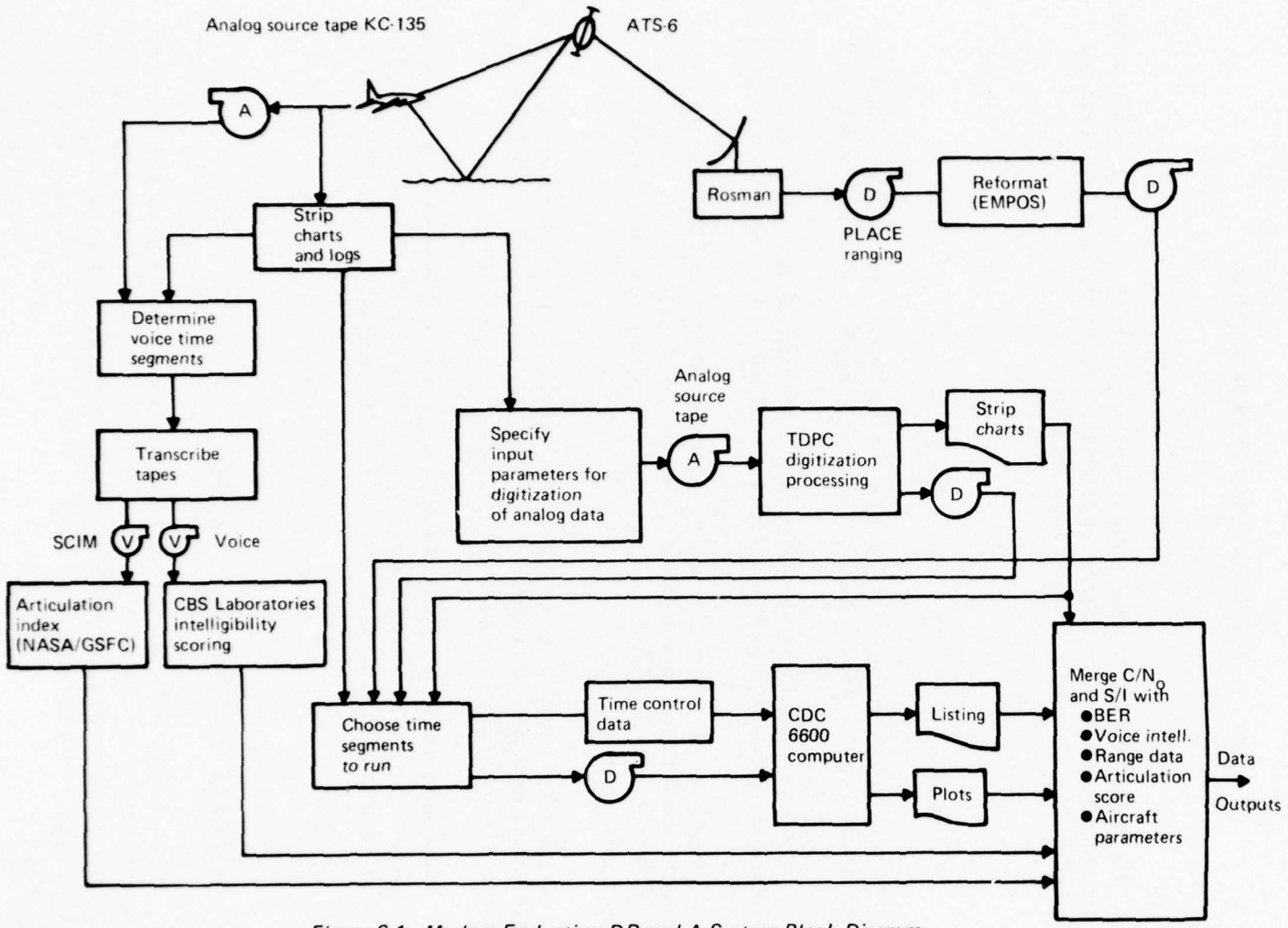


*Figure 6-1. Modem Evaluation DR and A System Block Diagram*

### 6.2.1 TDPC Processing of Antenna, Voice, and Ranging Tapes

A block diagram of the system used for all three types of data is shown in figure 6-2. A brief explanation of the formatting operation for the antenna, voice, and ranging data is given below.

Antenna data on the source tape consists of

| | |
|---|---|
| IRIG-B time code | WBFM |
| Signal strength (carrier detector) | WBFM |
| Channel event (A or B) | WBFM . |

These signals are recorded at 3-3/4 ips. At the transition of the event signal, time is read and 1025 samples of signal strength are acquired and formatted on the tape as shown in figure 6-3.

Voice data is recorded at 3-3/4 ips on the source tapes and consists of the following signals:

| | |
|---|---|
| IRIG-B time code | WBFM |
| Signal strength (carrier detector) | WBFM . |

For the voice data, sampling of the signal strength is under direct control of the time code rather than by a channel event signal. Beginning 15 sec after processing start time and repeating at 15-sec intervals, time is read and 1025 signal strength samples are taken and formatted on digital tape, again as shown in figure 6-3.

Ranging data is recorded at 3-3/4 ips on the source tapes and consists of the following signals:

| | |
|---|---|
| IRIG-B time code | WBFM |
| Signal strength | WBFM |
| Ranging data PCM | WBFM, Manchester code, 305 bps . |

Upon detection of a seven-bit synchronization pattern (Barker pattern) in the PCM track, the next 33 bits of PCM data are formatted with time and an identification (ID) word on digital tape as shown in figure 6-4. Each of these blocks consists of ten 12-bit words. After 16 of these blocks have been formatted, 1025 signal strength samples are taken and formatted on the digital tape (fig. 6-3). This completes one ranging data record. All these reformatted digital tapes are seven-track, 800-bpi tapes compatible with the CDC 6600.

The input to the system diagrammed in figure 6-2 is the source tape recorded on the airplane. The tapes are played back at 30 ips, which is a speed increase of X8. The signals applicable to the data being processed are demodulated by the DCS-2 demodulator. The time is patched to the range time decoder (RTD) and cross-coupled to the digital data converter (DDC). The signal strength and

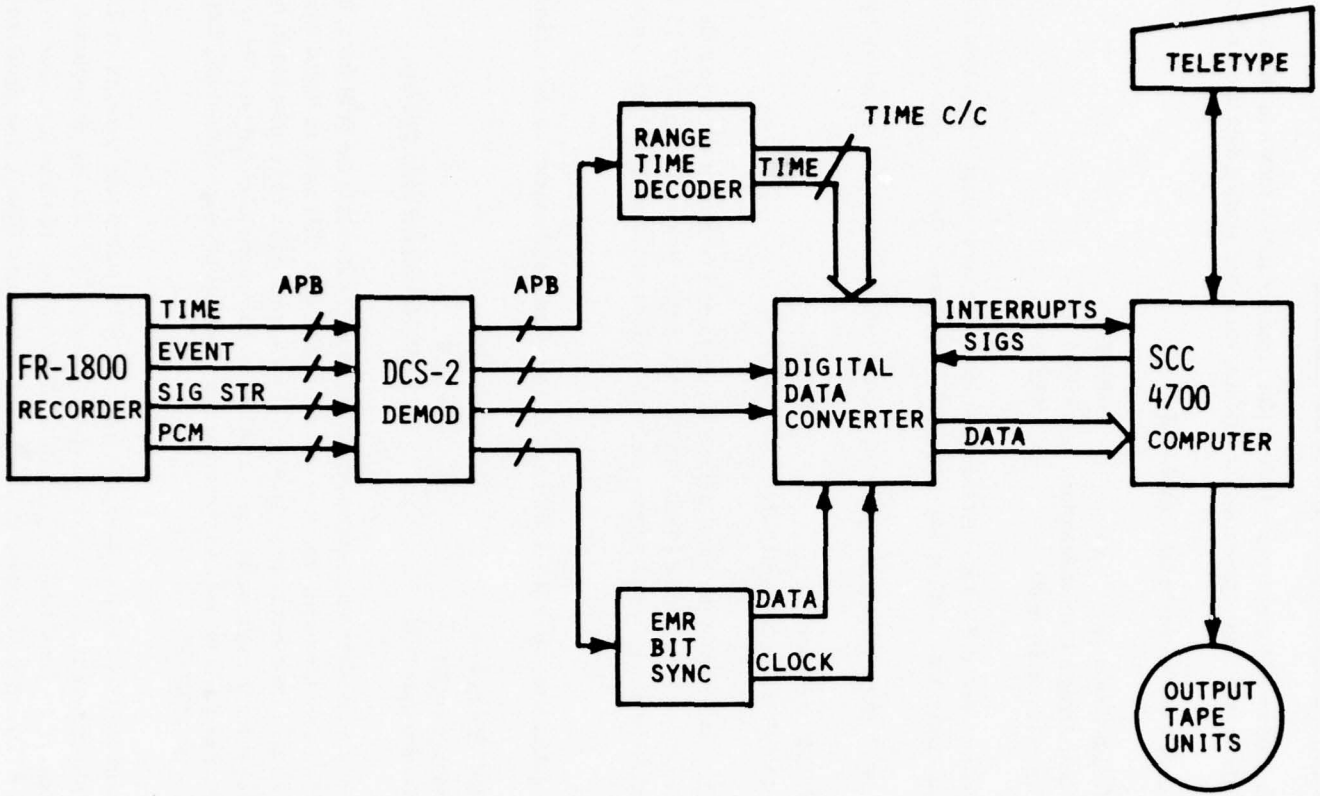


*Figure 6-2. ATSAVR Formatting System*

| Word | | Bit Position | | | | | | | | | | | |
|---|---|---|---|---|---|---|---|---|---|---|---|---|---|
| | | 1 | 2 | 3 | 4 | 5 | 6 | 7 | 8 | 9 | 10 | 11 | 12 |
| 1 | Hours | CC* | C | 0 | 0 | 20 | 10 | 0 | 0 | 8 | 4 | 2 | 1 |
| 2 | Minutes | 0 | 0 | 0 | 40 | 20 | 10 | 0 | 0 | 8 | 4 | 2 | 1 |
| 3 | Seconds | 0 | 0 | 0 | 40 | 20 | 10 | 0 | 0 | 8 | 4 | 2 | 1 |
| 4 | Msec | 0 | 0 | $2^9$ | $2^8$ | $2^7$ | $2^6$ | $2^5$ | $2^4$ | $2^3$ | $2^2$ | $2^1$ | $2^0$ |
| 5 | ID | See legend below | | | | | | | | | | | |
| 6 | Sample 1 | A | 0 | $2^9$ | $2^8$ | $2^7$ | $2^6$ | $2^5$ | $2^4$ | $2^3$ | $2^2$ | $2^1$ | $2^0$ |
| . | . | . | | | | | | | | | | | . |
| . | . | . | | | | | | | | | | | . |
| . | . | . | | | | | | | | | | | . |
| . | . | . | | | | | | | | | | | . |
| . | . | . | | | | | | | | | | | . |
| . | . | . | | | | | | | | | | | . |
| . | . | . | | | | | | | | | | | . |
| . | . | . | | | | | | | | | | | . |
| . | . | . | | | | | | | | | | | . |
| . | . | . | | | | | | | | | | | . |
| 1030 | Sample 1025 | A | 0 | $2^9$ | $2^8$ | $2^7$ | $2^6$ | $2^5$ | $2^4$ | $2^3$ | $2^2$ | $2^1$ | $2^0$ |

*CC = 1 time code out of sync, bad data possible

= 0 time code in sync, data acceptable

| | | | | | | | | | | | | | |
|---|---|---|---|---|---|---|---|---|---|---|---|---|---|
| ID = | 1 | 1 | 1 | 0 | 0 | 0 | 1 | 1 | 1 | 0 | 0 | 0 | voice |
| | 0 | 0 | 0 | 0 | 0 | 0 | 0 | 0 | 0 | 0 | 0 | 0 | digital data bit stream |
| | 1 | 1 | 1 | 1 | 1 | 1 | 1 | 1 | 1 | 1 | 1 | 1 | digital data amplitude samples |
| | 1 | 0 | 1 | 0 | 1 | 0 | 1 | 0 | 1 | 0 | 1 | 0 | ranging |
| | 0 | 0 | 0 | 1 | 1 | 1 | 0 | 0 | 0 | 1 | 1 | 1 | antenna evaluation (antenna 1) |

A = Event track status bit (antenna data only) in Words 6 to 1030

1 = event track on

0 = event track off

A = 0 for voice, ranging and digital data

*Figure 6-3. Signal Strength Format, 800-bpi Digital Tape*

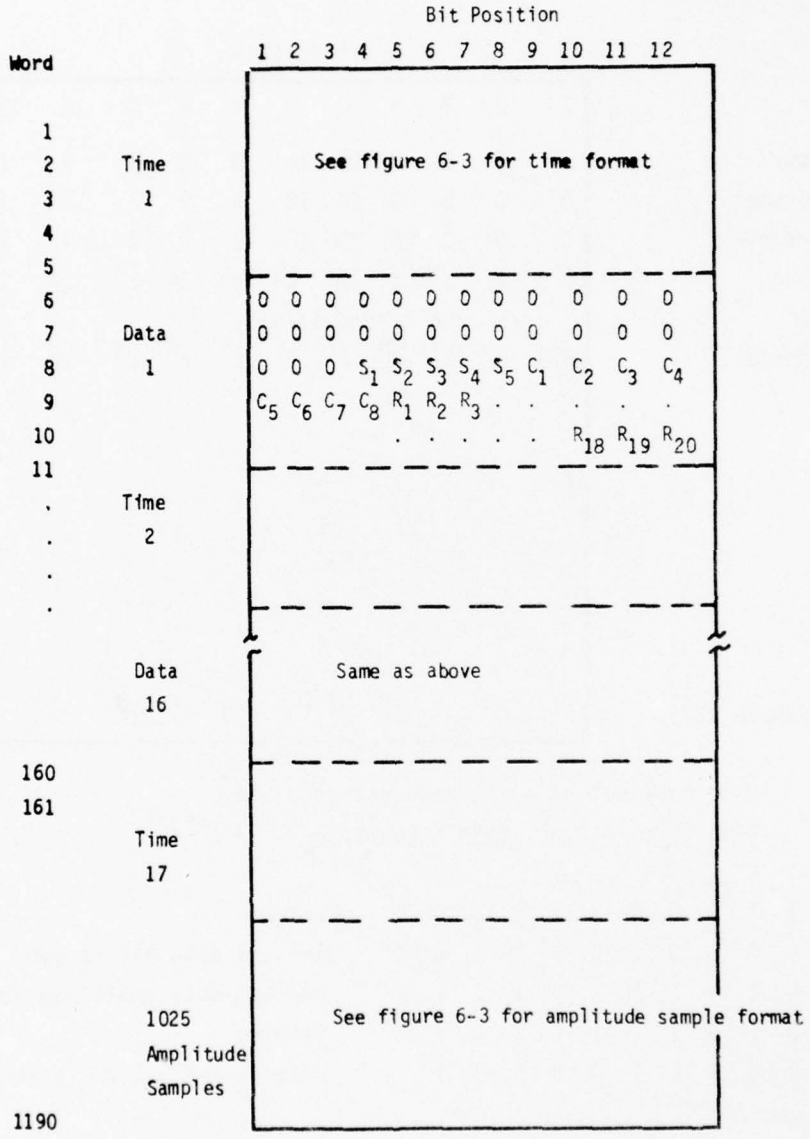


$S_1$-$S_5$ status bits

$C_1$-$C_8$ code information

$R_1$-$R_{20}$ range information

*Figure 6-4. Ranging Test Tape Format*

event tracks are patched to the DDC through the analog patch bay (APB). The serial PCM (ranging data) is decommutated by the EMR bit synchronizer and clocked into the DDC.

The signal strength data are sampled and digitized by the DDC. A 16-kHz clock (2-kHz real time) triggers an analog-to-digital converter, and the digitized samples are transferred to the SCC 4700 computer through the direct memory access (DMA).

The 7-bit PCM synchronization patterns preceding the 33-bit ranging data bursts are detected by the DDC. Following detection, the next 33 bits of PCM data are transferred to the SCC 4700 computer in one 9-bit word followed by two 12-bit words.

The ATSVAR computer program formats time, signal strength, and PCM data into records. ATSAVR is the SCC 4700 computer program that is operator controlled through teletype input. The operator selects the mode of operation according to the type of data to be processed and selects the number of output tapes necessary according to the quantity of input data.

Data is double buffered so that, while one record is being completed and written on tape, the formatting of the next may begin. This is necessary in the ranging mode where additional synchronization patterns may occur before the signal strength sampling of the previous record is completed.

Time editing is accomplished by the start-stop switches on the range time decoder. Processing may also be started or stopped manually. Each processing interval constitutes one file of data and at the conclusion of all processing intervals the operator terminates the processing mode. Data files are separated by one end-of-file mark. The last data file on the tape is terminated by two or more end-of-file marks.

### 6.2.2 Digital Communication Data

The digital data is recorded on the source tapes at either 3-3/4 or 7-1/2 ips and consists of the following signals:

| | |
|---|---|
| Five tracks, biphase level PCM | Direct record, one track per modem |
| Signal strength (carrier detector) | WBFM |
| IRIG-B time code | WBFM. |

The data rate of the digital data is 1200 bps, which results in the following relationship of record and playback speeds:

| Analog source tape record speed, ips | TDPC playback speed, ips |
|---|---|
| 3-3/4 | 15 |
| 7-1/2 | 30 |

During processing of the digital data analog tape (fig. 6-5), the PCM data is routed to the DDC, the analog signal strength to the DCS-2 demodulator, and time to the RTD. The signal strength is passed through a demodulator and sent to the DDC, where it is converted to a digital value by an analog-to-digital converter and written on tape, one record approximately every 15 data seconds.

Five-bit synchronizers have been patched on the DDC logic board, one for each recorded modem track. These bit synchronizers obtain bit synchronization and resolve Manchester phase ambiguity. The regenerated NRZ/PCM is written on tape in six-bit bytes, compatible with seven-track digital tape.

The frequency synthesizer on the analog patch bay is set to 1 kHz times the playback rate (X4) and patched to DDC input line 7. This signal is routed to a threshold detector. The leading and trailing edges are OR'ed together to give a 2K pulse/sec sample clock. This sample clock is used for the A/D conversion of the signal strength track.

The tape format of the digital data is illustrated in figure 6-6.

### 6.2.3 TDPC Chart Stripouts

The analog source tapes contain some data desirable to examine in analog visual form. Accordingly, the applicable channels are stripped out to yield the data shown in table 6-1.

All the above signals are recorded on chart paper for voice, data, and hybrid voice and data tests. Only the aircraft parameters are stripped out for ranging and antenna tests.

## 6.3 CDC 6600 PROCESSING

The data tapes formatted by TDPC are processed on a CDC 6600 computer under the KRONOS 2.1 operating system. Figure 6-7 gives the data flow of a computer run and is valid for all data processing: digital, ranging, voice, and antenna.

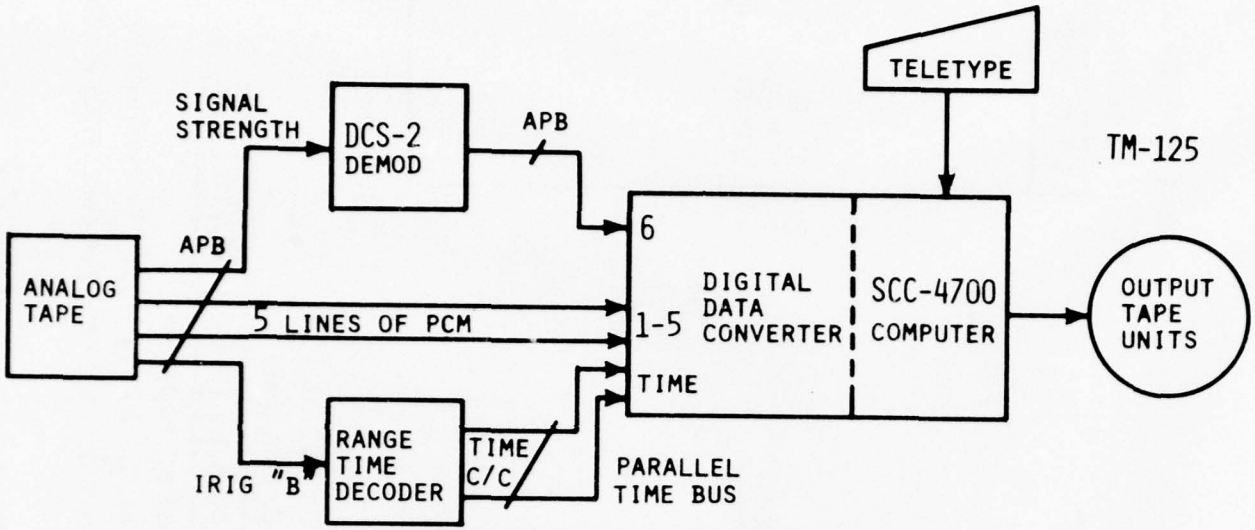


NOTES: (1) PCM = 1200 BPS
(2) TIME = X4
(3) DCS-2 CF = 27 KHz
(4) DEV = 10.8 KHz
(5) FILTER = 5000 Hz

*Figure 6-5. TDPC Digital Data Tape Formatting Process*

DIGITAL DATA FORMAT

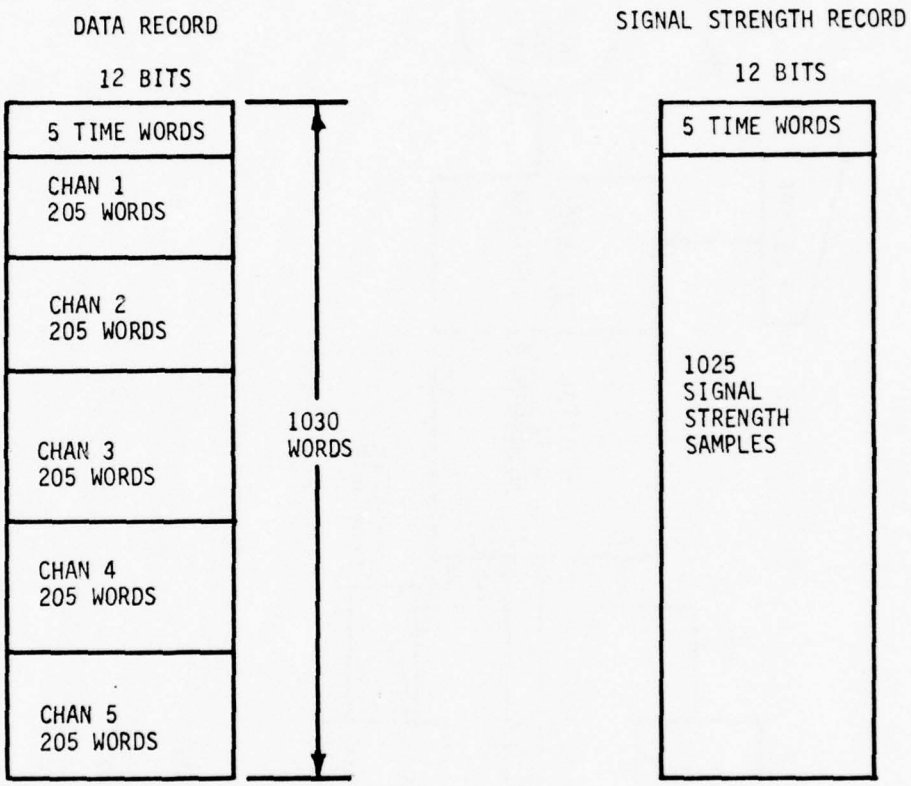


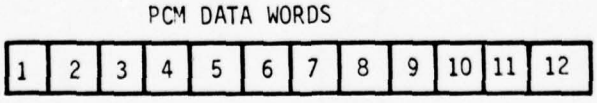


DATA BIT 1 IS THE FIRST BIT TRANSMITTED

SIGNAL STRENGTH IS SAMPLED EVERY 14 SECONDS (APPROXIMATELY)

FOR 1200 BPS THERE ARE 7 DATA RECORDS PER SIGNAL STRENGTH RECORD

*Figure 6-6. Digital Data Test Tape Format*

*TABLE 6-1. AIRCRAFT PARAMETERS*

| Information | Format |
|---|---|
| Aircraft heading (coarse) | 7.5% proportional to subcarrier FM |
| Aircraft heading (fine) | 7.5% proportional to subcarrier FM |
| Aircraft pitch | 7.5% proportional to subcarrier FM |
| Aircraft roll | 7.5% proportional to subcarrier FM |
| Hybrid No. 1 $C/N_0$ (dc voltage) | WBFM |
| Hybrid No. 2 $C/N_0$ (dc voltage) | WBFM |

The peripheral equipment necessary to run the program are card reader, printer, and two tape drives (one for the reformatted input data tape and one for the output plot file). Plotting is an off-line process performed on an SC 4020 Stromberg-Carlson plotter.

Although the programs are primarily coded in FORTRAN, a few subroutines are coded in assembly language to minimize run time.

Programs are run in a batch processing mode. The program inputs consist of the TDPC digital magnetic tapes and control data cards. These cards include start and stop times of each segment and program options. The outputs are a line printer listing and a plot of the signal spectrum. A more detailed description of program input/output is given under each program section.

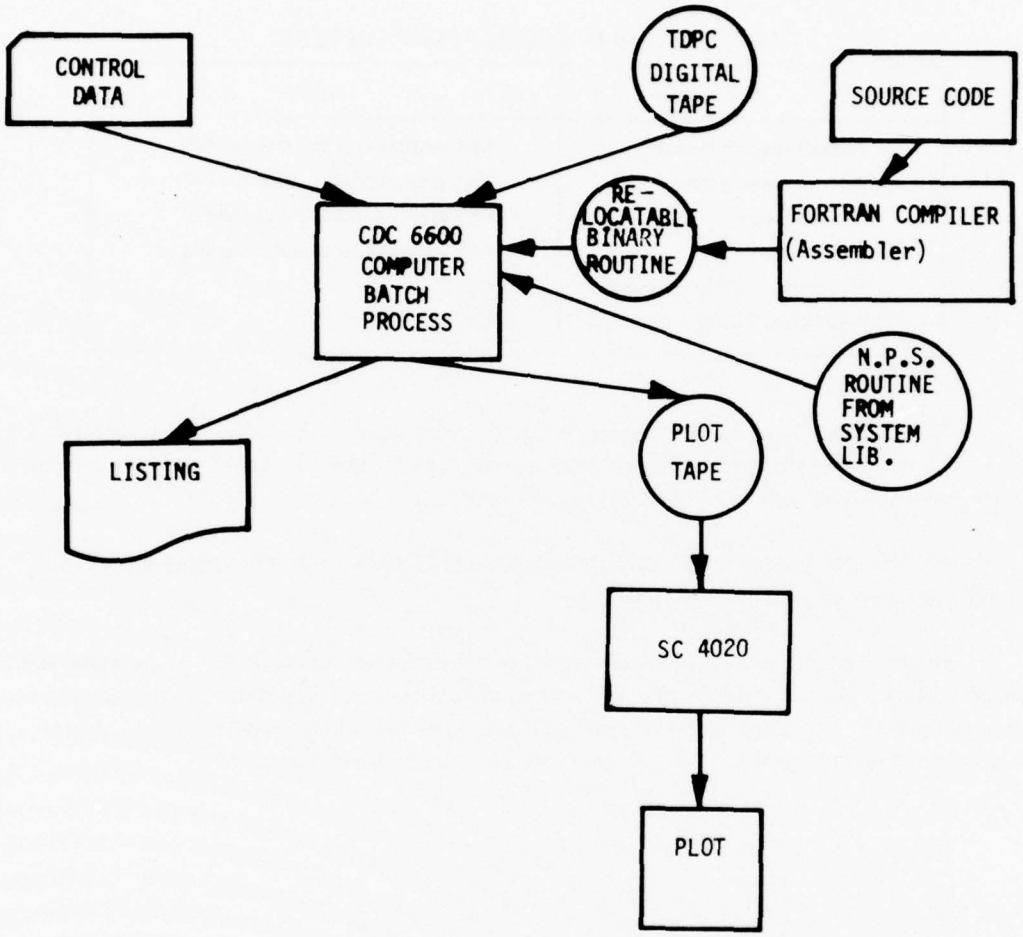


*Figure 6-7. CDC 6600 Computer Data Flow for Modem Evaluation Data Processing*

# 7. ANALYSIS OF ENVELOPE DETECTOR OUTPUT TO DETERMINE $C/N_o$ AND S/I

This section describes in detail the methodology and underlying theory for the determination of the carrier-to-noise power density ratio, $C/N_o$, and the direct signal-to-multipath signal ratio, S/I. The waveform utilized is the low-pass output of the carrier detector unit. The carrier detector unit processes an unmodulated carrier multiplexed into the satellite-aircraft transmission. The procedure is involved in analysis of voice, data, ranging, and antenna experiments.

## 7.1 BACKGROUND THEORY

The carrier detector unit incorporates a bandpass linear envelope detector (full-wave rectifier) to provide a measurement of channel character. The nonlinear approach was adopted to obviate the necessity for continuous Doppler compensation if a linear down-translation and analysis were used. Also, data sampling rates can be somewhat smaller with this approach.

The detector input signal is assumed to be the sum of (1) a sinusoid of frequency $f_o$ with average power $P^2/2$, i.e., its amplitude is P volts with a 1-ohm reference, (2) a diffuse multipath component having center frequency $f_o$ and power $\sigma_m{}^2$, and (3) wideband additive Gaussian noise with single-sided density of $N_o$, W/Hz.

Commensurate with the commonly accepted scatter model applicable for an aeronautical satellite oceanic system, the multipath return is assumed to have a complex Gaussian representation, with spectrum[1] given by

$$S_m(f) = \frac{\sigma_m{}^2}{\sqrt{2\pi B_m}}\, e^{-(f - f_o)^2/2B_m{}^2} \quad . \tag{7-1}$$

The parameter $B_m$ is the one-sided $e^{-1}$ bandwidth of the scattered signal. Theoretical and empirical results indicate that $B_m < 125$ Hz for the elevation angle/airspeed profile flown in the experiment.

The composite signal is initially prefiltered with a four-pole Bessel crystal filter to reject wideband noise and pass the signal components. The filter is modeled as having a Gaussian shape with

[1] A symmetric spectrum is obtained theoretically for cross-plane flights as in Type II tests but is not strictly true for other orientations.

bandwidth parameter $B_n$ for analytical simplicity. (Bessel and Gaussian characteristics are very similar to the 30-dB attenuation points.) Since noise and multipath are independent, the total interference spectrum at the detector input then becomes

$$S_I(f) = \frac{\sigma_m^2}{\sqrt{2\pi B_m}} e^{-(f - f_o)^2/2B_m^2} + \frac{\sigma_n^2}{\sqrt{2\pi B_n}} e^{-(f - f_o)^2/2B_n^2} . \tag{7-2}$$

Measurements have determined that $B_n$ = 2130 Hz for this experiment, with the result that all multipath energy is passed by this prefilter. Figure 7-1 shows the total spectrum, including the cw signal term.

The detector is modeled as an ideal linear, memoryless, full-wave device; i.e.,

$$y(t) = Ar(t) , \tag{7-3}$$

where:

y(t) = output
r(t) = input
A = arbitrary gain constant.

$\sigma_m^2$ = multipath power
$\sigma_n^2$ = noise power
$B_m$ = $e^{-½}$ multipath bandwidth, one sided
$B_n$ = $e^{-½}$ prefilter bandwidth, one sided

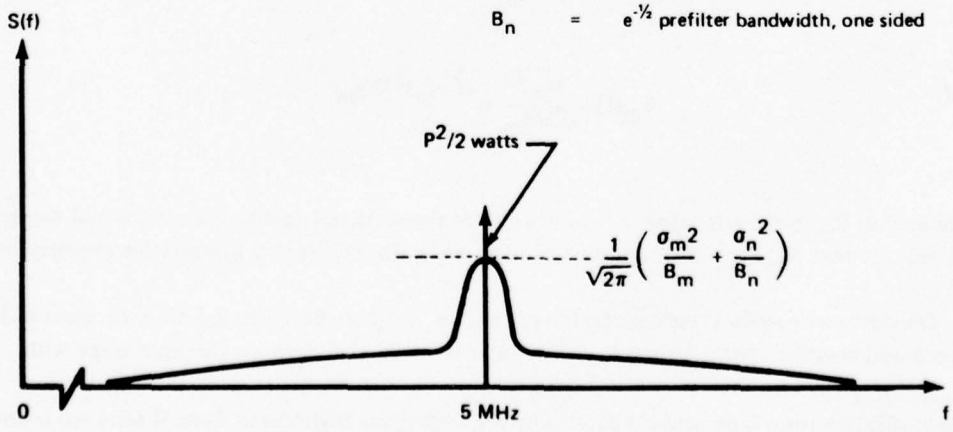


*Figure 7-1. Detector Input Spectrum*

Laboratory measurements have indicated that the actual detector is quite linear over a $\pm 8$ dB range about the nominal signal level.

Finally, the output is low-pass filtered with a two-pole Butterworth filter whose equivalent one-side rectangular bandwidth is 800 Hz. This signal is recorded for postflight analysis. The objective of the analysis is to determine $C/N_o$ and S/I of the signal.

Following Rice (ref. 7-1), Middleton (ref. 7-2), and Davenport and Root (ref. 7-3), the unfiltered output autocorrelation is expanded in a power series involving the input autocorrelation:

$$R_y(\tau) = h_{oo}^2 + 2\sum_{m=1}^{\infty} h_{mo}^2 \cos m\omega_o\tau + \sum_{k=1}^{\infty} \frac{h_{ok}^2}{k!} R_r^k(\tau)$$

$$+ 2\sum_{m=1}^{\infty}\sum_{k=1}^{\infty} \frac{h_{mk}^2}{k!} R_r^k(\tau) \cos m\omega_o\tau. \qquad (7\text{-}4)$$

This expansion displays the mean-value, signals harmonics, noise-cross-noise, and signal-cross-noise contributions, respectively.

The coefficients $h_{mk}$ are a function only of the total signal-to-input interference ratio, $P^2/2\sigma^2$, not the spectral distribution. The latter may be determined from

$$\left(P^2/2\sigma^2\right)^{-1} = \left(P^2/2\sigma_m^2\right)^{-1} + \left(P^2/2\sigma_n^2\right)^{-1}, \qquad (7\text{-}5)$$

Now, for the assumed Gaussian prefilter,

$$P^2/2\sigma_n^2 = (S/N_o)\left(\frac{1}{\sqrt{2\pi}\, B_n}\right). \qquad (7\text{-}6)$$

So

$$\left(P^2/2\sigma^2\right)^{-1} = (S/I)^{-1} + \left[(S/N_o)\left(\frac{1}{\sqrt{2\pi}\, B_n}\right)\right]^{-1}. \qquad (7\text{-}7)$$

The coefficients are (ref. 7-3):

$$h_{mk}^2 = \frac{\left(P^2/2\sigma^2\right)^m \, {}_1F_1{}^2\left(\frac{m+k-1}{2}\,;\, m+1\,;\, -P^2/2\sigma^2\right) 2^{k-1}}{(m!)^2\,\Gamma^2\left((3-m-k)/2\right)\,(\sigma^2)^{k-1}}\,, \tag{7-8}$$

where ${}_1F_1\,(.\,;.\,;.)$ is the confluent hypergeometric function.

By transforming equation (7-4), the output spectrum is obtained as

$$S_y(\omega) = h_{oo}^2\,\delta(\omega) + \sum_{m=1}^{\infty} h_{mo}^2\left[\delta(\omega - m\omega_o) + \delta(\omega + m\omega_o)\right]$$

$$+ \sum_{k=1}^{\infty}\sum_{m=0}^{\infty} \frac{h_{mk}^2}{k!}\left[S_k(\omega - m\omega_o) + S_k(\omega + m\omega_o)\right], \tag{7-9}$$

where $S_k(\omega)$ is the k-fold convolution of the input interference spectrum given by equation (7-2). In this convolution of spectra lies the appeal of the Gaussian input spectra.

Although the spectrum expansion appears rather formidable, the series converges rapidly for the cases of interest so that only a few terms need to be considered ($m \leq 2$, $k \leq 3$). Also, only products with $(m + k)$even yield energy in the low-frequency zone.

Using the spectrum of equation (7-2), the following relations can be written for the convolved spectra:

$$S_1(f) = \frac{\sigma_m^2}{2\sqrt{2\pi}\,B_m}\left[e^{-(f-f_o)^2/2B_m^2} + e^{-(f+f_o^2/2B_m^2}\right]$$

$$+ \frac{\sigma_n^2}{2\sqrt{2\pi}\,B_n}\left[e^{-(f-f_o)^2/2B_n^2} + e^{-(f+f_o)^2/2B_n^2}\right]$$

$$S_2(f) = \frac{\sigma_m^4}{4\sqrt{4\pi}\,B_m}\left[e^{-(f-2f_o)^2/4B_m^2} + 2e^{-f^2/4B_m^2} + e^{-(f+2f_o)^2/4B_m^2}\right]$$

$$+ \frac{\sigma_n^4}{4\sqrt{4\pi}\,B_n}\left[e^{-(f-2f_o)^2/4B_n^2} + 2e^{-f^2/4B_n^2} + e^{-(f+2f_o)^2/4B_n^2}\right]$$

$$+\frac{2\sigma_m^2\sigma_n^2}{4\sqrt{4\pi}\sqrt{B_m^2+B_n^2}}\left[e^{-(f-2f_o)^2/2(B_m^2+B_n^2)}+2e^{-f^2/2(B_m^2+B_n^2)}\right.$$

$$\left.+e^{-(f+2f_o)^2/2(B_m^2+B_n^2)}\right]$$

$$S_3(f)=\frac{\sigma_m^6}{8\sqrt{2\pi}\sqrt{3\,B_m}}\left[e^{-(f-3f_o)^2/6B_m^2}+3e^{-(f-f_o)^2/6B_m^2}+3e^{-(f+f_o)^2/6B_m^2}\right.$$

$$\left.+e^{-(f+3f_o)^2/6B_m^2}\right]$$

$$+\frac{\sigma_n^6}{8\sqrt{2\pi}\sqrt{3\,B_m}}\left[e^{-(f-3f_o)^2/6B_n^2}+3e^{-(f-f_o)^2/6B_n^2}+3e^{-(f+f_o)^2/6B_n^2}\right.$$

$$\left.+e^{-(f+3f_o)^2/6B_n^2}\right]$$

$$+\frac{3\sigma_m^4\sigma_n^2}{8\sqrt{2\pi}\sqrt{2B_m^2+B_n^2}}\left[e^{-(f-3f_o)^2/2(2B_m^2+B_n^2)}+3e^{-(f-f_o)^2/2(2B_m^2+B_n^2)}\right.$$

$$\left.+3e^{-(f+f_o)^2/2(2B_m^2+B_n^2)}+e^{-(f+3f_o)^2/2(2B_m^2+B_n^2)}\right]$$

$$+\frac{3\sigma_m^2\sigma_n^4}{8\sqrt{2\pi}\sqrt{B_m^2+2B_n^2}}\left[e^{-(f-3f_o)^2/2(B_m^2+2B_n^2)}+3e^{-(f-f_o)^2/2(B_m^2+2B_n^2)}\right.$$

$$\left.+3e^{-(f+f_o)^2/2(B_m^2+2B_n^2)}+e^{-(f+3f_o)^2/2(B_m^2+2B_n^2)}\right] \quad (7\text{-}10)$$

Substituting equation (7-10) in equation (7-9) and extracting only the low-frequency components gives, for the detector output low-pass spectrum with $B_n >> B_m$,

$$S(f)_{lf}=\frac{h_{02}^2}{16\sqrt{\pi}}\left\{\frac{2\sigma_m^4}{B_m}e^{-f^2/4B_m^2}+\frac{2\sigma_n^4}{B_n}e^{-f^2/4B_n^2}+\frac{4\sigma_m^2\sigma_n^2}{B_n}e^{-f^2/2B_n^2}\right\}$$

$$+\frac{h_{11}^2}{\sqrt{2\pi}}\left\{\frac{\sigma_m^2}{B_m}e^{-f^2/2B_m^2}+\frac{\sigma_n^2}{B_n}e^{-f^2/2B_n^2}\right\}$$

$$+\frac{h_{13}^2}{8\sqrt{2\pi}}\left\{\frac{\sigma_m^6}{\sqrt{3}\,B_m}e^{-f^2/6B_m^2}+\frac{\sigma_n^6}{\sqrt{3}\,B_n}e^{-f^2/6B_n^2}+\frac{3\sigma_m^4\sigma_n^2}{B_n}e^{-f^2/2B_n^2}\right.$$

$$\left.+\frac{3\sigma_m^2\sigma_n^4}{\sqrt{2}\,B_n}e^{-f^2/4B_n^2}\right\}$$

$$+\frac{h_{22}^2}{4\sqrt{4\pi}}\left\{\frac{\sigma_m^4}{B_m}e^{-f^2/4B_m^2}+\frac{\sigma_n^4}{B_n}e^{-f^2/4B_n^2}+\frac{2\sigma_m^2\sigma_n^2}{B_n}e^{-f^2/2B_n^2}\right\}. \qquad (7\text{-}11)$$

From equation (7-11), two important quantities are calculable. First, the noise floor is taken to be that value of the spectrum beyond the region of appreciable multipath energy. In the above equation this consists of only those terms with exponentials involving $B_n^2$ since for $f >> B_m$ the other terms are negligible. The noise floor can thus be calculated as a function of $C/N_o$ and S/I by evaluating the various coefficients and setting the remaining exponential multipliers to unity. This calculation is plotted in figure 7-2, where the ratio of mean value squared to noise floor is plotted. Fortunately, as discussed below, the ratio is largely insensitive to S/I for the parameter region of interest.

A second quantity of interest derived from equation (7-11) is the low-pass variance, mathematically defined as the spectral integral of (7-11) multiplied by the low-pass filter transfer function squared. The postdetection low-pass filter has an equivalent one-side bandwidth of 800 Hz, so it may be assumed that all terms having bandwidth related to $B_m$ are passed unattenuated, while the terms involving bandwidth $B_n$ may be considered as having a constant spectral density over the width of the low-pass filter. The variance of the low-pass filter output then becomes:

$$\sigma_{lp}^2=\frac{h_{02}^2\sigma_m^4}{4}+h_{11}^2\sigma_m^2+\frac{h_{13}^2\sigma_m^6}{8}+\frac{h_{22}^2\sigma_m^4}{4}$$

$$+\frac{2B_f}{B_n}\left\{\left(\frac{2\sigma_n^4}{4\sqrt{4\pi}}+\frac{4\sigma_m\sigma_n^2}{4\sqrt{4\pi}}\right)\frac{h_{02}^2}{2}+\frac{h_{11}^2\sigma_n^2}{\sqrt{2\pi}}+h_{13}^2\left(\frac{\sigma_n^6}{8\sqrt{2\pi}\sqrt{3}}+\frac{3\sigma_m^4\sigma_n^2}{8\sqrt{2\pi}}+\frac{3\sigma_m^2\sigma_n^4}{8\sqrt{2\pi}\sqrt{2}}\right)\right.$$

$$\left.+h_{22}^2\left(\frac{\sigma_n^4}{4\sqrt{4\pi}}+\frac{2\sigma_m^2\sigma_n^2}{4\sqrt{4\pi}}\right)\right\}. \qquad (7\text{-}12)$$

The mean value squared of the low-pass output is simply $h_{oo}^2$. The ratio of mean value squared to variance can be evaluated as a function of $C/N_o$ and S/I, since they jointly constrain the relationship between $\sigma_m^2$ and $\sigma_n^2$ in Equation (7-12). This ratio is shown in figure 7-3 as a function of $C/N_o$ with S/I varying.

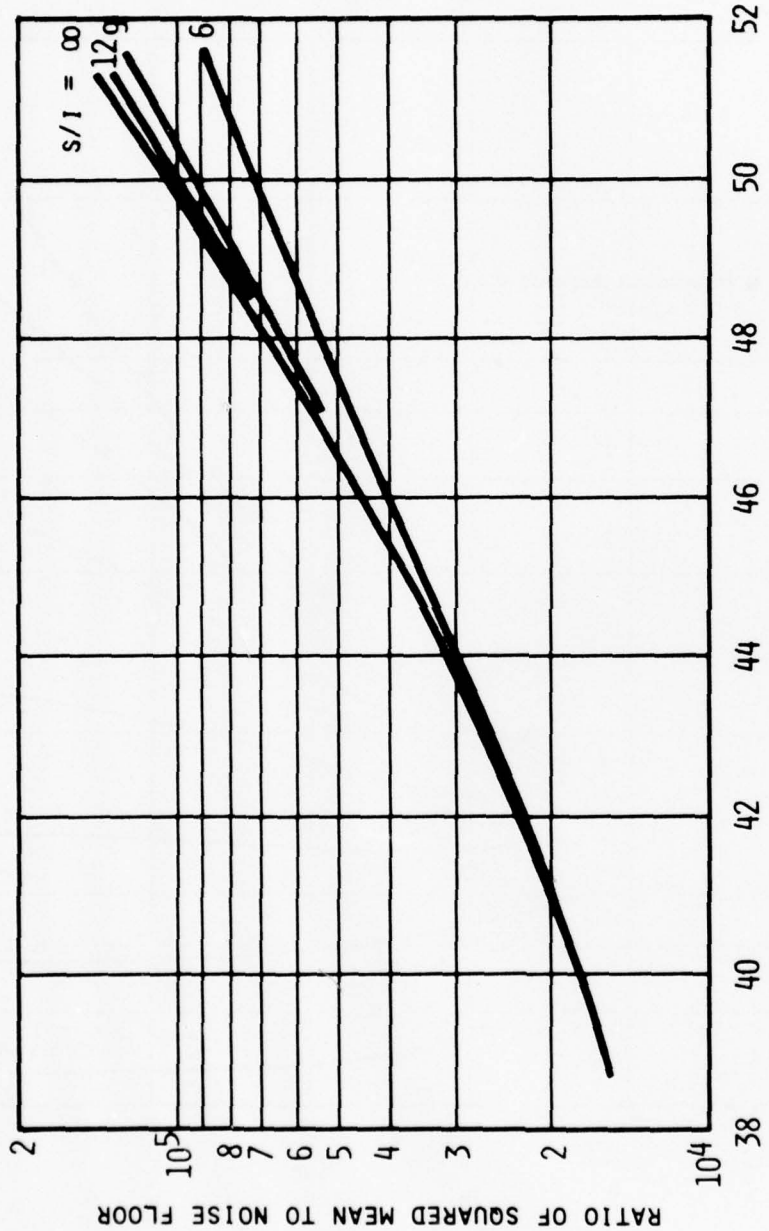


*Figure 7-2. Ratio of Squared Mean to Noise Floor – Low Pass Filter Output of Envelope Detector*

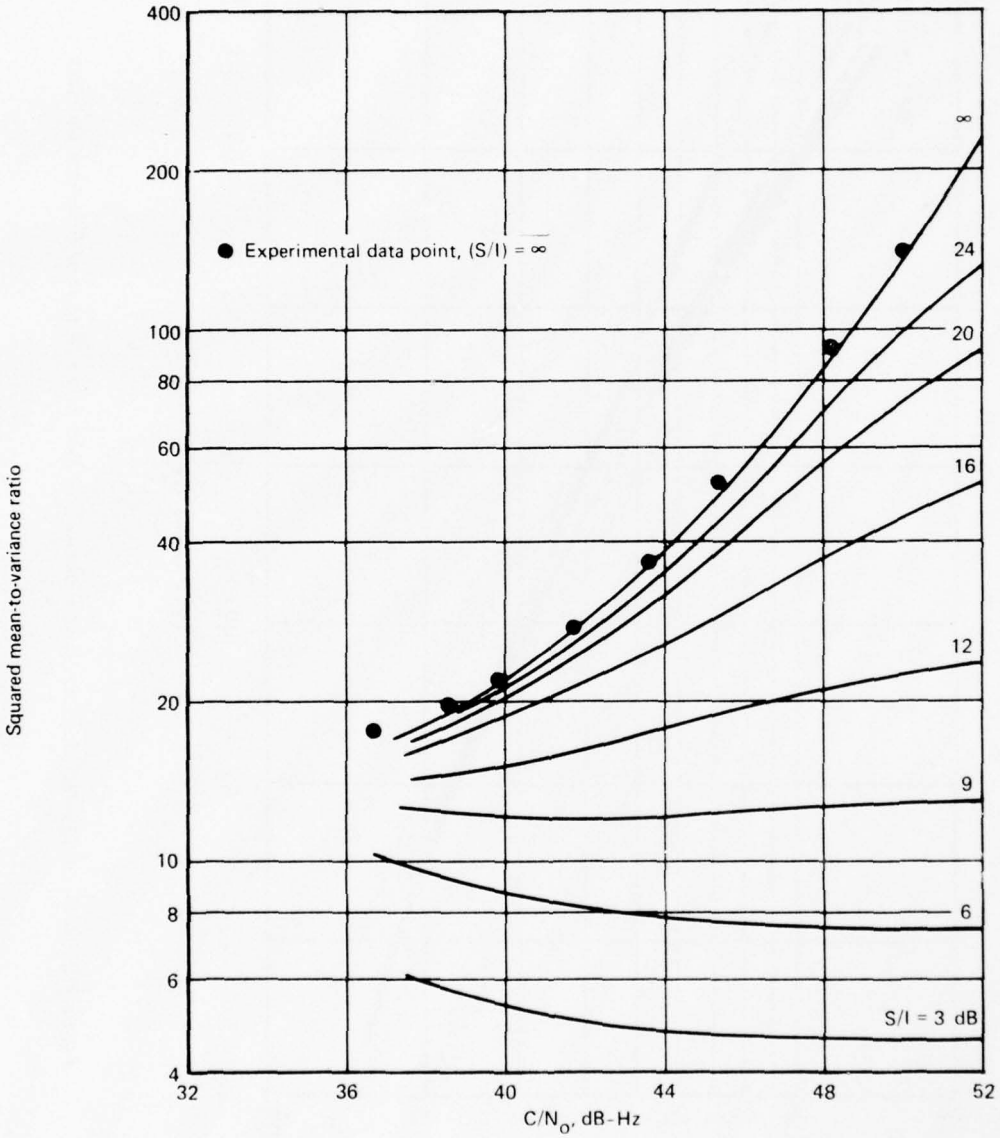


*Figure 7-3. Ratio of Squared Mean to Variance — Low-Pass Filter Output of Envelope Detector, $B_f$ = 800 Hz*

Note that at high $C/N_o$ the ratio is asymptotic to a value determined by the value of S/I, and this asymptote is an increasing function of S/I. On the other hand, at very poor $C/N_o$, additive noise dominates the multipath and a common asymptote is approached for all S/I.

Also shown in figure 7-3 are performance data taken in the laboratory for a no-multipath case ($S/I = \infty$). The experimental data confirm the above cw theory extremely well.

It is apparent from figure 7-3 that the observability of the S/I parameter is very poor at lower $C/N_o$ values. This results since the additive noise contribution to the variance dominates that of the multipath, and the curves tend to converge at low $C/N_o$ and become independent of S/I. Consequently, a modified variance calculation was employed that used a 250-Hz rectangular characteristic (this filtering was performed in the frequency domain by operating on the spectral estimates). Again it may be assumed that all multipath-related components are being passed unattenuated, while the noise contribution to the variance is reduced by a factor of roughly 250/800. Recalculation of equation (7-12) using $B_f = 250$ Hz then provides a theoretical relationship between the square of the process mean divided by the new variance and the parameters $C/N_o$ and S/I. This relationship is shown graphically in figure 7-4.

## 7.2 ENVELOPE DETECTOR OUTPUT PROCESSING PROCEDURE

The analog waveform is sampled at the Test Data Processing Center at a 2000-Hz rate using a 10-bit A/D quantizer (1024 levels). Little aliasing distortion is thus present. For every observation time, 1025 such samples (~0.5 sec) are written on magnetic tape along with the time code.

Processing of this time series consists of the following steps, illustrated in figure 7-5.

a. Estimate mean and mean-square value.

b. Remove mean and linear drift components, if any, from the time samples. This removes the dominance of the large dc component in the neighboring spectral estimates.

c. Taper the time series at each end of the record according to:

$$S(i) = S(i) \sin \frac{\pi(i-1)}{0.2N}, \quad 1 \le i < 0.1N$$

$$= S(i) \sin \frac{\pi(N-i)}{0.2N}, \quad 0.9N < i \le N$$

$$= S(i) \qquad \text{elsewhere} . \qquad (7\text{-}13)$$

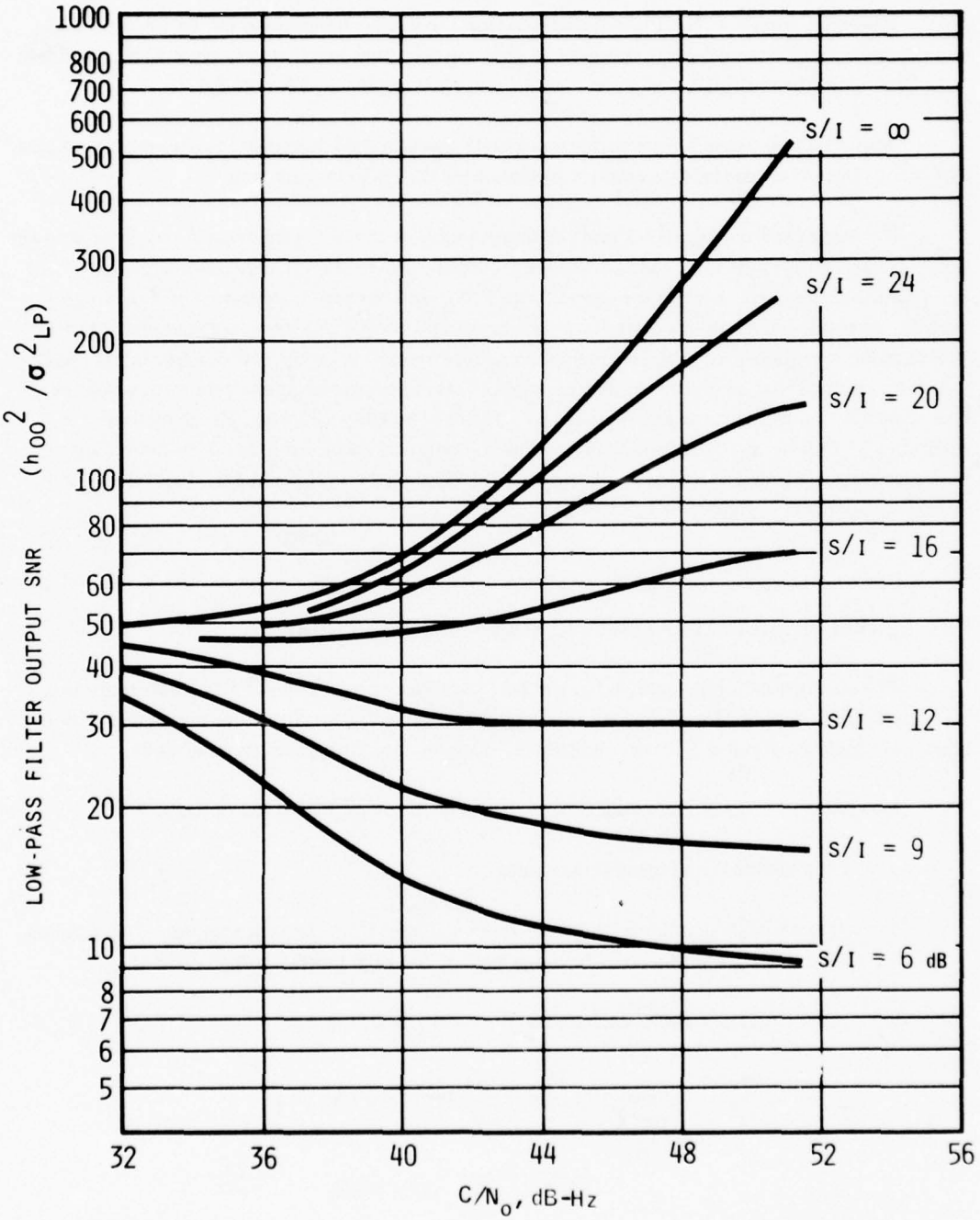


*Figure 7-4. Ratio of Squared Mean to Variance -- Low-Pass Filter Output of Envelope Detector, $B_f$ = 250 Hz*

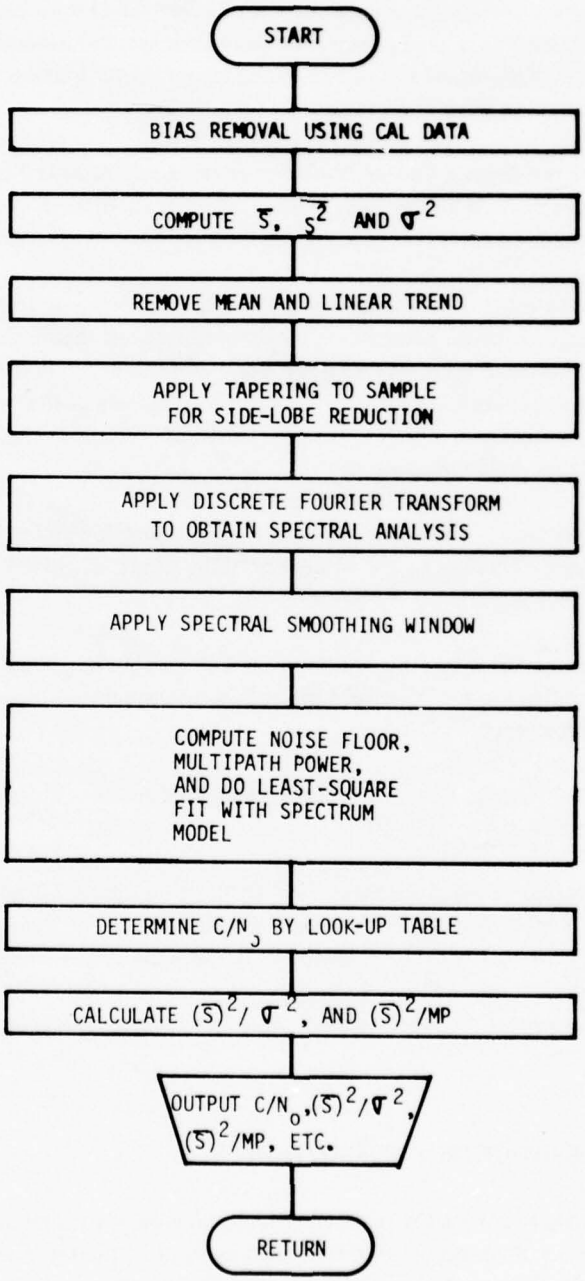


*Figure 7-5. Envelope Detector Data Analysis Algorithm*

This cosine tapering acts to convolve the observed random process with a "filter" having smoother impulse response; hence the equivalent spectral window has lower side lobes. This minimizes spectral bias due to strong components "looking through" the side lobe to contribute at other frequencies.

d. Compute the discrete Fourier transform of the resultant record and obtain the magnitude of the spectrum. With the data set given, spectral coefficients are available roughly every 2 Hz from dc to 1000 Hz.

e. Smooth the estimate in the frequency domain. The estimate from step d typically has rather large variance. Estimates of smaller variance are obtainable by weighting several adjacent coefficients on either side of a desired frequency. In the procedure given here, uniform weighting was used for 10 points on either side of the point in question.

f. Compute the following statistics:

   1) Noise floor – the average spectral level between 250 and 600 Hz, a region nominally devoid of multipath and within which the bandpass and low-pass filter rolloff are not yet important.

   2) Multipath power – the spectral energy lying between 2 and 250 Hz. This is the modified variance described previously, and which also includes some noise contribution.

   3) $(\text{Mean})^2$/noise floor and $(\text{mean})^2$/multipath power – these terms are used to estimate $C/N_o$ and S/I.

g. Using $(\text{mean})^2$/noise floor, determine $C/N_o$ from Figure 7-2 using the S/I = 16 dB curve. At this point S/I is an unknown parameter, but little error is incurred over the range of 38 dB-Hz < $C/N_o$ < 48 dB-Hz by using the S/I = 16 dB curve.

h. Using this same $C/N_o$ and $(\text{mean})^2$/multipath power, interpolate for S/I in figure 7-4.

## 7.3 PROGRAM INPUT/OUTPUT DESCRIPTION

The various programs using the envelope detector analysis algorithm have the same signal strength data outputs for all programs, with the minor exception of antenna test cases. The input data to this analysis algorithm is the same for all programs.

Input data specified whenever the signal strength analysis algorithm is used are as follows:

| | |
|---|---|
| Sample rate: | 2 kHz |
| Taper rate: | 0.1 |
| Spectral window width: | 40 Hz |
| Initial values of $a_1$, $a_2$, $a_3$: | Specified by user |
| Low-pass filter bandwidth: | 800 Hz |
| Bias value: | Specified by user |
| Signal strength record analysis skip factor: | Specified by user |
| Signal strength plot skip factor: | Specified by user. |

Direct output from the CDC 6600 computer is in the form of computer listings. This listing includes a printout of the smoothed spectrum as estimated from the signal strength time data, convergence data used in the least-squares-fit algorithm, and a printout of the fitted model spectrum. It also includes the following parameters as a tabulation:

Date and time of test
Mean value of the signal
Mean square value of the signal
Theoretical spectrum coefficients ($a_1$, $a_2$, $a_3$)
Ratio of squared mean/$a_3$ (noise floor)
Variance
Standard deviation
Ratio of squared mean/variance
MP, defined as multipath power plus noise power
Ratio of squared mean/multipath power
$C/N_0$.

A signal strength summary plot can be made for each of the summaries described above. The data to be plotted are output onto a plot tape, which is then run off-line on the SC 4020. The plots include the measured data-smoothed spectral estimate and the fitted model spectrum. In addition, several parameters, also printed on the listing, are included on the bottom of the plot output.

## 7.4 SAMPLE RESULTS

Figures 7-6 and 7-7 illustrate the smoothed spectral estimates for two cases selected arbitrarily. The first is for a Type I test when no appreciable multipath is anticipated. (Actually, the spectral analysis approach shows an absence of additional energy in the 0-100 Hz region for Type I tests, indicating that the antenna S/I is at least 15 dB in general.) The second plot (fig. 7-7) is for a Type II run

with intended S/I in the 8-dB range. A definite spectrum increase is observed in the multipath Doppler zone, and the curve fitting and parameter estimation procedures are illustrated below.

From figure 7-7 the squared mean/noise floor statistic is 52,500, and from figure 7-2 the estimated $C/N_0$ is 46.9 dB-Hz. Although the squared-mean-to-modified-variance ratio (250-Hz bandwidth) is not printed on figure 7-7, it is given in computer listings and for this case was 11.0. Use of figure 7-4 then yields an S/I of 6.5 dB.

Repetitive averaging of similar cases over a data run provides estimates with accuracy ascribed to be $\pm 0.5$ dB in $C/N_0$ and $\pm 1$ dB in S/I. Table 7-1 is an example printout, showing smoothed spectrum, best-fit spectrum, and statistical summary. The data interval does not correspond with the plots of figures 7-6 and 7-7.

As a check on the agreement between hardware $C/N_0$ measurements (for example those obtained with a wave analyzer or spectrum analyzer) and those generated with the computer procedure, a sample tape was generated for hardware-determined $C/N_0$ values of 38 to 50 dB-Hz. This tape was digitized and processed in the usual manner, and the calibration curve of figure 7-8 was generated. This curve was not used in the data reduction other than to show the rather good agreement between hardware and software approaches. The computer method becomes less accurate below 38 dB-Hz because the noise bandwidth at the detector input is 5 kHz, implying that the output statistics are quite insensitive to $C/N_0$ values lower than this point. For example, figure 7-2 is nearly horizontal in this region.

## TABLE 7-1. SIGNAL STRENGTH SUMMARY NUMERICAL OUTPUT

```
SMOOTHED SPECTRUM
    1  5.33E+00    2  5.34E+00    3  5.41E+00    4  5.32E+00    5  5.49E+00    6  5.70E+00    7  4.82E+00    8  4.96E+00
    9  4.66E+00   10  4.59E+00   11  4.52E+00   12  4.82E+00   13  4.84E+00   14  4.82E+00   15  4.27E+00   16  4.24E+00
   17  3.34E+00   18  2.78E+00   19  2.83E+00   20  2.77E+00
   25  3.0-E+00   30  2.40E+00   35  2.23E+00   40  2.27E+00   45  1.55E+00   50  9.12E-01   55  6.05E-01   60  3.98E-01
   65  3.15E-01   70  3.20E-01   75  2.67E-01   80  2.27E-01   85  2.39E-01   90  1.41E-01   95  1.15E-01  100  1.68E-01
  105  1.64E-01  110  1.93E-01  115  1.95E-01  120  1.55E-01  125  1.57E-01  130  1.33E-01  135  1.75E-01  140  1.68E-01
  145  1.37E-01  150  1.33E-01  155  1.51E-01  160  1.78E-01  165  2.04E-01  170  2.15E-01  175  1.92E-01  180  2.03E-01
  185  1.94E-01  190  1.54E-01  195  1.55E-01  200  1.31E-01  205  1.35E-01  210  1.25E-01  215  1.31E-01  220  1.17E-01
  225  1.24E-01  230  1.15E-01  235  1.16E-01  240  1.25E-01  245  1.28E-01  250  1.49E-01  255  1.24E-01  260  1.28E-01
  265  1.3-E-01  270  1.37E-01  275  1.24E-01  280  1.47E-01  285  1.53E-01  290  1.37E-01  295  1.23E-01  300  9.95E-02
CONVERGENCE
5.2    5.13255E+01   5.16613E+00   9.00003E+01   6.49478E+10  -3.51685E+01  -4.22638E-01  -1.02078E-10
5.2    2.77567E+01   3.02707E+00   9.50503E+01   6.49478E+10  -1.19747E+01   1.99981E-01  -1.17638E-11
5.2    1.26+13E+01   4.76255E+00   7.68081E+01   6.49478E+10   3.84210E+00   3.80923E-01   2.44993E-11
5.2    1.09526E+01   4.75347E+00   7.38572E+01   6.49478E+10   1.19288E+00   1.74285E-01   8.18037E-12
5.2    1.05281E+01   4.75291E+00   7.02215E+01   6.49478E+10  -1.62713E+00  -8.63905E-02  -1.10127E-11
5.2    1..418+E+01   4.79765E+00   7.13427E+01   6.49478E+10   2.61461E-01   2.99829E-02  -1.51773E-12
FITTED VAL
    1  4.95E+00    2  4.95E+00    3  4.94E+00    4  4.92E+00    5  4.90E+00    6  4.87E+00    7  4.83E+00    8  4.78E+00
    9  4.71E+00   10  4.67E+00   11  4.61E+00   12  4.54E+00   13  4.47E+00   14  4.39E+00   15  4.31E+00   16  4.21E+00
   17  4.12E+00   18  4.02E+00   19  3.92E+00   20  3.82E+00
   25  3.27E+00   30  2.71E+00   35  2.14E+00   40  1.69E+00   45  1.28E+00   50  9.52E-01   55  6.34E-01   60  5.12E-01
   65  3.91E-01   70  3.34E-01   75  2.38E-01   80  2.03E-01   85  1.83E-01   90  1.71E-01   95  1.65E-01  100  1.61E-01
  105  1.54E-01  110  1.54E-01  115  1.58E-01  120  1.58E-01  125  1.57E-01  130  1.57E-01  135  1.57E-01  140  1.56E-01
  145  1.53E-01  150  1.56E-01  155  1.55E-01  160  1.55E-01  165  1.55E-01  170  1.54E-01  175  1.54E-01  180  1.53E-01
  185  1.52E-01  190  1.52E-01  195  1.51E-01  200  1.50E-01  205  1.49E-01  210  1.48E-01  215  1.49E-01  220  1.47E-01
  225  1.43E-01  230  1.44E-01  235  1.43E-01  240  1.42E-01  245  1.41E-01  250  1.40E-01  255  1.38E-01  260  1.37E-01
  265  1.35E-01  270  1.34E-01  275  1.32E-01  280  1.30E-01  285  1.29E-01  290  1.27E-01  295  1.25E-01  300  1.23E-01

                              S I G N A L   S T R E N G H T   S U M M A R Y
                                        DATE        11/19/74-0
                                        TIME        14/48/ 4.707
        MEAN                             102.5
        MEAN SQUARE                    10349.7
        SPECTRUM COEFFICIENTS           4.7976          71.3427          .1586
        SQ.MEAN/NOISE FLOOR            65269.9
        VARIANCE                         40.8
        STANDARD DEVIATION               21.00
        SQ.MEAN/VAR                     23.737
        MULTIPATH POWER                356.19
        SQ.OF MEAN                     23.5016
        C/NO                             47.99
```

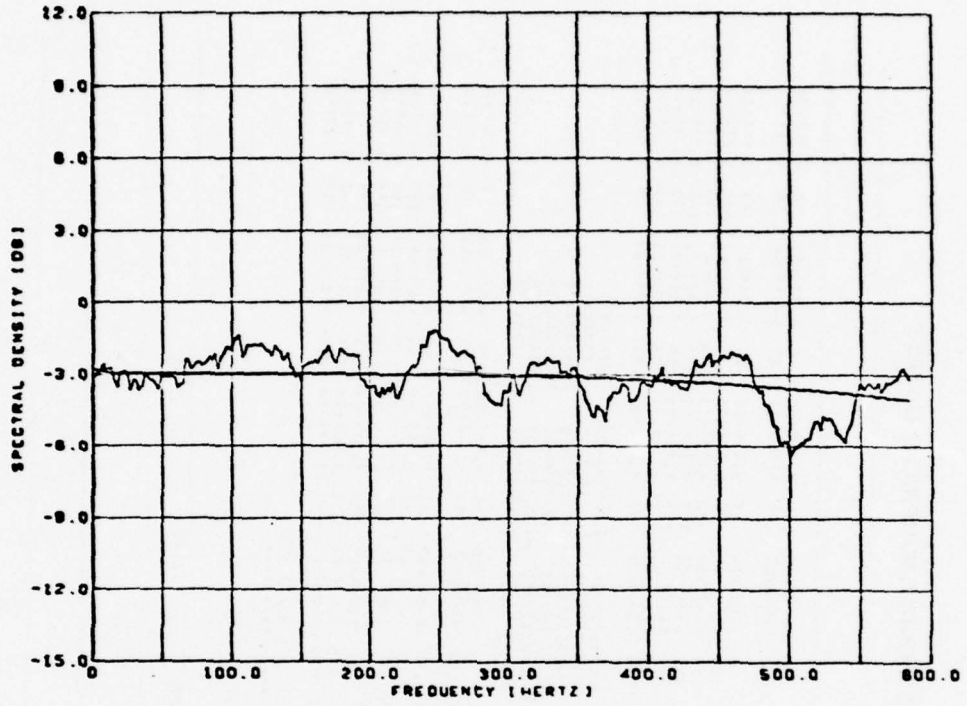


DATE 11/18/74-0 MEAN 108.7
START TIME 23/55/54.8 SO.MEAN/NOISE FLOOR 2.25E+04
SPECTRUM PARAMETER A1= .0171
A2= 10.9759
A3= .5053
SO.MEAN/VAR 29.581 C/NO 42.14

*Figure 7-6. Spectral Analysis Plot of Envelope Detector Output, S/I >15 dB*

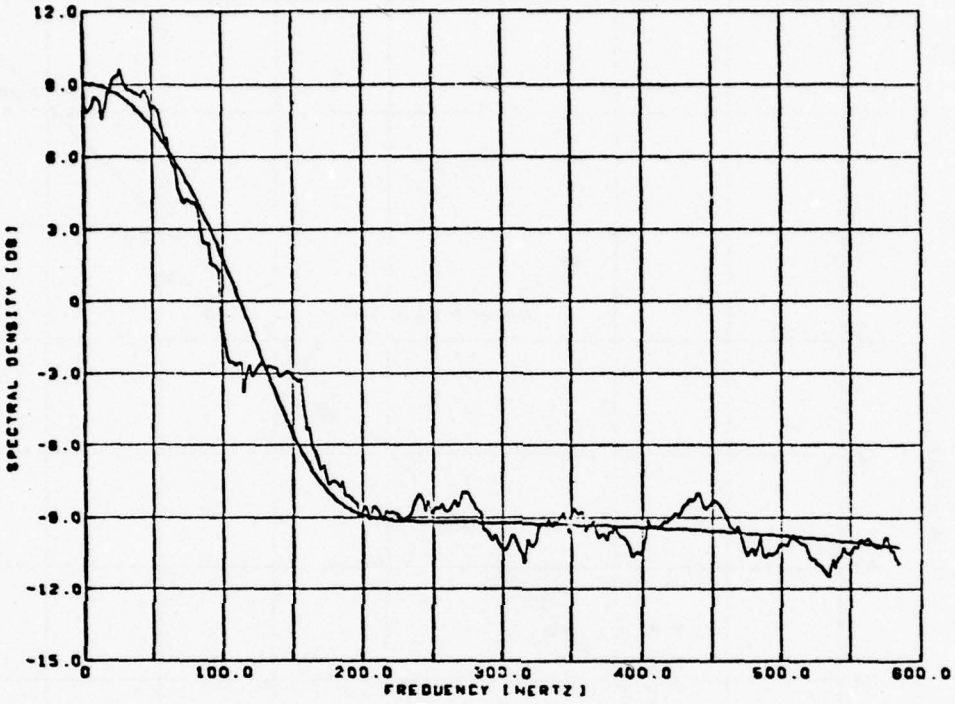


| | | | |
|---|---|---|---|
| DATE | 11/16/74-0 | MEAN | 79.9 |
| START TIME | 23/15/14.0 | SQ.MEAN/NOISE FLOOR | 5.25E+04 |
| | | SPECTRUM PARAMETER A1= | 7.9408 |
| | | A2= | 75.0360 |
| | | A3= | .1215 |
| SQ.MEAN/VAR | 0.015 | C/NO | 48.91 |

*Figure 7-7. Spectral Analysis Plot of Envelope Detector Output, S/I = 6.5 dB*

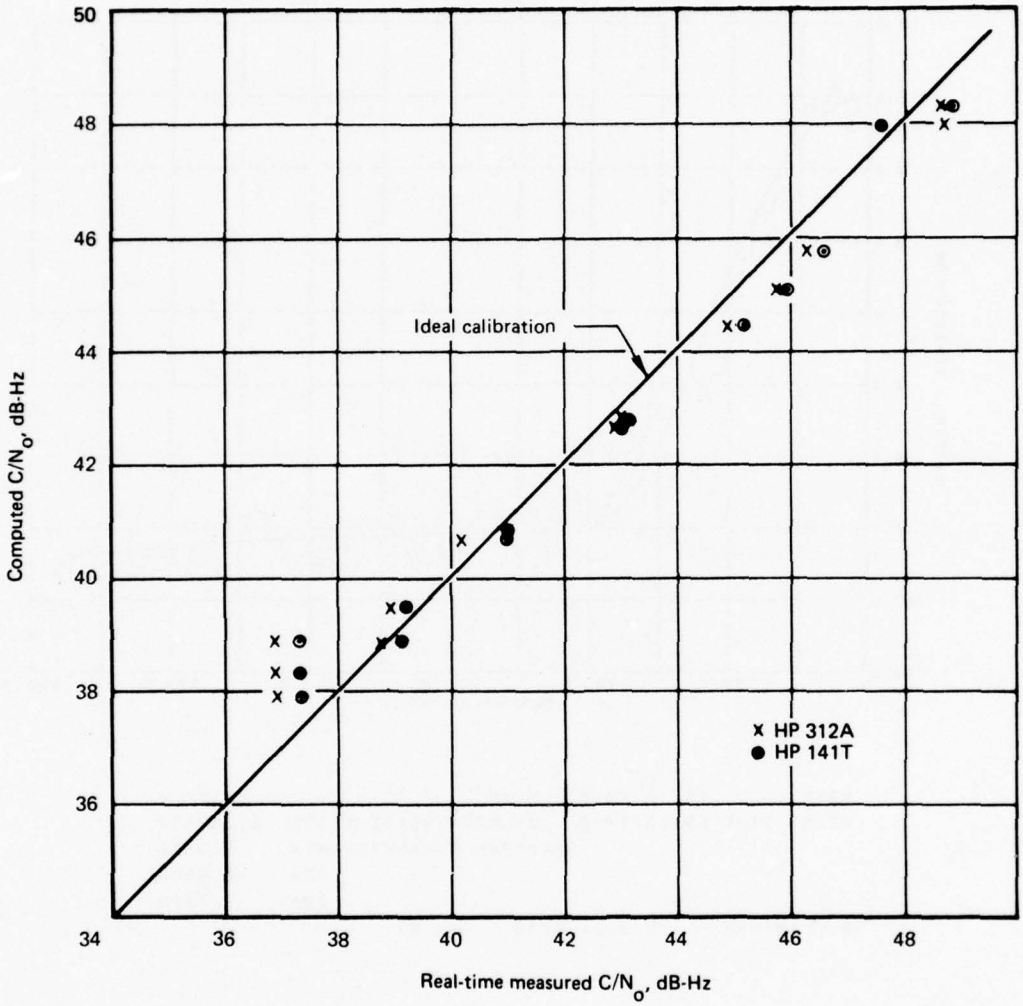


*Figure 7-8. Computed Versus Real-Time C/N$_o$*

# 8. VOICE MODEM DRandA PROCESSING

Voice data processing includes parallel efforts by Boeing and CBS Laboratories. CBS Laboratories provide intelligibility scoring using listener panels and supply test results to Boeing. Boeing processes the data to obtain $C/N_o$ and S/I, described below.

## 8.1 DETERMINATION OF $C/N_o$ AND S/I

The signal strength data are computer analyzed to determine $C/N_o$ and S/I for voice modem tests. Processing is controlled by a program that calls subroutines to position the data tape by using file numbers and segment times. The algorithm is shown in figure 8-1. The determination of $C/N_o$ and S/I uses algorithms described in section 7.

The digital tape format is as previously described in figure 6-3. Each signal strength record consists of four time words, one identification word, a 1025 signal strength sample words. Each signal strength word is 12 bits long. A record occurs e y 15 sec as controlled by the IRIG-B time code.

## 8.2 INPUT SPECIFICATIONS AND OUTPUT FORMATS

The input to voice program test segments consists of the entire specification of signal strength analysis related parameters as described in section 7.4. Further data specified for voice segments that relate to tape positioning and segment identification include:

Date of test
Tape number
Tape file
Start and end time of segment
Test mode (Type I or II).

The output from a voice analysis segment is described in section 7.4 and consists entirely of data resulting from signal strength analysis.

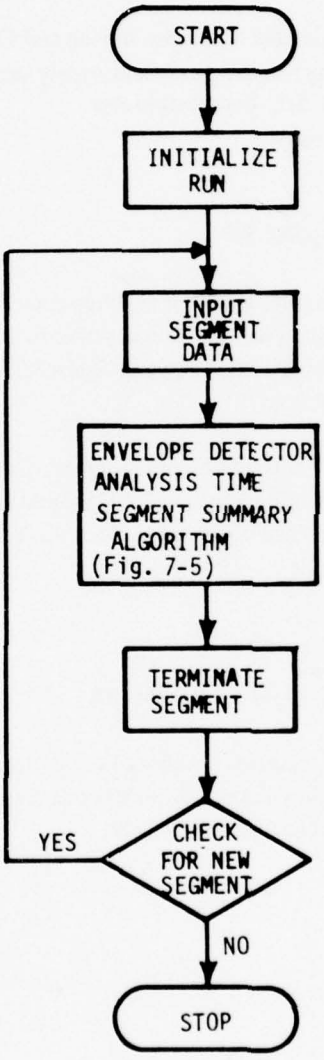


*Figure 8-1. Voice Data Processing Algorithm*

# 9. DIGITAL COMMUNICATION DATA MODEM DRandA PROCESSING

Digital data modem processing is controlled by a program that calls subroutines to position the tape at the correct file number and time, process the signal strength data to give $C/N_o$ and S/I statistics, and process the PN sequence digitial data message.

## 9.1 DIGITAL TAPE FORMAT

The digital tape format for digital segments is as previously shown in figure 6-6. This figure shows that each digital data record is comprised of four time words and one identification word, followed by five blocks of data bits. Each block (one per modem) contains 205 12-bit words (2460 bits per block) and corresponds to a digital data channel recorded on the airplane, thus corresponding to approximately 2 sec of data at 1200 bps. Signal strength is sampled every seven digital data records (approximately 14 sec) and is formatted with the applicable time code and ID shown in figure 6-3.

## 9.2 ALGORITHM FOR DIGITAL DATA PROCESSING

Processing the digital data involves signal strength parameter computation, bit-error rate determination, and error tabulation. Figure 9-1 illustrates the sequence of operations performed.

For the time segment defined for analysis, data is input and subroutines are initialized. Signal strength records are separated from digital data records and are processed to provide $C/N_o$ and S/I parameters as described in section 7. The digital data records are processed as described in the next section.

## 9.3 DIGITAL DATA RECORD PROCESSING ALGORITHM

The digital data record processing algorithm is shown in figure 9-2. Within each data record, the five blocks of data (one per recorded modem channel) are processed in turn starting with channel

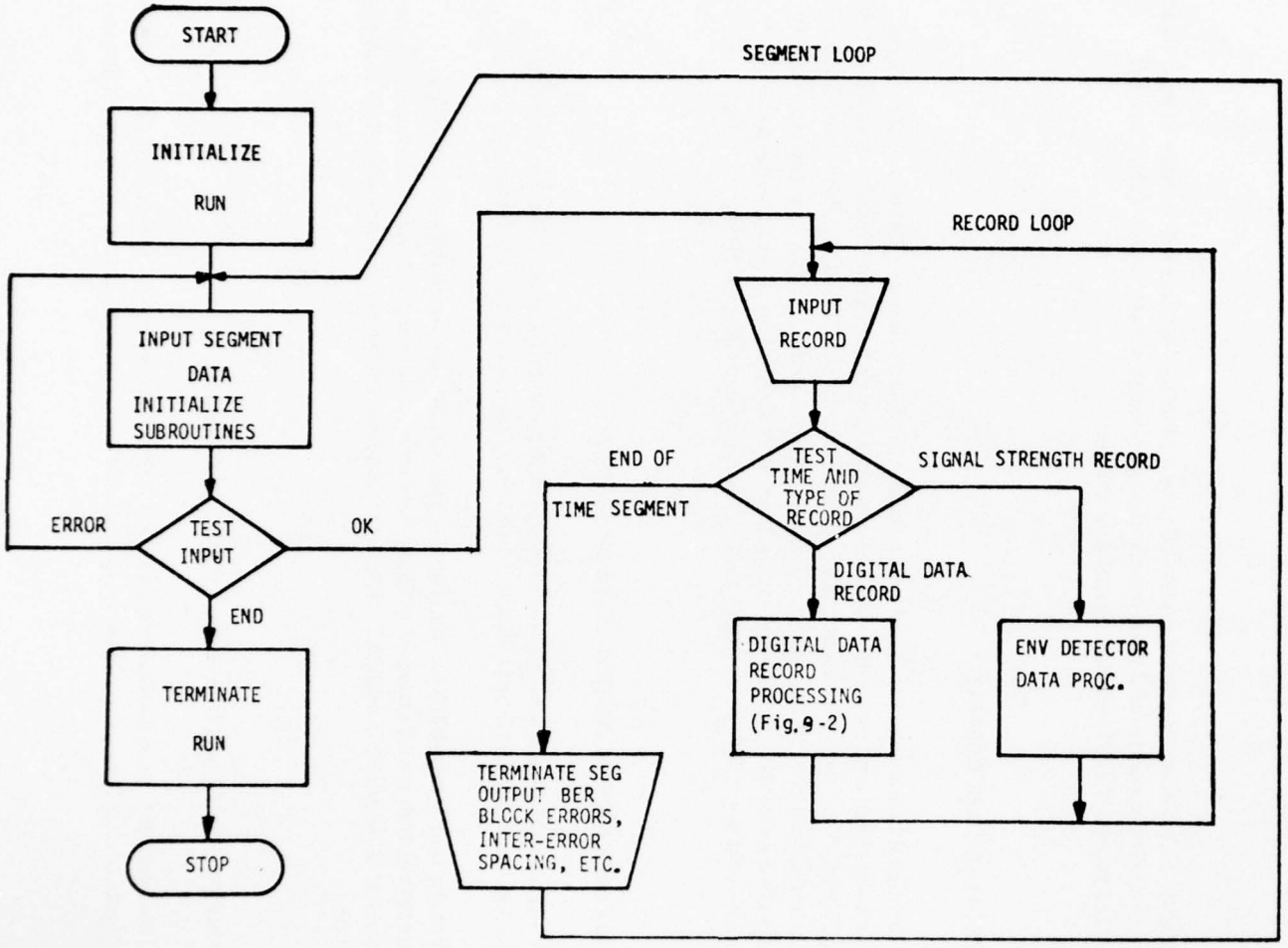


*Figure 9-1. Digital Data Processing Algorithm*

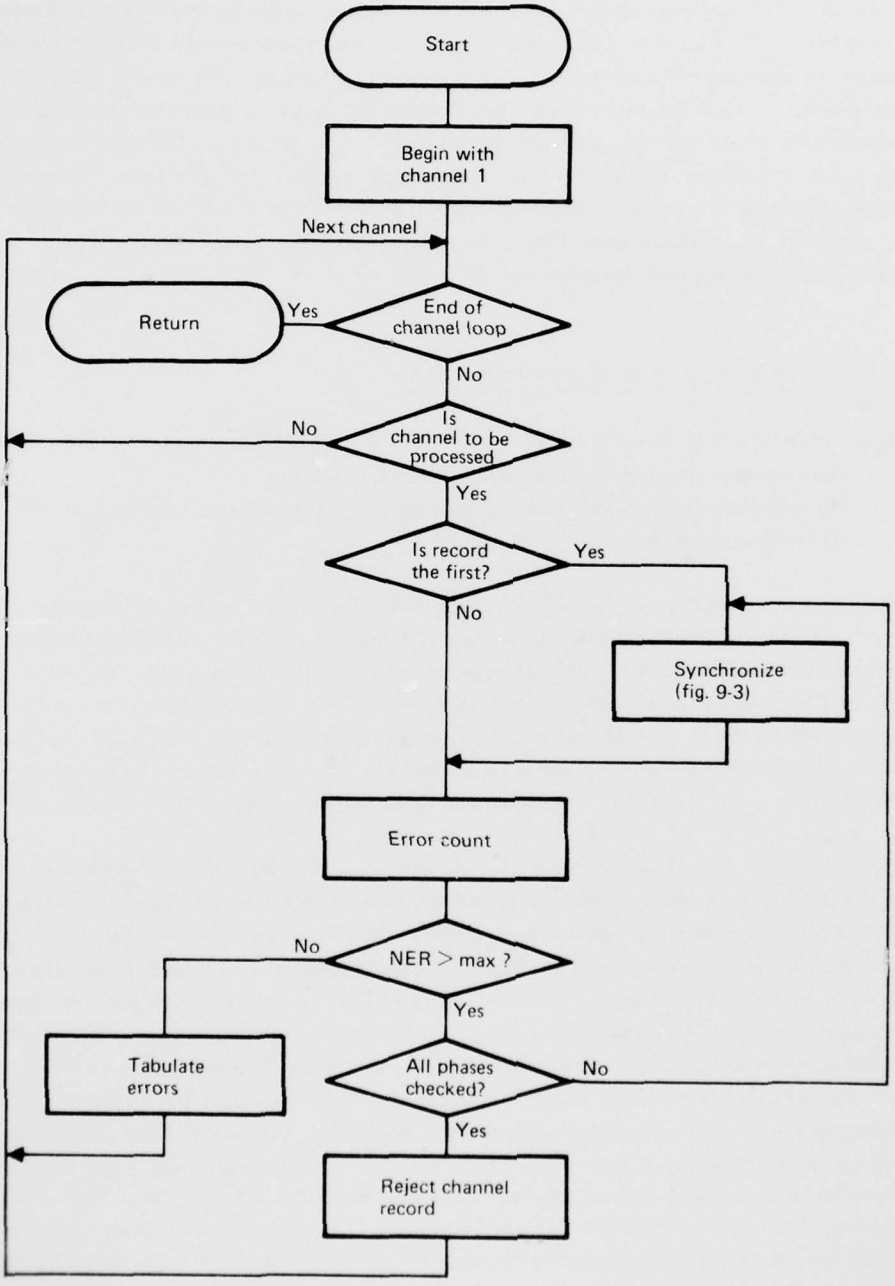


*Figure 9-2. Digital Record Processing Algorithm*

1. Since not all five channels are always active, a skip provision is made for omitting the processing for selected channels. If the data record to be processed is the first record within a time segment, data synchronization (reference PN sequence synchronization) is performed. This process will be described in detail in section 9.3.1. If the data record is not the first within a time segment, it is assumed that synchronization has been previously achieved and bit-error counts are made. The bit-error count is then subjected to an acceptance/rejection test. If the count exceeds a 10% error rate threshold, the resynchronization mode is entered. If the error count is accepted, the number of errors, the error locations, and other data are tabulated. Inter-error spacing and block error histograms are also computed and stored for the segment summary output.

### 9.3.1 Synchronization of Input Data to Reference Data

To process the digital data, two items associated with synchronization must be accomplished:

a. The error-free reference data sequence must be generated.
b. The reference sequence must be synchronized in phase with the received data for bit-by-bit comparison.

The transmitted PN data sequence is of length 2047, described by the generator polynomial $X^{11} + X^2 + 1$. An identical reference PN sequence is generated in the computer. Starting with each bit of the reference sequence, 2047 60-bit words are formed and stored in memory. Because of the properties of a PN sequence, each of these 2047 60-bit words has a unique 11-bit pattern in the 11 most significant bit positions. The remaining 49 bit positions are filled with the normal continuation of the PN sequence. A cross-reference table is created so that, given a particular 11-bit pattern, the 60-bit word with the same 11-bit pattern in the most significant bit positions can be found.

The algorithm for synchronization is illustrated in figure 9-3. Basically the method consists of extracting the first 11 bits from the input string and using the cross-reference table to determine which of the 2047 60-bit reference words has the same 11-bit pattern in the first 11 bits. The reference words are then called in the proper order to form the reference sequence. Bit-by-bit comparisons are then made with the input data string for the entire block of data bits in the record for that channel. If the two strings are not synchronized, the error rate will be approximately 50%, and the sync position will be rejected by the error rate threshold test (10% errors) that follows. If rejection occurs, the synchronization algorithm is repeated, this time using the second group of 11 bits from the input data stream. This process is continued until synchronization is achieved or the end of the channel block is reached. If synchronization is not achieved (all trials yield error rates greater than 0.10), the 2460 bits from that particular record and channel block are rejected. When the end of the data block for this channel is reached, the synchronization algorithm is applied to the data block for the next channel. Synchronization is performed independently for each of the five channels since bits from the various demodulators are not necessarily identically timed.

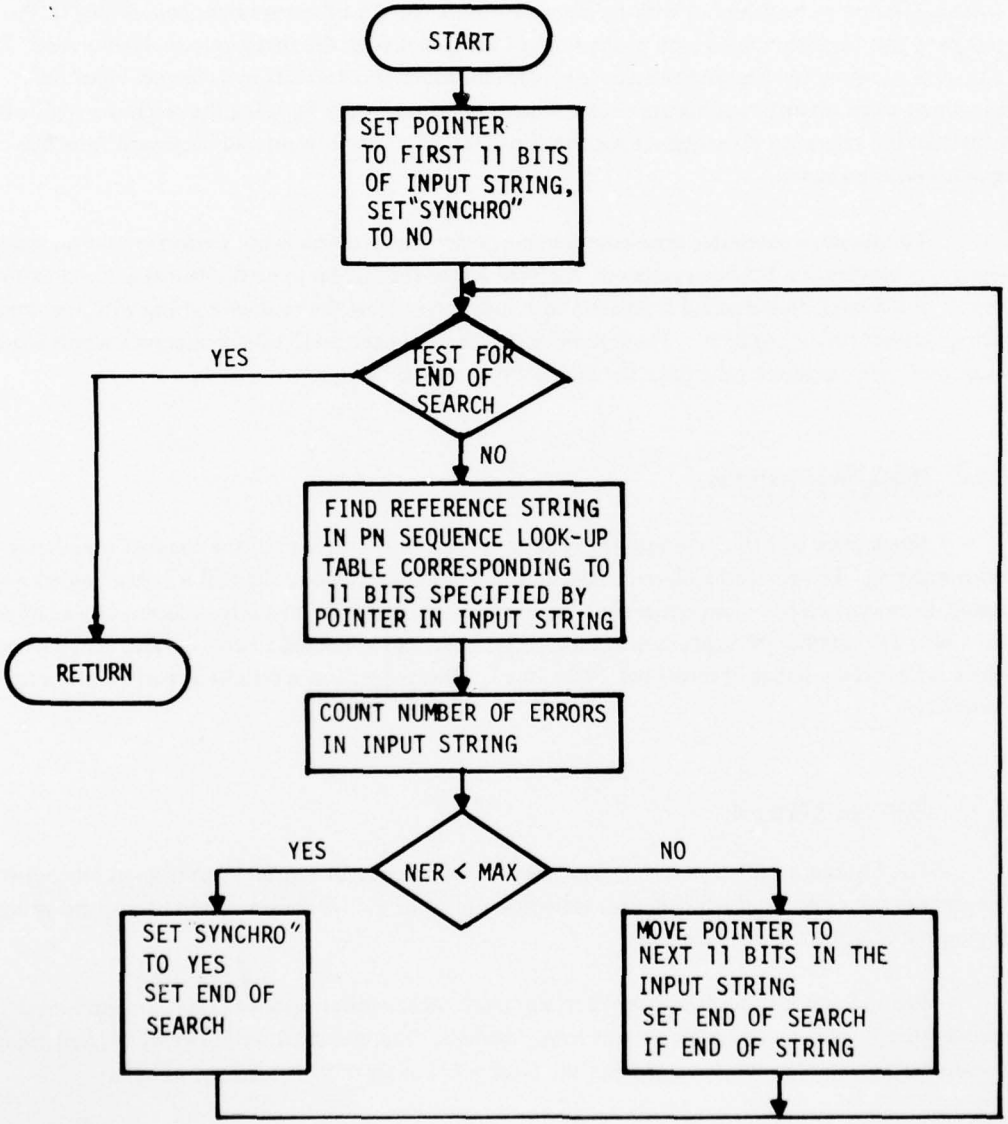


*Figure 9-3. Digital Message Synchronization Algorithm*

It is readily apparent that an error-free group of 11 bits in the input data string is required for synchronization to be achieved with the above method. At the bit-error rates encountered in this test program, this condition has a high probability of being met with the first group of 11 bits read. Even if several attempts are required to achieve synchronization, all 2460 bits in a channel block are examined when bit-error counts are made. This is achieved simply by using the reference words to construct the reference PN sequence for the entire record, both forward and backward from the synchronization point.

To minimize computer time requirements, resynchronization is not performed unless required. Once synchronization has been achieved, the position of the last bit in each channel is saved from one record to the next, thus making it possible to resume comparing the reference string with the input string without resynchronizing. The reference sequence and the 2047 60-bit reference words stored in memory are generated only once for each computer processing run.

### 9.3.2 Block Error Statistics

Block error statistics and inter-error spacings provide a measure of the channel's tendency for error bursting. To provide block error statistics, the input data of one channel is considered as a single string, from start to end of an entire time segment. The string is divided into adjacent blocks of n bits ($n = 24$). The number of errors in each block is counted and tabulated to give the frequency of occurrence for a given number of errors per 24-bit block. This tabulation is output as part of the segment summary.

### 9.3.3 Inter-Error Spacing

The histogram of inter-error spacing gives the frequency of a given separation in bits between successive errors. As for the block error statistics, the input data is considered to be a single string for a given channel and time segment.

Figure 9-4 illustrates the received string, with some error positions (x) and the inter-error spacing that is given by the difference in error positions. The tabulated output gives the frequency of occurrence for a given inter-error spacing and is included as part of the segment summary.

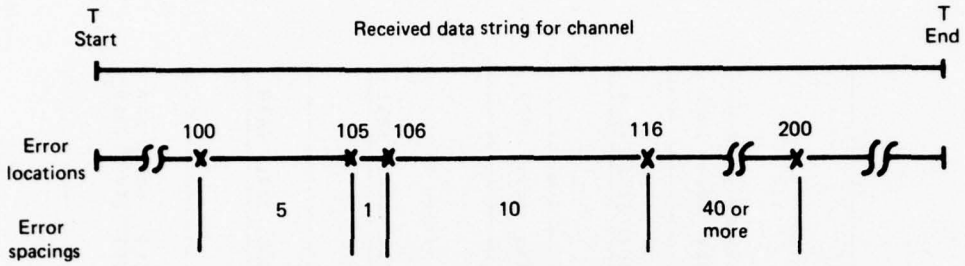


*Figure 9-4. Inter-Error Spacing Definition*

## 9.4 PROGRAM INPUT AND OUTPUT DESCRIPTION

Inputs to the digital data processing program include all the signal strength processing parameters explained in section 7.4. In addition, the following parameters are specified to position the tape, identify the test, and specify the channels to be analyzed:

Data of test
Tape number
Tape file
Start time of segment
End time of segment
Test mode (Type I or II)
Channels to be analyzed.

Outputs provided by the digital data analysis are as follows.

a. Error locations are tabulated for each record processed (table 9-1). The time of each record is printed and, if errors are present, the channel number containing errors, number of errors, and bit locations of the errors in the data block (locations run from bit 1 to 2460) are also given.

b. At the end of each time segment, a segment summary is provided (table 9-2). This summary includes the date, start and end time of segment, experiment mode identification, tabulation of number of bits analyzed for each of five channels, number of errors, and bit-error rate. Also included is the block error histogram for each channel for the segment and the inter-error spacing histogram (table 9-3). At the bottom of the inter-error histogram, the number of resynchronizations required during the segment is given for each channel.

## TABLE 9-1. ERROR LOCATIONS IN DIGITAL DATA RECORDS

| | | | | | | | | | | | | | | |
|---|---|---|---|---|---|---|---|---|---|---|---|---|---|---|
| 14/28/13.704 | | | | | | | | | | | | | | |
| | 4 | 8 | 149 | 173 | 174 | 567 | 1131 | 1423 | 1424 | 2309 | | | | |
| | 5 | 1 | 175 | | | | | | | | | | | |
| 14/28/15.034 | | | | | | | | | | | | | | |
| | 1 | 4 | 578 | 579 | 1454 | 1455 | | | | | | | | |
| | 2 | 2 | 577 | 578 | | | | | | | | | | |
| | 3 | 2 | 583 | 584 | | | | | | | | | | |
| | 4 | 18 | 21 | 169 | 507 | 508 | 555 | 570 | 577 | 578 | 1235 | 1259 | 1324 | 1415 |
| | | | 1715 | 1716 | 1846 | 1850 | 2009 | 2417 | | | | | | |
| | 5 | 1 | 561 | | | | | | | | | | | |
| 14/28/17.665 | | | | | | | | | | | | | | |
| | 4 | 18 | 199 | 200 | 371 | 376 | 769 | 843 | 855 | 892 | 1067 | 1098 | 1183 | 1304 |
| | | | 1305 | 1563 | 1594 | 2005 | 2189 | 2190 | | | | | | |
| 14/28/19.935 | | | | | | | | | | | | | | |
| | 1 | 4 | 1163 | 1164 | 1165 | 1167 | | | | | | | | |
| | 2 | 2 | 2094 | 2195 | | | | | | | | | | |
| | 4 | 18 | 82 | 475 | 663 | 839 | 1130 | 1419 | 1463 | 1794 | 1893 | 1894 | 1896 | 1973 |
| | | | 1974 | 2089 | 2090 | 2206 | 2322 | 2323 | | | | | | |
| | 5 | 6 | 567 | 1165 | 1166 | 2090 | 2091 | 2092 | | | | | | |
| 14/28/21.935 | | | | | | | | | | | | | | |
| | 1 | 3 | 1987 | 1988 | 1989 | | | | | | | | | |
| | 2 | 4 | 1989 | 1990 | 1986 | 1989 | | | | | | | | |
| | 3 | 1 | 1992 | | | | | | | | | | | |
| | 4 | 14 | 30 | 164 | 263 | 653 | 894 | 895 | 1056 | 1371 | 1415 | 1755 | 1890 | 1891 |
| | | | 1903 | 1911 | | | | | | | | | | |
| 14/28/24.635 | | | | | | | | | | | | | | |
| | 1 | 3 | 1063 | 1064 | 1065 | | | | | | | | | |
| | 2 | 4 | 1852 | 1853 | 1857 | 1858 | | | | | | | | |
| | 3 | 3 | 1887 | 1889 | 1890 | | | | | | | | | |
| | 4 | 12 | 569 | 570 | 852 | 859 | 860 | 962 | 1375 | 1516 | 1993 | 2330 | 2331 | 2439 |
| | 5 | 2 | 1138 | 1139 | | | | | | | | | | |
| 14/28/26.106 | | | | | | | | | | | | | | |
| | 2 | 1 | 563 | | | | | | | | | | | |
| | 3 | 2 | 579 | 1821 | | | | | | | | | | |
| | 4 | 26 | 149 | 153 | 154 | 193 | 222 | 388 | 412 | 413 | 559 | 568 | 825 | 827 |
| | | | 893 | 967 | 1000 | 1352 | 1166 | 1237 | 1659 | 1755 | 1766 | 1801 | 1803 | 1815 |
| | | | 1941 | 1942 | 2269 | 2424 | | | | | | | | |
| 14/28/28.246 | | | | | | | | | | | | | | |

## TABLE 9-2. DIGITAL SEGMENT SUMMARY AND BLOCK ERROR HISTOGRAM

SEGMENT SUMMARY

DIGITAL EXPERIMENT

DATE 1/24/75-02
START TIME 14/27/30.000
STOP TIME 14/30/ 0.000
MODE 2

| | CHANNEL 1 | CHANNEL 2 | CHANNEL 3 | CHANNEL 4 | CHANNEL 5 |
|---|---|---|---|---|---|
| NUMBER OF BITS | 173536 | 179580 | 167280 | 179580 | 164820 |
| NUMBER OF ERRORS | 251 | 261 | 74 | 1150 | 381 |
| BIT ERROR PROBABILITY | 1.44E-03 | 1.45E-03 | 4.42E-04 | 6.40E-03 | 2.31E-03 |
| BLOCK ERROR HISTOGRAM | | | | | |
| 1 | 6 | 13 | 16 | 481 | 52 |
| 2 | 34 | 28 | 26 | 156 | 25 |
| 3 | 7 | 10 | 2 | 39 | 13 |
| 4 | 5 | 10 | 0 | 16 | 10 |
| 5 | 4 | 5 | 0 | 11 | 4 |
| 6 | 5 | 5 | 0 | 5 | 3 |
| 7 | 4 | 5 | 0 | 2 | 1 |
| 8 | 2 | 1 | 0 | 4 | 2 |
| 9 | 1 | 1 | 0 | 1 | 2 |
| 10 | 1 | 0 | 0 | 0 | 0 |
| 11 | 1 | 0 | 0 | 0 | 0 |
| 12 | 1 | 0 | 0 | 2 | 0 |
| 13 | 0 | 0 | 0 | 0 | 2 |
| 14 | 0 | 0 | 0 | 0 | 0 |
| 15 | 0 | 1 | 0 | 0 | 0 |
| 16 | 0 | 0 | 0 | 0 | 1 |
| 17 | 0 | 0 | 0 | 0 | 1 |
| 18 | 0 | 0 | 0 | 0 | 0 |
| 19 | 0 | 0 | 0 | 0 | 1 |
| 20 | 0 | 0 | 0 | 0 | |
| 21 | 0 | 0 | 0 | 0 | 1 |
| 22 | 0 | 0 | 0 | 0 | 1 |
| 23 | 0 | 0 | 0 | 0 | 0 |
| 24 | 0 | 0 | 0 | 0 | 0 |

## TABLE 9-3. INTER-ERROR SPACING HISTOGRAM

| INTER ERROR SPACING | CHANNEL 1 | CHANNEL 2 | CHANNEL 3 | CHANNEL 4 | CHANNEL 5 |
|---|---|---|---|---|---|
| 1 | 115 | 104 | 29 | 253 | 143 |
| 2 | 87 | 40 | 2 | 59 | 54 |
| 3 | 12 | 12 | 1 | 33 | 20 |
| 4 | 7 | 6 | 0 | 23 | 15 |
| 5 | 9 | 4 | 0 | 20 | 12 |
| 6 | 2 | 5 | 0 | 14 | 5 |
| 7 | 7 | 3 | 0 | 15 | 12 |
| 8 | 0 | 2 | 0 | 18 | 9 |
| 9 | 4 | 6 | 0 | 12 | 5 |
| 10 | 2 | 6 | 0 | 9 | 4 |
| 11 | 5 | 0 | 0 | 15 | 2 |
| 12 | 4 | 1 | 0 | 7 | 5 |
| 13 | 4 | 2 | 0 | 5 | 2 |
| 14 | 2 | 2 | 0 | 3 | 3 |
| 15 | 1 | 4 | 0 | 4 | 2 |
| 16 | 1 | 1 | 0 | 3 | 6 |
| 17 | 0 | 1 | 0 | 5 | 2 |
| 18 | 1 | 1 | 0 | 5 | 4 |
| 19 | 3 | 1 | 0 | 3 | 2 |
| 20 | 2 | 2 | 0 | 5 | 4 |
| 21 | 0 | 2 | 0 | 4 | 2 |
| 22 | 0 | 2 | 1 | 3 | 1 |
| 23 | 0 | 0 | 0 | 2 | 1 |
| 24 | 0 | 0 | 0 | 10 | 1 |
| 25 | 0 | 0 | 0 | 2 | 1 |
| 26 | 0 | 1 | 0 | 1 | 2 |
| 27 | 1 | 1 | 0 | 3 | 1 |
| 28 | 0 | 0 | 0 | 4 | 0 |
| 29 | 0 | 1 | 0 | 2 | 1 |
| 30 | 0 | 0 | 0 | 2 | 0 |
| 31 | 1 | 0 | 0 | 2 | 0 |
| 32 | 1 | 0 | 0 | 4 | 0 |
| 33 | 0 | 0 | 0 | 2 | 0 |
| 34 | 0 | 1 | 0 | 1 | 0 |
| 35 | 0 | 0 | 0 | 5 | 0 |
| 36 | 0 | 1 | 0 | 6 | 1 |
| 37 | 1 | 0 | 0 | 4 | 1 |
| 38 | 1 | 0 | 0 | 4 | 0 |
| 39 | 0 | 0 | 0 | 4 | 0 |
| 40 | 38 | 36 | 41 | 570 | 58 |
| NUMBER OF RESYNC | 0 | 0 | 4 | 0 | 6 |

# 10. RANGING MODEM DRandA PROCESSING

Analysis of TSC and NASA ranging data is provided by the same ranging software. The analysis, performed on time segments up to 5 min in length, includes both relative ranging error and signal strength analysis. The time segments analyzed are chosen for their relatively constant aircraft parameters and for the constancy of $C/N_o$ and S/I.

## 10.1 DIGITAL TAPE FORMAT (TSC RANGING)

Source tapes are converted to digital tape for the TSC ranging modem at TDPC. NASA information is received in digital form. The digital tape format for the TSC digital ranging modem data was shown in figure 6-4. Table 10-1 describes the meaning of each of the status bits and code information bits. Each bit in the range information corresponds to 25 nsec in range time. For each range value there is a corresponding time and for every 16 range readings there is a signal strength record.

*TABLE 10-1. TSC DIGITAL RANGING TAPE LEGEND*

| | |
|---|---|
| BIT 1 THRU 27 | 0 FILLER |
| BIT 28 | 70 MHz PLL LOCKED + |
| BIT 29 | 70 MHz PLL LOCKED - |
| BIT 30 | CLOCK PLL LOCKED |
| BIT 31 | CORRECT CORRELATION |
| BIT 32 | --- |
| BIT 33 | CODE FORMAT 1 |
| BIT 34 | CODE FORMAT 3 |
| BIT 35 | CODE FORMAT 5 |
| BIT 36 | CODE FORMAT 7 |
| BIT 37 | CODE FORMAT 2 |
| BIT 38 | CODE FORMAT 4 |
| BIT 39 | CODE FORMAT 6 |
| BIT 40 | CODE FORMAT 8 |
| BIT 41 | MSB |
| . | RANGE DATA |
| . | 1 BIT = 25 nsec |
| BIT 60 | LSB |

## 10.2 RANGING DATA ANALYSIS ALGORITHMS

The overall ranging data processing block diagram is given in figure 10-1. The signal strength records are separated from the ranging data records and are analyzed as described in section 7 to yield estimates of $C/N_o$ and S/I. All processes described in that section apply to the ranging data signal strength samples.

The major blocks of the ranging analysis algorithm are shown in figure 10-2. These blocks are described below.

### 10.2.1 Purge of Unreasonable Range Values

Before the range values are analyzed, the entire array of range values is examined to determine if the values are reasonable. Specifically, the second range value is initially assumed to be correct and any change from this range to the range at the next data time will be less than some specified threshold value. This test is repeated on the entire array with the differential in range being calculated for all adjacent ranging values. For acceptance

$$|r(t_{i+1}) - r(t_i)| \leq R_p, \tag{10-1}$$

where:

$r(t_i)$ = range at time $t_i$

$r(t_{i+1})$ = range at the next range reading output time

$R_p$ = differential range threshold that may not be exceeded ($R_p$ usually 10,000 meters).

The values of range that do not meet this criterion are purged from the ranging data array and the rejected data is printed out. When a range value is rejected, the last valid value of range is saved and used as $r(t_i)$ until a point is found that meets the above criterion.

### 10.2.2 Least-Squares Fit and Error Array

Values of time and relative range are read from the digital tape into an array in the computer. Following the initial purge of unreasonable values, a least-squares fit to the empirical data is made using a second-order curve:

$$r(t) = at^2 + bt + c. \tag{10-2}$$

The method of the least-squares fit is explained in appendix A.

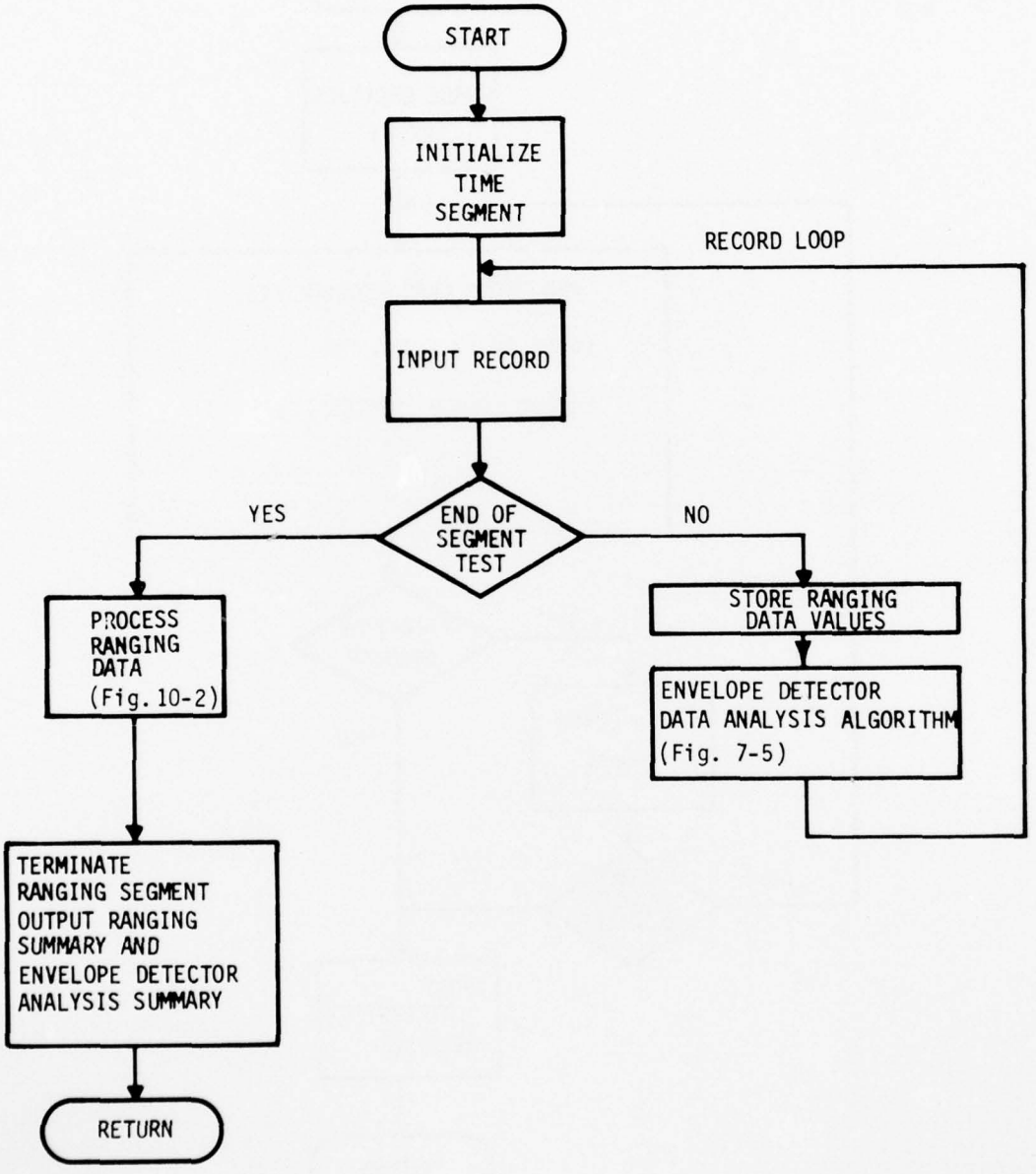


*Figure 10-1. Ranging Time Segment Processing Algorithm*

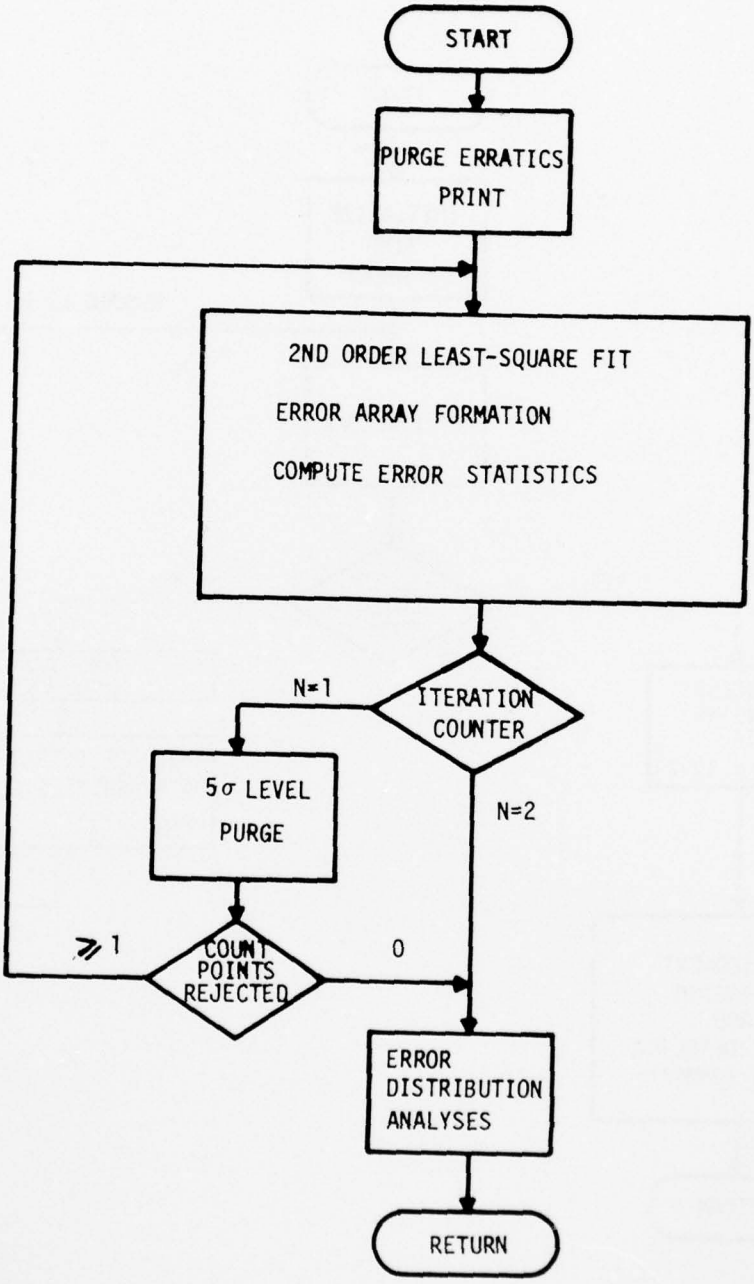


*Figure 10-2. Ranging Values Processing Algorithm*

When the least-squares-fit curve has been determined, an error array is formed using the least-squares curve as the assumed actual path. The array is formed using the following algorithm:

$$\Delta_R(t_i) = r_i(t_i) - r(t_i) , \tag{10-3}$$

where:

$r_i(t_i)$ = real-time-measured range at time $t_i$

$r(t_i)$ = assumed actual range at time $t_i$ as estimated by the least-squares-fit curve from equation (10-2).

10.2.3 Error Statistics

Error analysis is performed on the error array formed above. The mean and mean squared values of the error array are calculated as:

$$\overline{\Delta_R} = \frac{\sum_{i=1}^{n} \Delta_R(t_i)}{n} \tag{10-4}$$

$$\overline{\Delta_R^2} = \frac{\sum_{i=1}^{n} \Delta_R^2(t_i)}{n} , \tag{10-5}$$

where n is the number of range values in the array.

The variance and standard deviation are then calculated from

$$\sigma^2 = \overline{\Delta_R^2} - (\overline{\Delta_R})^2 . \tag{10-6}$$

A second purge is now performed on the data. Any points found outside the $5\sigma$ limits are deleted since they are assumed to be caused by equipment malfunction or incorrect ambiguity resolution and would corrupt the processed outputs. The purge is accomplished by eliminating the ranging values from the data corresponding to points outside the $5\sigma$ limits. Purged events are printed as part of the output. If this second purge operation occurs, the least-squares fit is repeated to form a new error array and new values are computed for mean, mean square, and variance.

### 10.2.4 Error Distribution Histogram

The error distribution histogram is formed as part of the analysis that leads to a chi-squared goodness-of-fit test. The lower limit for the frequency distribution is chosen to be $X_L = \bar{\Delta}_R - 2\sigma$ and the upper limit is $X_U = \bar{\Delta}_R + 2\sigma$. Typically, eight bins are used in computing the histogram. The midpoint of each bin is found by

$$X_L - \frac{\Delta X}{2}, X_L + \frac{\Delta X}{2}, \ldots, X_U - \frac{\Delta X}{2}, X_U + \frac{\Delta X}{2} ,$$

where:

$\Delta X = (X_U - X_L)/(K - 2)$

$K$ = number of intervals or bins.

In forming the actual error histogram, the two tail intervals contain all the points outside the upper and lower frequency distribution limits. The remaining error points are contained within their proper interval, between the upper and lower limits of the histogram as determined above.

### 10.2.5 Chi-Squared Goodness-of-Fit Test

A chi-squared goodness-of-fit test is made on the range error data. The mean and standard deviation of the observed error array are used as estimation parameters to determine a theoretical Gaussian distribution with the same total number of points as the observed sample of range error values. This theoretical distribution is used to construct an expected observations histogram having the same number of cells and bin size as the error histogram constructed. From these two histograms, the following test statistic is computed:

$$\chi^2 = \sum_{i=1}^{K} \frac{(0_i - E_i)^2}{E_i} , \qquad (10\text{-}7)$$

where:

$K$ = number of bins

$0_i$ = number of observed ranging errors in sample bin i

$E_i$ = theoretically expected number of errors within sample bin i.

AD-A041 864 BOEING COMMERCIAL AIRPLANE CO SEATTLE WASH F/G 9/5
AIR TRAFFIC CONTROL EXPERIMENTATION AND EVALUATION WITH THE NAS--ETC(U)
SEP 76 A D THOMPSON, S C WILSON, P F RIEDER DOT-TSC-707-4

UNCLASSIFIED D6-44049 FAA RD-75-173-4 NL

3 OF 3
ADA041864

END

DATE
FILMED
8 - 77

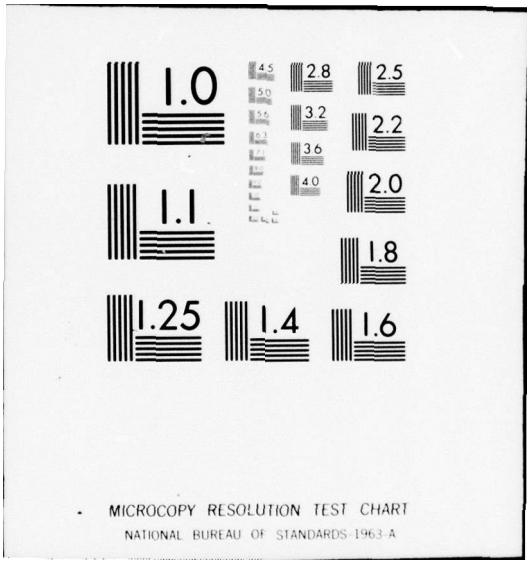
1.0
1.1
1.25
1.4
1.6
1.8
2.0
2.2
2.5
2.8
3.2
3.6
4.0
4.5
5.0
5.6
MICROCOPY RESOLUTION TEST CHART
NATIONAL BUREAU OF STANDARDS-1963-A

The $\chi^2$ test statistic is used in combination with the number of degrees of freedom to determine the probability that a sample of the same size, randomly chosen from a known normally distributed population of large size and having the same mean and standard deviation, will have a $\chi^2$ statistic greater than or equal to that of the observed sample.

The number of degrees of freedom is known to be equal to $K - k$, where $k = 1 +$ number of parameters estimated from the observed data. Since mean and standard deviation are both estimated, $k = 1 + 2 = 3$ and the degrees of freedom are found to be $K - 3$. The probability values are determined by a look-up table contained in a subroutine known as the chi-square distribution percentage point table.

## 10.3 INPUT SPECIFICATION AND OUTPUT FORMAT

The input to ranging program test segments consists of the entire specification of signal strength analysis related parameters (described in sec. 7.4). Further data specified for ranging segments relate to tape positioning and segment identification:

Date of test
Tape number
Tape file
Start time of segment
End time of segment
Test mode (Type I or II).

The output from the CDC 6600 consists of (1) signal strength summaries, plots, and time segment information discussed in section 7.4 and (2) range data information. The range data information outputs include the following:

a. Input data read from the digital ranging test tape, as shown in the example of table 10-2. The items listed are:

1) Point: Number n, identifying $n^{th}$ measurement of segment being analyzed

2) Status bit:
1 70 MHz PLL LOCKED +
2 70 MHz PLL LOCKED -
3 CLOCK PLL LOCKED
4 CORRECT CORRELATION
5 ---

## TABLE 10-2. PRINTOUT OF DIGITAL RANGING OBSERVATIONS

| | | | | | | | | | | |
|---|---|---|---|---|---|---|---|---|---|---|
| POINT | 145 | ST.BIT | 1 0 1 1 1 | TIME | 22/53/31.105 | RANGE | 2059357 | R.IN NSEC | 6864525 |
| POINT | 146 | ST.BIT | 1 0 1 1 1 | TIME | 22/53/31.315 | RANGE | 2059357 | R.IN NSEC | 6864525 |
| POINT | 147 | ST.BIT | 1 0 1 1 1 | TIME | 22/53/31.525 | RANGE | 2059237 | R.IN NSEC | 6864125 |
| POINT | 148 | ST.BIT | 1 0 1 1 1 | TIME | 22/53/31.735 | RANGE | 2059357 | R.IN NSEC | 6864525 |
| POINT | 149 | ST.BIT | 1 0 1 1 1 | TIME | 22/53/31.944 | RANGE | 2059357 | R.IN NSEC | 6864525 |
| POINT | 150 | ST.BIT | 1 0 1 1 1 | TIME | 22/53/32.154 | RANGE | 2059237 | R.IN NSEC | 6864125 |
| POINT | 151 | ST.BIT | 1 0 1 1 1 | TIME | 22/53/32.364 | RANGE | 2059237 | R.IN NSEC | 6864125 |
| POINT | 152 | ST.BIT | 1 0 1 1 1 | TIME | 22/53/32.573 | RANGE | 2059357 | R.IN NSEC | 6864525 |
| POINT | 153 | ST.BIT | 1 0 1 1 1 | TIME | 22/53/32.783 | RANGE | 2059357 | R.IN NSEC | 6864525 |
| POINT | 154 | ST.BIT | 1 0 1 1 1 | TIME | 22/53/32.993 | RANGE | 2059357 | R.IN NSEC | 6864525 |
| POINT | 155 | ST.BIT | 1 0 1 1 1 | TIME | 22/53/33.203 | RANGE | 2059357 | R.IN NSEC | 6864525 |
| POINT | 156 | ST.BIT | 1 0 1 1 1 | TIME | 22/53/33.412 | RANGE | 2059357 | R.IN NSEC | 6864525 |
| POINT | 157 | ST.BIT | 1 0 1 1 1 | TIME | 22/53/33.622 | RANGE | 2059357 | R.IN NSEC | 6864525 |
| POINT | 158 | ST.BIT | 1 0 1 1 1 | TIME | 22/53/33.832 | RANGE | 2059357 | R.IN NSEC | 6864525 |
| POINT | 159 | ST.BIT | 1 0 1 1 1 | TIME | 22/53/34.041 | RANGE | 2059357 | R.IN NSEC | 6864525 |
| POINT | 160 | ST.BIT | 1 0 1 1 1 | TIME | 22/53/34.251 | RANGE | 2059357 | R.IN NSEC | 6864525 |
| POINT | 161 | ST.BIT | 1 0 1 1 1 | TIME | 22/53/34.461 | RANGE | 2059357 | R.IN NSEC | 6864525 |
| POINT | 162 | ST.BIT | 1 0 1 1 1 | TIME | 22/53/34.671 | RANGE | 2059357 | R.IN NSEC | 6864525 |
| POINT | 163 | ST.BIT | 1 0 1 1 1 | TIME | 22/53/34.880 | RANGE | 2059357 | R.IN NSEC | 6864525 |
| POINT | 164 | ST.BIT | 1 0 1 1 1 | TIME | 22/53/35.090 | RANGE | 2059357 | R.IN NSEC | 6864525 |
| POINT | 165 | ST.BIT | 1 0 1 1 1 | TIME | 22/53/35.300 | RANGE | 2059357 | R.IN NSEC | 6864525 |
| POINT | 166 | ST.BIT | 1 0 1 1 1 | TIME | 22/53/35.510 | RANGE | 2059357 | R.IN NSEC | 6864525 |
| POINT | 167 | ST.BIT | 1 0 1 1 1 | TIME | 22/53/35.719 | RANGE | 2059477 | R.IN NSEC | 6864925 |
| POINT | 168 | ST.BIT | 1 0 1 1 1 | TIME | 22/53/35.929 | RANGE | 2059477 | R.IN NSEC | 6864925 |
| POINT | 169 | ST.BIT | 1 0 1 1 1 | TIME | 22/53/36.139 | RANGE | 2059477 | R.IN NSEC | 6864925 |
| POINT | 170 | ST.BIT | 1 0 1 1 1 | TIME | 22/53/36.348 | RANGE | 2059357 | R.IN NSEC | 6864525 |
| POINT | 171 | ST.BIT | 1 0 1 1 1 | TIME | 22/53/36.558 | RANGE | 2059477 | R.IN NSEC | 6864925 |
| POINT | 172 | ST.BIT | 1 0 1 1 1 | TIME | 22/53/36.768 | RANGE | 2059357 | R.IN NSEC | 6864525 |
| POINT | 173 | ST.BIT | 1 0 1 1 1 | TIME | 22/53/36.977 | RANGE | 2059477 | R.IN NSEC | 6864925 |
| POINT | 174 | ST.BIT | 1 0 1 1 1 | TIME | 22/53/37.187 | RANGE | 2059357 | R.IN NSEC | 6864525 |
| POINT | 175 | ST.BIT | 1 0 1 1 1 | TIME | 22/53/37.397 | RANGE | 2059357 | R.IN NSEC | 6864525 |
| POINT | 176 | ST.BIT | 1 0 1 1 1 | TIME | 22/53/37.607 | RANGE | 2059357 | R.IN NSEC | 6864525 |

3) Time: GMT at which range measurement was made.

4) Range: Range in meters

5) Range in nsec: Range in nanoseconds

b. Purged range errors, censored range error values, and range error array (output not shown).

c. The ranging segment summary, as shown in table 10-3. The mode type refers to Type I or II and the code status bits refer to table 10-1. Other items are self-explanatory.

## 10.4 PLACE RANGING DATA ANALYSIS

PLACE ranging tapes recorded and furnished by NASA for analysis are reformatted from nine- to seven-track digital tape compatible with the Boeing CDC 6600 computer. The slot and row data pertaining to the KC-135 are used to determine which records are to be analyzed. Time and range are read from the chosen records and put into storage in memory. At the end of the segment the range values that have been stored in memory are analyzed using the algorithms described.

The ranging data analysis outputs are essentially the same in format as those described in section 10.3 except that printouts specific to the TSC digital ranging modem and signal strength analysis are not included. An example output is given in table 10-4.

*TABLE 10-3. RANGING SEGMENT SUMMARY, TSC MODEM*

RANGING SEGMENT SUMMARY

| | | | |
|---|---|---|---|
| DATE | 3/25/75-R | | |
| START TIME | 11/17/10.00 | | |
| STOP TIME | 11/18/15.00 | | |
| MODE | 1 | | |
| 2ND ORDER FIT COEFFICIENTS | .0093 | -50.5763 | -1.1363 |
| NUMBER OF POINTS | 256 | | |
| NUMBER OF POINTS CENSORED | 1 | | |
| MEAN ERROR, METERS | -.0 | | |
| RMS ERROR, METERS | 71.3 | | |

ERROR DISTRIBUTION

| INTERVAL | MID POINT | NUMBER OF OBSER. | EXPECTED NB. OF OBS. |
|---|---|---|---|
| 1 | -156.935 | 7 | 5.8 |
| 2 | -128.402 | 10 | 8.2 |
| 3 | -99.868 | 12 | 15.4 |
| 4 | -71.334 | 24 | 24.7 |
| 5 | -42.801 | 30 | 33.8 |
| 6 | -14.267 | 36 | 39.6 |
| 7 | 14.267 | 49 | 39.6 |
| 8 | 42.801 | 33 | 33.8 |
| 9 | 71.334 | 24 | 24.7 |
| 10 | 99.868 | 21 | 15.4 |
| 11 | 128.402 | 4 | 8.2 |
| 12 | 156.935 | 5 | 5.8 |

PROBABILITY THAT CHI-SQUARED VARIATE IS GREATER THAN TEST STATISTIC .646

CODE/STATUS BITS 0 0 0 0 0 1 0 0

*TABLE 10-4. RANGING SEGMENT SUMMARY, PLACE MODEM*

R A N G I N G  S E G M E N T  S U M M A R Y

| | |
|---|---|
| DATE | 3/ 27/ 75 DOC-5 TYPE 2 |
| START TIME | 12/20/20.00 |
| STOP TIME | 12/33/ .00 |
| MODE | 3 |

| | | | |
|---|---|---|---|
| 2ND ORDER FIT COEFFICIENTS | -.0017 | 47.7378 | -416.6024 |
| NUMBER OF POINTS | 121 | | |
| NUMBER OF POINTS CENSORED | 0 | | |
| MEAN ERROR, METERS | .0 | | |
| RMS ERROR, METERS | 334.4 | | |

ERROR DISTRIBUTION

| INTERVAL | MID POINT | NUMBER OF OBSER. | EXPECTED NO. OF OBS. |
|---|---|---|---|
| 1 | -1504.596 | 0 | .2 |
| 2 | -501.063 | 69 | 59.8 |
| 3 | 501.663 | 51 | 59.8 |
| 4 | 1504.996 | 0 | .2 |

PROBABILITY THAT CHI-SQUARED VARIATE IS GREATER THAN TEST STATISTIC .387

| | | | | | | | |
|---|---|---|---|---|---|---|---|
| POINT | 1 | ID | 22 | 444TIME | 12 2 20.120 | RANGE | 154621874 |
| POINT | 2 | ID | 22 | 444TIME | 12 20 26.519 | RANGE | 154622455 |
| POINT | 3 | ID | 22 | 444TIME | 12 2 32.920 | RANGE | 154622396 |
| POINT | 4 | ID | 22 | 444TIME | 12 2 39.320 | RANGE | 154622694 |
| POINT | 5 | ID | 22 | 444TIME | 12 20 45.720 | RANGE | 154622679 |
| POINT | 6 | ID | 22 | 444TIME | 12 20 52.120 | RANGE | 154869222 |
| POINT | 7 | ID | 22 | 444TIME | 12 20 58.519 | RANGE | 154623326 |
| POINT | 8 | ID | 22 | 444TIME | 12 21 4.920 | RANGE | 154623243 |
| POINT | 9 | ID | 22 | 444TIME | 12 21 11.319 | RANGE | 154623223 |
| POINT | 10 | ID | 22 | 444TIME | 12 21 17.719 | RANGE | 154623953 |
| POINT | 11 | ID | 22 | 444TIME | 12 21 24.119 | RANGE | 154624049 |
| POINT | 12 | ID | 22 | 444TIME | 12 21 30.519 | RANGE | 154624534 |
| POINT | 13 | ID | 22 | 444TIME | 12 21 36.919 | RANGE | 154624459 |
| POINT | 14 | ID | 22 | 444TIME | 12 21 43.321 | RANGE | 154625195 |
| POINT | 15 | ID | 22 | 444TIME | 12 21 49.719 | RANGE | 154624656 |

# 11. ANTENNA TEST DRandA PROCESSING

The antenna test data is processed in the same manner as the voice data with one minor deviation: it is identified as antenna data in the identification word as shown in figure 6-3. The signal strength records described below are examined for the 1 or 0 antenna bit to determine to which antenna the signal strength record applies. The algorithm flow is essentially the same as for the voice case (fig. 8-1). The signal strength data is processed to obtain $C/N_o$ and S/I using the algorithm described in section 7.

## 11.1 DIGITAL TAPE FORMAT

The digital tape format for antenna tests was shown in figure 6-3. Each signal strength record consists of four time words (hours, minutes, seconds, and milliseconds), one identification word, and 1025 signal strength sample words. The most significant bit of each signal strength sample word is either 1 or 0 depending on the receiver to which the carrier detector unit is connected. The number and spacing of signal strength samples are under the control of the receiver multiplex signal, which also determines whether the signal strength bit is 1 or 0.

## 11.2 INPUT SPECIFICATION AND OUTPUT FORMAT

The input to antenna program test segments includes the entire specification of signal strength analysis related parameters as required (described in sec. 7.4). Further data specified for antenna test segments relate to tape position and segment identification:

Date of test
Tape number
Tape file
Start time of segment
End time of segment.

The output from an antenna analysis segment is as described in section 7.4, consisting entirely of data resulting from envelope detector data analysis. The antenna bit is printed on the envelope detector analysis output to indicate to which antenna the data is applicable.

## REFERENCES


4-1. P. A. Bello and R. Esposito, "Measurement Techniques for Time-Varying Dispersive Channels," Alta Frequenza, no. 11, vol. XXXIX, 1970, p. 980-310E to 996-326E.

4-2. C. Cox and W. Munk, "Slopes of the Sea Surface Deduced from Photographs of Sun Glitter," University of California Press, Berkeley and Los Angeles, 1956, p. 431.

5-1. W. H. Peake, "Satellite to Aircraft Multipath Signals Over the Ocean," final report 3266-2, Ohio State University Electro-Science Laboratory, May 1974.

7-1. S. O. Rice, "Mathematical Analysis of Random Noise," Bell System Technical Journal, vol. 23, 1944, and vol. 24, 1945.

7-2. D. Middleton, AN INTRODUCTION TO STATISTICAL COMMUNICATION THEORY, McGraw-Hill, New York, 1960, p. 161-195.

7-3. W. B. Davenport and W. L. Root, INTRODUCTION TO SIGNALS AND NOISE, McGraw-Hill, New York, 1958, p. 288-300.

## APPENDIX A

## LEAST-SQUARES-FIT ALGORITHM

The least-squares-fit method is used several times in the processing of the modem evaluation data. Although this method is well known and documented, some explanation is necessary to describe the software used in one of the ATS-6 processing cases (signal strength processing). Solving a least-squares fit consists mainly in finding the minimum of a function of one or more variables. In the case of signal strength, a method was found that is an efficient tradeoff, insofar as implementation is concerned, between a numerical and an analytical approach. The least-squares method used in modem evaluation programs is presented in general terms first, then each particular case is explained.

### A.1 GENERAL CASE

Suppose n measurements $(X_i, Y_i)$ are given. The least-squares fit is a method for finding m unknown parameter values of an analytical model $Y = F(X,a_1,a_2,\ldots,a_m)$, that give the best fit to these points in the squared-error sense. The fit is considered best when an "error" E, function of $a_j$ parameters and input points $X_i, Y_i$ is minimum. E is defined as:

$$E(a_1,a_2,\ldots,a_m) = \sum_{i=1}^{n} \left(F(X_i,a_1,a_2,\ldots,a_m) - Y_i\right)^2 . \qquad \text{(A-1)}$$

In the general case the partial derivative of E with respect to $a_1,a_2,\ldots,a_m$ is taken and set equal to zero. The resulting m equations are then solved simultaneously for $a_1,a_2,\ldots,a_m$.

Specific cases of least-squares fit used in the analysis of ATS-6 data are discussed individually in the following sections.

### A.2 FITTING WITH A LINEAR FUNCTION FOR LINEAR DRIFT REMOVAL

The function $F(X,a_j)$ chosen is:

$$F = a_1 + a_2X .$$

Substitution in equation (A-1) gives:

$$E = \sum_{i=1}^{n} (a_1 + a_2 X_i - Y_i)^2.$$

The minimum E is given for $\frac{\partial E}{\partial a_1} = \frac{\partial E}{\partial a_2} = 0$; that is,

$$\frac{1}{2}\frac{\partial E}{\partial a_1} = \sum_{i=1}^{n} (a_1 + a_2 X_i - Y_i) = 0$$

$$\frac{1}{2}\frac{\partial E}{\partial a_2} = \sum_{i=1}^{n} X_i(a_1 + a_2 X_i - Y_i) = 0$$

or

$$a_1 \sum_{1}^{n} 1 + a_2 \sum_{i=1}^{n} X_i - \sum_{i=1}^{n} Y_i = 0$$

$$a_1 \sum_{1}^{n} X_i + a_2 \sum_{i=1}^{n} X_i^2 - \sum_{i=1}^{n} X_i Y_i = 0.$$

This is a linear system with two equations and two unknowns.

## A.3 FITTING WITH A SECOND-DEGREE POLYNOMIAL FOR RANGING DATA

For a second-degree polynomial, the function used is:

$$F(X,a_j) = a_1 + a_2 X + a_3 X^2.$$

The same previously described steps yield linear equations with three unknowns, which are solved for $a_1, a_2, a_3$.

$$a_1 \sum_{i=1}^{n} 1 + a_2 \sum_{i=1}^{n} X_i + a_3 \sum_{i=1}^{n} X_i^2 - \sum_{i=1}^{n} Y_i = 0$$

$$a_1 \sum_{i=1}^{n} X_i + a_2 \sum_{i=1}^{n} X_i^2 + a_3 \sum_{i=1}^{n} X_i^3 - \sum_{i=1}^{n} X_i Y_i = 0$$

$$a_1 \sum_{i=1}^{n} X_i^2 + a_2 \sum_{i=1}^{n} X_i^3 + a_3 \sum_{i=1}^{n} X_i^4 - \sum_{i=1}^{n} X_i^2 Y_i = 0.$$

## A.4 SPECTRUM MODEL

The spectrum model used is not linear relative to the $a_j$ parameters, a fact that complicates the derivative expression. Short of an analytical solution, we use a iterative numerical solution. Convergence by iteration involves computing the function with an initial set of values for $a_j$ and varying the parameters in search of the minimum $E(a_1, a_2, \ldots, a_n)$. The function derivatives $\partial E/\partial a_j$ provide useful information to increment the parameters. Note that most of the operations needed to compute E are common to the computation of each $\partial E/\partial a_j$. The function evaluation, derivative computation, and the convergence algorithm are the main parts of the least-squares fit in this case.

### A.4.1 Function and Derivative Computation

The function used is:

$$F(X, a_j) = a_1 e^{-X^2/a_2^2} + \frac{a_3}{X^4 + 800^4},$$

where:

- $X$ = frequency variable
- $a$ = proportional to multipath power density
- $a_2$ = one-sided multipath bandwidth
- $a_3$ = proportional to the noise power density.

This may be rewritten as

$$F(X,a_j) = a_1 F_1(a_2,X) + a_3 F_2(X).$$

By substitution in equation (A-1):

$$E = \sum_{i=1}^{n} \left(a_1 F_1(a_2,X_i) + a_3 F_2(X_i) - Y_i\right)^2. \qquad \text{(A-2)}$$

The following notation is used for simplification:

$$F_{1i} \text{ for } F_1(a_2,X_i), \quad F_{2i} \text{ for } F_2(X_i),$$

$$FP_i \text{ for } \frac{\partial F_1(a_2,X_i)}{\partial a_2}.$$

The derivatives of E are:

$$\frac{1}{2}\frac{\partial E}{\partial a_1} = \sum_{i=1}^{n} F_{1i}(a_1 F_{1i} + a_3 F_{2i} - Y_i)$$

$$\frac{1}{2}\frac{\partial E}{\partial a_2} = \sum_{i=1}^{n} a_1 FP_i(a_1 F_1 i + a_3 F_{2i} - Y_i)$$

$$\frac{1}{2}\frac{\partial E}{\partial a_3} = \sum_{i=1}^{n} F_{2i}(a_1 F_{1i} + a_3 F_{2i} - Y_i).$$

The previous equations can be rewritten:

$$\frac{1}{2}\frac{\partial E}{\partial a_1} = a_1 \sum_{i=1}^{n} F_{1i}^2 + a_3 \sum_{i=1}^{n} F_{2i} F_{1i} - \sum_{i=1}^{n} Y_i F_{1i}$$

$$\frac{1}{2}\frac{\partial E}{\partial a_2} = a_1^2 \sum_{i=1}^{n} FP_i F_{1i} + a_3 a_1 \sum_{i=1}^{n} F_{2i} FP_i - a_1 \sum_{i=1}^{n} Y_i FP_i$$

$$\frac{1}{2}\frac{\partial E}{\partial a_3} = a_1 \sum_{i=1}^{n} F_{2i} F_{1i} + a_3 \sum_{i=1}^{n} F_{2i}^2 - \sum_{i=1}^{n} Y_i F_{2i} .$$

In this relation $F_{1i}$, $F_{2i}$, $FP_i$ are an array of values. $F_{2i}$ is independent of the $a_j$ parameters. This array is computed only once. $F_{1i}$ and $FP_i$ are functions of $a_2$ and should be recomputed at each iteration. The array $FP_i$ is computed from $F_{1i}$ values:

$$FP_i = \frac{\partial F_1(a_2, X_i)}{\partial a_2}$$

$$= \frac{2 X_i^2 F_1(a_2, X_i)}{a_2^3} .$$

A.4.2 Convergence

The convergence algorithm used to find the minimum of the function E is given in figure A-1. The algorithm computes the function and its derivatives with a given set of parameter values. The parameters are then increased or decreased depending on the sign of the corresponding derivative. The increment step is initially defined to be 20% of the parameter value. The following rule is used to vary the step size: if in two consecutive steps the corresponding derivative does not change sign, the step size is doubled (up to a maximum of 20% of the parameter value); if the derivative does change sign, the step size is halved. Convergence is stopped after a given number of iterations.

In the algorithm of figure A-1, the previous step parameters are denoted $A_j$, the corresponding function and derivatives are denoted EA and $\partial EA/\partial A_j$, and B is used for next iteration value. $A_j$ is the increment size.

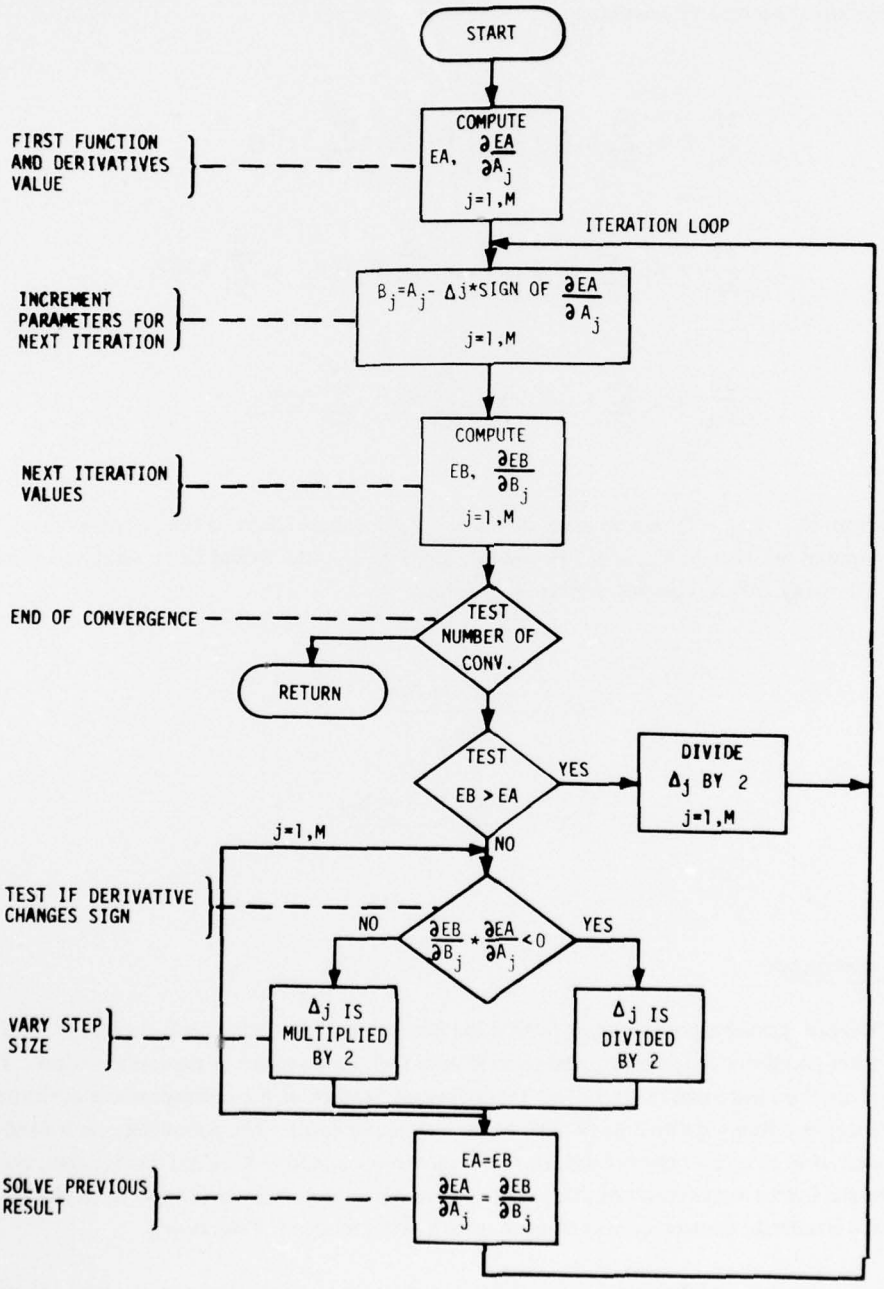


*Figure A-1. Convergence Algorithm*

## APPENDIX B

## SEA-STATE DATA REDUCTION

### B.1 MEASURED PARAMETERS

The sea-state measurements available from the buoy can be listed as follows:

Compass bearing
Roll angle
Pitch angle
Acceleration along three axes
Wave staff height measurements.

These variables are discussed below in terms of their code and calibration properties.

#### B.1.1 Magnetic Compass Bearing

The compass bearing is obtained as a parallel digital output. The code is a seven-bit Gray code shown in table B-1, with one division equivalent to approximately $3^{o}$ (i.e., 360/128). The time constant of the compass is roughly 3 sec. The reference line on the buoy is in the pitch plane, as shown in figure B-1. Clockwise rotation results in an increasing angle.

#### B.1.2 Roll Angle

Roll angle is available as a 12-bit output from a synchro/digital converter. The roll angle is offset so that in a calm sea the digital output is 2048, i.e., an offset binary code with one least significant bit corresponding to

$$\Delta = 360 \times 2^{-12} \text{ degrees}$$
$$= 5.4 \text{ minutes.}$$

Depression of the buoy port side (relative to the reference line) results in an increasing roll angle indication.

The roll (and pitch) angles are derived from displacement gyros that are gimballed to indicate angular displacement from horizontal or, more precisely, angular displacement from the long-term (5-min) average. Figure B-1 indicates the orientation of pitch and roll angles.

*TABLE B-1. GRAY CODE*

| Weights 64 | 32 | 16 | 8 | 4 | 2 | 1 | Order | Weighted Decimal | Degrees |
|---|---|---|---|---|---|---|---|---|---|
| Code | | | | | | | | | |
| 0 | 0 | 0 | 0 | 0 | 0 | 0 | 0 | 0 | 000 |
| 0 | 0 | 0 | 0 | 0 | 0 | 1 | 1 | 1 | 003 |
| 0 | 0 | 0 | 0 | 0 | 1 | 1 | 2 | 3 | 006 |
| 0 | 0 | 0 | 0 | 0 | 1 | 0 | 3 | 2 | 008 |
| 0 | 0 | 0 | 0 | 1 | 1 | 0 | 4 | 6 | 011 |
| 0 | 0 | 0 | 0 | 1 | 1 | 1 | 5 | 7 | 014 |
| 0 | 0 | 0 | 0 | 1 | 0 | 1 | 6 | 5 | 017 |
| 0 | 0 | 0 | 0 | 1 | 0 | 0 | 7 | 4 | 020 |
| 0 | 0 | 0 | 1 | 1 | 0 | 0 | 8 | 12 | 022 |
| 0 | 0 | 0 | 1 | 1 | 0 | 1 | 9 | 13 | 025 |
| 0 | 0 | 0 | 1 | 1 | 1 | 1 | 10 | 15 | 028 |
| 0 | 0 | 0 | 1 | 1 | 1 | 0 | 11 | 14 | 031 |
| 0 | 0 | 0 | 1 | 0 | 1 | 0 | 12 | 10 | 034 |
| 0 | 0 | 0 | 1 | 0 | 1 | 1 | 13 | 11 | 037 |
| 0 | 0 | 0 | 1 | 0 | 0 | 1 | 14 | 9 | 039 |
| 0 | 0 | 0 | 1 | 0 | 0 | 0 | 15 | 8 | 042 |
| 0 | 0 | 1 | 1 | 0 | 0 | 0 | 16 | 24 | 045 |
| 0 | 0 | 1 | 1 | 0 | 0 | 1 | 17 | 25 | 048 |
| 0 | 0 | 1 | 1 | 0 | 1 | 1 | 18 | 27 | 051 |
| 0 | 0 | 1 | 1 | 0 | 1 | 0 | 19 | 26 | 053 |
| 0 | 0 | 1 | 1 | 1 | 1 | 0 | 20 | 30 | 056 |
| 0 | 0 | 1 | 1 | 1 | 1 | 1 | 21 | 31 | 059 |
| 0 | 0 | 1 | 1 | 1 | 0 | 1 | 22 | 29 | 062 |
| 0 | 0 | 1 | 1 | 1 | 0 | 0 | 23 | 28 | 065 |
| 0 | 0 | 1 | 0 | 1 | 0 | 0 | 24 | 20 | 068 |
| 0 | 0 | 1 | 0 | 1 | 0 | 1 | 25 | 21 | 070 |
| 0 | 0 | 1 | 0 | 1 | 1 | 1 | 26 | 23 | 073 |
| 0 | 0 | 1 | 0 | 1 | 1 | 0 | 27 | 22 | 076 |
| 0 | 0 | 1 | 0 | 0 | 1 | 0 | 28 | 18 | 079 |
| 0 | 0 | 1 | 0 | 0 | 1 | 1 | 29 | 19 | 082 |
| 0 | 0 | 1 | 0 | 0 | 0 | 1 | 30 | 17 | 084 |
| 0 | 0 | 1 | 0 | 0 | 0 | 0 | 31 | 16 | 087 |
| 0 | 1 | 1 | 0 | 0 | 0 | 0 | 32 | 48 | 090 |
| 0 | 1 | 1 | 0 | 0 | 0 | 1 | 33 | 49 | 093 |
| 0 | 1 | 1 | 0 | 0 | 1 | 1 | 34 | 51 | 096 |

*TABLE B-1(Continued)*

| Weights 64 | 32 | 16 | 8 | 4 | 2 | 1 | Order | Weighted Decimal | Degrees |
|---|---|---|---|---|---|---|---|---|---|
| Code | | | | | | | | | |
| 0 | 1 | 1 | 0 | 0 | 1 | 0 | 35 | 50 | 098 |
| 0 | 1 | 1 | 0 | 1 | 1 | 0 | 36 | 54 | 101 |
| 0 | 1 | 1 | 0 | 1 | 1 | 1 | 37 | 55 | 104 |
| 0 | 1 | 1 | 0 | 1 | 0 | 1 | 38 | 53 | 107 |
| 0 | 1 | 1 | 0 | 1 | 0 | 0 | 39 | 52 | 110 |
| 0 | 1 | 1 | 1 | 1 | 0 | 0 | 40 | 60 | 112 |
| 0 | 1 | 1 | 1 | 1 | 0 | 1 | 41 | 61 | 115 |
| 0 | 1 | 1 | 1 | 1 | 1 | 1 | 42 | 63 | 118 |
| 0 | 1 | 1 | 1 | 1 | 1 | 0 | 43 | 62 | 121 |
| 0 | 1 | 1 | 1 | 0 | 1 | 0 | 44 | 58 | 124 |
| 0 | 1 | 1 | 1 | 0 | 1 | 1 | 45 | 59 | 127 |
| 0 | 1 | 1 | 1 | 0 | 0 | 1 | 46 | 57 | 129 |
| 0 | 1 | 1 | 1 | 0 | 0 | 0 | 47 | 56 | 132 |
| 0 | 1 | 0 | 1 | 0 | 0 | 0 | 48 | 40 | 135 |
| 0 | 1 | 0 | 1 | 0 | 0 | 1 | 49 | 41 | 138 |
| 0 | 1 | 0 | 1 | 0 | 1 | 1 | 50 | 43 | 141 |
| 0 | 1 | 0 | 1 | 0 | 1 | 0 | 51 | 42 | 143 |
| 0 | 1 | 0 | 1 | 1 | 1 | 0 | 52 | 46 | 146 |
| 0 | 1 | 0 | 1 | 1 | 1 | 1 | 53 | 47 | 149 |
| 0 | 1 | 0 | 1 | 1 | 0 | 1 | 54 | 45 | 152 |
| 0 | 1 | 0 | 1 | 1 | 0 | 0 | 55 | 44 | 155 |
| 0 | 1 | 0 | 0 | 1 | 0 | 0 | 56 | 36 | 158 |
| 0 | 1 | 0 | 0 | 1 | 0 | 1 | 57 | 37 | 160 |
| 0 | 1 | 0 | 0 | 1 | 1 | 1 | 58 | 39 | 163 |
| 0 | 1 | 0 | 0 | 1 | 1 | 0 | 59 | 38 | 166 |
| 0 | 1 | 0 | 0 | 0 | 1 | 0 | 60 | 34 | 169 |
| 0 | 1 | 0 | 0 | 0 | 1 | 1 | 61 | 35 | 172 |
| 0 | 1 | 0 | 0 | 0 | 0 | 1 | 62 | 33 | 174 |
| 0 | 1 | 0 | 0 | 0 | 0 | 0 | 63 | 32 | 177 |
| 1 | 1 | 0 | 0 | 0 | 0 | 0 | 64 | 96 | 180 |
| 1 | 1 | 0 | 0 | 0 | 0 | 1 | 65 | 97 | 183 |
| 1 | 1 | 0 | 0 | 0 | 1 | 1 | 66 | 99 | 186 |
| 1 | 1 | 0 | 0 | 0 | 1 | 0 | 67 | 98 | 188 |
| 1 | 1 | 0 | 0 | 1 | 1 | 0 | 68 | 102 | 191 |
| 1 | 1 | 0 | 0 | 1 | 1 | 1 | 69 | 103 | 194 |

*TABLE B-1 (Continued)*

| Weights 64 | 32 | 16 | 8 | 4 | 2 | 1 | Order | Weighted Decimal | Degrees |
|---|---|---|---|---|---|---|---|---|---|
| Code | | | | | | | | | |
| 1 | 1 | 0 | 0 | 1 | 0 | 1 | 70 | 101 | 197 |
| 1 | 1 | 0 | 0 | 1 | 0 | 0 | 71 | 100 | 200 |
| 1 | 1 | 0 | 1 | 1 | 0 | 0 | 72 | 108 | 202 |
| 1 | 1 | 0 | 1 | 1 | 0 | 1 | 73 | 109 | 205 |
| 1 | 1 | 0 | 1 | 1 | 1 | 1 | 74 | 111 | 208 |
| 1 | 1 | 0 | 1 | 1 | 1 | 0 | 75 | 110 | 211 |
| 1 | 1 | 0 | 1 | 0 | 1 | 0 | 76 | 106 | 214 |
| 1 | 1 | 0 | 1 | 0 | 1 | 1 | 77 | 107 | 217 |
| 1 | 1 | 0 | 1 | 0 | 0 | 1 | 78 | 105 | 219 |
| 1 | 1 | 0 | 1 | 0 | 0 | 0 | 79 | 104 | 222 |
| 1 | 1 | 1 | 1 | 0 | 0 | 0 | 80 | 120 | 225 |
| 1 | 1 | 1 | 1 | 0 | 0 | 1 | 81 | 121 | 228 |
| 1 | 1 | 1 | 1 | 0 | 1 | 1 | 82 | 123 | 231 |
| 1 | 1 | 1 | 1 | 0 | 1 | 0 | 83 | 122 | 233 |
| 1 | 1 | 1 | 1 | 1 | 1 | 0 | 84 | 126 | 236 |
| 1 | 1 | 1 | 1 | 1 | 1 | 1 | 85 | 127 | 239 |
| 1 | 1 | 1 | 1 | 1 | 0 | 1 | 86 | 125 | 242 |
| 1 | 1 | 1 | 1 | 1 | 0 | 0 | 87 | 124 | 245 |
| 1 | 1 | 1 | 0 | 1 | 0 | 0 | 88 | 116 | 247 |
| 1 | 1 | 1 | 0 | 1 | 0 | 1 | 89 | 117 | 250 |
| 1 | 1 | 1 | 0 | 1 | 1 | 1 | 90 | 119 | 253 |
| 1 | 1 | 1 | 0 | 1 | 1 | 0 | 91 | 118 | 256 |
| 1 | 1 | 1 | 0 | 0 | 1 | 0 | 92 | 114 | 259 |
| 1 | 1 | 1 | 0 | 0 | 1 | 1 | 93 | 115 | 262 |
| 1 | 1 | 1 | 0 | 0 | 0 | 1 | 94 | 113 | 264 |
| 1 | 1 | 1 | 0 | 0 | 0 | 0 | 95 | 112 | 267 |
| 1 | 0 | 1 | 0 | 0 | 0 | 0 | 96 | 80 | 270 |
| 1 | 0 | 1 | 0 | 0 | 0 | 1 | 97 | 81 | 273 |
| 1 | 0 | 1 | 0 | 0 | 1 | 1 | 98 | 83 | 276 |
| 1 | 0 | 1 | 0 | 0 | 1 | 0 | 99 | 82 | 278 |
| 1 | 0 | 1 | 0 | 1 | 1 | 0 | 100 | 86 | 281 |
| 1 | 0 | 1 | 0 | 1 | 1 | 1 | 101 | 87 | 284 |
| 1 | 0 | 1 | 0 | 1 | 0 | 1 | 102 | 85 | 287 |
| 1 | 0 | 1 | 0 | 1 | 0 | 0 | 103 | 84 | 290 |
| 1 | 0 | 1 | 1 | 1 | 0 | 0 | 104 | 92 | 292 |

*TABLE B-1(Concluded)*

| Weights 64 | 32 | 16 | 8 | 4 | 2 | 1 (Code) | Order | Weighted Decimal | Degrees |
|---|---|---|---|---|---|---|---|---|---|
| 1 | 0 | 1 | 1 | 1 | 0 | 1 | 105 | 93 | 295 |
| 1 | 0 | 1 | 1 | 1 | 1 | 1 | 106 | 95 | 293 |
| 1 | 0 | 1 | 1 | 1 | 1 | 0 | 107 | 94 | 301 |
| 1 | 0 | 1 | 1 | 0 | 1 | 0 | 108 | 90 | 304 |
| 1 | 0 | 1 | 1 | 0 | 1 | 1 | 109 | 91 | 306 |
| 1 | 0 | 1 | 1 | 0 | 0 | 1 | 110 | 89 | 309 |
| 1 | 0 | 1 | 1 | 0 | 0 | 0 | 111 | 88 | 312 |
| 1 | 0 | 0 | 1 | 0 | 0 | 0 | 112 | 72 | 315 |
| 1 | 0 | 0 | 1 | 0 | 0 | 1 | 113 | 73 | 316 |
| 1 | 0 | 0 | 1 | 0 | 1 | 1 | 114 | 75 | 321 |
| 1 | 0 | 0 | 1 | 0 | 1 | 0 | 115 | 74 | 323 |
| 1 | 0 | 0 | 1 | 1 | 1 | 0 | 116 | 78 | 326 |
| 1 | 0 | 0 | 1 | 1 | 1 | 1 | 117 | 79 | 329 |
| 1 | 0 | 0 | 1 | 1 | 0 | 1 | 118 | 77 | 332 |
| 1 | 0 | 0 | 1 | 1 | 0 | 0 | 119 | 76 | 335 |
| 1 | 0 | 0 | 0 | 1 | 0 | 0 | 120 | 68 | 338 |
| 1 | 0 | 0 | 0 | 1 | 0 | 1 | 121 | 69 | 340 |
| 1 | 0 | 0 | 0 | 1 | 1 | 1 | 122 | 71 | 343 |
| 1 | 0 | 0 | 0 | 1 | 1 | 0 | 123 | 70 | 346 |
| 1 | 0 | 0 | 0 | 0 | 1 | 0 | 124 | 66 | 349 |
| 1 | 0 | 0 | 0 | 0 | 1 | 1 | 125 | 67 | 352 |
| 1 | 0 | 0 | 0 | 0 | 0 | 1 | 126 | 65 | 354 |
| 1 | 0 | 0 | 0 | 0 | 0 | 0 | 127 | 64 | 357 |

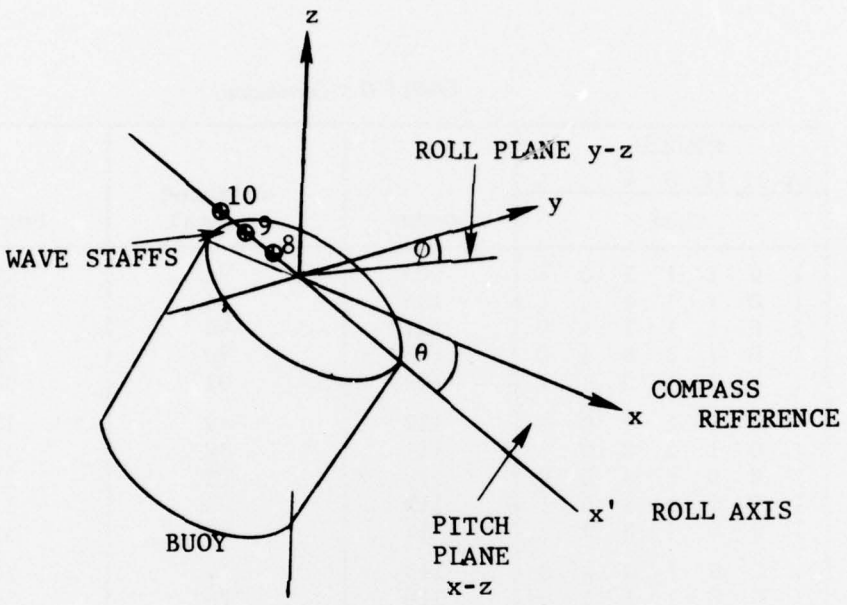


*Figure B-1. Buoy Roll and Pitch Coordinate System*

B.1.3 Pitch Angle

This measurement is similar to that for roll angle. The angular deviation from horizontal is output as an offset binary number (12 bits). The resolution is 5.4 min. As shown in figure B-1, pitch and roll are defined relative to horizontal, so that depression of the pitch line causes a positive increase in pitch angle.

Note that x' satisfies the usual definition of roll axis, i.e., the axis about which rotation takes place. Similarly, y satisfies the usual definition of pitch axis, with x-z referred to as the pitch plane.

B.1.4 Three-Axis Acceleration

Strap-down accelerometers provide the three components of acceleration of the buoy. The output in each case is a 12-bit word, offset so that zero acceleration indicates 2048. The sensitivity of each accelerometer can be summarized in the following way:

Vertical acceleration (z) $\pm 0.3g$

$$\text{Resolution} = \frac{0.6g}{4096} .$$

Horizontal acceleration (x and y) $\pm 0.5$ g

$$\text{Resolution} = \frac{g}{4096} .$$

It is assumed that the x- and y-axes lie in the pitch and roll planes, respectively.

B.1.5 Wave Staffs

Wave height relative to the buoy is sensed by means of a 10-element array. The array elements are numbered and spaced as shown in figure B-2, with the reference axis (numbers 1, 3, 2) lying in the pitch plane of the buoy, i.e., orthogonal to the y-axis shown.

All the variables are sampled at a 25-Hz sampling rate and, with the exception of the compass, all sensors are capable of 25-Hz response.

The wave staffs are variable-resistance devices, with resistance decreasing as a function of immersion depth. Ideally, the resistance value should be sensed electrically by driving the wave staff with a constant-current source (ac) and measuring voltage. However, a simpler approach is to employ a constant-voltage source with series resistance (see fig. B-3). When the series resistance $R_o$ is considerably larger than the maximum wave staff resistance, the net effect is equivalent to a constant-current generator. For smaller values of $R_o$, the wave staff voltage can be expressed as

$$V_s = \left(\frac{R_s}{R_s + R_o}\right)V ,$$

where:

$V_s$ = measured staff voltage
$R_s$ = wave staff resistance
$R_o$ = series resistance
$V$ = voltage source.

In processing the sea-state data, a relationship between the measured voltage and wave height is needed. Thus,

$$\frac{R_s}{R_o} = \frac{V_s}{V - V_s} .$$

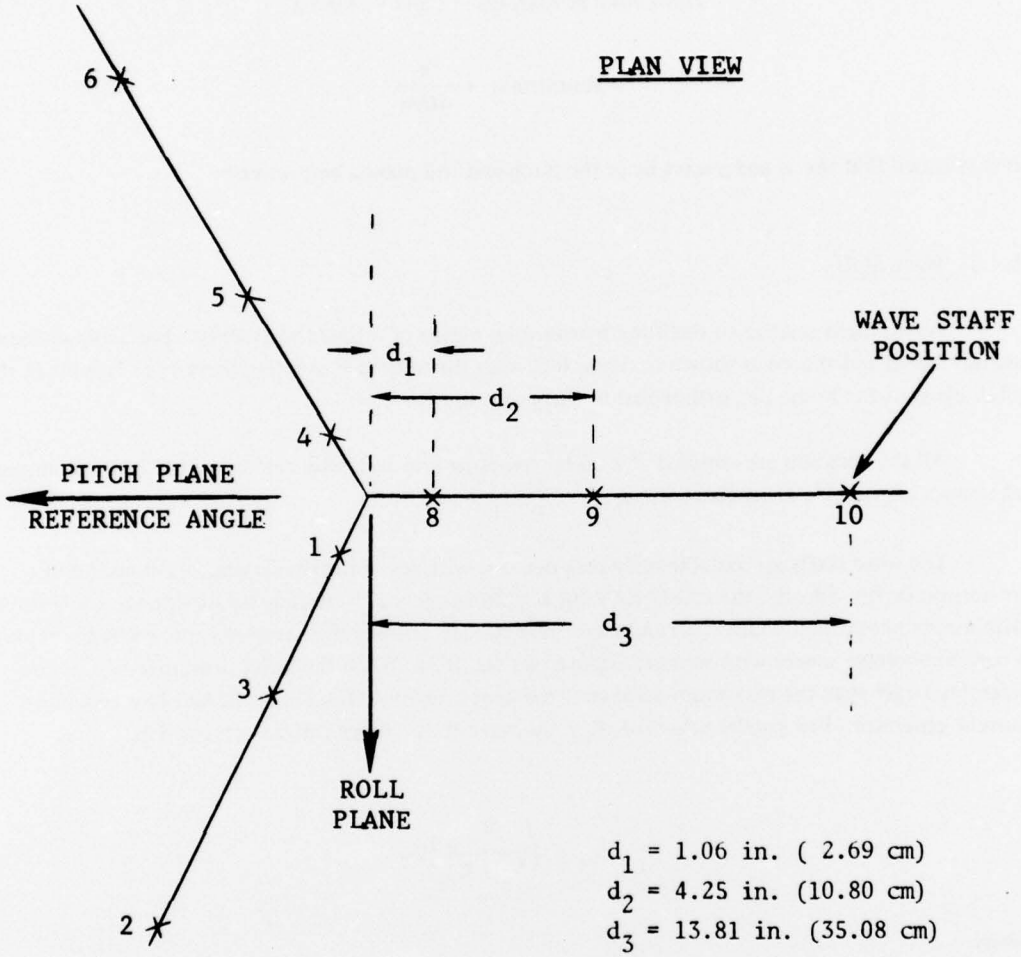


$d_1$ = 1.06 in. ( 2.69 cm)
$d_2$ = 4.25 in. (10.80 cm)
$d_3$ = 13.81 in. (35.08 cm)

$d_2 \approx 4\ d_1$
$d_3 \approx 13\ d_1$

Wave Staff Diameter = 0.128 in.

*Figure B-2. Wave Staff Geometry*

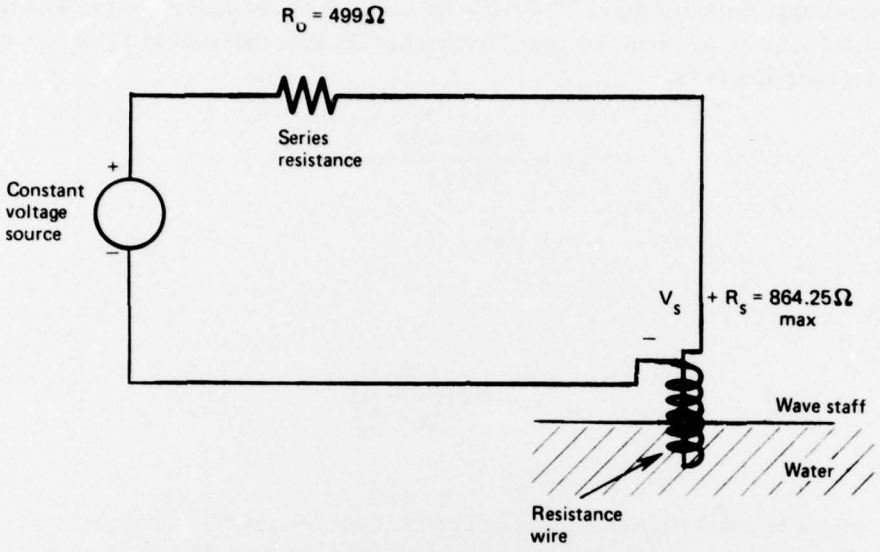


*Figure B-3. Wave Staff Circuitry*

Assuming a linear relationship between height h and resistance ratio $R_s/R_o$,

$$h = a \frac{R_s}{R_o},$$

we find that

$$h = \frac{a V_s}{V - V_s}.$$

The resistive values of interest are known to be:

$$R_o = 499\Omega \pm \frac{1}{2}\Omega$$

$$R_{s_{max}} = 864.25\Omega .$$

This maximum value occurs with the wave staff out of the water. With the staff partially immersed, it is assumed that that portion of the winding below the surface is totally short-circuited. With full immersion, the value of $R_s$ should be zero. The length of the wave staff is 31 in. (78.8 cm), so the constant a is computed to be:

$$a = \frac{0.788 \times 499}{864.25} \text{ meters}$$

$$= 0.45,$$

and, hence,

$$h = 0.45\left(\frac{V_s}{V - V_s}\right).$$

It should be noted that three analog calibration signals are supplied from the buoy. These signals are generated by the same means as the wave staff voltages except that a dummy resistor is used in place of a physical wave staff. These resistors were chosen to simulate the resistance of a wave staff when it is extended by roughly 10%, 50%, and 90% of full scale. In practice, the resistance values corresponded to wave staff extensions of 11.57%, 45.36%, and 86.78%. The corresponding voltages will, of course, not indicate this same percentage of full scale because of the nonlinear relationship between resistance and measured voltage.

By observing the calibration signals and maximum staff resistance signals while the buoy is on the Coast Guard cutter deck, it is possible to provide a check on the unknown constants in the expression for $R_s$. Four points are plotted in figure B-4 corresponding to the voltage $V_s$ that results for 11%, 46%, 86%, and 100% of the maximum $R_s$. The voltage scale is expressed as an integer where the maximum value of 4096 corresponds to the A/D converter reference voltage.

With the aid of these plotted points, it is found that

$$V = 3910 \quad \text{(same units as } V_s\text{)},$$

and

$$\frac{R_s}{R_{s_{max}}} = 0.59.$$

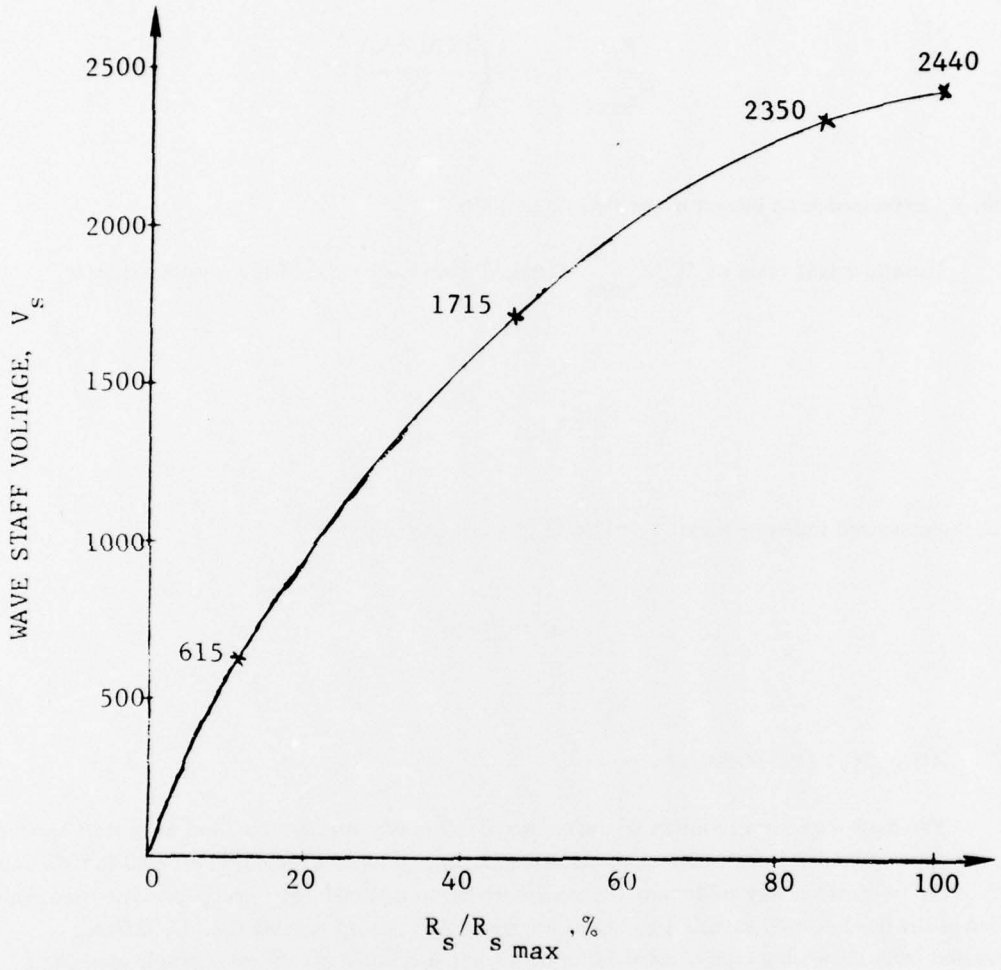


CALIBRATION RESISTORS 11%, 46%, & 25%
OF $R_{s\ max}$

*Figure B-4. Voltage/Resistance Calibration Curve*

Thus,

$$\frac{R_S}{R_{S_{max}}} = 0.59\left(\frac{3910 - V_S}{V_S}\right),$$

with $V_S$ expressed as an integer in the range 0 to 4095.

The equivalent value of $R_O/R_{S_{max}}$ obtained from knowledge of the resistor values is

$$\frac{R_O}{R_{S_{max}}} = 0.578.$$

With the measured full-scale value $V_S$ of 2440, V is computed to be

$$V = 3860.$$

## B.2 ANALOG TAPE FORMAT

The basic data frame consists of the compass, roll, pitch, acceleration, and wave staff samples to which are appended three calibration samples indicating voltages representative of 10%, 50%, and 90% of the full-scale analog voltages in the system under normal operation. A 33-bit sync train is also added at the head of each frame. The composite frame is indicated in table B-2. Each frame is extracted from the analog tape in serial form, with most significant bits of each sample appearing first. In the analog-to-digital tape conversion, the software is set up to handle 12-bit bytes of data. The total data segment of 223 bits is therefore extended to cover five bits of the sync code to give a multiple of 12; i.e., the equipment is set up to search for the abridged sync code (octal):

0 0 3 6 0 7 0 6 2 2 (28 bits).

*TABLE B-2. DATA FRAME FORMAT*

Sync bits (octal)

0 1 7 0 3 4 3 1 1 2 5

| DATA | BITS | DATA | BITS |
|---|---|---|---|
| Compass | 7 | $S_1$ | 12 |
| Roll | 12 | $S_2$ | 12 |
| Pitch | 12 | ⋮ | |
| $A_z$ | 12 | $S_{10}$ | 12 |
| $A_x$ | 12 | $Cal_1$ | 12 |
| $A_y$ | 12 | $Cal_2$ | 12 |
| | | $Cal_3$ | 12 |

The remaining five bits are then treated as data and appear in the five most significant bit locations of the 12-bit compass word. The actual compass bearing must, therefore, be extracted by first eliminating these bits and then decoding the seven-bit Gray code.

## B.3 CONVERSION OF ANALOG TAPES TO DIGITAL

The EMR tape-stripping facility at TSC was used to convert the analog tapes to digital form. Analog tape speed was 3-3/4 ips and the data rate was 6.4 Kbps. The EMR bit and frame synchronizer were loaded with the following contents (octal):

Bit Synchronizer

| Register | Contents |
|---|---|
| 1 | 1 4 4 |
| 2 | 0 3 1 |
| 3 | 2 2 1 |
| 4 | 0 4 2 |
| 5 | 0 2 0. |

Frame Synchronizer

| Register | Contents |
|---|---|
| 1 | 0 0 0 |
| 2 | 1 7 0 |
| 3 | 1 6 1 |
| 4 | 2 2 2 |
| 5 | 0 1 7 |
| 6 | 2 0 7 |
| 7 | 2 2 6 |
| 8 | 1 5 5 |
| 9 | 0 0 4 |
| 10 | 0 0 0 |
| 11 | 0 0 0 |
| 12 | 0 0 0 |
| 13 | 0 7 0 |
| 14 | 0 2 3 |
| 15 | 0 4 1 |
| 16 | 0 0 0 |
| 17 | 1 4 1. |

The program DFS.LDA[12,1] was loaded into the PDP-11 by means of the absolute loader and the desired parameters were entered. A concise summary of the parameters required is given in section 3.2, along with a listing of the digital tape file structure for each analog tape stripped. The data segments are referenced by experiment time in the form: hours: minutes: seconds.

## B.4 PROCESSING OF THE JOINT WAVE SLOPE PROBABILITY DENSITY FUNCTION

In this section three topics relative to the measurements leading to the joint probability density functions for the wave slopes are discussed:

a. Bias removal
b. Measurement geometry
c. Coordinate rotation.

In item c, transformation to a fixed coordinate system is required because of the nonnegligible time variability of the magnetic compass bearing. The fixed reference was chosen to be in the direction of the satellite so that the results could be easily related to the multipath scattering measurements for in-plane and cross-plane flights.

### B.4.1 Bias Removal

During the programming, a question arose relative to the removal of bias: At what point in the processing should the bias be removed? We chose to remove the bias from the raw roll and pitch data; this choice guarantees that an unbiased angle $\theta$ with value at or near $0^{o}$ is mapped into a slope value via that part of the tan $\theta$ curve near the origin.

### B.4.2 Measurement Geometry

The conventions used to describe roll and pitch are illustrated in figure B-5a. The x-axis is the reference direction and points to the "bow." The negative y-axis points in the starboard direction. When the +x axis is depressed in the x-z plane, this is considered to be an increase from 0, i.e., a positive-valued pitch angle $\theta$. Positive values of $\phi$, the roll angle, result from depression of the +y axis (port arm) in the y-z plane.[1]

The sense of angular dependence is appropriately illustrated in figure B-5a. We point out that all the tape data on sea slope are referred to the buoy coordinate system according to the convention illustrated in figure B-5a.

### B.4.3 Coordinate Rotation

The fact that the buoy coordinate system itself rotates is one major reason for the need to rotate each data point to a single fixed coordinate system. Because of convenience, the aircraft heading is chosen as the reference direction. The transformations required are illustrated in figure B-5b. To summarize briefly, note that all sea-slope measurements are referenced to the buoy coordinate system, which has a nonconstant bearing $\alpha$. It is desired to reference these quantities to the constant aircraft heading at $\beta$. To do this, a coordinate transformation through the variable angle $\xi = \beta - \alpha$ is required. Using primed variables to indicate the location of a point in the "new" coordinate system, the transformation is governed by:

$$x = x' \cos \xi + y' \sin \xi$$

$$y = y' \cos \xi - x' \sin \xi$$

$$z = z'. \qquad \text{(B-1)}$$

[1] Actually the pitch depression is an increase above $180^{o}$ ($172.7^{o}$ was measured for an $8^{o}$ lift), whereas a depression of the starboard arm causes a decrease in $\phi$ relative to $180^{o}$ (a $12^{o}$ depression resulted in a measured value of $167.5^{o}$). We have subtracted the $180^{o}$ from the data, however.

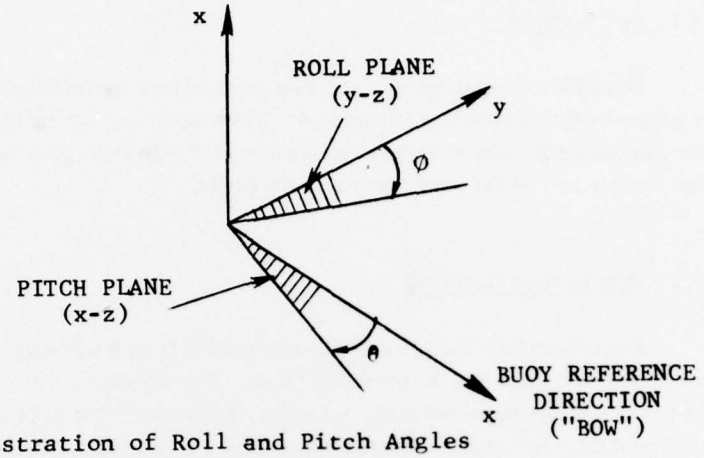


(a) Illustration of Roll and Pitch Angles

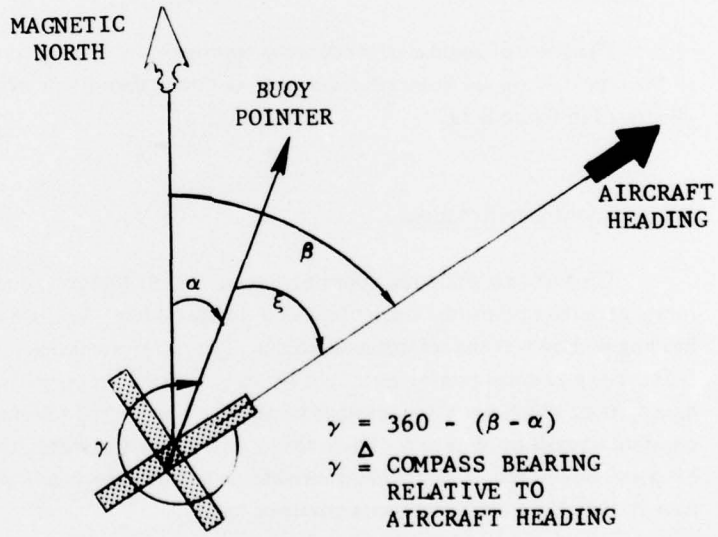


(b) Transformation to Fixed Reference System

$\phi \triangleq$ ROLL ANGLE

$\rho \triangleq$ PITCH ANGLE

$\beta \triangleq$ AIRCRAFT HEADING

$\alpha \triangleq$ MAGNETIC COMPASS READING

*Figure B-5. Sea-State Geometries*

In the "old" coordinate system, the equation for a plane passing through the origin was governed by:

$$Ax + By + Cz = 0. \tag{B-2}$$

Using the fact that a vector with components A, B, and C is normal to the plane, it is an easy matter to show that

$$\tan \phi = -\frac{B}{C} , \tag{B-3}$$

and

$$\tan \phi = -\frac{A}{C} . \tag{B-4}$$

Additionally, one can show by using the transformation properties in equation (B-1) that the equation for the plane in the "new" coordinate system

$$A'x' + B'y' + C'z' = 0 , \tag{B-5}$$

has the coefficients

$$A' = A \cos \xi - B \sin \xi$$

$$B' = A \sin \xi + B \cos \xi$$

$$C' = C . \tag{B-6}$$

Relations (B-3) and (B-4) hold for the primed coordinate system as well as the unprimed. By substituting equation B-6 into (B-3) and (B-4), it is easily shown that the roll and pitch angles in the new coordinate system are governed by

$$\tan \phi' = \tan \theta \sin \xi + \tan \phi \cos \xi , \tag{B-7}$$

and

$$\tan \theta' = \tan \theta \cos \xi - \tan \phi \sin \xi . \tag{B-8}$$

As an important example, we look at the case

$$\beta = 270^{o}.$$

For this case, $\sin \xi = - \cos \alpha$ and $\cos \xi = - \sin \alpha$, so that finally we have

$$\tan \phi' = - \tan \theta \cos \alpha - \tan \phi \sin \alpha , \tag{B-9}$$

and

$$\tan \theta' = \tan \theta \sin \alpha + \tan \phi \cos \alpha . \tag{B-10}$$

The sign assignment in equations (B-9) and (B-10) can be checked quickly by drawing a few sketches and testing for $\alpha = 0^{o}$ and $\alpha = 90^{o}$.

Summarizing, we note from figure B-5 that the slopes in the x- and y-directions are given by $\eta_{x'} = \tan \theta'$ and $\eta_{y'} = \tan \phi'$. Thus, in the final reference system (positive x-axis aligned with aircraft heading), the wave slopes are given by:

$$\eta_{x'} = \tan \theta \cos \xi - \tan \phi \sin \xi$$

$$\eta_{y'} = \tan \theta \sin \xi + \tan \phi \cos \xi$$

$$\xi = \beta - \alpha .$$

U.S. GOVERNMENT PRINTING OFFICE: 1976—700-696/124